Positioning mechanisms in bacterial cells

Midcell sensing in *Myxococcus xanthus*

Silke Bergeler

München 2018

Positioning mechanisms
in bacterial cells

Midcell sensing in *Myxococcus xanthus*

Silke Bergeler

Dissertation

an der Fakulät für Physik

der Ludwig–Maximilians–Universität München

vorgelegt von

Silke Bergeler

aus Mainz

München, den 1. Juni 2018

Erstgutachter: Prof. Dr. Erwin Frey

Zweitgutachter: Prof. Dr. Ulrich Gerland

Tag der mündlichen Prüfung: 13. Juli 2018

Zusammenfassung (Summary in German)

Die räumliche und zeitliche Regulierung der Positionierung von Proteinen an bestimmten Stellen innerhalb einer Bakterienzelle ist wichtig für viele lebensnotwendige Prozesse, unter anderem der Zellteilung. In dem Bakterium *Myxococcus xanthus* formen so genannte Pom Proteine ein Cluster, das sich auf dem Nukleoid von einer Position nahe eines Nukleoid Endes zur Mitte der Zelle bewegt und dort die Zellteilung positiv stimuliert. In meiner Doktorarbeit habe ich mich mit der Modellierung dieser Dynamik beschäftigt, wobei sowohl numerische als auch analytische Methoden angewandt wurden.

1. Ein Fluss-basierter Mechanismus für die Lokalisierung der Zellmitte in *M. xanthus*
mit Dominik Schumacher, Lotte Søgaard-Andersen und Erwin Frey.

Im ersten Projekt haben wir, in enger Zusammenarbeit mit unseren experimentellen Kollaborationspartnern Dominik Schumacher und Lotte Søgaard-Andersen vom MPI for Terrestrial Microbiology (Marburg), ein Modell entwickelt, das die Dynamik des Pom-Clusters auf dem Nukleoid beschreibt. Diese wird reguliert durch die ATPase PomZ. Wir konnten zeigen, dass die Positionierung des Pom-Clusters in der Mitte der Zelle durch einen Mechanismus beschrieben werden kann, der auf den Flüssen von PomZ auf dem Nukleoid beruht. Mit Hilfe unseres Modells haben wir Vorhersagen gemacht, die experimentell bestätigt werden konnten. Dieses Projekt hat zu einer Publikation (Developmental Cell) geführt, die dieser Doktorarbeit angefügt ist.

2. Regulierung der Pom Cluster Dynamik in *M. xanthus* *mit Erwin Frey.*

Das zweite Projekt hatte das Ziel die Clusterbewegung genauer zu untersuchen. Hierzu haben wir Simulationen durchgeführt, bei denen die Modell-Parameter über einen großen Bereich variiert wurden. Unter anderem haben wir herausgefunden, dass die Cluster auf dem Nukleoid oszillieren, wenn die Zeitskalen der Cluster- und PomZ-Dynamik vergleichbar werden. Für den Fall, dass die Cluster-Dynamik deutlich langsamer ist als die PomZ-Dynamik, was den experimentellen Beobachtungen entspricht, konnten wir einen theoretischen Ansatz entwickeln, der die gemittelte Cluster-Trajektorie durch eine effektive Gleichung beschreibt. Dadurch konnten wir erklären wie die stochastischen Interaktionen von PomZ Proteinen mit dem Cluster zu einer gerichteten Bewegung und Positionierung führen. Ein Manuskript wurde zur Veröffentlichung eingereicht und befindet sich gerade im Peer-Review Prozess.

3. Positionierung von Protein-Clustern in der dreidimensionalen Zellgeometrie
mit Matthias Kober und Erwin Frey.

Im dritten Projekt haben wir unser Modell von einer eindimensionalen Geometrie auf eine biologisch realistischere, dreidimensionale Geometrie erweitert. Bisher war unklar, ob ein Fluss-basierter Mechanismus auch Objekte positionieren kann, wenn die Proteine um diese herum diffundieren können, da so die Asymmetrien in der Proteinverteilung ausgeglichen werden könnten. Wir haben gezeigt, dass eine Positionierung auch in einem solchen Fall möglich ist und die Abhängigkeit von der Clustergröße auf den Positionierungsprozess analysiert. Die Simulation der Dynamik von zwei Proteinclustern ergab eine Positionierung bei ein und drei viertel der Nukleoidlänge. Eine Publikation zu unseren Ergebnissen ist in Vorbereitung.

Overview of the thesis

My thesis is concerned with an intracellular protein patterning system: the Pom system in the bacterium *Myxococcus xanthus* that regulates the positioning of the cell division site at midcell. In this system, a protein cluster forms, which is tethered to the nucleoid by the ATPase PomZ and moves in a biased random-walk towards midcell. There, it positively stimulates the FtsZ ring formation. This thesis is organized into three parts corresponding to three projects to which I contributed to.

1. **A flux-based mechanism for midcell positioning in *M. xanthus***
   with Dominik Schumacher, Lotte Søgaard-Andersen, and Erwin Frey
   In this project, we developed together with our experimental collaboration partners Dominik Schumacher and Lotte Søgaard-Andersen from the MPI of Terrestrial Microbiology (Marburg) a model for the Pom cluster dynamics. Our results showed that a flux-based mechanism can explain midcell localization of the cluster. We made several model predictions that were verified experimentally. The results from this project are published in "The PomXYZ Proteins Self-Organize on the Bacterial Nucleoid to Stimulate Cell Division", *Dev Cell* **41**(3), 299–314 (2017) (reprinted in section 3.1). In section 1.4, I summarize the experimental findings of our collaboration partners. Chapter 2 gives details on the computational model, including the parameter choice.

2. **Regulation of Pom cluster dynamics in *M. xanthus***   *with Erwin Frey*
   In the second project we studied the proposed one-dimensional model using extensive *in silico* parameter sweeps. We found that cluster dynamics changes from localization at to oscillatory movement around midcell, when the time scale of the PomZ dynamics and the cluster dynamics become comparable. We showed that in the adiabatic limit, i.e. if the PomZ dynamics is faster than cluster dynamics, the average cluster trajectories can be described by the flux difference of PomZ dimers into the cluster, the forces a single PomZ dimer exerts on the cluster and an effective friction coefficient of the cluster. With our analyses we gained new mechanistic insights into the positioning process. Our results are presented in chapter 4. A manuscript about the results discussed in sections 4.1–4.7 is currently under review for publication and as a preprint available on arXiv ("Regulation of Pom cluster dynamics in *Myxococcus xanthus*", arXiv:1801.06133).

3. **Flux-based positioning of protein clusters in three-dimensional cell geometry**
   with Matthias Kober and Erwin Frey
   In the third project, we generalized our model to one that incorporates a three-dimensional nucleoid geometry. We showed that a flux-based mechanism can explain midcell positioning of a Pom cluster also in a geometry, where it is possible that PomZ dimers diffuse past the cluster. The results presented in section 5.2 are currently prepared for submission with Matthias Kober and me as shared first authors.

Abstracts of the projects

Intracellular positioning of proteins is crucial for several vital processes in bacterial cells, including cell division. In the bacterium *Myxococcus xanthus* three proteins (PomX, PomY, and PomZ) are found to be important for the positioning of the cell division site at midcell [1, 2]. Similar to other positioning systems such as the MinCDE system in *Escherichia coli* and ParAB*S* systems for plasmid and chromosome segregation, the Pom system involves an ATPase (PomZ) that cycles between two states: bound to the nucleoid or unbound in the cytosol. There is experimental evidence that PomX and PomY form a cluster, which is tethered to the nucleoid by PomZ dimers and the cluster moves in a PomZ-dependent manner towards midnucleoid, which coincides with midcell.

During my doctoral studies, I worked on the theoretical investigation of this protein-based midcell positioning system in *M. xanthus*. The work to which I contributed can be grouped into three projects. In the first project, Erwin Frey and I developed a computational model for the Pom cluster dynamics in *M. xanthus*. Our experimental collaboration partners Dominik Schumacher and Lotte Søgaard-Andersen from the Max Planck Institute for Terrestrial Microbiology in Marburg performed the experiments, which our theoretical analyses are based on. We showed that our proposed model can explain midcell localization of the Pom cluster on the experimentally observed time scale for physiologically relevant parameters. Based on our findings we proposed a mechanism for midcell localization in *M. xanthus* that relies on a flux-balance argument as previously proposed to explain equidistant positioning of plasmids [3]. In the second project, we investigated our proposed model further using analytical and computational methods to increase our mechanistic understanding of the positioning process. To this end, we studied the influence of each of the model parameters on the cluster trajectories in our simulations and developed an approach to estimate the average cluster trajectory. In both projects we considered a reduced model geometry: the nucleoid and the cluster are modeled as one-dimensional lattices. To study the effect of the three-dimensionality of the nucleoid on the cluster dynamics, in the third project, we simulated the cluster dynamics on the surface of a cylinder. Furthermore, we investigated the role of the cytosolic PomZ distribution on the cluster dynamics and also considered the dynamics of two clusters on the same nucleoid.

Since the Pom system has similarities with ParAB*S* systems for plasmid and chromosome segregation, our findings might be relevant also for this system. On a broader perspective, our work might be of interest also for a general biophysics / statistical physics community as we theoretically investigated a transport and localization process of cargoes in a non-equilibrium system. Non-equilibrium transport processes are also

important e.g. in eukaryotic cells where cargoes are transported by molecular motors that move on microtubules or actin filaments [4].

1. A flux-based mechanism for midcell positioning in *M. xanthus*
with Dominik Schumacher, Lotte Søgaard-Andersen, and Erwin Frey

Summary

In the first project we investigated the midcell positioning process of the Pom cluster in *M. xanthus* cells. We searched computationally for a mechanism to explain the localization of the cluster at midcell. Previously, the nucleoid has been observed to have elastic properties, which might lead to the forces that translocate a macromolecular object interacting with proteins bound to the nucleoid [5, 6]. We followed this idea by modeling the PomZ dimers effectively as springs to account for the elasticity of the nucleoid and, to a minor extent, the proteins. Simulations of our model showed that the cluster moves in a biased stochastic manner towards midcell and at midcell its movement is constrained, for physiologically relevant parameters. Based on the fast diffusion of PomZ dimers on the nucleoid observed experimentally, we proposed a flux-based mechanism for midcell positioning of the protein cluster (similar to a previously proposed mechanism for equal plasmid spacing [3]). The idea is that the ATPase fluxes on the nucleoid differ at the cargo (in our case the Pom cluster) if the cargo is positioned away from midcell: More PomZ dimers are arriving from the side with the longer distance between the cluster and the nucleoid end. Since PomZ dimers can exert forces on the cluster due to the elastic properties of the nucleoid, the asymmetry in the fluxes can guide the cluster to midcell. To further test our proposed model we made several model predictions that are in qualitative agreement with the experimental findings.

Background

Bacterial cell division starts by the formation of a ring consisting of the tubulin homologue FtsZ at the future division site, which then recruits further proteins involved in the cell division process. Interestingly, the proteins of the cell division machinery are conserved among various bacteria, but the proteins that regulate the positioning of the FtsZ ring are not [7–9]. Recently, our collaboration partners discovered a set of proteins that are important for defining the cell division site in *M. xanthus* cells. Here, a protein cluster forms that moves on the nucleoid from an off-center position towards midcell and positively regulates the FtsZ ring formation there. The movement depends on the ATPase PomZ, which binds in its ATP-bound dimeric state to the nucleoid and its ATPase activity is stimulated when bound to the PomXY cluster. Upon ATP hydrolysis PomZ undergoes a conformational change and detaches from the nucleoid and cluster into the cytosol as two ADP-bound monomers. The midcell positioning process of the PomXY cluster is reminiscent of the positioning of low-copy number plasmids at equally spaced distances along the nucleoid by the ParABS system, involving an ATPase, ParA. How macromolecular objects such as protein clusters,

plasmids or partition complexes can be translocated and positioned by ATPases is an intriguing question and an active field of research.

Motivation and research question

The aim of this project was to identify and analyze a computational model that explains the experimentally observed cluster dynamics: a random-walk like movement from an off-center position towards midcell in about 80 min. In addition, the model should qualitatively agree with the following experimental observations: i) a high density of PomZ in direct association with the cluster, ii) a slowly moving cluster compared to quickly diffusing PomZ dimers on the nucleoid and in the cytosol, iii) a large Pom cluster size, iv) no depletion zone in the wake of the cluster as observed for several Par systems.

Summary of results

A flux-based positioning mechanism can explain midcell localization of the Pom cluster. In close collaboration with Dominik Schumacher and Lotte Søgaard-Andersen we developed a computational model for the stochastic dynamics of PomZ on the nucleoid and the PomXY cluster that is tethered to the nucleoid via PomZ. In this model, we reduced the nucleoid and the cluster to one-dimensional lattices. To account for exclusion effects we limited the number of PomZ dimers per lattice site on both the nucleoid and cluster. We implemented the model using a Gillespie algorithm and showed that the experimentally observed Pom cluster movement from close to the nucleoid pole to midcell can be reproduced on the biological time scale. The parameters we used were either determined experimentally, or estimated from literature values for the related Par systems, or varied over a broad range. Our simulation results showed a high density of PomZ at the cluster as observed in the fluorescence images. The number of PomZ dimers bound to the cluster increase when the cluster moves towards midcell, because it becomes more accessible for PomZ dimers. As expected for a flux-based mechanism we observed an asymmetric PomZ density distribution on the nucleoid [3], if the cluster is located off-center, which implies a difference in the protein fluxes from each side into the cluster. In addition, we observed an asymmetric distribution of nucleoid-bound proteins that are also bound to the cluster, which was not considered previously [3]. If the cluster is positioned at midcell, the PomZ profile, both on the nucleoid and bound to the cluster, is symmetric. A first analysis of this asymmetry in the biological system indeed showed a slightly, but significantly asymmetric PomZ distribution on the nucleoid for Pom clusters at an off-center position.

Our model predictions agreed with the experimental findings. We made three model predictions that were qualitatively tested against the experiments. First, for a reduced ATP hydrolysis rate of PomZ (= detachment rate of the protein at the cluster), the simulation results showed a decreased bias in the cluster movement towards midcell. This can be attributed to the fact that a reduced ATPase activity leads to a reduced cycling frequency of PomZ between the cytosolic and nucleoid-bound state, which decreases the flux difference at the cluster. Thus the bias in the cluster's movement

is reduced. For very low hydrolysis rates the high density of PomZ at the cluster reduces the mobility of the cluster due to crowding effects. These observations are in qualitative agreement with the following two experiments. First, in cells with a mutant of PomZ that cannot hydrolyze ATP the cluster was stalled at its initial position and fluctuated only slightly around this position. Since the ATPase activity of PomZ is synergistically stimulated by PomX, PomY and DNA, it is reduced in the absence of PomY. Hence, in a second experiment, we could use cells that do not express PomY to study the effect of a lowered hydrolysis rate. In these cells, the clusters were still biased in their movement towards midcell. They were less mobile compared to clusters in wild type cells, but more mobile than clusters in cells with the ATP hydrolysis mutant, in qualitative agreement with our predictions.

Next, we considered a variation of the total PomZ dimer number, N_{total}, in the cell. When we reduced N_{total} by a factor of two in the simulations, the clusters still moved towards midcell, but more slowly. In experiments with a reduced PomZ dimer number, the clusters showed a bias towards midcell, but the mean squared displacement was lower compared to that of clusters in wild type cells, suggesting that they move more slowly towards midcell as predicted by theory. Interestingly, when we increased N_{total} in the simulations, we also observed a reduced bias of the clusters towards midcell and, for very large N_{total} values, the clusters were stalled at their initial positions. This can be explained by exclusion effects of PomZ dimers at the cluster: PomZ dimers might not be able to bind to a cluster site if this site is already occupied, whereby the flux of PomZ in the system is reduced. Furthermore, a high amount of cluster-bound PomZ leads to crowding and thereby reduces the mobility of the cluster, similar to the case of very small hydrolysis rates. The flux difference in PomZ at the cluster might also be reduced due to exclusion on the nucleoid, but since the proteins have more space to explore on the nucleoid compared to the cluster region, this is a minor effect if N_{total} is not too large. In *M. xanthus* cells with PomZ > 50-fold overexpressed, the clusters did not show directed movement towards midcell and moved only slightly in general, in line with our theoretical predictions.

Relevance and outlook

We proposed a flux-based mechanism for midcell localization of the Pom cluster in *M. xanthus* that is in qualitative agreement with experimental observations. Our model has similarities to models for the Par system regulating chromosome and plasmid segregation, though some observations for the Pom system in *M. xanthus* differ from those made for Par systems. Among others, these include the high density of PomZ at the cluster and the fast PomZ dynamics compared to the slow cluster dynamics. The latter is crucial for a flux-based positioning mechanism and also explains the lack of a depletion zone in the wake of the cluster, which is observed for cargoes translocated by Par systems [10]. Understanding the differences and commonalities between the Pom and other positioning systems will increase our understanding of intracellular positioning processes in general. Our proposed model is one-dimensional, which is suitable for a conceptual and mechanistic understanding of the process. However, for a

quantitative description, a one-dimensional model geometry might be oversimplified. Furthermore, not all parameters of the model are determined experimentally yet, which remains to be done in the future.

The results from this project were published in "The PomXYZ Proteins Self-Organize on the Bacterial Nucleoid to Stimulate Cell Division", Dev Cell **41**(3), 299–314 (2017) (reprinted in section 3.1).

2. Regulation of Pom cluster dynamics in *M. xanthus*
with Erwin Frey

Summary
In the second project we theoretically investigated our proposed model for midcell positioning in *M. xanthus* with the aim to get further mechanistic insights into the positioning process. First, we performed broad *in silico* parameter sweeps to study how each of the model parameters influences the cluster dynamics. Though the time the clusters needed to reach midcell varied, we found midcell positioning in a large region of parameter space. In this case, we showed that the average cluster trajectory can be described by three factors: the fluxes of nucleoid-bound PomZ dimers into the cluster, the force a single dimer exerts on the cluster and the effective friction coefficient of the cluster. We were able to derive analytical expressions for the fluxes of PomZ on the nucleoid and for the effective friction coefficient of a cluster that is tethered to the nucleoid via PomZ dimers. The average force a single PomZ dimer exerts on the cluster was determined by simulations. This approach, which we refer to as *semi-analytical approach*, allowed us to gain further insights into the dependence of the cluster trajectories on the model parameters and thereby to increase our understanding of the mechanism itself. A qualitatively different behavior was observed for small diffusion constants of PomZ on the nucleoid. Here, the clusters started to oscillate around midcell. In general, oscillatory cluster movements occurred when the dynamics of the PomZ dimers on the nucleoid was slow compared to the dynamics of the Pom cluster, because then the cluster moved faster than the PomZ density profile adapted to the new cluster position.

Motivation and research question
In the first project, we proposed a mechanism that relies on the fluxes of the ATPase PomZ on the nucleoid to regulate the cluster position. However, several open questions remained regarding the positioning process, including: i) Which of the model parameters are crucial for the cluster's movement and how is the cluster's trajectory affected by a change of these parameters? ii) How do the PomZ dimers that are model effectively as springs exert forces on the cluster? iii) Which factors determine the net velocity of the cluster's movement towards midcell?

Summary of results

In silico parameter sweeps showed interesting cluster dynamics when the ATP hydrolysis rate of PomZ and the mobility of PomZ on the nucleoid and cluster were varied. First, we performed broad parameter sweeps that serve several purposes, including: i) get the dependence of the cluster trajectories on each parameter, ii) make model predictions, and iii) cope with the fact that not all parameters are measured experimentally. Reassuringly, we found midcell localization of the cluster for a broad range of parameters. Typically, a change in one of the parameters either led to an increased or decreased bias in the cluster's movement towards midcell. However, for some of the model parameters we observed a distinct behavior. For the ATP hydrolysis rate of PomZ we found that there exists a rate for which the time the clusters need to reach midcell is minimized. A qualitatively different cluster dynamics was observed when the diffusion constant of PomZ on the nucleoid was decreased: the clusters oscillate around midcell. Furthermore, we observed that the cluster's velocity towards midcell increased when the PomZ dimers diffused more quickly on the PomXY cluster.

The average cluster trajectory can be approximated by a semi-analytical approach in the adiabatic limit. To understand the observed changes in the cluster dynamics when one of the parameters was varied, we aimed at an effective equation for the average cluster trajectories in dependence of the model parameters. In the adiabatic limit, i.e. when the cluster moves slowly compared to the PomZ dimers, the cluster position can be regarded as constant on the time scale of the PomZ dynamics. We found that, if the adiabatic assumption holds true, the net force acting on the cluster can be approximated by the product of the flux difference of PomZ dimers approaching the cluster from either side and the force a single dimer exerts on the cluster averaged over time. Solving a continuum model that resembles the stochastic model allowed us to derive an analytical expression for the flux difference into the cluster. We determined the forces a single PomZ dimer exerts on the cluster using simulations and verified that a PomZ dimer that approaches the cluster from one side also exerts, on average, a force to this side. Interestingly, we observed that forces are not only generated when the PomZ dimer just attached to the cluster in a stretched configuration (as in the DNA-relay model, [6]), but every time the dimer encounters the cluster's edge it can exert a net force on the cluster. Since the PomZ dimers tether the cluster to the nucleoid, they are not only responsible for exerting a net force on the cluster, but also decrease the mobility of the cluster. We showed that the tethering can be described by a frictional force acting on the cluster, for which we could derive an analytical expression. Altogether, we obtained an approximation for the average cluster trajectory that matched our simulation results well, showing that, in the adiabatic limit, the cluster dynamics can be solely described by the flux difference in PomZ, the force a single PomZ dimer exerts and an effective friction coefficient of the cluster.

The semi-analytical approach offers new insights into the simulated cluster trajectories. Next, we used our semi-analytical approach to gain a better understanding of the observed cluster dynamics. We found an interesting behavior when the ATP hydrolysis rate of PomZ, k_h, was varied: The bias in the cluster movements towards midcell is maximal for an intermediate k_h value. In the semi-analytical approach we

approximated the average cluster trajectory by an expression that only depends on the flux difference of PomZ into the cluster, the single particle force and the effective friction coefficient of the cluster. To investigate the effect of the hydrolysis rate on the cluster dynamics, we considered these different constituents separately. The flux difference increased with an increasing ATP hydrolysis rate, because k_h sets the rate with which PomZ dimers cycle between the nucleoid-bound and cytosolic state. In contrast, the single particle force showed a decrease with increasing k_h. This can be attributed to the fact that the larger the ATP hydrolysis rate, the shorter the time PomZ is attached to the cluster (average residence time $\tau = 1/k_h$) and hence the time to exert a force. The effective friction coefficient of the cluster also decreased with increasing k_h since less PomZ dimers are bound to the cluster and thereby restrict the cluster's movement. In total, this results in a net velocity of the cluster that is maximal for intermediate k_h values.

Clusters oscillate around midcell if the PomZ dynamics is slow compared to the cluster dynamics. Midcell positioning changed to oscillations of the clusters around midcell when the time scale for the PomZ dynamics became comparable to that of the cluster dynamics. We investigated the oscillatory cluster dynamics by varying both the diffusion constant of PomZ on the nucleoid and the friction coefficient of the cluster. Our simulation results showed that the clusters localize at midcell if PomZ dimers diffuse quickly on the nucleoid and the cluster moves slowly (high friction coefficient). When the diffusion constant of PomZ on the nucleoid and cluster was decreased, the clusters started to oscillate around midcell as indicated by a peak in the Fourier spectrum. Lowering the diffusion constant even further resulted in cluster trajectories that not only have a defined peak in the Fourier spectrum, but also a bimodal distribution of the cluster positions. To estimate the onset of oscillations we used a time-scale argument.

Relevance and outlook

With the parameter sweeps we could make several model predictions that would be interesting to test experimentally. A key prediction is that the Pom clusters start to oscillate if the PomZ dynamics is slowed down compared to the cluster dynamics. This might be possible to realize experimentally by increasing the binding affinity of PomZ to the DNA and thereby reducing the mobility of PomZ on the nucleoid. Furthermore, our observation of an ATP hydrolysis rate that minimizes the time the clusters need to reach midcell, is in accordance with the experimental finding that the clusters move more slowly towards midcell for a reduced (PomY deletion mutant) or zero (PomZ-D90A mutant) ATP hydrolysis rate. It would be interesting to also perform experiments with PomZ proteins that have an increased hydrolysis rate. In our model we assumed that the PomZ dimers diffuse on both the cluster and the nucleoid. This assumption is motivated by the experimental finding that in fluorescence images PomZ has a high density along the entire cluster and not only at the cluster's edges. Since there is experimental evidence that PomZ dimers only attach to the PomXY cluster when they are nucleoid-bound, this could suggest that PomZ is mobile when in

direct association with the cluster. However, since the resolution of fluorescence images is about 200 nm and the cluster has a length of about 700 nm, further experiments with a higher resolution are necessary to test this model assumption. In this project, we investigated our proposed model for the Pom cluster dynamics in *M. xanthus* using *in silico* parameter sweeps and analytical calculations and thereby gained mechanistic understanding of the positioning mechanism. An approach similar to our semi-analytical approach might proof useful also for other positioning systems such as the Par system.

We submitted a manuscript with our results to PLoS Computational Biology, which is currently in the peer-review process.

3. Flux-based positioning of protein clusters in three-dimensional cell geometry
with Matthias Kober and Erwin Frey

Summary

In this project we investigated the PomZ and cluster dynamics in a three-dimensional cell geometry. First, we described the PomZ dynamics for a stationary cluster in terms of reaction-diffusion equations and solved the equations using finite element methods. We found an asymmetry in the PomZ fluxes into the cluster also when PomZ can diffuse past the cluster, a necessary requirement for a flux-based mechanism. Next, we investigated the Pom cluster dynamics using an extension of our stochastic, particle-based model that incorporates the three-dimensional geometry of the nucleoid. We found that the cluster still moves to and localizes at midcell in this geometry. In accordance with our findings from the reaction-diffusion equations, we observed an asymmetric PomZ density distribution on the nucleoid if the cluster is positioned off-center and a symmetric distribution for a cluster at midcell. To investigate the effect of the PomZ fluxes around the cluster on its dynamics, we performed simulations with different width and length of the cluster. We observed that the time the clusters need to reach midcell decreases with both the cluster's length and width. These observations can be explained heuristically by the changes in the PomZ fluxes and the forces a single PomZ dimer exerts on the cluster. Moreover, we studied the dependence of the cluster dynamics on the cytosolic distribution of PomZ. Previously, we assumed that the PomZ density in the cytosol is well-mixed, which is justified by a time delay between detachment of PomZ from and reattachment to the nucleoid as well as fast cytosolic diffusion of PomZ. In this project, we generalized our model by explicitly including the cytosolic distribution, though in a simplified manner to be computationally feasible. Our simulation results showed that the closer the cytosolic distribution is to the homogeneous one, the faster the cluster moves towards midcell. Finally, we studied the dynamics of two clusters in the three-dimensional cell geometry, which resulted in the localization of the clusters at the one- and three-quarter positions along the nucleoid.

Motivation and research question

In the first two projects we considered a computational model for the Pom cluster dynam-

ics in *M. xanthus* in which we reduced the nucleoid and the cluster to one-dimensional lattices. However, the bacterial nucleoid is a highly complicated, three-dimensional structure that is constantly reshaped, e.g. due to DNA transcription/replication and chromosome segregation. Since the geometry of the nucleoid likely affects the Pom cluster dynamics, it is important to investigate the cluster dynamics also in a biologically more realistic, three-dimensional cell geometry. In particular, for a flux-based mechanism the asymmetry in the PomZ density and fluxes on the nucleoid is crucial. However, in the three-dimensional cell geometry, PomZ dimers can more easily pass a cluster without interacting with it compared to the one-dimensional geometry, if the cluster is small compared to the nucleoid. Hence, it was questioned whether a flux-based mechanism can lead to midcell positioning in this case [3]. Motivated by these observations, we wanted to answer the following research questions: i) Can a flux-based mechanism explain midcell positioning of the Pom cluster also in a three-dimensional cell geometry? ii) How does the cytosolic PomZ distribution affect the cluster dynamics? In particular, is the homogeneous distribution, which we assumed previously, optimal in the sense that it leads to midcell positioning fastest? iii) What happens if we include a second Pom cluster in our system similar to multiple plasmids in Par systems?

Summary of results

An asymmetry in the PomZ fluxes is still observed in the three-dimensional cell geometry. A flux-based positioning mechanism requires an asymmetry of the PomZ fluxes into the cluster for the guidance of the cluster towards midcell. To investigate if a flux asymmetry is possible also in a three-dimensional cell geometry, we considered a fixed cluster position and described the PomZ dynamics in terms of reaction-diffusion equations. We solved these equations using the finite element solver COMSOL [11]. We found a flux difference of PomZ dimers at the cluster along the long cell axis also in the full three-dimensional cell geometry. This difference was maintained when PomZ can diffuse past the cluster.

   A flux-based mechanism can explain midcell positioning also in the three-dimensional cell geometry. To investigate the cluster dynamics in a three-dimensional cell geometry, we generalized our previous stochastic, particle-based model such that it incorporates the same biochemical processes of PomZ, but the nucleoid is modeled as a cylinder and the PomXY cluster as a rectangular sheet. Recently, Le Gall et al. [12] showed that partition complexes and plasmids move within the nucleoid volume. However, since the PomXY cluster is relatively large ($0.7\,\mu m$) compared to plasmids / partition complexes (about $0.1\,\mu m$, [6]), we expect that the cluster does not penetrate into the nucleoid volume and therefore restricted the movement of a cluster tethered by PomZ to the nucleoid's surface. We further assumed that PomZ dimers do not penetrate into the nucleoid volume. Our simulation results showed that the cluster moves towards and localizes at midcell also for the three-dimensional cell geometry and the movement can be explained by the PomZ fluxes on the nucleoid. We observed that the cluster needs slightly longer to reach midcell compared to the one-dimensional case if the cluster

does not cover the complete nucleoid circumference. This can be attributed to the fact that, in the three-dimensional geometry, nucleoid-bound PomZ dimers can diffuse into the cluster from the short cell axis direction or diffuse past the cluster. Hence, the asymmetry in the fluxes of nucleoid-bound PomZ into the cluster from each side along the long cell axis is decreased, which also reduces the bias in the cluster's movement.

A larger cluster moves faster towards midcell. To study the effect of the nucleoid geometry on the movement of the cluster, we varied the cluster's length, l_{clu}, and width, w_{clu}, in our simulations. We found that the time the clusters need to reach midcell decreases with increasing l_{clu} or w_{clu}. Based on our insights from the one-dimensional model we expected that, in the three-dimensional cell geometry, the cluster's velocity is also mainly determined by the flux difference of PomZ into the cluster and the forces exerted by a single PomZ dimer. We measured the flux difference along the long cell axis for static clusters at different positions along the nucleoid and found an increased flux difference for longer and wider clusters. The increase can be attributed to the fact that a larger cluster is more accessible for PomZ dimers on the nucleoid such that the cycling frequency of PomZ between the nucleoid-bound and cytosolic state is increased. The second factor that contributes to the net force exerted on the cluster, is the force a single PomZ dimer exerts. For a small cluster size, an originally asymmetric density profile of cluster-bound PomZ dimers quickly approaches a homogeneous distribution due to diffusion of PomZ on the nucleoid and the cluster. Since forces are exerted at the cluster's edges, the net force vanishes in this case. This effect is reduced for longer clusters, such that not only the frequency with which PomZ dimers interact with the cluster, but also the forces PomZ dimers exert on average on the cluster, are increased for longer clusters. With these observations we can heuristically explain the observation that larger Pom clusters move faster towards midcell.

Spatial redistribution of PomZ in the cytosol is important for midcell positioning. In all simulation results discussed so far, we assumed that the cytosolic PomZ density is homogeneous. This is a simplifying assumption based on the observation that PomZ diffuses quickly in the cytosol and detaches as ADP-bound monomers from the nucleoid and cluster, such that the monomers first have to exchange ADP for ATP and dimerize before they can rebind to the nucleoid. To analyze the effect of a non-homogeneous cytosolic PomZ density, we explicitly included the cytosolic distribution in a simplified manner, as follows: We formulated the cytosolic PomZ dynamics in terms of one-dimensional reaction-diffusion (RD) equations with a point source accounting for the cluster position. Since the PomZ dynamics in the cytosol is fast, we solved the RD equations in the steady state and used the normalized cytosolic PomZ-ATP density profile as probability distribution for cytosolic PomZ to bind to the nucleoid, in our model. Simulations with this model variant showed that it takes longer for the clusters to reach midcell if the cytosolic PomZ distribution deviates more from the homogeneous distribution. Hence, we concluded that spatial redistribution of PomZ in the cytosol is important for the positioning process.

Two clusters localize at the one- and three-quarter positions. Motivated by equal plasmid spacing observed in Par systems [3, 10, 13–15], we also investigated the dynamics of two Pom clusters on the three-dimensional nucleoid. The simulation

results showed a localization of the clusters at the one- and three-quarter positions along the long cell axis. This can be explained by a repelling force between the two clusters since they compete for the PomZ dimers in the region between them [3, 16]. Interestingly, when we changed the parameter values (smaller diffusion constant of PomZ on the nucleoid and cluster and larger total PomZ dimer number), the clusters oscillate around the one- and three-quarter positions, similar to our observations for one cluster in the one-dimensional model.

Relevance and outlook
In this project we studied the PomZ and cluster dynamics in the three-dimensional cell geometry. We generalized our stochastic model to one that incorporates the nucleoid as a cylindrical object and the cluster as a rectangular sheet, moving on the surface of the nucleoid. We could show that a flux-based mechanism can lead to midcell positioning of the cluster also if the PomZ dimers can diffuse past the cluster and that two cluster are positioned equidistantly. Our findings might be of relevance also for other positioning system involving relatively large cargoes such that it is unlikely that the cargo moves through the interior of the nucleoid (e.g. carboxysomes [17] or clusters of plasmids). Though three-dimensional, the cylindrical geometry we chose to mimic the nucleoid in our model is still very simplified. Further experimental evidence is needed to clarify whether the Pom cluster is really confined to the nucleoid's surface or penetrates into the nucleoid volume. Including more details on the chromosome structure and its reorganization during segregation will be an important task for future research.

Contents

Chapter 1

Introduction

1.1 Intracellular positioning in bacterial cells

The interior of bacterial cells is highly organized, which is remarkable as bacteria lack a nucleus and other organelles found in eukaryotic cells [18]. Proteins form various spatio-temporal patterns inside the cell [19, 20], including localization at midcell [21] or at the cell poles [9, 22, 23], pole-to-pole oscillations [24, 25], gradients along the cell length [6] or from the poles towards midcell [8] as well as foci distributed along the membrane [26]. These patterns serve several important cellular functions, such as the placement of the cell division site, correct chromosome and plasmid segregation as well as the positioning of chemotactic protein clusters and flagella [19].

To form and maintain their intracellular structure, bacterial cells consume energy, which is supplied by the environment (e.g. via food or sunlight). Since they exchange energy and matter with the environment, the processes in a bacterial cell are out of thermodynamic equilibrium. The energy produced in a metabolic reaction is stored in the energy-rich molecule adenosine triphosphate (ATP). In this way, energy can be transferred to a specific position inside the cell and released by the hydrolysis of ATP into adenosine di- or monophosphate (ADP/AMP) and an inorganic phosphate.

An important cellular process that is highly spatio-temporally regulated is chromosome segregation and the subsequent cell division. In a bacterial cell, the chromosome is not enclosed by a membrane as it is in the nucleus in eukaryotic cells, but instead forms a highly condensed structure, which - together with proteins and RNA bound to it - is called the *nucleoid*. Though bacterial cells can exhibit different shapes and accordingly there are various ways how they divide, most of the prokaryotic model organisms are rod-shaped and divide at midcell (e.g. *Myxococcus xanthus*, *Escherichia coli*, *Bacillus subtilis*, *Caulobacter crescentus*). To ensure that both daughter cells inherit the same genetic information, first, the chromosome needs to be duplicated and spatially separated into the two cell halves. Then, the cell has to divide precisely at midcell. This raises two important questions:

1. How are the sister chromosomes segregated?

2. How does the cell identify midcell to divide there?

In bacterial cells, cell division starts by the assembly of the FtsZ-ring (or Z-ring) [9, 27], which then recruits the rest of the proteins involved in the cytokinetic machinery [9]. Interestingly, the proteins of the cytokinetic machinery are highly conserved in different

bacteria, while the protein systems to position the Z-ring are not [7–9]. Accordingly, there are various ways how Z-ring positioning at midcell is ensured. In *E. coli* the MinCDE system (short: Min system) restricts the Z-ring formation to midcell (see section 1.2).

Bacterial chromosome segregation is also regulated by proteins, which can be grouped into three types [28, 29]: (i) actin-like ATPases (e.g. ParM) (ii) tubulin-like GTPases (e.g. TubZ) and (iii) P-loop ATPase (e.g. ParA). ParM and TubZ form filaments *in vivo* and position objects by pushing them apart [30] or treadmilling dynamics [31]. These two kinds of proteins resemble eukaryotic actin and microtubules. Interestingly, in prokaryotes, homologues of all three type of eukaryotic filaments (actin, microtubules, intermediate filaments) have been identified [29, 32]. For the third group of proteins involved in bacterial chromosome segregation, the P-loop ATPases, no homologues are known in eukaryotes so far [28]. It is still under debate if they form filaments *in vivo* and how they regulate chromosome segregation (see section 1.3.2). Interestingly, MinD a constituent of the Min system in *E. coli* and the ParA P-loop ATPases belong to the same superfamily of P-loop NTPases (they have structural similarities) [9, 33].

ATPases are enzymes that can bind and catalyze the hydrolysis of ATP, whereby energy is released. These proteins typically show different intracellular localizations depending on their nucleotide state. As an ATP-bound dimer, the ATPase can bind nonspecifically to DNA (e.g. ParA) or the membrane (e.g. MinD), whereas otherwise it resides in the cytosol [9]. For some ATPases of the ParA/MinD superfamily it is known that they bind cooperatively to the respective surface [34, 35]. The ATPase activity of ATP-bound dimers on the membrane or the nucleoid ("active" form) can be stimulated by so called *ATPase activating proteins* (AAPs), which leads to a conformational change of the protein and finally to the release of ADP-bound monomers ("inactive" form) into the cytosol. The cytosolic form of the ATPase then first needs to become active again before it reattaches to the respective surface. Thus the ATPase cycles between the active, nucleoid- or membrane-bound state and the inactive, cytosolic state.

The topic of this thesis is midcell positioning of the cell division site in the bacterium *M. xanthus*. Here, three proteins (PomX, PomY and PomZ) form a cluster that moves towards midcell and positively regulates Z-ring formation there (see section 1.4). Interestingly, the positioning of the clusters relies on a protein that is a member of the ParA/MinD superfamily of P-loop ATPases [1]. Before we present the details of this system (called Pom system), we discuss two well-studied positioning systems in bacterial cells in order to later explain commonalities and differences to the system under study in this thesis (see section 1.5): the Par system for plasmid and chromosome segregation and the Min system in *E. coli* for midcell localization of the Z-ring.

1.2 Min system for midcell positioning

The Min system in *E. coli* cells is an extensively studied system for midcell positioning of the Z-ring. Here, the Min proteins (MinC, MinD and MinE) ensure the robust positioning of the cell constriction site at midcell [36]. The key biochemical reactions of the Min proteins are: MinD, an ATPase, binds as an ATP-bound dimer to the membrane, where it forms a complex with MinC, which is an inhibitor of FtsZ-ring formation [24, 35, 37, 38]. Furthermore, MinD recruits both MinD and MinE to the membrane [35, 36]. The protein MinE stimulates the ATPase activity of MinD and thereby triggers the release of the membrane-attached Min proteins into the cytosol [39]. Upon detachment from the membrane, MinD is in its ADP-bound monomeric form and first needs to exchange ADP for ATP and dimerize before it can rebind to the membrane [35, 38, 39]. In wild type cells the Min proteins show oscillatory dynamics from pole to pole [24, 25], which results in an average concentration profile of MinC, which is lowest at midcell. Since MinC inhibits the Z-ring formation, the FtsZ proteins are assembled at midcell [40]. To explain the observed Min oscillations, reaction-diffusion models for the Min protein dynamics have been proposed [40–54]. Models based on cooperative membrane attachment and cytosolic nucleotide exchange [43, 46, 48] have been successfully tested experimentally [50, 51, 55]. Besides the nonlinear dynamics of the MinD proteins (MinD recruits further MinD and MinE to the membrane), the cell geometry and the cycling of the MinD proteins between its ADP- and ATP-bound state are crucial to explain the experimentally observed protein patterns [48, 56]. The findings from the Min system can be generalized: the self-organized formation of intracellular protein patterns relies on the cycling of proteins between different states (e.g. membrane-bound and cytosolic) and the spatial redistribution of the proteins via diffusion in the cytosol [53, 54].

Although the Min system in *E. coli* and the Pom system in *M. xanthus* have several commonalities (most obvious they have the same biological function, which is midcell positioning of the Z-ring), from a modeling point of view the Pom system turns out to be closer to Par systems for plasmid and chromosome segregation (see chapter 2). Hence, we do not dive into the various models proposed for the Min system in detail here, but rather continue with a summary of the experimental and theoretical findings for Par systems for chromosome and plasmid segregation.

1.3 Par system for chromosome and plasmid segregation

Another well-studied positioning system in bacteria is the ParABS system (or short Par system) for chromosome and plasmid segregation. During a cell cycle, the bacterial chromosome needs to be duplicated and segregated such that each daughter cell inherits one copy. Apart from the chromosome, bacterial cells contain plasmids, which are smaller, circular DNA molecules that duplicate independent of the cell cycle [57]. Plasmids are important for bacterial cells because they can be transferred from one

cell to another by a process called horizontal gene transfer and in this way genetic information is quickly spread over a population. If there is a large number of the same plasmid inside the cell, both daughter cells inherit roughly the same amount of plasmids when the cell divides because diffusion of the plasmids in the cytosol distributes them between the two cell halves, though the plasmids are likely not homogeneously distributed inside the cell, but rather localize to the nucleoid-free regions at the cell poles [58]. However, for low-copy-number plasmids diffusion is not enough to ensure that each daughter cell inherits the same amount or even one plasmid. In this case, active mechanisms are required to distribute the plasmids to the two daughter cells [59]. ParABS systems ensure equal plasmid distribution by tethering the plasmids to the nucleoid and distributing them along the nucleoid equidistantly. Besides plasmids, also chemotaxis protein clusters [21, 60], carboxysomes (bacterial microcompartments for carbon fixation) [17] and storage granules [61–63] are found to be equidistantly positioned along the cell.

ParABS systems are conserved across many bacterial species [64]. They consist of three different components: An ATPase ParA, that binds in its ATP-bound dimeric form non-specifically to the nucleoid [34, 65, 66], a genomic sequence *parS* on the chromosome or the plasmid and a protein ParB that bind specifically to the *parS* DNA sequence [9]. We refer to the ParBS complex as *partition complex* (PC). DNA-bound ParA dimers can interact with the ParB proteins in the partition complex. This leads to a stimulation of ParA's ATPase activity and two ADP-bound monomers are released into the cytosol [67–69]. To ensure the positioning of plasmids of different kind without interference, each plasmid type typically has a different ParABS system, though some Par systems are not compatible [70, 71].

1.3.1 Experimental observations

Par systems are involved in the positioning of different objects, such as plasmids, partition complexes and protein clusters. In the following we will refer to these macromolecular objects as cargoes. Different patterns of the cargo and the ATPase ParA are observed experimentally. For one cargo, positioning at midcell [3, 14, 15], oscillatory movement of the cargo and the ATPase [10, 13, 72], and movement from one nucleoid pole to the other are observed [6]. Multiple plasmids are found to equidistantly position along the nucleoid [3, 10, 13–15, 72].

1.3.2 ParA-mediated cargo movement

Experiments show that the cargo movement crucially depends on the ParA dynamics [59]: ParA binds in its ATP-bound dimeric form to the nucleoid and its ATPase activity is stimulated by ParB proteins bound to the *parS* site on the plasmid or partition complex. Two key questions remain: How does the ParA dynamics lead to directional movement of a cargo and how are cargoes positioned inside the cell? To address these questions, various mechanisms have been proposed so far [73] (Fig 1.1). Based on experimental observations that ParA forms filaments *in vitro* and hints for ParA

structure formation *in vivo*, cargo translocation was attributed to a pulling force of a depolymerizing ParA filament bundle acting on the cargo (see Fig. 1.1A). However, recent experiments challenge the assumption that ParA forms filament *in vivo* [6, 69]. Instead, ParA dimers are observed to form dynamic patterns on the nucleoid, including a gradient of ParA on the nucleoid [6]. To explain the movement of a cargo into the direction of a higher ParA concentration, a chemophoresis force [74–77], and the elasticity of the chromosome have been proposed [6, 78, 79], which will be discussed next.

1.3.2a Chemophoresis force vs. nucleoid elasticity

A macromolecular object to which a chemical can adsorb experiences a force in a gradient of this chemical that points in the direction of an increased chemical potential [74] (Fig. 1.1A). The force is called *chemophoresis* force, inspired by other phoretic phenomena such as electro-, thermo- or diffusiophoresis [82–84]. These phenomena all have in common that particles move due to gradients of thermodynamic variables (electrical potential, temperature, concentration of chemical species, respectively) [82, 84]. Chemophoresis has an entropic origin [74]. *Proteophoresis* or volumetric chemophoresis refers to a similar phenomenon as chemophoresis, except that the chemical can react with the whole volume of the macromolecular object [75]. Both diffusiophoresis and chemophoresis describe forces acting on an object in a concentration gradient of a chemical species. However, in contrast to chemophoresis, where the force is due to adsorption reactions of the chemicals to the macromolecular object, diffusiophoresis typically refers to processes in which hydrodynamic effects are important and no reactions between the object and a chemical occur [74, 82–84].

The generic concept of chemophoresis has been applied to the Par system to explain plasmid and chromosome segregation [74, 75, 77, 85, 86]: The free energy is decreased by an increasing number of ParA dimers bound to ParB. Hence, a concentration gradient of ParA leads to a force exerted on the cargo into the direction of a higher chemical potential, i.e. a larger ParA concentration [74, 86].

As an alternative to chemophoresis, the nucleoid has been proposed as a source to generate the forces that translocate the cargo [6]. The bacterial chromosome is a highly organized and dynamic structure [87–89]. Measuring the dynamics of genomic loci positions revealed that the nucleoid has elastic properties [5, 6, 90]. Based on this observation, Lim et al. proposed a so called DNA-relay mechanism for the movement of a cargo into the direction of a larger ParA concentration [6] (see Fig. 1.1): ATP-bound ParA dimers bind to the nucleoid and due to the elasticity of the nucleoid and thermal fluctuations the dimers "wiggle" around the equilibrium position of the underlying DNA loci. When they reach the cargo, they bind to it - typically in a stretched configuration - and then relay the cargo towards the equilibrium position until they are released into the cytosol upon ATP hydrolysis. If there is a concentration gradient in nucleoid-bound ParA, it is more likely that a ParA dimer reaches the cargo from the side where the concentration is higher, which leads to the movement of the cargo into the direction of a larger ParA density.
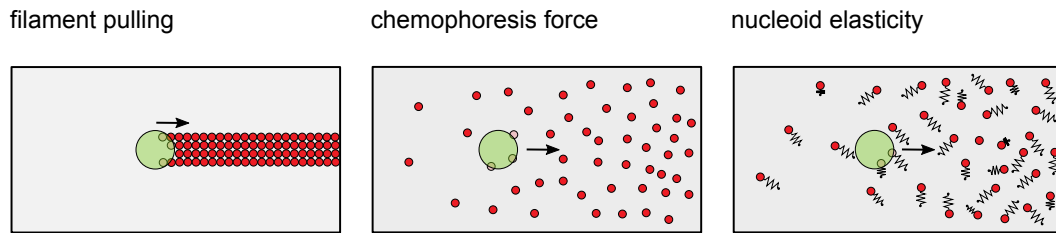
A   How does ParA mediate cargo **movement**?

B   How does ParA mediate cargo **positioning**?
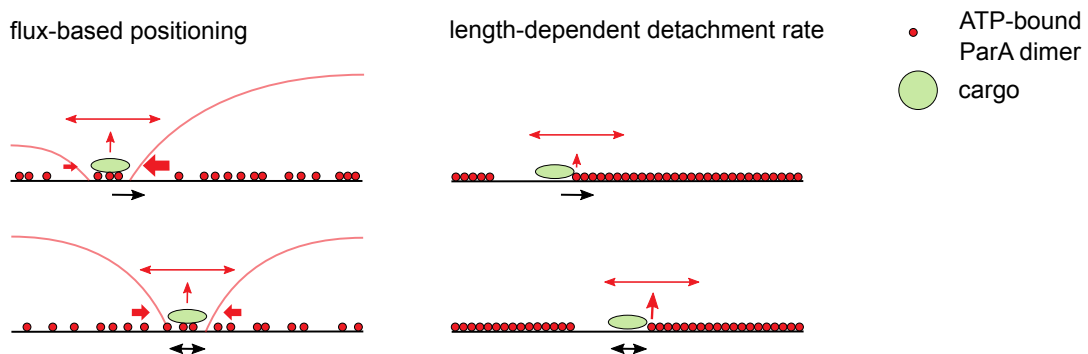
Figure 1.1 ParA-mediated cargo movement and positioning. (A) Different mechanisms for the unidirectional movement of a cargo (e.g. a partition complex, a plasmid or a protein cluster) by nucleoid-bound ParA have been proposed: the cargo follows a retracting ParA-filament bundle [80, 81] ("filament pulling"), the cargo moves into the direction of a higher ParA density by a chemophoresis force [74] or due to the elasticity of the nucleoid [6]. ParB proteins at the cargo (not explicitly shown in the Figure) stimulate the ATPase activity of ParA, which leads to detachment of ADP-bound ParA monomers from the nucleoid into the cytosol. Hence the cargo and ParA dynamics are correlated: an asymmetric distribution of ParA leads to the movement of the cargo, which in turn has an effect on the ParA distribution by stimulating the dissociation of ParA. (B) Positioning of a single cargo at midcell has been explained by a flux-based mechanism that relies on the fluxes of ParA dimers on the nucleoid (ParA might form structures, but this is not a prerequisite) [3]. If ParA forms filaments, positioning of a cargo can be achieved by a length-dependent detachment rate of the cargo from the ParA structure (smaller detachment rates for longer ParA structures) [10].

1.3.2b Brownian ratchets

ParA-mediated cargo movement by a filament-pulling mechanism, a chemophoresis force or a DNA-relay mechanism rely on an asymmetric distribution of ParA on the nucleoid. Here, the movement of a diffusing cargo becomes directed by its interactions with the ParA dimers. Hence, these systems resemble Brownian ratchets [79], which can be defined by two conditions: i) the cargo performs Brownian motion (diffusion)

and ii) it experiences a force due to an asymmetric potential [79, 91]. The asymmetry in the potential leads to a bias in the movement of the cargo though it intrinsically moves in an unbiased manner - by diffusion. To generate and maintain the asymmetric potential, energy needs to be supplied to the system. In the case of the ParABS system, the energy likely comes from ATP that is bound to the ParA dimers. Upon ATP hydrolysis, ATP dimers detach into the cytosol as ADP-bound monomers and this step is irreversible. Hence, detailed balance is broken and the system is out of equilibrium. Interestingly, in the Par system, the cargo and ParA dynamics are coupled: Since ParA dimers detach from the nucleoid when they interact with the ParB dimers bound to the cargo, the cargo influences the ParA distribution on the nucleoid, which in turn determines the movement of the cargo.

A specific class of Brownian ratchet models are so called *burnt-bridge Brownian ratchets*. Since several of the models for the Par system discussed later are similar to this class of Brownian ratchets, we shortly introduce them here. Burnt-bridge Brownian ratchets were originally introduced to understand the movement of track-altering molecular motors [92–94]. Such molecular motors move along a track (e.g. a microtubule or actin), but they can also change the track, which in turn influences the dynamics of the motor. In the standard burnt-bridge Brownian ratchet model the motor protein performs a random walk on a one-dimensional lattice. The lattice contains weak and strong links and the weak ones can be destroyed by the motor with a probability $0 < p \leq 1$. If the link is broken, the motor cannot pass it again, which affects the overall dynamics of the motor. To summarize, burnt-bridge Brownian ratchet models mainly rely on the property that the track on which a cargo moves can be burnt in the wake of the cargo such that a contiguous forward movement of the cargo is achieved.

1.3.3 Models for Par positioning systems

In the following, various models proposed in the literature for chromosome and plasmid segregation by Par systems are discussed.

1.3.3a Filament-based models

Based on the experimental evidence that ParA proteins form filaments or structures *in vitro* and *in vivo* [10, 34, 73], models that include the dynamic polymerization and depolymerization of ParA have been introduced. In these models, ParA forms filaments and depolymerization of the filaments is triggered by the interaction of the filaments with the cargo. Different mechanisms have been proposed for how a ParA filament can position a cargo, including mitotic-like mechanisms [70, 95]. Ringgaard et al. proposed a filament-pulling mechanism to explain the experimentally observed dynamics of one plasmid and equipositioning of multiple plasmids [10]. Interestingly, they find that equipositioning can be obtained by a length-dependent rate for the plasmids to detach from the filament upon depolymerization. If plasmids have a reduced probability to detach from long filaments, a single plasmid is on average positioned at midcell (see

Fig. 1.1B). This model assumption is in accordance with experimental data showing that long ParA filaments pull plasmids over longer distances (also relative to their initial filament length). However, the biological justification of a length-dependent detachment rate of the plasmid remained unclear. Ringgaard et al. hypothesized that the detachment rate might be length-dependent because not a single filament, but filament bundles interact with the cargo and longer filament bundles might contain more protofilaments and hence lead to stronger interactions between the plasmid and the filament bundle.

How ParA filaments can pull a cargo that in turn triggers the depolymerization of the filaments is not intuitively clear. To investigate this question Banigan et al. simulated different modes for the ParA-ParB interaction [80]. They find that if the cargo (here a ParB complex) is allowed to bind to the ParA filament also away from the tip, but depolymerization of ParA occurs only at the tip, the most robust translocation of the cargo is obtained (compared to binding of the complex to the tip only or binding also away from the tip, but also disassembling the filament there). The disassembly of ParA at the filament's tip leads to a ParA gradient that moves together with the cargo such that the cargo keeps moving towards a higher ParA density (see Fig. 1.1A). This is reminiscent of a chemophoretic / diffusiophoretic force [80]. A similar mechanism was proposed for chromosome segregation in *C. crescentus* [81] based on experimental evidence in [67, 68].

In most of the filament-based models discussed here, the cargo follows a ParA filament (bundle) and there are no ParA filaments in the wake of the cargo [10, 80, 81]. Therefore, these systems can be considered as burnt-bridge Brownian ratchets. If the cargoes stay attached to the ParA filaments and the filaments retract, the cargo effectively cannot move back. Since there is evidence against filament formation of ParA in *in vivo* systems [6, 12, 14, 76, 96], also models that do not include polymerization of ParA have been suggested, which are discussed in the remaining part of this section.

1.3.3b Diffusion-ratchet model

Vecchiarelli et al. proposed a diffusion-ratchet mechanism to explain the ParA-mediated ParA movement [69, 76, 86, 97, 98]. This mechanism relies on the property of ParA to switch between an 'active' form, which can bind to the DNA non-specifically, and an 'inactive', cytosol form. Based on *in vitro* experiments they found that it takes a long time for ParA proteins that just detached from the nucleoid upon interacting with ParB proteins until they can rebind to the DNA [97]. This delay can be attributed to the fact that the released ParA-ADP monomers need to bind ATP, dimerize and gain the ability to bind DNA non-specifically before they can reattach to the nucleoid [97]. In the diffusion-ratchet mechanism, ParB bound to the cargo stimulates the ATPase activity of nucleoid-bound ParA, which leads to the release of 'inactive' ParA into the cytosol and a depletion of ParA in the vicinity of the cargo. The cargo then diffuses in the confined space between the nucleoid and the cell membrane until it binds to new ParA dimers on the nucleoid. Because of the depletion zone in its wake, once the cargo started to move in one direction, it continues to move in the same direction, due to

a chemophoresis force. To obtain directed and persistent movement of the cargo as observed for ParB-coated beads in DNA-carpeted flow cells [76], an elastic tethering of the cargo to the nucleoid via ParA dimers was proposed [78]. The tethering of ParB via ParA leads to persistent forward movement of the cargo by quenching orthogonal diffusion [78]. This model can explain diffusive, static and oscillatory cargo movements (from nucleoid pole to pole) as well as equidistant spacing of cargoes on a nucleoid that is modeled as a rectangular sheet [79].

In order for the diffusion-ratchet mechanism to lead to directional movement of the cargo, the following conditions need to be satisfied: (i) ParB bound to the cargo needs to interact weakly and transiently with the ParA proteins, (ii) the diffusion constant of the cargo must not be too large such that it keeps inside the depletion zone, (iii) there needs to be a time delay between the 'inactive' and 'active' form of ParA as otherwise ParA would rebind to close to the cargo and the depletion zone would refill [76]. Depletion zones in ParA are also observed in cell-free *in vitro* systems in agreement with the model [69]. Due to the depletion zone, the diffusion-ratchet mechanism can be regarded as another realization of a burnt-bridge Brownian ratchet.

1.3.3c Diffusion-immobilization mechanism

For the movement of a cargo into the direction of a higher ParA density, a diffusion-immobilization mechanism was proposed. The idea is that a cargo diffuses in the cytosol and is immobilized by binding to ParA dimers on the nucleoid. Due to the interaction of ParA with ParB on the cargo, the ATPase activity of ParA is stimulated, which leads to the release of the ParA dimers and the cargo into the cytosol. The cargo is then again free to diffuse and the cycle repeats. Since the cargo becomes immobilized more often in regions with a high ParA density and therefore stays longer in these regions, it is asserted that the cargo moves on average into the direction of a higher ParA density [3, 68]. The asymmetric ParA distribution is ensured by the release of ParA dimers bound to the cargo upon the stimulation of ATP hydrolysis by ParB.

Ietswaart et al. investigated such a diffusion-immobilization mechanism in a stochastic model: ParA dimers bind to the nucleoid, diffuse on the nucleoid and detach from the nucleoid upon interacting with the cargo, which in turn is immobilized if at least one nucleoid-bound ParA dimer is bound to it. They found that such a mechanism can produce equal plasmid spacing, however experimental observations speak against this mechanism: In order for the cargo to be immobilized by the ParA tethers, the cargo needs to diffuse more quickly than ParA dimers on the nucleoid [3]. This is in contrast to observations for plasmids in *E. coli*, which show very little mobility in the cytosol and an increased mobility if ParA is present in the cell [3]. A diffusion-immobilization mechanism was also investigated by Lim et al. [6]. In their model the ParA dimers, which form a gradient on the nucleoid, are immobile. Stochastic simulations of their model do not show a directional bias in the movement of the cargo [6].

In general, the cargoes (plasmids and partition complexes) are relatively large (about 100 nm in length [6]) and hence diffuse only slowly in the cytosol. Intermittent immobilization of the cargo would reduce their mobility even further, such that it seems

unlikely how a diffusion-immobilization mechanism can explain the experimentally observed cargo dynamics. The experiments rather suggest an active mechanism to move the cargoes [3, 6].

1.3.3d DNA-relay model

Based on the observation that the nucleoid has elastic properties [5, 6], Lim et al. proposed a DNA-relay model for chromosome segregation in *C. crescentus* [6]. The original models proposed for chromosome segregation in *Caulobacter* relied on filament formation of ParA [67, 80, 81]. However, Lim et al. made several experimental observations that speak against the filament forming property of ParA in this system: (i) there is no evidence for filament formation in *in vitro* experiments, (ii) the cargo shows movement along the short cell axis while it translocates along the long cell axis, (iii) the concentration of ParA in the cell seems to be too low for a filament of the size of the cell and (iv) super resolution experiments do not show ParA filaments, but rather a concentration gradient of ParA in the cell [6]. The gradient of nucleoid-bound ParA with the highest density at the future position of the cargo [99] can explain cargo movement from one end of the nucleoid to the other by a DNA-relay mechanism, as explained before (see section 1.3.2a). When the cargo reaches the cell pole, it is tethered to the pole by additional proteins [6].

The DNA-relay model without an externally imposed ParA gradient, but homogeneous attachment of ParA all over the nucleoid, results in pole-to-pole oscillations of one cargo and equidistant positioning of multiple cargoes over the nucleoid [100]. Here, the gradient of ParA dimers changes in a self-organized manner with the position of the cargo such that the cargo always follows the highest ParA density.

1.3.3e Flux-based positioning

To understand the localization of one cargo at midcell or equidistant positioning of multiple cargoes, Ietswaart et al. proposed a flux-balance argument (see Fig. 1.1B) [3]: If ParA dimers homogeneously attach to the nucleoid, diffuse on the nucleoid and are released into the cytosol locally at the cargo and the cargo moves only slowly, the fluxes of nucleoid-bound ParA into the cargo from either side differ if the cargo is positioned off-center. More ParA dimers reach the cargo from the site with the longer cargo to nucleoid end distance. Hence, if the cargo moves into the direction from which more ParA dimers are interacting with the cargo, it moves towards midcell. At midcell, the mechanism is self-correcting: If the cargo moves away from this position, the fluxes are such that it moves back towards midcell. Based on this flux-balance argument Ietswaart et al. proposed a model where competing ParA structures on the nucleoid guide the plasmids to equally distant positions as long as they move into the direction of a higher ParA concentration [3]. The same argument was used to explain the positioning of dynamic protein clusters on the nucleoid [16]. Prerequisites for the positioning of cargoes by a flux-based mechanism are: (i) the ATPase diffuses on the nucleoid, faster than the cargo [3, 16], (ii) it cycles between a nucleoid-bound and

cytosolic state, and (iii) the typical length the ATPase diffuses on the nucleoid before it spontaneously detaches (without interacting with the cargo) has to be large compared to the nucleoid length [16].

1.3.3f Phenomenological models

The ParA dynamics in the cell can be described in terms of reaction-diffusion equations [3, 74, 75, 85]. However, to describe the movement of fixed structures such as plasmids or the partition complex, an equation of motion for the cargo needs to be defined. Models that combine RD equations for the ParA dynamics with a phenomenological equation for the movement of the cargo can explain experimentally observed cargo dynamics for the *in vivo* [75] and the *in vitro* system [85]. Walter et al. considered a phenomenological model that leads to ParA-mediated transport of the cargo by proteophoresis [75]. Interestingly, they observe both oscillatory cargo movements and equidistant positioning of cargoes depending on the model parameters.

1.3.3g Summary and discussion

The variety of models proposed for ParA-mediated cargo movement might suggest different mechanisms for cargo translocation / positioning depending on the Par systems under consideration. However, there are still several model assumptions that are under debate (such as the filament forming property of ParA) and need to be tested further to verify or falsify the models. For sure, some differences in the cargo and ParA patterns observed in the bacterial cells are due to the biological details of the specific systems. In *Caulobacter* for example there is a polar protein that tethers the cargo to the cell pole once it arrived there [67, 68, 81]. The key differences between the models for Par systems presented here are:

1. ParA is either assumed to form filaments or not.

2. Apart from the Brownian motion of the cargo, the forces that lead to the directional movement of the cargo are assumed to either have a chemophoretic origin or are due to the elasticity of the nucleoid (see section 1.3.2a).

3. The velocity of the cargo is faster or slower than the ParA dynamics on the nucleoid.

4. The cargo refers to a plasmid, a partition complex or another macromolecular object.

These differences have important implications on the movement of the cargo: For example, how mobile nucleoid-bound ParA dimers are compared to the cargo affects the ParA distribution on the nucleoid and hence the cargo's movement. A faster dynamics of ParA reduces the depletion zone in the wake of the cargo (or even eliminates it) as the ParA density quickly replenishes while the cargo is slowly moving. A depletion zone in the wake of the cargo leads to contiguous forward-movement of the

cargo (e.g. by a diffusion-ratchet mechanism), whereas fast dynamics of PomZ on the nucleoid results in midcell positioning by a flux-balance argument. More generally, since the cargo is tethered to the nucleoid via the ParA dimers, its mobility also depends on the mobility of the ParA dimers bound to the cargo and the nucleoid. Furthermore, it makes a difference if the cargo is a macromolecular object (plasmid, carboxysome, chemotactic cluster, ...) tethered to the nucleoid or if the cargo refers to the partition complex, which is part of the bacterial chromosome itself. Since the partition complex is moved through the cell while DNA replication is ongoing, the movement of the partition complex is restricted by the speed of the replication machinery. In a model by Shtylla et al. [81] this backward pulling force is accounted for by a load acting on the partition complex.

To explain the directional movement of a cargo via nucleoid-bound ParA, mechanisms that resemble a burnt-bridge Brownian ratchet mechanism have been proposed (including the diffusion-ratchet and the DNA-relay model). Here, the depletion zone in ParA in the wake of the cargo is crucial for a continuous forward movement of the cargo. Only if the cargo encounters the nucleoid end or another cargo, the depletion zone replenishes and the cargo turns, which leads to oscillatory cluster movements. To explain midcell localization of one cargo, however, the cargo's average velocity needs to reflect its position on the nucleoid, i.e. the bias in the cargo's movement needs to vanish at midcell. One possible explanation for midcell sensing of the cargo is via a tug-of-war mechanism (see Fig. 1.1A). If ParA dimers do not only interact with the cargo from one side along the long cell axis, but from both sides and the forces exerted on the cargo reflect the length between the cargo and the nucleoid end (e.g. by a length-dependent detachment rate of the cargo from a ParA filament [10] or different fluxes of ParA on the nucleoid into the cluster [3]), midcell sensing is possible.

1.4 Midcell localization in *Myxococcus xanthus*

So far, I introduced two well-studied positioning systems in bacterial cells, the Min system for midcell localization in *E. coli* and the Par system for plasmid and chromosome segregation found in several bacteria. Now we focus on the positioning system, which will be in the focus of this work: the Pom system for midcell localization in *M. xanthus*. In the following, I shortly summarize the experimental findings of our collaboration partners, Dominik Schumacher and Lotte Søgaard-Andersen (Max Planck Institute for Terrestrial Microbiology, Marburg), which are published in [1, 2, 101]. On the basis of their findings, we developed a mathematical model for the positioning mechanism (see chapter 2).

1.4.1 PomX, PomY and PomZ proteins are important for midcell positioning

In *M. xanthus* cells three proteins are found to be important for cell division at midcell: PomX, PomY and PomZ. When one of the three proteins is deleted the cells divide
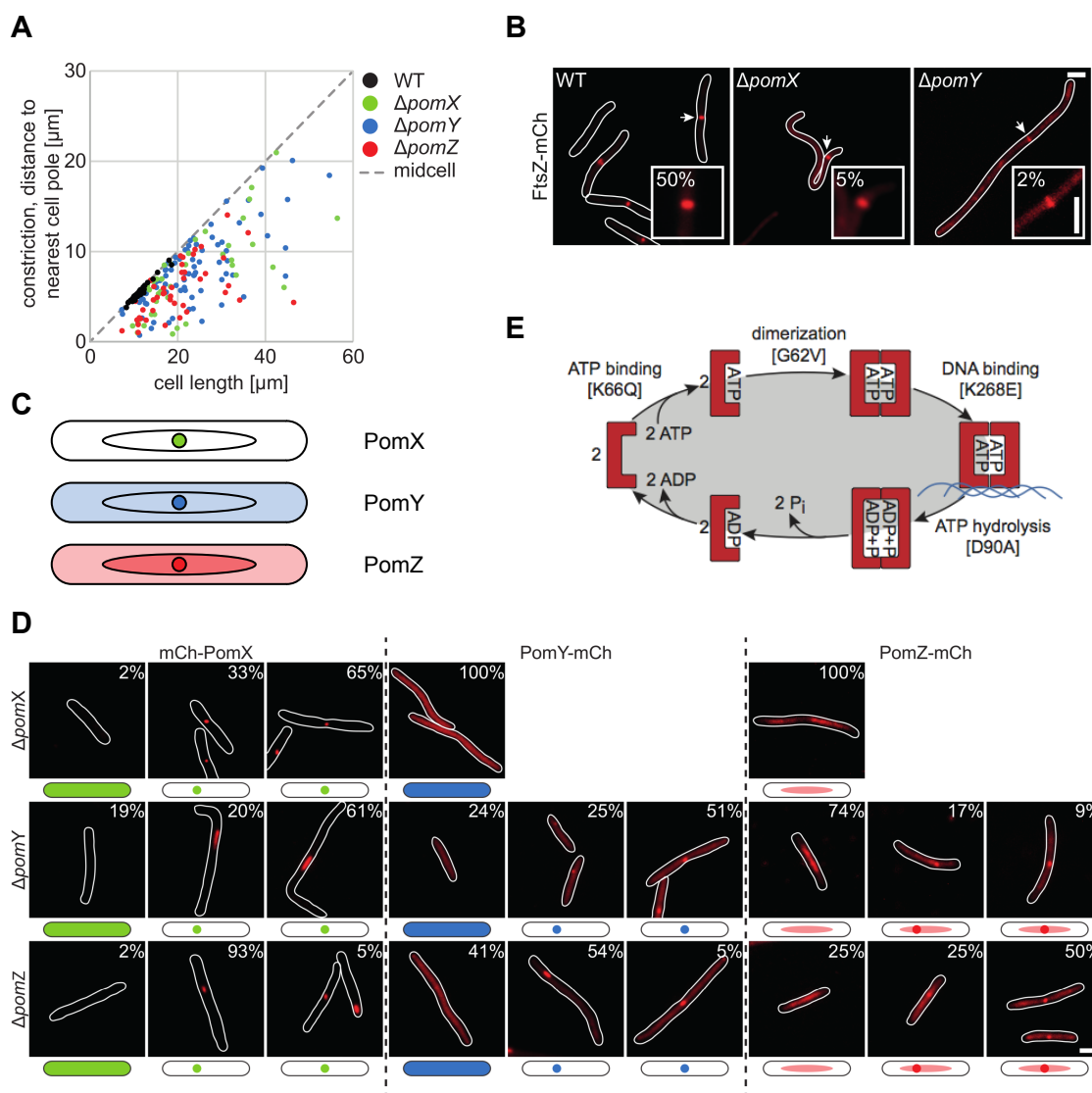
Figure 1.2 Pom proteins are important for division at midcell. (A) Position of the cell constriction site in dependence of cell length for wild type *M. xanthus* cells and single deletion mutants. Wild type cells divide at midcell and have a cell length of $(7.7 \pm 1.9)\,\mu$m, whereas deletion mutants show constrictions over the entire cell length and hence deviate remarkably in cell length. (B) In wild type cells, 50% of the cells show a Z-ring, which is located at midcell (defined as $50\% \pm 5\%$ of cell length). In contrast, cells that lack PomX or PomY form Z-rings less frequently (5% and 2%) and over the entire cell length. (C) Sketch of the typical localization patterns of PomX, PomY and PomZ inside the cell (based on experimental data shown in D). The ellipsoidal region inside the cell indicates the nucleoid. (D) Localization of fluorescently tagged Pom proteins in the absence of PomX, PomY or PomZ. (E) Illustration of typical ParA ATPase cycle with names of mutants in PomZ for which one step of the cycle is inhibited. Subfigures (A, B, D, E) are taken from [2].

somewhere along the cell length, but not robustly at midcell as observed for the wild type cells (Fig. 1.2A). In these single deletion mutants, the Z-ring, which assembles at the future constriction site, forms in less cells compared to wild type and the position of the Z-ring is not restricted to midcell (Fig. 1.2B). We conclude that all three proteins are important for the regulation of cell division at midcell. They function together to stimulate the Z-ring formation at midcell, which also explains their name: Pom stands for *positioning at midcell for FtsZ*.

To investigate the role of each Pom protein in this process, experiments with fluorescently tagged PomX, PomY or PomZ proteins in single deletion mutants ($\Delta pomX$, $\Delta pomY$, $\Delta pomZ$) were performed (Fig. 1.2D). A fluorescently tagged version of PomX, PomY and PomZ can be expressed in each single deletion mutant, resulting in nine different experiments. From the experiments that investigate the localization of a fluorescent fusion protein in a mutant that has a deletion of the respective protein as it occurs natively (e.g. mCh-PomX in $\Delta pomX$ mutants), the typical location of the Pom proteins inside the cell can be inferred (Fig. 1.2D, data shown on diagonal). The majority of cells contain a single cluster and, if existent, all three Pom proteins colocalize in this cluster, which we refer to as *Pom cluster*. Interestingly, experiments show that the cluster is located over the nucleoid, either at an off-center position or around the midpoint of the nucleoid along the long cell axis (in the following called *midnucleoid*), which coincides with midcell. Besides accumulation in the cluster, the localization patterns of the three Pom proteins inside the cell vary (Fig. 1.2CD): For mCh-PomX, a high fraction of the protein is associated with the cluster. PomY-mCh proteins outside the cluster show a diffuse pattern inside the cell. A large fraction of PomZ-mCh colocalizes with the nucleoid (about 90%), resulting in a high density at the cluster and also a patchy signal over the nucleoid. This indicates that PomZ binds non-specifically to the nucleoid.

Apart from this, it is insightful to consider the localization of the proteins in the absence of one of the other Pom proteins, e.g. mCh-PomX in $\Delta pomY$ mutants (Fig. 1.2, data shown on off-diagonal). Interestingly, PomX proteins still form a cluster if PomY or PomZ proteins are absent, though in $\Delta pomY$ mutants the cluster is longer than in the presence of PomY proteins. If PomX is absent, neither PomY nor PomZ show an accumulation in a cluster. Hence, we conclude that PomX nucleates the formation of a cluster in which all three proteins colocalize. PomY proteins also seem to be involved in cluster formation, but rather in making it round shaped instead of forming a cluster at all. *In vitro* experiments show that PomX can form filaments and these filaments are bundled to larger structures if PomY is added. This might explain the different shape of the cluster if PomY is absent observed *in vivo*. In mutants that lack PomZ, mCh-PomX and PomY-mCh still form a cluster, however, the cluster is rarely at midcell. In fact, a more detailed analysis of the localization of the cluster shows that it also localizes in the subpolar DNA-free regions of the cell. In contrast, if PomZ is present, the clusters are positioned over the nucleoid. These observations suggest that PomZ is important for the localization of the cluster at midcell and PomZ associates the cluster to the nucleoid.

Since PomZ seems to play a crucial role in positioning the cluster at midcell, it is important to understand its dynamics and how it interacts with the other components (Pom proteins, DNA) involved. PomZ is a ParA-like ATPase and its ATPase activity is stimulated synergistically by PomX, PomY and DNA. If PomZ is only in contact with non-specific DNA, it has an ATP turnover rate of (1.7 ± 1.2) ATP/h, whereas this turnover increases to (34.0 ± 1.3) ATP/h if PomX and PomY proteins are present. PomZ variants (one specific amino acid substituted by another) can be used to infer in which state PomZ binds to the DNA and interacts with the PomX and PomY proteins. Fluorescence images of cells with these variants indicate that PomZ binds only in the ATP-bound dimeric form to the nucleoid and recruits the PomXY cluster only in this state to the nucleoid (see Fig. 1.2E).

So far, we observed that PomX and PomY proteins form a cluster and PomZ is necessary for positioning this cluster at midcell, but how does the Pom cluster influence the Z-ring formation at midcell, which then constricts the cell? To investigate this question, experiments with both PomX or PomY proteins and FtsZ fluorescently labelled were performed. They show that the PomX and PomY proteins localize to midcell before FtsZ. Further experiments show that the Pom proteins also localize to midcell in the absence of FtsZ, indicating that the Pom cluster is positioned at midcell first and then recruits the Z-ring to this position. Furthermore, there is experimental evidence that PomY and PomZ interact with FtsZ and PomY in the Pom cluster is important for the recruitment of the Z-ring to the division site. However, the details of the recruitment process are not known and need to be investigated further.

1.4.2 Pom cluster dynamics

The experimental results discussed so far indicate that three proteins (PomX, PomY, PomZ) are important for the localization of the cell division site at midcell and they have different roles in this positioning process. As a next step, we consider the dynamics of the Pom cluster. Time-lapse experiments show that the Pom cluster moves from an off-center position (close to the cell pole) towards midcell in about 80 min (Fig. 1.3A), which is about 1/4 of the generation time of the cells. When considering the cluster dynamics with a higher temporal resolution (Fig. 1.3B), the stochasticity of the cluster movement becomes more evident. It seems that the cluster is performing a random walk on the nucleoid with a bias towards midcell. At midcell, the cluster fluctuates around this position, but overall its movement is confined to a region around midcell. Interestingly, if PomZ is absent in the cell, the cluster is not only stalled at its initial position, it also moves less in general (Fig. 1.3BC). From these observations we conclude that the PomZ dimers are important for the movement of the cluster and its positioning at midcell, in agreement with the findings from the deletion mutants in PomZ.

To quantify the observed cluster dynamics, the mean squared displacement (MSD) of the cluster trajectories was calculated. The MSD of off-center clusters increases over time and the data suggests that this increase is more than linearly (Fig. 1.3C). Thus, the movement of these clusters is not purely diffusive, but also has a directed component. For clusters at midcell the situation is different: Here, the MSD first
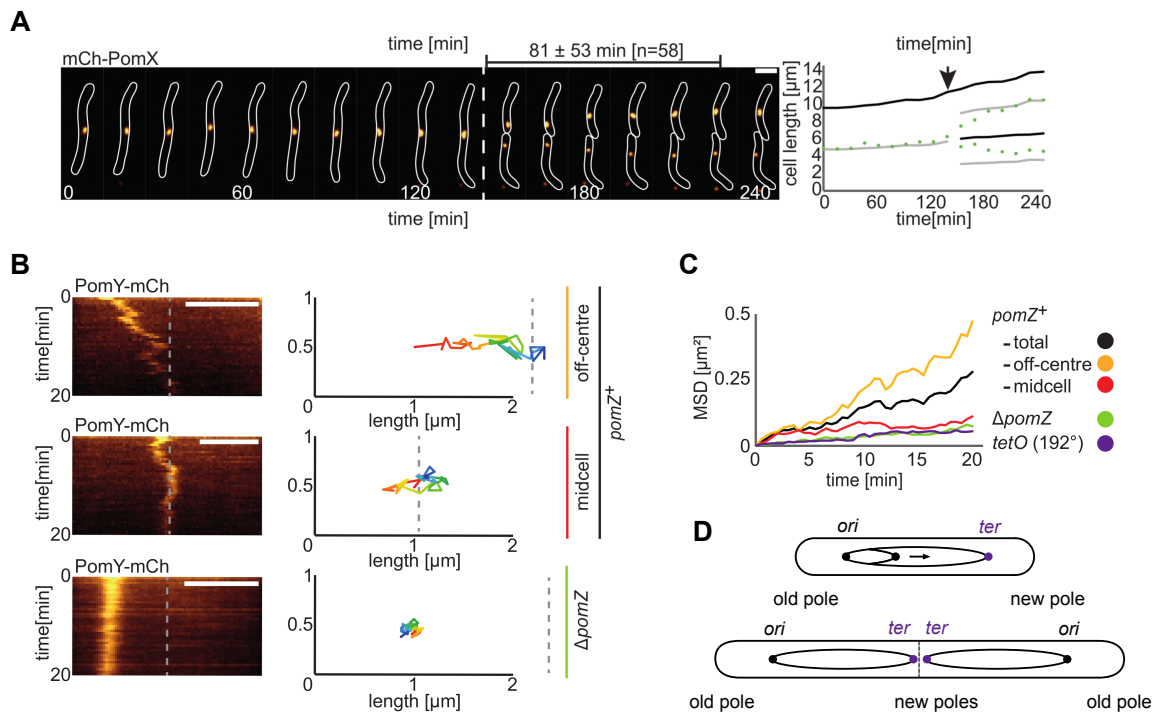
Figure 1.3 Dynamics of the Pom cluster. (A) Time-lapse images of a *M. xanthus* cell with PomX labelled. PomX proteins accumulate in a cluster and this cluster moves from a position close to the cell poles to midcell in about 80 min. (B) Time-lapse images with a higher temporal resolution (PomY is labelled) for clusters starting off-center or at midcell and cells that lack PomZ proteins. If PomZ is absent, the cluster is stalled at its initial position, showing that PomZ is important for the positioning of the Pom cluster. (C) Mean square displacement curves of the cluster over time for cells with and without PomZ. A locus on the genome (*tetO*) shows only little motion, indicating that the cluster is not "piggybacked" on the terminus region of the chromosome. (D) Sketch of chromosome segregation in *M. xanthus*. DNA replication starts at the origin (*ori*) close to one of the cell poles. During chromosome segregation the duplicated origin moves across the cell until the chromosome is fully replicated. The cell then divides such that the terminus regions of the chromosome (*ter*) are close to the new cell poles. Subfigures (A-C) are taken from [2].

increases and then seems to reach a plateau. This is in accordance with the constrained movement of the clusters at midcell observed in the time-lapse experiments. In Δ*pomZ* mutants we do not distinguish between off-center and midcell clusters as no bias in the cluster's movement is observed independent of the position of the cluster in the cell. These clusters show a small MSD, in agreement with the observation that PomZ is important for the clusters mobility.

In order to explain the cluster's movement from an off-center position to midcell, one could argue as follows: In *M. xanthus* the bacterial chromosome is oriented inside the cell such that the origin of replication, *ori* region (DNA sequence that signals

the start of replication) is close to the old pole and the terminus region, *ter* (stop sequence) is at the opposite site [102]. When the bacterial chromosome is segregated, the terminus moves from a position close to the cell pole to midcell [103] (see sketch, Fig. 1.3D). As this dynamics resembles the observed dynamics of the Pom cluster, one might hypothesize that the Pom cluster is just "piggybacked" on the terminus site of the chromosome. However, the terminus is a lot less mobile than Pom clusters starting from an off-center position (Fig. 1.3C), which speaks against such a mechanism. Other facts disfavoring this mechanism are that PomZ dimers bind, in their ATP-bound dimeric state, non-specifically to the nucleoid and the Pom cluster localizes at midcell when DNA replication is still ongoing.
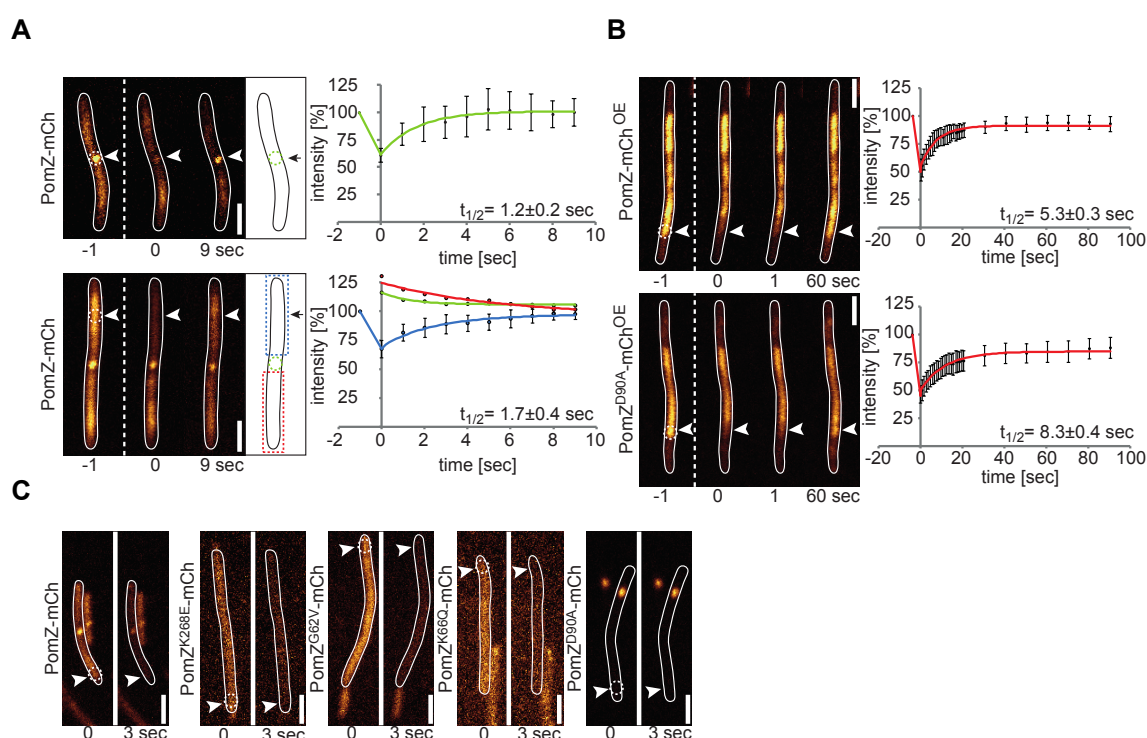
Figure 1.4 PomZ is highly dynamic. (A) FRAP experiments of PomZ-mCh with a bleach spot over the cluster and over the nucleoid. On the right side, the fluorescence recovery curves of the regions indicated in the sketch of the cell are shown. (B) FRAP data for PomZ-mCh and PomZ^{D90A}-mCh overexpressed more than 50-fold. (C) Fluorescence signal of PomZ-mCh, the variants that cannot bind DNA (PomZ^{K268E}-mCh, PomZ^{G62V}-mCh, PomZ^{K66Q}-mCh) and the ATP hydrolysis mutant (PomZ^{D90A}-mCh) before and after bleaching for 3 s. The figure is taken from [2].

If the cluster is not "piggybacked" on a specific chromosome site, how do PomZ dimers lead to the movement of the cluster? To shed light on this question, the dynamics of the PomZ dimers was investigated. So far, we know that PomZ binds in its ATP bound dimeric state to the nucleoid and interacts with the PomXY cluster. A

common method to study the dynamics of proteins inside cells is FRAP, *fluorescence recovery after photobleaching.* Here, the fluorescence fusion protein (PomZ-mCh) is bleached with a laser in a small spot inside the cell and the recovery of the fluorescence signal at this spot is recorded. Such experiments are typically used to measure the diffusion constants of proteins and other rate constants (see section 2.2).

If PomZ is bleached over the cluster, the fluorescence intensity recovers quickly (half recovery time: $t_{1/2} = (1.2 \pm 0.2)\,\mathrm{s}$) (Fig. 1.4A). This indicates that there is a fast turnover of PomZ dimers at the cluster. Already during bleaching with a laser pulse of 60 ms duration, the fluorescence signal of PomZ over the nucleoid outside of the bleaching spot is reduced (Fig. 1.4A), which shows that PomZ dimers are highly dynamic on the nucleoid. Fast dynamics of PomZ is also observed when PomZ-mCh is bleached over the chromosome instead of the cluster. After the 60 ms laser pulse, the fluorescence intensity on the chromosome of the site of the cluster where the bleach spot was located is drastically reduced (Fig. 1.4A).

To analyze diffusion of PomZ dimers on the nucleoid FRAP experiments of cells with PomZ-mCh and PomZ^{D90A}-mCh (mutant that does not hydrolyze ATP) overexpressed more than 50-fold were performed (Fig. 1.4B). First, we observe that the fluorescence intensity is high over the region where we expect the nucleoid and no cluster is visible although PomX and PomY proteins are present. Hence, we conclude that the capacity of PomZ dimers that can interact with the cluster at the same time is exceeded in these cells with PomZ overexpressed. Furthermore, if PomZ-mCh or PomZ^{D90A}-mCh is bleached (bleach spot over the nucleoid), the intensity recovers quickly, but more slowly compared to cells with less PomZ dimers in the cell. This can be attributed to the fact that PomZ dimers hinder each other in their movement because of crowding effects. PomZ^{D90A} binds in its ATP-bound dimeric state to the nucleoid, but cannot hydrolyze ATP. Experiments show that these proteins primarily localize over the nucleoid, indicating that detachment from the nucleoid is ATP hydrolysis dependent. Since the ATPase activity of PomZ is stimulated by PomX, PomY and DNA, release of nucleoid-bound PomZ dimers mainly occurs at the Pom cluster for PomZ-mCh and no significant detachment from the nucleoid is expected for PomZ^{D90A}-mCh. Hence, the recovery of PomZ^{D90A}-mCh is mainly due to diffusion of PomZ proteins on the nucleoid instead of an exchange with the cytosol. In the case of PomZ-mCh, the fluorescence recovery is due to both diffusion on the nucleoid and exchange via the cytosol, thus explaining the slightly shorter recovery time. However, the recovery times for PomZ-mCh or PomZ^{D90A}-mCh overexpressed are very close, which suggests that the main factor that leads to the fluorescence recovery is fast diffusion of PomZ on the nucleoid in both cases.

If the dynamics of a protein is very fast, it is difficult to perform FRAP experiments, as a large fraction of the signal around the bleaching spot is gone after the laser pulse was applied (as observed for the PomZ dimers, see Fig. 1.4A). Hence, our collaboration partners performed the following bleaching experiments: They bleach at a spot over the nucleoid for 3 s and image the intensity distribution inside the cell before and after bleaching (Fig. 1.4C). For three variants of PomZ that cannot bind to the nucleoid (PomZ^{K268E}-mCh, PomZ^{G62V}-mCh and PomZ^{K66Q}-mCh) the intensity is drastically

reduced after 3 s showing that their dynamics in the cell is fast. Since they cannot bind to the nucleoid, they most likely diffuse in the cytosol, which is typically a fast process (the diffusion constant for Min proteins in the cytosol is on the order of $10\,\mu m^2/s$, [104]). Another interesting observation is that in cells with PomZ^{D90A}-mCh (not overexpressed) the proteins accumulate in a cluster and bleaching outside of the cluster does not change the intensity of the cluster significantly, whereas for PomZ-mCh the intensity is reduced a lot. This suggests that ATP hydrolysis is essential for the fast turnover of PomZ at the cluster and binding of nucleoid-bound PomZ dimers to the cluster occurs more frequently than detachment of PomZ dimers from the cluster such that they stay bound to the nucleoid, if this process occurs at all.

1.5 Comparison of Pom, Min and Par system

The Pom system in *M. xanthus*, the Min system in *E. coli* and the Par systems for plasmid and chromosome segregation have in common that they are all positioning systems that include an ATPase (PomZ, MinD and ParA), whose ATPase activity is stimulated by at least one partner protein, the ATPase activating protein (AAP). Depending on the nucleotide state, the ATPase's affinity to bind to the nucleoid (in the case of PomZ, ParA) or membrane (in the case of MinD) is increased. Hence, in all three systems the ATPase cycles between a cytosolic and a bound state. Another common feature is the temporal delay between detachment of the ATPase from the respective scaffold (nucleoid or membrane) upon interaction with the AAP, and rebinding to it, which leads to a spatial redistribution of the protein in the system by cytosolic diffusion. However, these systems also differ in several aspects, which are discussed in the following (see Table 1.1).

Both the Pom and the Min system are important for midcell localization of the Z-ring and hence for the correct placement of the cell division site. Although they have the same biological function, there are several differences between the two systems: First, how they ensure that the Z-ring is robustly formed at midcell, differs. In *E. coli* cells, MinC inhibits the Z-ring formation away from midcell ("negative regulation"), whereas the Pom cluster promotes the assembly of FtsZ into a ring at midcell ("positive regulation") in *M. xanthus* cells [1].

Second, the scaffolds the ATPases bind to differ: MinD binds in its ATP-bound dimeric form to the membrane and ATP-bound PomZ dimers attach to the nucleoid. In contrast to the rather smooth surface of the membrane, the nucleoid is a very complex structure that is continuously remodeled during the cell cycle [89]. Since *E. coli* cells are rod-shaped, the curvature of the membrane at the pole is distinct from the membrane's curvature at midcell. Hence, also the ratio of the bulk volume to the membrane area differs at midcell compared to the cell poles, which is key for the resulting Min protein patterns on the membrane [48, 56]. If we consider the nucleoid, in a simplified manner, as an ellipsoid inside the cell, the geometry of the reactive surface for PomZ can be regarded as inverted compared to the cell membrane, to which the Min proteins bind.

	Pom system	Min system	Par systems
ATPase	PomZ	MinD	ParA
AAP	PomX, PomY	MinE	ParB
ATPase binds to ...	nucleoid	cell membrane	nucleoid
Biological function	midcell positioning of cell division site (positive regulation)	midcell positioning of cell division site (negative regulation)	chromosome / plasmid segregation
Cargo(es) of fixed structure	yes (PomXY cluster)	no	yes (plasmids / partition complex)
Typically observed patterns	midcell localization of Pom cluster	pole-to-pole oscillations of Min proteins	one cargo: midcell localization / oscillations / movement from one pole to the other; multiple cargoes: equidistant positioning; . . .

Table 1.1 Comparison between the Pom system in *M. xanthus*, the Min system in *E. coli* and the Par systems for chromosome and plasmid segregation.

For the cell membrane, the bulk-to-boundary ratio is low at the cell poles, whereas, for the nucleoid, the bulk-to-boundary ratio is high at its poles.

Finally, the key difference between the Min and the Pom system that also necessitate different theoretical approaches, is the following: In contrast to the Min proteins, PomX and PomY form a cluster inside the cell and experiments suggest that this cluster can be regarded as a fixed structure (PomX forms filaments *in vitro* and a high fraction of PomX accumulates in the cluster [2]). The cluster is likely to be actively translocated towards midcell via its interactions with PomZ dimers [2]. In contrast, the Min proteins form dynamic patterns on the membrane, which can be described in terms of mass-conserving reaction-diffusion equations [54]. Here, patterns emerge in a self-organized manner due to the cycling of MinD between the membrane and the cytosol, where MinD quickly diffuses, and the nonlinearities in the equations (recruitment of MinD and MinE by membrane-bound MinD) [48, 52–54]. Whether or not PomZ proteins recruit further PomZ to the nucleoid is not known and needs to be investigated further.

In summary, the Min and the Pom system both regulate the Z-ring formation at midcell, but in very different ways. Par systems for plasmid and chromosome segregation do not regulate the positioning of the cell division site, but instead ensure that the genomic information (on the plasmids or on the chromosome) is equally distributed to the two daughter cells. Like PomZ, the ATPase ParA also binds in its ATP-bound dimeric state to the nucleoid and is crucial for the movement of a cargo

(plasmids or partition complex). Hence, from a mechanistic point of view the Pom system is closer to Par systems for plasmid and chromosome segregation than to the Min system in *E. coli*.

For a more detailed comparison between the Pom and Par systems it is not feasible to compare the Pom system to all Par systems at once since there are various ParAB*S* systems in several bacterial species, which differ in the details. Here we highlight key experimental observations for the Pom system and compare these to Par systems for plasmid and chromosome segregation.

One important observation is that the density of PomZ in direct association with the PomXY cluster is high as observed from the fluorescence micrographs [2]. This is in contrast to a low density of ParA at a ParB-coated bead in an *in vitro* Par system [76] and at plasmids as observed *in vivo* [10]. However, there are also Par systems that show an accumulation of ParA at the cargo [60, 99]. Another observation made for some Par systems is that there is a depletion zone in the wake of the cargo's movement. In *M. xanthus* the nucleoid region in close proximity of the Pom cluster is depleted in PomZ dimers, however we do not observe a clear depletion zone in the trail of the cluster when it moves to midcell [2].

Moreover, PomZ dimers diffuse quickly on the nucleoid [2], whereas the PomXY cluster does hardly not move if PomZ is not present in the cell. This is in contrast to experimental observations for Par systems that show a fast diffusing cargo and slowly diffusing ParA dimers [6, 79, 100]. The low mobility of the PomXY cluster might be due to its relatively large size (diameter of $0.7\,\mu m$ along the long cell axis), compared to the size of plasmids/partition complexes of about $0.1\,\mu m$. For plasmids and partition complexes Le Gall et al. showed that they are moved through the interior of the nucleoid while being segregated [12]. However, due to the large size of the PomXY cluster, we expect that the cluster does not penetrate into the nucleoid volume.

Finally, the Pom cluster typically moves from a position close to the nucleoid pole to midnucleoid (Fig 1.3), when the cell divides, it splits into two and the same dynamics repeats. Though positioning at midcell is also observed for plasmids by the Par system, Par systems show also various other patterns as mentioned before, including oscillations of ParA and the cargo and movement from one nucleoid end to the other.

Chapter 2

Stochastic model for midcell positioning in *M. xanthus*

2.1 Introduction of the model

To investigate the experimentally observed dynamics of the Pom cluster in *M. xanthus* theoretically and thereby gain a better mechanistic understanding of the positioning process, we searched for a computational description of the system. In this chapter we give an overview of the models we consider in chapter 3 to 5 to investigate the Pom cluster dynamics. We give details on the model and estimates for the model parameters based on the experimental findings. Further information on the models and the exact parameter values used in the simulations can be found in the corresponding chapters.

Due to the similarities between the Pom system and the Par systems for chromosome and plasmid segregation (see section 1.5), we thought about whether an existing model for the Par system might also explain the observed Pom cluster dynamic. However, there is no experimental evidence that PomZ forms filaments [1] and therefore we did not consider filament-based models. Also, several experimental observations in *M. xanthus* cells [2] speak against a diffusion-ratchet or diffusion-immobilization mechanism (as discussed in section 1.3.2): (i) time-lapse experiments show that the Pom cluster is more mobile if PomZ is present than without PomZ, (ii) FRAP / bleaching experiments indicate that the PomZ dynamics is fast (in the cytosol and on the nucleoid), and (iii) no clear depletion zone in PomZ in the wake of the cluster is visible. Finally, in the DNA-relay mechanism the nucleoid-bound ParA dimers wiggle around their equilibrium position, but cannot diffuse on the nucleoid, which is in contrast to the experimentally observed fast dynamics of PomZ on the nucleoid. Hence, the previously proposed models for Par systems do not capture all experimental observations for the Pom system in *M. xanthus*. Therefore, we developed, together with our experimental collaboration partners, Dominik Schumacher and Lotte Søgaard-Andersen, a mathematical model for the Pom system that accounts for the key experimental observations.

Based on the observation that PomX and PomY form a cluster and PomZ is important for the movement and positioning of the cluster, we abstracted the biological system to three model components: the nucleoid, the cluster of PomX and PomY proteins (PomXY cluster), and the PomZ dimers. We assume that the PomXY cluster is an object of fixed structure, as PomX forms structures *in vitro* and a high fraction of PomX accumulates in the Pom cluster *in vivo* (see Fig. 1.3A). Since the Pom cluster is

typically inherited from one cell to the next (the cluster is splitted into two when the cell divides), we do not include *de novo* formation of the PomXY cluster in our model.

We considered two different geometries for the nucleoid and the PomXY cluster (Fig. 2.1A). Either we modeled the nucleoid and the cluster in a simplified manner as one-dimensional objects, or we modeled the nucleoid as a cylinder and the cluster as a two-dimensional sheet. In the later case, we assume that the cluster cannot penetrate into the nucleoid volume, based on the experimental observation that the PomXY cluster is large.

These two model geometries both have their advantages: A one-dimensional geometry is suitable to calculate analytical solutions for the observables of interest, which might result in further insights into the mechanistic details of the positioning process. On the other hand, the three-dimensional geometry resembles the biological cell more closely. Hence, it is suitable for a quantitative description of the system. Furthermore, it captures effects that are not included in the 1D model. One such effect is that Pom dimers can diffuse past the cluster as long as the cluster's width does not cover the entire nucleoid circumference. Here, we refer to PomZ dimers that diffuse on the nucleoid from one side of the cluster (along the long cell axis) to the other without entering the region that is covered by the cluster. PomZ can in principle also pass the cluster by diffusing through the nucleoid region where the cluster is located without binding to the cluster. This event is also possible in the 1D model. However, since we typically assume a high attachment rate, the probability for this event becomes very small. FRAP experiments show that diffusion of PomZ past the cluster occurs also in the *in vivo* system. If PomZ is bleached over the nucleoid its intensity is reduced also on the nucleoid on the other side of the cluster (Fig. 1.4A). Although the intensity is reduced, the experiments show that PomZ is hindered in diffusing on the nucleoid from one side of the cluster to the other side (Fig. 1.4A).

Fluorescence micrographs show a biased, though very stochastic movement of the Pom cluster (Fig. 1.3B). This stochasticity can be explained by thermal fluctuations and the relatively small number of PomZ proteins in the cell. A Western blot analysis reveals that the number of PomZ molecules in the cell is about 200 [2]. To account for the stochasticity of the Pom cluster and PomZ dimer dynamics in our model, we chose a stochastic lattice gas model. Based on the experimentally suggested ATPase cycle of PomZ and its interactions with DNA and the other Pom proteins, we model the PomZ dynamics as follows (see Fig. 2.1B). PomZ dimers can attach to the nucleoid with rate k_{on}, on which they diffuse with diffusion constant D_{nuc}. In the case of the three-dimensional geometry we assume that the PomZ dimers do not penetrate into the nucleoid volume, but instead bind to and diffuse on the surface of the nucleoid. Similar to the DNA-relay model [6], we incorporate the elasticity of the nucleoid [5] and the PomZ proteins in our model by describing the PomZ dimers as effective springs. Proteins have been modeled as springs or network of springs [105–107]. The values for the spring stiffnesses reported in these models vary significantly, but are typically very large — on the order of 10^7–10^9 $k_B T/\mu m^2$ (or 10–10^3 pN/nm) [106, 107]. In contrast, the elasticity of the nucleoid was measured to be much softer, 100 $k_B T/\mu m^2$ (or about
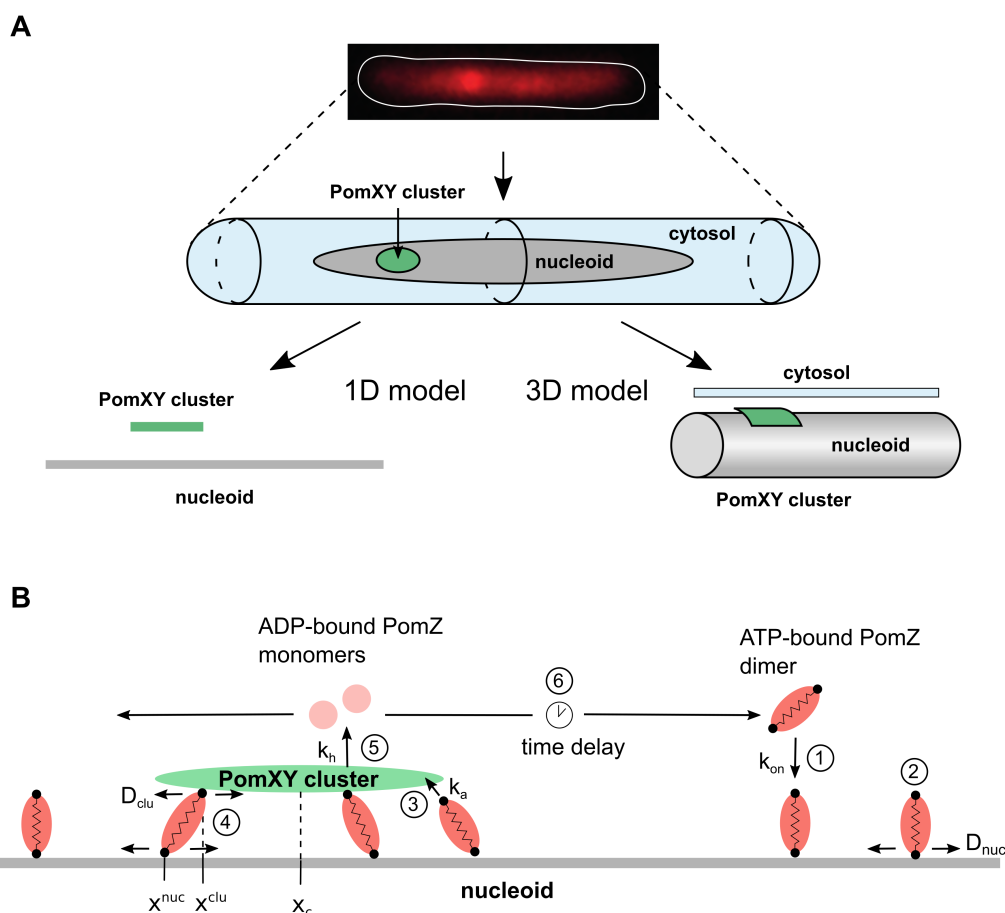
Figure 2.1 Models for Pom cluster dynamics. (A) Sketch of a *M. xanthus* cell based on experimental data (a microscopy image with PomZ fluorescently tagged is shown, modified from [2]). The nucleoid is depicted in grey and the PomXY cluster in green. We considered two different model geometries, which reduce the complexity of the biological system: In the one-dimensional (1D) model, the nucleoid and cluster are one-dimensional lattices. In contrast, in the three-dimensional (3D) model the nucleoid is incorporated as a cylinder and the cluster as a rectangular sheet. (B) Stochastic dynamics of the PomZ dimers considered in both the 1D and 3D model: PomZ dimers can attach to the nucleoid in the ATP-bound dimeric state (1) and diffuse on the nucleoid (2). At the nucleoid ends we assume reflecting boundary conditions for the PomZ movement. PomZ dimers are modeled as springs to account for the elasticity of the nucleoid and the protein itself. A nucleoid-bound PomZ dimer can bind to the Pom cluster, also in a stretched configuration (3). We assume that cluster- and nucleoid-bound PomZ dimers can diffuse on both the cluster and the nucleoid (4). Cluster-bound PomZ dimers are released into the cytosol as two ADP-bound monomers upon ATP hydrolysis (5). The ADP-bound monomers first need to exchange ADP for ATP and dimerize before they can rebind to the nucleoid, which leads to a time delay (6). Subfigure B is a modified version of Fig. 4.1.

10^{-3} pN/nm) [6]. Hence, we expect that the nucleoid's elasticity mainly determines the elasticity of the link between the nucleoid and the PomXY cluster via the PomZ dimer.

A nucleoid-bound PomZ dimer can bind, with a second binding site, to the PomXY cluster. We assume that the binding rate, k_a, depends on the degree of stretching of the spring (similar to [105]):

$$k_a = k_a^0 \exp\left(-\frac{k}{2k_BT}(x^{\mathrm{clu}} - x^{\mathrm{nuc}})^2\right), \tag{2.1}$$

with x^{clu} and x^{nuc} the cluster and nucleoid binding site of the PomZ dimer (Fig. 4.1B). Alternatively, we could consider the PomZ dimer as two beads (one denotes the cluster and the other the nucleoid binding site) connected by a spring and explicitly model also diffusion of the cluster binding site. For a fixed position of the nucleoid binding site, the dynamics of the cluster binding site can be described by an Ornstein-Uhlenbeck process, i.e. a Brownian particle in a potential. For this process the stationary probability distribution is given by

$$p_s(x^{\mathrm{clu}}) = \frac{1}{\sqrt{2\pi k_BT/k}} \exp\left(-\frac{k}{2k_BT}(x^{\mathrm{clu}} - x^{\mathrm{nuc}})^2\right), \tag{2.2}$$

which is the same distribution as above (Eq. 2.1).

The details of the interaction of PomZ dimers with the PomXY cluster in the *in vivo* system are not known yet. In our model we assume that cluster-bound PomZ dimers can diffuse on both the nucleoid and the cluster with diffusion constants D_{nuc} and D_{clu}, respectively. This assumption is motivated by the following two experimental observations: First, in experiments with PomZ mutants that cannot bind to DNA, the proteins do not accumulate in a cluster although PomX and PomY is present [2], indicating that PomZ dimers only bind to the PomXY cluster when they are nucleoid-bound. Second, in fluorescence images the density of PomZ at the Pom cluster is high over the entire cluster. If PomZ dimers attach quickly to the cluster and cannot move further upon binding, the PomZ density distribution should be strongly peaked at the cluster's edges. However, since we do not see such a distribution in the experiments, the observations suggest that nucleoid-bound PomZ dimers are mobile also when bound to both the nucleoid and the cluster.

We implemented diffusive motion of PomZ as a hopping process on a lattice (lattice spacing a). The hopping rates on the nucleoid and the PomXY cluster are then given by $k_{\mathrm{hop}}^0 = D_{\mathrm{nuc}}/a^2$ and $k_{\mathrm{hop}}^0 = D_{\mathrm{clu}}/a^2$, respectively. PomZ dimers bound to both, the cluster and the nucleoid, can hop on both scaffolds with the rate (as in [105])

$$k_{\mathrm{hop}} = k_{\mathrm{hop}}^0 \exp\left[-\frac{1}{4}\frac{k}{k_BT}\left((x_i^{\mathrm{clu,\,to}} - x_i^{\mathrm{nuc,\,to}})^2 - (x_i^{\mathrm{clu,from}} - x_i^{\mathrm{nuc,\,from}})^2\right)\right], \tag{2.3}$$

with $x_i^{\mathrm{clu,\,from}}$, $x_i^{\mathrm{nuc,\,from}}$ and $x_i^{\mathrm{clu,\,to}}$, $x_i^{\mathrm{nuc,\,to}}$ denoting the positions of the binding sites of the i-th PomZ dimer to the cluster and nucleoid before and after hopping, respectively.

For these hopping events we assume that detailed balance holds (as in [105]). Let us consider a single hopping event of a PomZ dimer bound to both the nucleoid and the cluster. From this state (state 1), either the nucleoid or the cluster binding site can hop to a neighboring lattice site (state 2). Then, detailed balance implies

$$p_1 k_{12} = p_2 k_{21},$$

and hence $p_1/p_2 = k_{21}/k_{12}$. The rates k_{12} and k_{21} denote the rates from state 1 to 2 and vice versa. If both states are distributed according to a Boltzmann distribution

$$p_1 = \frac{1}{\mathcal{Z}} e^{-\frac{E_1}{k_B T}}, \quad p_2 = \frac{1}{\mathcal{Z}} e^{-\frac{E_2}{k_B T}},$$

we obtain

$$\frac{k_{21}}{k_{12}} = \frac{p_1}{p_2} = \exp\left[-\frac{E_1 - E_2}{k_B T}\right] = \exp\left[-\frac{k}{2 k_B T}\left((x^{\text{clu}, 1} - x^{\text{nuc}, 1})^2 - (x^{\text{clu}, 2} - x^{\text{nuc}, 2})^2\right)\right].$$

In the last step we inserted the energies of the springs. Hence, in order for detailed balance to hold only the ratio of the rates is determined. We fixed this degree of freedom by choosing the rates such that k_{12} is the inverse of k_{21}, which leads to the factor of $1/4$ in the exponent in Eq. 2.3 (see also [105]).

Experiments with the ATP hydrolysis mutant of PomZ suggest that detachment of PomZ from the nucleoid depends on ATP hydrolysis. In these cells, PomZ colocalizes with the nucleoid if no cluster is present [2] and is stuck at the cluster otherwise (Fig. 1.4C). Since the ATPase activity of PomZ is low when only DNA is present, but synergistically stimulated by PomX, PomY and DNA, we expect that PomZ primarily detaches at the cluster. Therefore we typically chose a zero detachment rate for nucleoid-, but not cluster-bound, PomZ in the simulations. To study the effect of a non-zero detachment rate we also performed simulations with such a process included (see section 4.3).

Upon the stimulation of the ATPase activity, PomZ proteins change their conformational state and finally, two ADP-bound monomers are released into the cytosol. In our model, we account for these processes by combining them into one detachment process of cluster-bound PomZ dimers (rate k_h). Experiments suggest that PomZ proteins are released into the cytosol as ADP-bound monomers that first need to bind ATP and dimerize before they can rebind to the nucleoid [2]. Since these processes take some time (for ParA proteins on the order of minutes [97]), the PomZ dimers, which diffuse quickly in the cytosol, are spatially redistributed inside the cell. We typically do not explicitly model the processes in the cytosol, but instead assume that a cytosolic PomZ dimer can bind to each site on the nucleoid with the same rate. In this way, the spatial redistribution of the PomZ dimers in the cytosol is accounted for.

For the 3D model we also consider a variant that explicitly incorporates the cytosolic processes (nucleotide exchange and diffusion) in an effective manner (see chapter 5). Since the dynamics of PomZ in the cytosol is very fast and the cargo moves only slowly

(see section 1.4), we can make an adiabatic assumption by assuming that the cytosolic PomZ distribution instantaneously reaches its steady state while the cluster is moving. The one-dimensional steady-state reaction-diffusion equations for the cytosolic PomZ distribution along the long cell axis through the cluster (see Fig. 2.1A) can be solved analytically and used as an input for the nucleoid attachment rate in the stochastic model. Then, a PomZ dimer in the cytosol attaches to the nucleoid with a probability distribution of the same shape as the ATP-bound PomZ density in the cytosol.

Next, we consider whether crowding effects of PomZ dimers play a role. In the experiments with the ATP hydrolysis mutant of PomZ overexpressed more than 50-fold, the PomZ intensity was also high on the nucleoid away from the cluster such that the cluster was not visible (see Fig. 1.4B). We conclude that for high PomZ densities the cluster is saturated in PomZ and thus crowding effects need to be accounted for. However, for the wild type PomZ dimer number they should not matter, because PomZ dimers cover only a small fraction of the nucleoid. If we estimate the nucleoid by an ellipsoid (5 μm in length and 0.6 μm in width), the fraction 100 PomZ dimers (approximated as discs with radius 2 nm [6, 34]) cover, is approximately 0.02%. Hence, crowding effects are only relevant in the case of very large particle numbers. Therefore, we limited the number of binding sites for PomZ per nucleoid and cluster binding site in our simulations only in these cases (in chapter 3).

So far, we have discussed the stochastic dynamics of the PomZ dimers in the system. When they are bound to the cluster, they can exert forces on it, which lead to movement of the cluster. The position of the cluster, $x_c(t)$, evolves according to the following force-balance equation (overdamped limit):

$$\gamma_c \partial_t x_c(t) = -k \sum_{i=1}^{N} (x_i^{\text{clu}}(t) - x_i^{\text{nuc}}), \tag{2.4}$$

with the number of cluster-bound PomZ dimers, N. Here, we neglect the vertical distance of the cluster from the nucleoid. When we rewrite the cluster binding site position as $x_i^{\text{clu}}(t) = x_c(t) + \Delta x_i^{\text{clu}}$, the equation of motion can be solved analytically

$$x_c(t) = \left(x_{c,0} + \frac{1}{N} \sum_{i=1}^{N} (\Delta x_i^{\text{clu}} - x_i^{\text{nuc}}) \right) e^{-\frac{Nkt}{\gamma_c}} - \frac{1}{N} \sum_{i=1}^{N} (\Delta x_i^{\text{clu}} - x_i^{\text{nuc}}). \tag{2.5}$$

Here we do not include an additional noise term that accounts for Brownian motion of the cluster, because the experimental data suggests that the cluster is very immobile compared to the PomZ dynamics.

2.2 Estimating the model parameters

Diffusion constant of PomZ on the nucleoid and in the cytosol

The diffusion constant of PomZ on the nucleoid and in the cytosol can be estimated from the FRAP / bleaching experiments shown in Fig. 1.4. A precise determination of

the values is challenging, because a *M. xanthus* cell is relatively small (length of about 7.7 µm and width of about a micrometer) and the PomZ dimers are very dynamic.

In the FRAP experiments a region over the nucleoid (of diameter 0.35 µm) was bleached. Experiments with a short laser pulse of 60 ms showed a reduced signal intensity not only at the bleaching spot, but also around it (see Fig. 1.4A,B). This observation indicates that the PomZ dynamics is fast and diffusion during photobleaching cannot be neglected. Because bleaching affects the intensity signal in the whole cell, it is difficult to obtain a value for the diffusion constants only from the signal recovery curves. Several factors contribute to signal recovery, including diffusion of PomZ on the nucleoid, but also exchange with highly dynamic, cytosolic PomZ. A solution might be to simulate the dynamics of PomZ in the cell and fit the results with the experimentally obtained kymographs [99, 108].

To get insights into the dynamics of the quickly moving PomZ dimers, a variation of the typical FRAP experiment was considered. Instead of analyzing the fluorescence recovery after a very short laser pulse, a spot was bleached for $t_{\text{bleach}} = 3\,\text{s}$. The experiments show that after 3 s of bleaching the fluorescence intensity of labelled PomZ is reduced remarkably (see Fig. 1.4C). This implies that most of the PomZ dimers either reach the bleaching spot directly or diffuse to the cluster and then detach into the cytosol. In the cytosol they diffuse quickly and hence reach the bleaching spot after only a short time. If detachment of PomZ dimers from the nucleoid into the cytosol away from the cluster can be neglected, nucleoid-bound PomZ dimers need to reach the cluster by diffusion in 3 s.

The longest distance a PomZ dimer needs to cover until it reaches the cluster is $\Delta x \approx 2\,\text{µm}$ (half the nucleoid length and accounting for the length of the cluster). From this observation we get the following estimate for the diffusion constant of PomZ on the nucleoid:

$$D_{\text{nuc}} \approx \frac{\Delta x^2}{2t_{\text{bleach}}} \approx 0.66\,\text{µm}^2/\text{s}. \tag{2.6}$$

However, this value is only a rough estimate for the diffusion constant. It is likely that the real value is lower because PomZ dimers might, although to a minor extent, detach into the cytosol from the nucleoid away from the cluster. Furthermore, the fluorescence intensity on the nucleoid is not entirely gone after 3 s of bleaching.

The diffusion constant of PomZ in the cytosol can be obtained from bleaching experiments in mutants with PomZ that cannot bind to the nucleoid. In these experiments the fluorescence intensity is also nearly gone after 3 s of bleaching (see Fig. 1.4C). Hence, a significant fraction of PomZ dimers has to pass through the bleaching region in the time interval of 3 s. Hence, we get the following estimate for the diffusion constant of cytosolic PomZ:

$$D_{\text{cyt}} \approx \frac{l_{\text{cell}}^2}{2t_{\text{bleach}}} \approx \frac{(7.7\,\text{µm})^2}{2 \cdot 3\,\text{s}} \approx 10\,\text{µm}^2/\text{s}, \tag{2.7}$$

with the average length of the cell, $l_{\text{cell}} = 7.7\,\text{µm}$. This value for the cytosolic diffusion constant of PomZ is on the same order as the diffusion constant of MinD and MinE

proteins in the cytosol [104] and, as expected, larger than the diffusion constant of PomZ on the nucleoid.

ATP hydrolysis rate of PomZ bound to the cluster

The rate k_h in our model combines ATP hydrolysis of PomZ in contact with PomX, PomY and DNA, the conformational change and the detachment process. Initially we estimated k_h by the ATP hydrolysis rate of PomZ obtained from an *in vitro* assay. The measured value of $k_h = 0.01\,\mathrm{s}^{-1}$ is in the lower range of values used in models for the related Par system ($0.03\,\mathrm{s}^{-1}$[6] - $70\,\mathrm{s}^{-1}$[3]). Using this value as an estimate for the rate k_h in our model is not ideal, because i) it is obtained from an *in vitro* assay and ii) the turnover rate changes with the concentration of PomX, PomY and DNA. However, we do not know the exact values of the number of PomX and PomY proteins with which PomZ interacts when bound to the cluster. Alternatively, the rate k_h can be estimated from FRAP experiments with a bleaching spot over the cluster. These experiments show that PomZ dimers quickly exchange at the cluster (see Fig. 1.4A) with a half recovery time of $t_{1/2} = (1.2 \pm 0.2)\,\mathrm{s}$. This finding suggests that the ATP hydrolysis and detachment rate of PomZ at the cluster is at least $1\,\mathrm{s}^{-1}$, which is a lot larger than the value obtained from the *in vitro* assay.

Diffusion constant of the PomXY cluster in the cytosol

In the PomZ deletion mutant the cluster is often observed to be in the nucleoid free region [2], which suggested that the PomZ dimers tether the cluster to the nucleoid. Hence, this mutant strain can be used to estimate the diffusion constant of the PomXY cluster in the cytosol. From the mean squared displacement curves (using an time- and ensemble average) we get a diffusion constant of the Pom cluster of about $10^{-5}\,\mathrm{\mu m^2/s}$ (Fig. 2.2). This is likely a lower estimate of the diffusion constant because of two reasons: i) the cell membrane constricts the movement of the cluster, and ii) experiments show that Pom clusters often localize close to the nucleoid poles in the absence of PomZ. This might suggest that the cluster binds to a specific regions on the chromosome (at the nucleoid poles) although in the absence of PomZ, which would be another factor that reduces the diffusion constant of the cluster.

With this estimate, we can calculate how long it would take the cluster to reach midcell by diffusion only. The time scale to travel from a far off-center position to midcell ($\Delta x \approx 2\,\mathrm{\mu m}$) is given by

$$t = \frac{\Delta x^2}{2D} \approx 3300\,\mathrm{min},$$

which is a lot larger than the experimentally measured value of about $80\,\mathrm{min}$. Although the actual diffusion constant of the Pom cluster might be larger than the value estimated here, a mechanism that does not include active translocation is very unlikely.
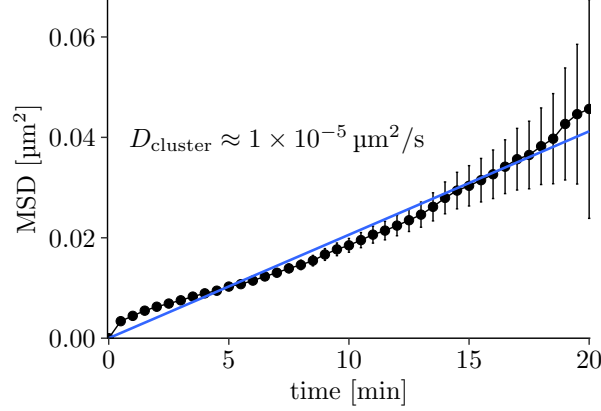
Figure 2.2 Mean squared displacement of the Pom cluster in PomZ deletion mutants. We measured the mean squared displacement (MSD) of the Pom cluster for 37 cluster trajectories obtained from time-lapse experiments. We assumed that the system is ergodic and therefore averaged the data not only over the ensemble, but also over time (data shown in black with error bars denoting the standard error of the mean). This procedure improved the statistics significantly. We fitted the data to a linear curve with zero off-set, which resulted in a diffusion constant of $D_{\text{cluster}} \approx 10^{-5}\,\mu\text{m}^2/\text{s}$.

Estimating the forces acting on the cluster

With the diffusion constant of the cluster, D_{cluster}, and the time the clusters need to reach midcell, $t_{\text{mid}} = 80\,\text{min}$, we can estimate the average force that needs to act on the cluster such that movement from off-center to midcell is achieved. Here, we assume that the cluster moves with a constant speed, which is in contrast to a slowing down of the net movement at midcell observed experimentally. For $D_{\text{cluster}} = 10^{-5}\,\mu\text{m}^2/\text{s}$ we get:

$$F = \gamma_c v = \gamma_c \frac{l_{\text{nuc}}}{2t_{\text{mid}}} = \frac{k_B T}{D_{\text{cluster}}} \frac{l_{\text{nuc}}}{2t_{\text{mid}}} \approx \frac{4\,\text{pN}\,\text{nm}}{10^{-5}\,\mu\text{m}^2/\text{s}} \frac{2.5\,\mu\text{m}}{4800\,\text{s}} = 0.2\,\text{pN}. \tag{2.8}$$

We used the Stokes-Einstein equation to rewrite the friction coefficient of the cluster: $\gamma_c = k_B T/D_{\text{cluster}}$. The diffusion constant of the cluster is likely larger than $10^{-5}\,\mu\text{m}^2/\text{s}$ as discussed before. For $D_{\text{cluster}} = 10^{-4}\,\mu\text{m}^2/\text{s}$, the net force is of the order $0.02\,\text{pN}$, which is similar to the estimated force for translocation acting on plasmids in Par systems ($0.03\,\text{pN}$ [109]). Though the forces are on the same order of magnitude, the average net velocity of plasmids ($0.007\,\mu\text{m}/\text{s}$ [109]) is likely larger than that of a Pom cluster ($l_{\text{nuc}}/(2t_{\text{mid}}) \approx 0.0005\,\mu\text{m}/\text{s}$). On the other hand, the friction coefficient of plasmids is likely smaller than that of the Pom cluster, because of the larger size of the cluster compared to plasmids.

2.3 Implementation as a stochastic simulation

We implemented our model using a stochastic simulation algorithm, the Gillespie algorithm [110–112]. For a system that can be described in terms of chemical Master equations [113], the algorithm generates realizations of the system over time. The occurrence of these realizations is distributed according to the exact solution of the underlying Master equations.

The Gillespie algorithm consists of two steps. First, the time until any event occurs is drawn from an exponential waiting time distribution, and second a random number is drawn to choose which event is realized. The first step can be implemented using an uniformly distributed random variable $\xi \in (0, 1]$. Then, the time step, Δt can be obtained from the following equation

$$-\ln(\xi) = \int_t^{t+\Delta t} \alpha(t')dt',\qquad(2.9)$$

with $\alpha(t)$ the sum over the rates for all possible events. For time-independent rates, $\alpha(t) = \alpha$, the time step is given by $\Delta t = -\ln(\xi)/\alpha$. However, if any of the rates is time-dependent, the integral in Eq. 2.9 becomes more difficult to solve. For some cases an analytical solution can be found, but otherwise the equation has to be solved numerically, which increases the computational time of the algorithm significantly.

Gillespie simulation with time-dependent rates

In our model, the rates for attachment of a nucleoid-bound PomZ dimer and hopping of PomZ dimers bound to the nucleoid and cluster depend on the cluster position and are therefore time-dependent. In both cases, the rates are of the form

$$e^{-c_1 e^{-2c_2 t}+c_3 e^{-c_2 t}},\qquad(2.10)$$

with constants c_1, c_2 and c_3 (see Eq. 2.1, 2.3 and 2.5). This term needs to be integrated over time, which is not feasible analytically. Hence, the integration has to be done numerically, which is computationally costly. However, for the parameters we used in our simulations (as given in the respective chapters) we could show that the time-dependence of the rates does not lead to significant changes in the simulation results compared to approximating the rates as time-independent. Therefore, we approximated the rates to be time-independent in our simulations.

We used two different methods to investigate the time-dependence of the rates. The first method is based on a personal communication with Karl Wienand. Here, we added an event that occurs frequently to the list of all actions and if it is selected, no action is performed. This additional "empty" event has the effect that the time step is decreased and hence the cluster position is updated more frequently. In the second method, the effect of the time-dependence is estimated based on the time scales for the next action to occur and the time scale with which the time-dependent rates change. Since the time dependence in the rates is due to the time dependence of the cluster

position, the time scale with which the rates change is the one of the cluster movement, which can be read off from Eq. 2.5: $\tau_{\mathrm{cluster}} = \gamma_c/(Nk)$. The typical time until the next event occurs, Δt, is given by the sum of all rates. In our simulations the hopping rate of PomZ on the nucleoid is typically the largest rate. Hence, a lower bound for the sum of all rates is given by the product of the number of PomZ dimers on the nucleoid, the directions on the lattice a PomZ dimer can hop to and the hopping rate. This value yields an upper bound for Δt. If Δt is a lot smaller than τ_{cluster}, the rates can be approximated as constant.

We also solved Eq. 2.9 numerically using a 4th-order Runge-Kutta method (odeint solver in the boost C++ library [114]) and compared the time step obtained from this method to the time step if the rates are approximated as constants. Using different sizes of the time step for the numerical integration of Eq. 2.9 yields a method to estimate the error we make by choosing the time step based on the time-independent rates. To estimate how much the rates change during the time until the next reaction occurs, we drew the time step using the rates at time t and the actions either based on the rates at time t or $t + \Delta t$ and compared the results. For the parameters we considered, we found similar results when we replaced the time-dependent rates by their time-independent approximations.

Chapter 3

A flux-based mechanism for midcell positioning in *M. xanthus*

3.1 Publication

The PomXYZ Proteins Self-Organize on the Bacterial Nucleoid to Stimulate Cell Division

by

D. Schumacher[1], S. Bergeler[2], A. Harms[1], J. Vonck[3], S. Huneke-Vogt[1], E. Frey[2] and L. Søgaard-Andersen[1]

[1]Department of Ecophysiology, Max Planck Institute for Terrestrial Microbiology, Karl-von-Frisch Straße 10, 35043 Marburg, Germany,

[2]Arnold Sommerfeld Center for Theoretical Physics and Center for NanoScience, Department of Physics, Ludwig-Maximilians-Universität München, Theresienstraße 37, 80333 Munich, Germany,

[3]Department of Structural Biology, Max Planck Institute of Biophysics, 60438 Frankfurt am Main, Germany

Reprinted on pages 36–76.

The main part of the supplemental material is reprinted on pages 77–98.

The PomXYZ proteins self-organize on the bacterial nucleoid to stimulate cell division

Dominik Schumacher[1], Silke Bergeler[2], Andrea Harms[1], Janet Vonck[3], Sabrina Huneke-Vogt[1], Erwin Frey[2] & Lotte Søgaard-Andersen[1, 4]

[1] Department of Ecophysiology, Max Planck Institute for Terrestrial Microbiology, Karl-von-Frisch Str. 10, 35043 Marburg, Germany

[2] Arnold Sommerfeld Center for Theoretical Physics and Center for NanoScience, Department of Physics, Ludwig-Maximilians-Universität München, Theresienstr. 37, 80333 Munich, Germany.

[3] Department of Structural Biology, Max Planck Institute of Biophysics, 60438 Frankfurt am Main, Germany.

[4] Corresponding author & Lead Contact
Tel. +49-6421-178 201
Fax +49-6421-178 209
E-mail: sogaard@mpi-marburg.mpg.de

Summary

Cell division site positioning is precisely regulated to generate correctly sized and shaped daughters. We uncover the strategy used by the social bacterium *Myxococcus xanthus* to position the FtsZ cytokinetic ring at midcell. PomX, PomY and the nucleoid-binding ParA/MinD ATPase PomZ self-assemble forming a large nucleoid-associated complex that localizes at the division site before FtsZ to directly guide and stimulate division. PomXYZ localization is generated through self-organized biased random motion on the nucleoid towards midcell and constrained motion at midcell. Experiments and theory show that PomXYZ motion is produced by diffusive PomZ fluxes on the nucleoid into the complex. Flux differences scale with the intracellular asymmetry of the complex and are converted into a local PomZ concentration gradient across the complex with translocation towards the higher PomZ concentration. At midcell, fluxes equalize resulting in constrained motion. Flux-based mechanisms may represent a general paradigm for positioning of macromolecular structures in bacteria.

Introduction

Correct positioning of the cell division site requires exquisite spatiotemporal control to ensure the formation of daughter cells of correct size, shape and chromosome complement. In bacteria, cell division initiates with the assembly of the tubulin-like protein FtsZ into a ring-like structure, the Z-ring, at the future division site (Bi and Lutkenhaus, 1991; Lutkenhaus et al., 2012). The Z-ring directly or indirectly recruits the remaining proteins of the cytokinetic machinery (Lutkenhaus et al., 2012). Consistently, systems that regulate positioning of the cell division site control Z-ring formation and positioning (Lutkenhaus et al., 2012). The proteins of the cytokinetic machinery are conserved in different bacterial lineages. By

contrast, the systems that regulate when and where the Z-ring forms are diverse and incompletely understood.

The systems that regulate Z-cell division in the rod-shaped cells of *Escherichia coli*, *Bacillus subtilis* and *Caulobacter crescentus* inhibit Z-ring formation throughout cells except at midcell and all systems incorporate a member of the ParA/MinD superfamily of P-loop ATPases. In *B. subtilis* proteins of the Min system bind to the cell poles (Lutkenhaus, 2012). By contrast, proteins of the Min system in *E. coli* self-organize (Howard et al., 2001; Meinhardt and de Boer, 2001; Kruse, 2002; Huang et al., 2003; Fange and Elf, 2006; Touhami et al., 2006; Loose et al., 2008; Halatek and Frey, 2012) to undergo coupled pole-to-pole oscillations (Hu and Lutkenhaus, 1999; Raskin and de Boer, 1999). In this system, MinD in its ATP-bound dimeric form, binds to the cytoplasmic membrane and forms a complex with MinC that inhibits Z-ring formation (Hu and Lutkenhaus, 1999; Hu et al., 1999; Hu et al., 2002; Lackner et al., 2003). MinD also recruits its ATPase Activating Protein (AAP) MinE to the membrane triggering ATPase activity and membrane unbinding of monomeric MinD. After nucleotide exchange, MinD rebinds to the membrane (Hu and Lutkenhaus, 2001; Hu et al., 2002; Lackner et al., 2003). Over time the lowest concentration of MinD-ATP/MinC is at midcell, thus, restricting Z-ring assembly to midcell (Meinhardt and de Boer, 2001). In *C. crescentus*, the ParA/MinD ATPase MipZ directly inhibits FtsZ polymerization (Thanbichler and Shapiro, 2006). MipZ is recruited to the cell poles by ParB and forms gradients on the nucleoid extending from the poles towards midcell restricting division to midcell.

ParA/MinD ATPases are also involved in chromosome and plasmid segregation as well as in positioning of macromolecular structures (Lutkenhaus, 2012). Among these systems, the ParABS systems involved in chromosome and plasmid segregation are best understood. Here, ParA dimerizes upon ATP binding and binds nonspecifically to the nucleoid (Leonard et al., 2005; Hester and Lutkenhaus, 2007; Scholefield et al., 2011). ParB binds to *parS* sequences close to the chromosomal origin of replication or on a plasmid (Lutkenhaus, 2012). ParB/*parS* interacts with nucleoid-bound ParA dimers and with the AAP ParB stimulating ParA ATPase activity resulting in ParA dissociation from the nucleoid (Ptacin et al., 2010; Schofield et al., 2010; Vecchiarelli et al., 2013). Subsequently, ParB/*parS* interacts with flanking nucleoid-bound ParA dimers. Repeated cycles of these events result in translocation of the ParB/*parS* complex across the nucleoid and a zone depleted of ParA is generated in the wake of the translocating complex. The directionality of translocation is thought to be determined by the concentration gradient of nucleoid-bound ParA that spans across the entire nucleoid (Ringgaard et al., 2009; Ptacin et al., 2010; Schofield et al., 2010).

Regulation of Z-ring formation and cell division at midcell in the rod-shaped cells of *Myxococcus xanthus* depend on the ParA/MinD ATPase PomZ (Treuner-Lange et al., 2013). PomZ has a unique localization pattern among characterized ParA/MinD ATPases (Treuner-Lange et al., 2013): Upon cell division, PomZ forms a cluster over the nucleoid; later, this cluster localizes at midcell and here PomZ colocalizes with FtsZ. Intriguingly, PomZ localizes to midcell before as well as in the absence of FtsZ suggesting that PomZ could be part of a spatiotemporal control system that directly recruits FtsZ to midcell. However, the mechanisms underlying midcell localization of PomZ and stimulation of Z-ring formation remain unknown.

Here, we identify two previously uncharacterized proteins, PomX and PomY, and show that they function in concert with PomZ to directly recruit FtsZ to midcell and stimulate Z-ring formation. We demonstrate that the PomXYZ proteins self-assemble to form a large complex on the nucleoid that translocates to the midnucleoid, which coincides with midcell, in a biased random walk. At midnucleoid, the complex undergoes constrained motion and stimulates Z-ring formation. By combining experimental work and theory, we provide evidence that the motion pattern of this complex arise from a mechanism that depends on the diffusive flux of nucleoid-bound PomZ into the PomXYZ cluster as previously suggested for equipositioning of plasmids (Ietswaart et al., 2014). These analyses explain how interactions at the molecular scale are transformed into cellular organization at the μm scale.

Results

<u>PomX and PomY are important for cell division, Z-ring formation and positioning</u>
While searching for proteins important for midcell localization of PomZ, we noticed that *pomZ* (MXAN_0635) is flanked by conserved genes in myxobacterial genomes (Fig. S1A). MXAN_0634 (henceforth PomY for <u>Po</u>sitioning at <u>m</u>idcell of FtsZ <u>Y</u>) as well as MXAN_0636 (henceforth PomX for <u>Po</u>sitioning at <u>m</u>idcell of FtsZ <u>X</u>) are rich in protein-protein interaction domains (Fig. S1B).

Similar to the Δ*pomZ* mutant, mutants with in-frame deletions in *pomX* or *pomY* had a growth rate comparable to wild-type (WT), formed long filamentous cells and short anucleate minicells, and had fewer cell division constrictions that were distributed along the cell length but did not occur over the nucleoid (Fig. 1A-C; S1CD). Overall, all double and the triple mutants had similar phenotypes (Fig. 1AB; S1C) suggesting that PomXYZ function together to stimulate cell division at midcell. However, the mutants display different cell length distributions suggesting that PomX, PomY and PomZ have different functions in cell division or that lack of one protein causes dominant negative effects. The division defects in the Δ*pomX* and Δ*pomY* mutants were complemented by ectopic expression at native or above native levels of mCherry (mCh)-PomX and PomY-mCh, respectively (Fig. 1B; S1CE). Moreover, PomX, PomY and PomZ accumulated independently of each other (Fig. 1D).

The number of nucleoids per cell length in the Δ*pomX* and Δ*pomY* mutants were not significantly different to that in untreated WT or WT treated with the division inhibitor cephalexin (t-test, p>0.05). Also, using the midpoint of the nucleoid (henceforth, referred to as midnucleoid) as a marker, nucleoids showed similar localization patterns in a two one-sided equivalence test (Fig. S2AB). Using a ParB-eYFP fusion (Harms et al., 2013) as a marker for the origin of replication, the number of origins per cell length (t-test, p>0.05) and the localization of origins (two one-sided equivalence test) were similar in the Δ*pomX* and Δ*pomY* mutants compared to WT (Fig. S2AC). We conclude that PomX and PomY, similarly to PomZ (Treuner-Lange et al., 2013), are not important for replication and chromosome segregation.
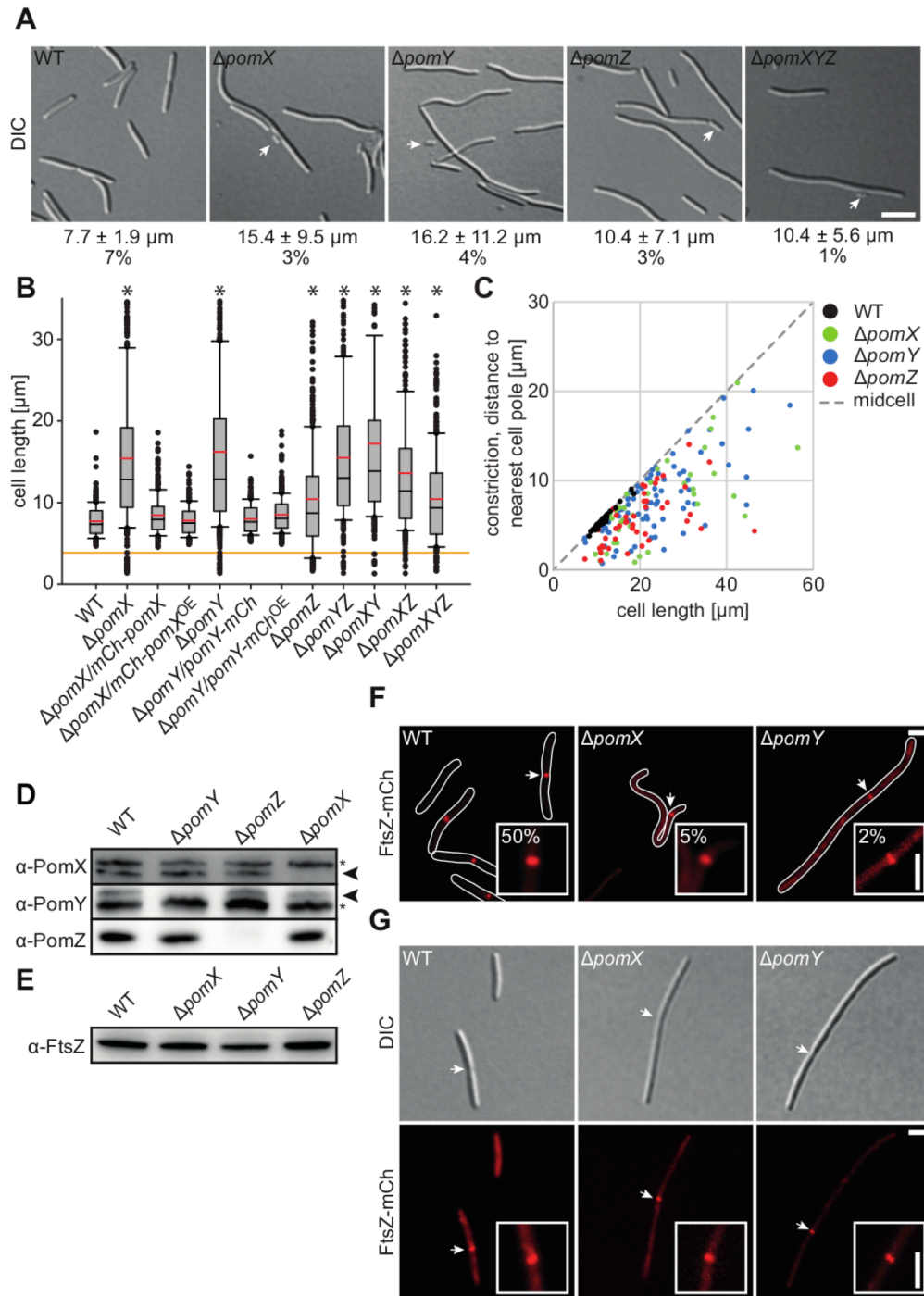
Figure 1: PomX and PomY are important for cell division and Z-ring formation and positioning.
A. Morphology of cells of indicated genotypes. Arrows indicate minicells, numbers mean cell length ± standard deviation (SD) and constriction frequency (n>200 cells). Scale bar, 5µm.
B. Cell length distributions of cells of indicated genotypes. Same cells analyzed as in A. The few cells longer than 35µm are not included in the box plots. Dots below orange line indicate minicells. Strains labelled *mCherry-PomX^{OE}* or *PomY-mCherry^{OE}* overexpress the two proteins. * indicate strains with a cell length distribution significantly different from WT (t-test, p<0.05).
C. Lack of PomX, PomY or PomZ leads to misplaced constrictions. Same cells analyzed as in A. Dots represent constrictions in individual cells.

D. Immunoblot analysis of PomX, PomY and PomZ accumulation. Equal amounts of protein were loaded. * indicate cross-reacting proteins and arrows PomX and PomY.

E. Immunoblot analysis of FtsZ accumulation. Analysis done as in D.

F. PomX and PomY are important for Z-ring formation and positioning. *ftsZ*^{+} cells expressing FtsZ-mCh were visualized. Strains used from left to right: SA3139, SA4228, SA4707. Arrows indicate Z-rings shown at higher magnification in insets. Numbers represent Z-ring frequencies (n>1000 cells). Scale bars, 2µm.

G. FtsZ-mCh colocalizes with constrictions. Cells and strains as in F. Arrows indicate constrictions. Marked Z-rings shown at higher magnification in insets. Scale bars, 2µm.

See also Fig. S1 and S2.

All three *pom* mutants accumulated FtsZ at WT levels (Fig. 1E). As shown (Treuner-Lange et al., 2013), in ~50% of WT cells FtsZ-mCh was diffusely localized in the cytoplasm and formed a Z-ring at midcell (defined as 50±5% of cell length) in the remaining cells (Fig. 1F). ~10% of these Z-rings colocalized with a constriction (Fig. 1G). In ΔpomX and ΔpomY cells, FtsZ-mCh predominantly localized in the diffuse pattern and only 2-5% of cells contained a Z-ring and these Z-rings were not restricted to midcell but localized along the cell length (Fig. 1F). As in the ΔpomZ mutant, ~50% of the Z-rings in the ΔpomX and ΔpomY mutants colocalized with a constriction (Fig. 1G). These observations suggest that the Z-ring in WT stably assembles at midcell well before constriction and that PomX, PomY and PomZ function to stimulate Z-ring formation and stability as well as positioning at midcell. Because many of the Z-rings in the *pom* mutants colocalize with constrictions and the frequency of cells with a Z-ring colocalizing with a constriction in these mutants is similar to the frequency of constrictions, these data also suggest that constriction initiates shortly after assembly of a Z-ring in the *pom* mutants.

PomX, PomY and PomZ form a complex that is positioned at midcell by PomZ

To uncover the function of PomX and PomY in Z-ring formation and division, we determined their subcellular localization using active mCh-PomX and PomY-mCh fusions expressed at native levels. Overall, the two proteins showed the same localization pattern as PomZ [(Treuner-Lange et al., 2013); Fig. 2A)]. mCh-PomX and PomY-mCh gave no signal or a diffuse signal in 10 and 26% of cells, respectively, formed a single cluster in an off-centre position (defined as clusters outside of the midcell region at 50±5% of cell length) in 34 and 22% of cells, respectively, and a cluster at midcell in the remaining 56 and 52% of cells, respectively. Off-centre clusters colocalized with the nucleoid (Fig. 2A). ~75% of midcell clusters localized over the midnucleoid (Fig. 2A, third row) and the remaining ~25% localized between two fully segregated nucleoids (Fig. 2A, fourth row). Moreover, PomX and PomY colocalized with constrictions (Fig. S3A).

In addition to forming a cluster, ~90% of PomZ-mCh colocalized with the nucleoid generating a patchy localization pattern (Fig. S3B) suggesting that PomZ binds nonspecifically to the nucleoid. The patchy PomZ signal over the nucleoid is almost symmetrically distributed around the cluster as indicated by an asymmetry measure normalized for nucleoid area of 0.10±0.03 (n=52) for off-centre clusters and 0.05±0.04 (n=44) for midcell clusters (Fig. S3B). This asymmetry is slightly but significantly higher in the case of cells with an off-centre cluster (t-test, $p<0.01$) and with the highest intensity on the side of the cluster containing

most of the nucleoid. For comparison, the same asymmetry measure for Pico Green stained nucleoids is 0.07±0.06 (n=49).
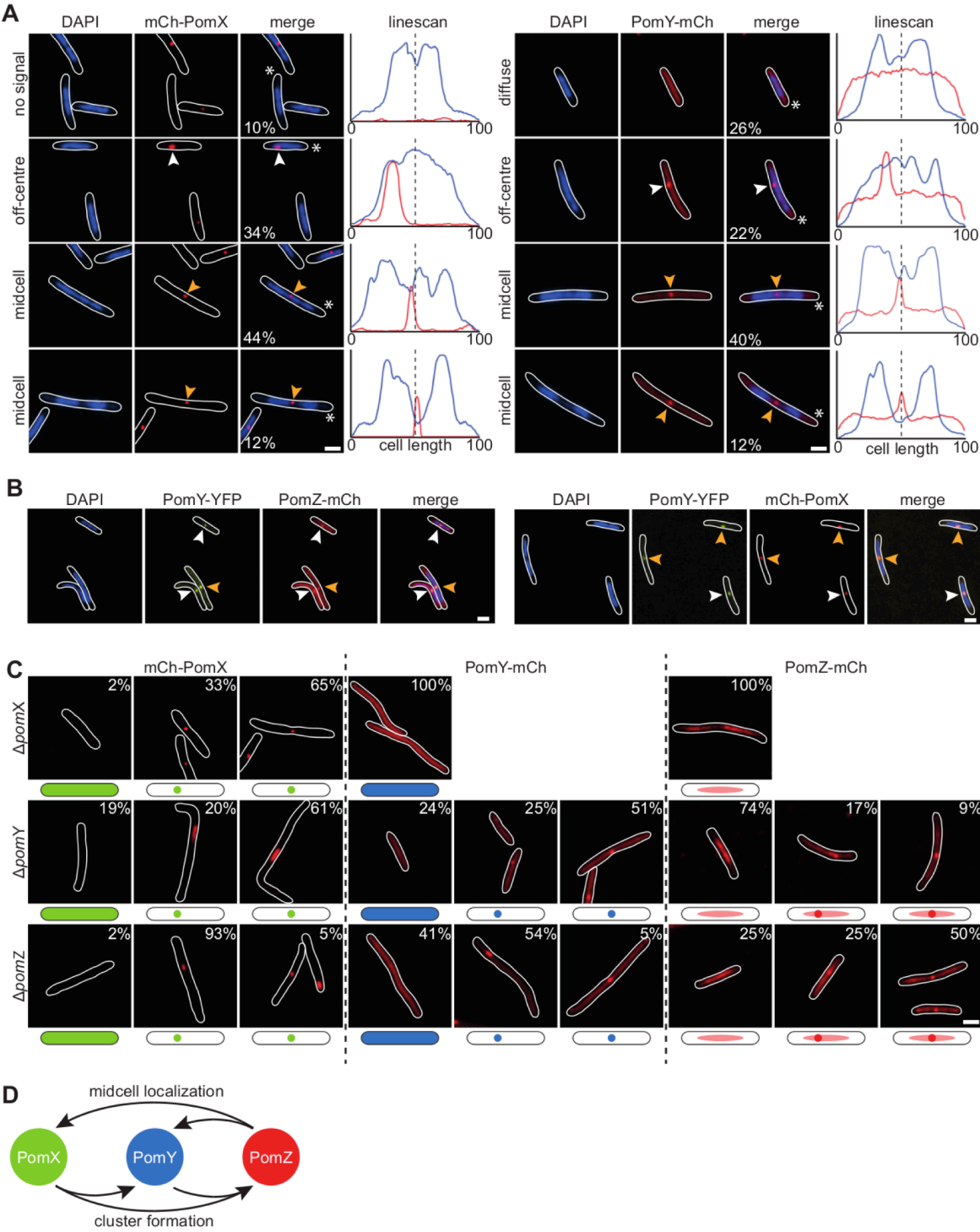

Figure 2: PomX, PomY and PomZ form a complex that is positioned at midcell by PomZ.
(A, B). PomX, PomY and PomZ localize similarly and colocalize. Fluorescent fusion proteins were localized in the corresponding in-frame deletion mutants (n>200). White and orange arrows indicate off-centre and midcell clusters. DAPI was used to stain nucleoids. In A, numbers indicate % of cells

with that localization pattern. Linescans show fluorescence intensity of DAPI (blue) and mCh-PomX/PomY-mCh (red) fluorescence for cells marked *. Stippled line indicates midcell. In lower two rows, midcell clusters are divided into those localizing at midnucleoid and those localized between two segregated nucleoids. Strains used in A from left to right: SA4229, SA4713 (n>200). In B, PomY-eYFP expression was induced by 150µM Cu^{2+}.Strains used from left to right: SA7020, SA7041.

C. PomX, PomY and PomZ localize interdependently. Fusion proteins were analyzed in the indicated in-frame deletion mutants. Numbers indicate % of cells with that localization (n>200). Cartoons illustrate localization patterns schematically. Strains used in C from left to right: Top row SA4252, SA4737, SA4232; middle row SA4739, SA4712, SA4706; bottom row SA5821, SA4720, SA3131.

D. Schematic of localization dependency of PomX, PomY and PomZ.

Scale bar, 2µm in all panels.

See also Fig. S1F and S3.

PomY-eYFP/PomZ-mCh and PomY-eYFP/mCh-PomX perfectly colocalized in off-centre clusters and at midnucleoid (Fig. 2B). Using an Ssb-eYFP fusion as a proxy for assembled replisomes (Harms et al., 2013), we observed that PomX and PomY localized at midnucleoid while replication was ongoing (Fig. S3C). We conclude that PomXYZ early in the cell cycle colocalize in an off-centre position on the nucleoid, later at the midnucleoid at midcell before termination of replication, and this midcell localization persists at least until division initiates.

We hypothesized that if PomXYZ interact to form a complex, then lack of one of the proteins would perturb complex formation and/or localization. To this end, we localized each Pom protein in the absence of one or the other Pom protein (Fig. 2C). mCh-PomX formed clusters and localized independently of PomY; however, the clusters had an aspect ratio of 3.6±2.9 compared to 1.2±0.2 in the presence of PomY. mCh-PomX also formed clusters independently of PomZ; however, these clusters were rarely at midcell and often in the large nucleoid-free subpolar regions (Fig. S3D). By contrast, PomY-mCh was dispersed in the absence of PomX, formed slightly fewer clusters in the absence of PomZ and these clusters were rarely at midcell and frequently in the nucleoid-free subpolar regions (Fig. S3D). PomZ-mCh only localized in the patchy pattern over the nucleoid in the absence of PomX. In the absence of PomY, PomZ-mCh also mostly localized in the patchy pattern over the nucleoid. Among the few clusters formed, ~35% were at midcell (Fig. 2C). Finally, mCh-PomX and PomY-eYFP colocalized in the absence of PomZ (Fig. S3E).

Altogether, these observations are consistent with PomX nucleating the formation of a complex that contains all three Pom proteins and with PomZ being central to localization of this complex at midcell (Fig. 2D). From the frequent localization of the PomXY complex to the nucleoid-free subpolar regions in the absence of PomZ, we infer that PomZ also associates this complex with the nucleoid.

<u>PomX and PomY localize to midcell in the absence of FtsZ</u>
To address the causal relationship between midcell localization of PomX/PomY and FtsZ, we localized FtsZ-GFP expressed at native levels in the presence of unlabeled FtsZ in strains expressing mCh-PomX or PomY-mCh. Importantly, in a large fraction of cells, mCh-PomX (49%) or PomY-mCh (28%) were at midcell without FtsZ-GFP and we did not observe the opposite pattern (Fig. 3A). FtsZ-GFP was perfectly superimposable with mCh-PomX and

PomY-mCh at midcell but not in the off-centre position (Fig. 3A). In otherwise WT cells, FtsZ-GFP forms Z-rings in ~50% of cells suggesting that mCh-PomX or PomY-mCh may interfere with Z-ring formation by FtsZ-GFP. Nonetheless, these observations are in agreement with previous findings that PomZ localizes to midcell before FtsZ (Treuner-Lange et al., 2013).
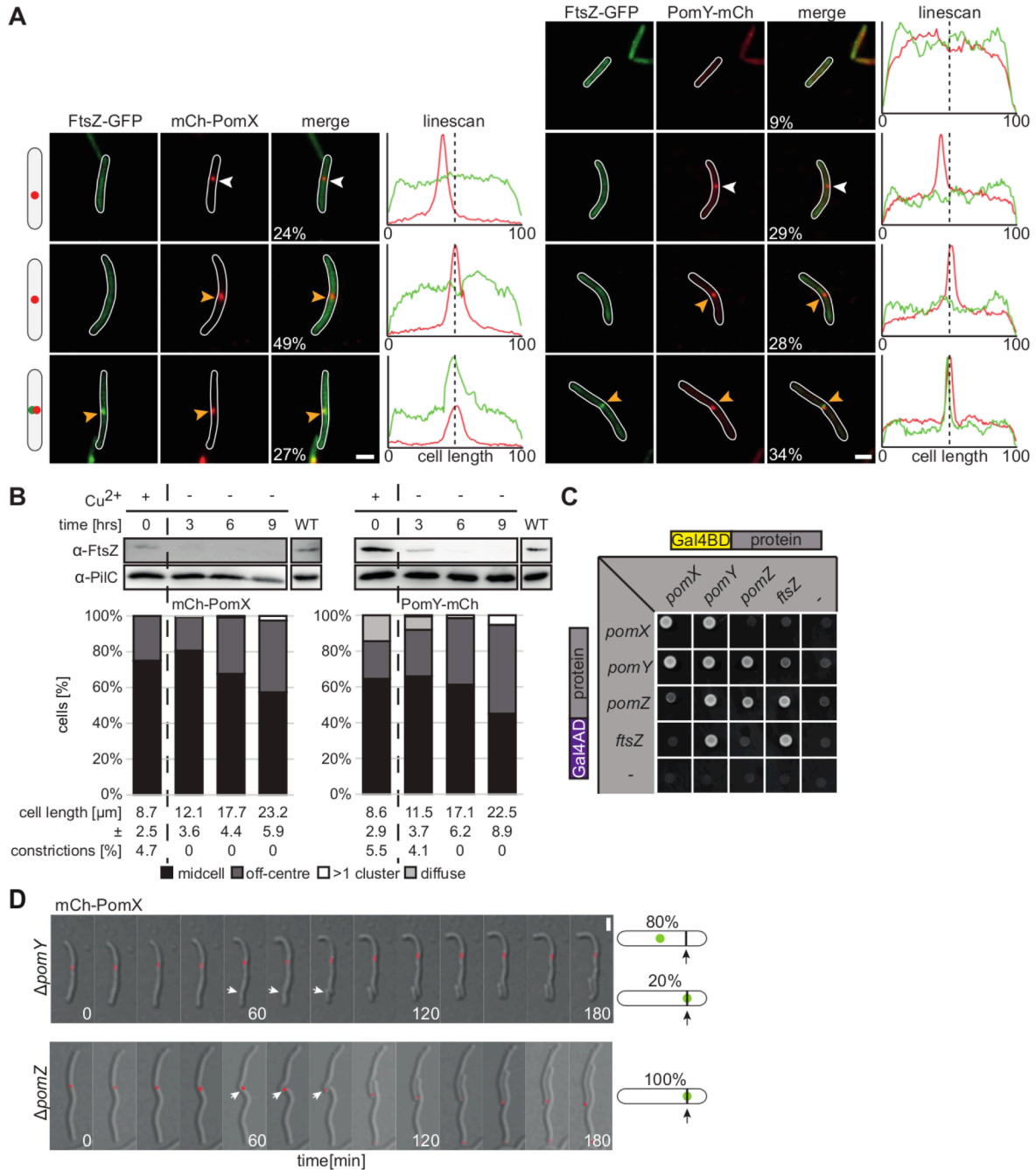

Figure 3: PomX and PomY localize at midcell before and in the absence of FtsZ.
A. mCh-PomX and PomY-mCh localize at midcell before FtsZ. mCh-PomX/PomY-mCh were expressed in the presence of 150μM Cu^{2+}. Numbers indicate % of cells with that localization pattern (n>200). Linescans as in Fig. 2A with FtsZ (green) and mCh-PomX/PomY-mCh (red). Cartoons indicate localization patterns of FtsZ (green) and PomX/PomY (red). White and orange arrows indicate off-centre and midcell clusters, respectively. Scale bar, 2μm. Strains used from left to right: SA4295, SA4736.

B. PomX and PomY localize at midcell in the absence of FtsZ. FtsZ was expressed in the presence of 300µM Cu^{2+} and depleted by removal of Cu^{2+} from the growth medium (t = 0 hrs); samples withdrawn at indicated time points. Upper panel, FtsZ during Cu^{2+} depletion. Lower panel, PilC loading control in same cells. For comparison, FtsZ accumulation in WT is included on the right. For each time point, cells (n>200) were analyzed for cell length ± SD, constriction frequency and localization of mCh-PomX/PomY-mCh. Strains used from left to right: SA5809, SA4718.
C. Yeast two hybrid analysis for interactions between Pom proteins and FtsZ. Yeast strain AH109 expressing indicated variants of Gal4-AD and Gal4-BD were analyzed for growth selective medium. Negative control, AH109 with bait plasmid containing Gal4-AD or Gal4-BD fusion and a plasmid expressing native Gal4-AD or Gal4-BD.
D. PomY is required to align cell division with PomX cluster. Images were recorded every 15 min. Shown are merged DIC and fluorescence microscopy images. White arrows indicate constrictions. Right, cartoons show schematically constrictions (black arrow) relative to the mCh-PomX clusters (green) and frequency of indicated patterns (n>25 per strain). Strains used top to bottom: SA7008, SA7009.
See also Fig. S1 and S4.

To localize mCh-PomX and PomY-mCh in cells depleted for FtsZ, we expressed the only copy of *ftsZ* from a Cu^{2+} inducible promoter. In the presence of Cu^{2+} the two strains displayed normal cell length distributions and constriction frequencies (Fig. 3B). FtsZ accumulation decreased over time in the absence of Cu^{2+} and was not detectable in immunoblots after 3-6 hrs. In parallel, the frequency of constrictions decreased and cell length increased. After 9 hrs of FtsZ depletion, all cells contained mCh-PomX or PomY-mCh clusters (Fig. 3B; S4A). Importantly, these clusters often localized at midcell. Thus, similarly to PomZ (Treuner-Lange et al., 2013), PomX and PomY localize at midcell in the absence of FtsZ. In control experiments, we observed that PomX and PomY also remained at midcell in a large fraction of cells treated with cephalexin (Fig. S4B). Moreover, the cell division protein FtsK, which is recruited late to the cytokinetic machinery in an FtsZ-dependent manner (Lutkenhaus et al., 2012), did not form midcell clusters after depletion of FtsZ (Fig. S4C). Altogether, these data suggest that the PomXYZ complex localizes at midcell independently of FtsZ and function to recruit FtsZ to midcell.

PomY and PomZ interact directly with FtsZ
We carried out a yeast two hybrid screen for direct interactions between the Pom proteins and FtsZ. FtsZ self-interacted; moreover, PomY and PomZ interacted with FtsZ (Fig. 3C). Using purified native FtsZ (Fig. S4D) we observed that FtsZ in a GTP-dependent manner formed higher order structures as shown by right angle light scattering (Fig. S4E) and filaments as shown by negative stain transmission electron microscopy (EM) (Fig. S4F). We previously reported that *M. xanthus* FtsZ has cooperative GTPase activity *in vitro* but did not form filaments visible by right angle light scattering and EM (Treuner-Lange et al., 2013). Here, we used a different purification protocol and performed the experiments at slightly lower pH. We attribute the different results to these differences in experimental setups.

Consistent with direct interactions between PomY or PomZ and FtsZ, only 20% of the divisions in the Δ*pomY* mutant occurred over mCh-PomX clusters some of which also contain PomZ (Fig. 3D; Cf. 2C) while all divisions in the Δ*pomZ* mutant occurred over the mCh-PomX cluster all of which contain PomY (Fig. 3D; Cf. 2C; S3E). We conclude that FtsZ

9

interacts directly with PomY and PomZ. Moreover, our data suggest that PomY in the PomXYZ complex has an important function in recruiting FtsZ to the division site in WT, and that all three Pom proteins are important for efficient Z-ring formation.
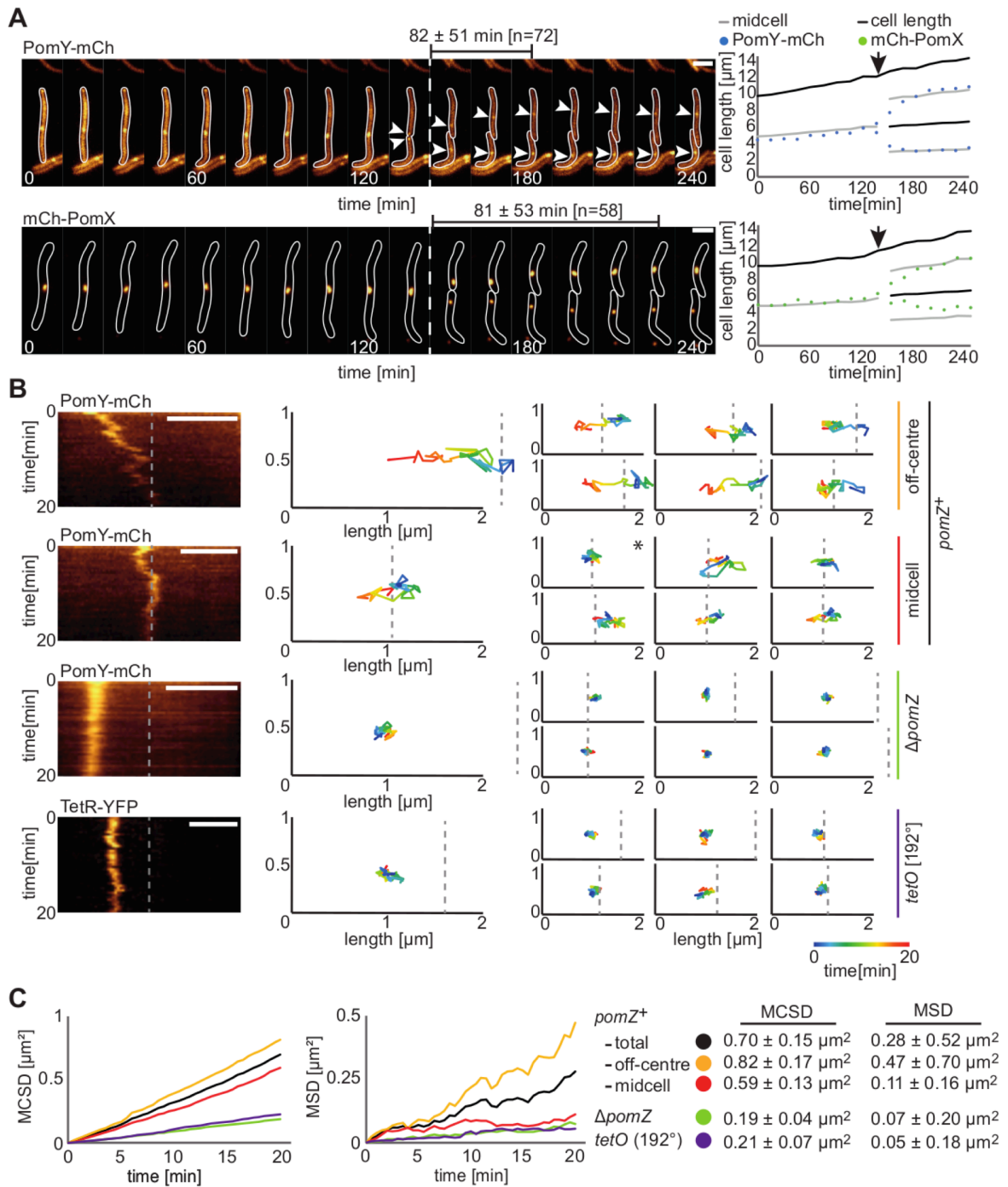

Figure 4: PomX and PomY form dynamically localized clusters that are positioned at midcell by PomZ.

A. mCh-PomX and PomY-mCh are dynamically localized. Time-lapse microscopy as in Fig. 3D. White arrows mark PomY-mCh clusters. Stippled line indicates a division. Numbers above images indicate mean ± SD translocation time from the release of a cluster at a division site until it reached the new

midcell. Black lines indicate this translocation time for the cells shown. Right, schematics illustrate cluster localization in cells on the left with divisions marked by arrows. Scale bar, 2µm.

B. Kymographs of PomY-mCh and TetR-eYFP localization. Images were recorded every 30 sec. Right panels, representative two-dimensional cluster trajectories color-coded for time. Stippled lines indicate midcell. Large panels refer to clusters shown in kymographs. Scale bars, 2µm. TetR-eYFP was expressed in presence of 150µM vanillate. * marks cell in which midcell cluster was essentially non-motile. Strains used from top to bottom: SA4746 (two top panels), SA4796, SA6757.

C. Quantification of PomY-mCh and TetR-eYFP cluster translocation. Cluster centroids were tracked (n >30 per strain) and used to calculate MCSD and MSD.

See also Fig. S5.

The PomXYZ complex relocates to midcell by PomZ-dependent translocation

To resolve how the PomXYZ complex shifts from an off-centre to a midnucleoid position at midcell, we performed time-lapse microscopy (images every 15 min). PomX and PomY behaved similarly (Fig. 4A) and colocalized during translocation (Fig. S5A): Starting with a midcell cluster, this cluster splits into two during division resulting in two daughters each with an off-centre cluster close to the new cell pole. Subsequently, each cluster slowly migrated to midcell, and remained there. Occasionally, PomX and PomY were asymmetrically distributed to the daughters (Fig. S5B) likely giving rise to cells with no or a diffuse signal of the Pom proteins in snapshots (Cf. Fig. 2A). PomX and PomY had the same translocation time to midcell after release from a division site (Fig. 4A). The generation time of *M. xanthus* under the conditions of the experiment is ~5 hrs. Thus, the PomXYZ complex localizes at midnucleoid 3-4 hrs before division.

Next, we monitored the PomY-mCh cluster as a marker for the PomXYZ complex at higher temporal resolution (images every 30 sec). At this temporal resolution, PomY-mCh clusters moved along the long and the short axes of cells (Fig. 4B). Qualitatively, cluster dynamics varied depending on cluster position and with off-centre clusters displaying long periods of wandering towards midcell reminiscent of a two-dimensional biased random walk while clusters in the midcell region had less directional bias. Finally, ~10% of midcell clusters, and these were mostly in long cells, essentially displayed no motion. We speculate that these cells are undergoing division and that the PomXYZ proteins are associated with the cytokinetic machinery and, therefore, display less motion.

To quantify cluster motion, we calculated the mean cumulative squared distance (MCSD) (STAR*Methods) and the mean squared displacement (MSD) from the PomY-mCh cluster trajectories (Fig. 4C). Off-centre and midcell clusters had similar MCSD. However, the MSD showed clear differences with the MSD for off-centre clusters displaying a slope over time, which seems to increase, indicating that they exhibited directed motion whereas the MSD for midcell clusters reached a plateau demonstrating that cluster motion was constrained to midcell.

Strikingly, lack of PomZ strongly reduced the MCSD of PomY-mCh clusters and MSD reached a plateau slightly lower than for midcell clusters in a *pomZ*$^+$ background (Fig. 4BC). Thus, these clusters are essentially stalled somewhere in a cell. We conclude that PomZ is

essential for cluster motion with translocation to midcell by a biased random walk and constrained motion at midcell.

The *M. xanthus* chromosome is arranged about a longitudinal axis with the origin of replication and the terminus region close to the old and new poles, respectively (Harms et al., 2013). During replication, the terminus region displaces towards midcell in a manner somewhat comparable to that of the PomXYZ cluster. To test whether PomXYZ translocation to midcell occurs by "piggybacking" on the terminus, we quantified the dynamics of the terminus region using FROS (Fluorescence Repressor Operator System) with TetR-eYFP bound to a *tetO* array at 192° on the *M. xanthus* chromosome. Similarly to the PomXY cluster in the absence of PomZ, this locus displayed very little motion (Fig. 4BC), suggesting that the PomXYZ complex is not "piggybacking" on the terminus to midcell.

PomX and PomY form a complex that stimulates ATPase activity by DNA bound PomZ

To determine how PomZ promotes the motion of the PomXYZ complex, we tested for direct interactions between the Pom proteins. In the yeast two hybrid system, all three proteins self-interact and interact in all pairwise combinations (Fig. 3C). Next, we expressed the active Pom-fusion proteins alone or together in *E. coli*, which lacks close relatives of the Pom proteins (Fig. 5A). PomZ-mCh alone perfectly colocalized with the nucleoid without forming clusters, supporting the notion that PomZ binds nonspecifically to DNA. PomY-eYFP displayed a diffuse signal throughout cells and often also formed a polar cluster in nucleoid-free areas. mCh-PomX formed small patches and longer filamentous structures in nucleoid-free areas. Co-expressed PomY-eYFP and mCh-PomX colocalized in filamentous patches whereas co-expressed PomZ-mCh and PomY-eYFP colocalized on the nucleoid without forming clusters. Remarkably, co-expression of PomY-eYFP, PomZ-mCh and unlabeled PomX resulted in the formation of clusters in 64% of cells; these clusters had the same dimensions as those in *M. xanthus* and contained both PomY-eYFP and PomZ-mCh. While *M. xanthus* cells contain a single PomXYZ cluster until it splits late during division, *E. coli* cells generally contained a cluster over each nucleoid. We speculate that more than one cluster is formed in *E. coli* because the Pom proteins are not associated with the cytokinetic machinery. We conclude that the three Pom proteins interact directly in all pairwise combinations and that all three proteins are required and sufficient for the formation of nucleoid-associated clusters.

To independently test for interactions between the Pom proteins, we overexpressed and purified soluble full length variants of the WT proteins as well as PomZ^{D90A}, which is predicted to be blocked in ATP hydrolysis and is non-functional *in vivo* (Treuner-Lange et al., 2013) (Fig. S4D). After high-speed centrifugation, 90% of PomX-His$_6$ was recovered in the pellet fraction whereas PomY-His$_6$ was equally distributed in the pellet and soluble fractions (Fig. S6A). By contrast, PomY-His$_6$ mixed with an equimolar amount of PomX-His$_6$ was almost entirely recovered in the pellet fraction. In EM analyses, PomX-His$_6$ alone formed long thin filaments 8.3±1.9nm in width and several μm in length (Fig. 5B) whereas PomY-His$_6$ under the same conditions did not form higher order structures. However, when mixed in a 1:1 molar ratio, PomX-His$_6$ and PomY-His$_6$ formed thick bundles up to 150nm in width and

several µm in length. Thin filaments emerged from these bundles suggesting that these structures consist of PomX-His$_6$ filaments bundled by PomY-His$_6$.
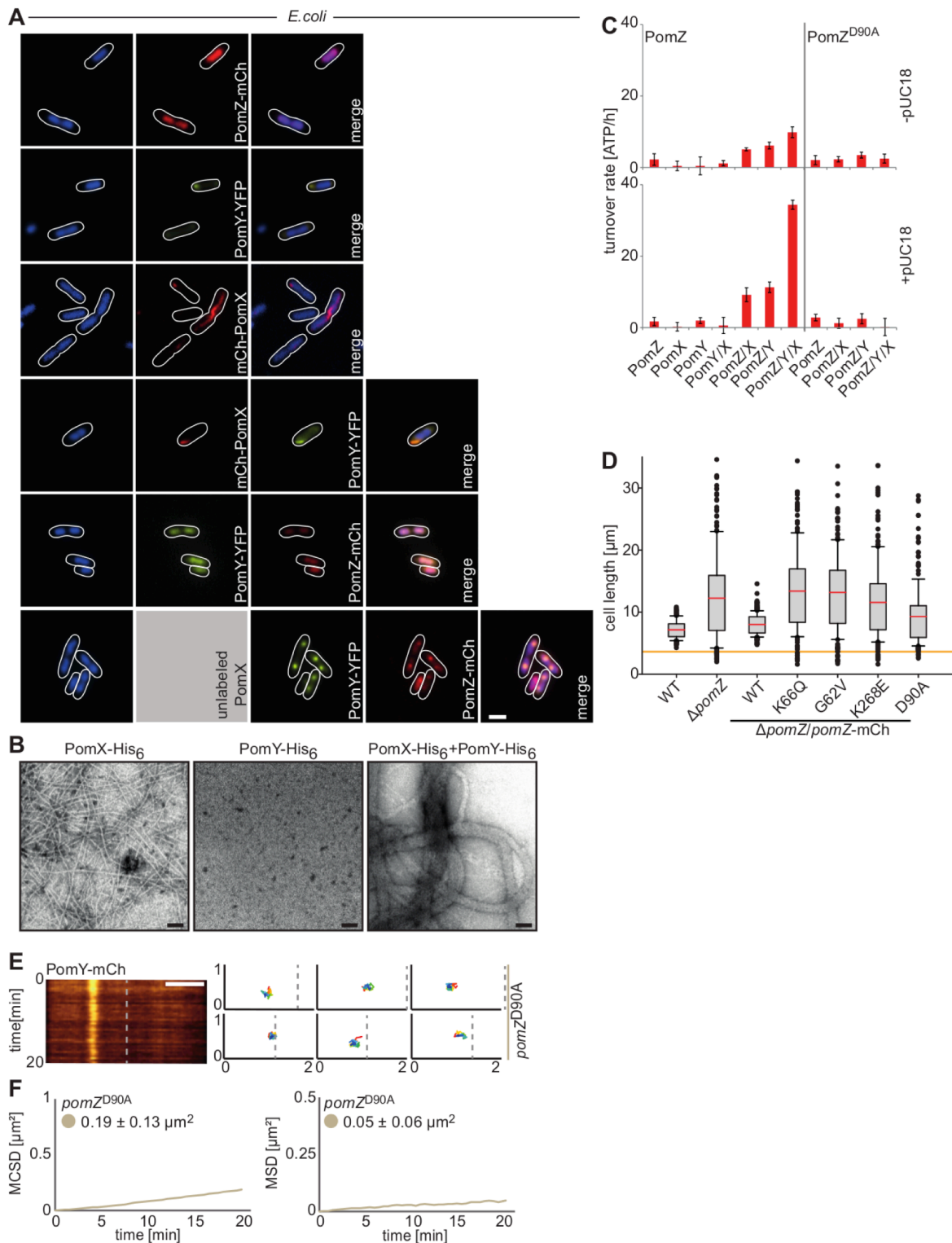

Figure 5: PomX, PomY and PomZ interact in all pairwise combinations and PomXY stimulate PomZ ATPase activity.

A. PomX, PomY and PomZ self-assemble to form clusters that colocalize with the nucleoid in *E. coli*. PomX, PomY, and PomZ were expressed separately (top three rows) or in different combinations

13

(bottom three rows) and cells DAPI-stained (left column) to visualize nucleoids. Note that PomX was expressed without a fluorescent tag in the experiments in the bottom row (grey box). In three top rows, PomZ-mCh, mCh-PomX and PomY-eYFP expression was induced in *E. coli* BL21 DE3 by 0.05mM IPTG for 1 hr. For PomZ-mCh/PomY-eYFP and mCh-PomX/PomY-eYFP co-expression, PomZ-mCh and mCh-PomX expression was induced as described and PomY-eYFP by 0.015% arabinose. For PomZ-mCh/PomY-eYFP/PomX co-expression, PomZ-mCh and PomY-eYFP expression was induced for 1 hr with 0.05mM IPTG before PomX expression was induced with 0.015% arabinose for 30 min. Cells were treated with chloramphenicol for 30 min before DAPI staining. Scale bar, 2µm.

B. PomX-His$_6$ forms filaments that are bundled by PomY-His$_6$ *in vitro*. EM images of negatively stained PomX-His$_6$ (final concentration 3µM) and PomY-His$_6$ (final concentration 3µM) alone and after mixing in a 1:1 molar ratio (final concentration 3µM each). Scale bar, 100nm.

C. MalE-PomZ ATPase activity is stimulated by PomXY complex. Specific ATPase activity of MalE-PomZ and MalE-PomZ^{D90A} (final concentration 2µM) was measured in the presence of 1mM ATP, with or without PomX-His$_6$/PomY-His$_6$ (final concentration 2µM each) and with or without 5nM pUC18 plasmid. Experiments were performed in triplicates and results shown as mean ± SD.

D. PomZ variants affected in ATPase cycle do not correct division defects in Δ*pomZ* mutant. Box plots as in Fig. 1B. Strains used from left to right: DK1622, SA3108, SA3131, SA5001, SA5000, SA5837, SA3146.

E. Kymographs and two-dimensional trajectories of PomY-mCh translocation in presence of PomZ^{D90A}. Kymographs and trajectories as in Fig. 4B. Cells expressing *pomZ*^{D90A} rarely have PomY-mCh clusters at midcell and therefore clusters were not divided into off-centre and midcell. Scale bar, 2µm.

F. Quantification of PomY-mCh cluster translocation in presence of PomZ^{D90A}. Cluster centroids were tracked (n >50) and used to calculate MCSD and MSD.

See also Fig. S4 and S6.

Next, we tested if PomX and/or PomY affect PomZ ATPase activity *in vitro* (Fig. 5C). In agreement with previous data (Treuner-Lange et al., 2013), ATPase activity by MalE-PomZ^{WT} alone was low (2.2±1.6 ATP hr^{-1}). As expected, MalE-PomZ^{D90A} alone also had a low ATPase activity (2.1±1.3 ATP hr^{-1}). Equimolar amounts of PomX-His$_6$ or PomY-His$_6$ stimulated MalE-PomZ^{WT} ATPase activity ~2- and ~3-fold, respectively and PomX and PomY together stimulated PomZ ATP hydrolysis ~5-fold resulting in a turnover rate of 9.9±1.5 ATP hr^{-1}. By contrast, PomX-His$_6$ and PomY-His$_6$ alone or together had no effect on MalE-PomZ^{D90A} ATPase activity.

Because PomZ-mCh binds nonspecifically to the nucleoid in *M. xanthus* and in *E. coli*, contains the conserved amino acid residue important for nonspecific DNA binding by other ParA ATPases (Fig. S6BC), and ATP hydrolysis by ParA ATPases is stimulated by nonspecific DNA binding, we tested ATP hydrolysis by MalE-PomZ^{WT} in the presence of nonspecific DNA. Under these conditions, ATPase activity by MalE-PomZ^{WT} alone was not stimulated (1.7±1.2 ATP hr^{-1}). PomX-His$_6$ and PomY-His$_6$ independently stimulated MalE-PomZ^{WT} ATPase activity to 9.2±1.9 ATP hr^{-1} and 11.3±1.5 ATP hr^{-1}; however, the two proteins synergistically stimulated MalE-PomZ^{WT} ATPase activity to 34.4±1.3 ATP hr^{-1}. PomX-His$_6$ and PomY-His$_6$ alone or together did not stimulate ATPase activity of MalE-PomZ^{D90A} in the presence of DNA. PomX and PomY do not contain DNA binding domains and do not appear to bind to the nucleoid *in vivo*. Therefore, these observations strongly suggest that PomX and PomY in the PomXY complex function synergistically to stimulate

ATP hydrolysis by PomZ bound nonspecifically to DNA. Moreover, we conclude that PomZ^{D90A} is severely reduced in ATP hydrolysis.

ATP-bound dimeric PomZ recruits the PomXY complex to the nucleoid

To analyze if the ATPase cycle of PomZ is important for function, we introduced substitutions into PomZ that block this cycle at specific steps (Fig. S6BC). These substitutions in PomZ correspond to PomZ^{K66Q} and PomZ^{G62V}, which are predicted monomeric variants, PomZ^{K268E}, which is predicted to be blocked in DNA binding, and PomZ^{D90A}, which is strongly reduced in ATP hydrolysis as shown above and is predicted to be locked in the ATP-bound dimeric form that binds DNA nonspecifically. As expected, in *E. coli* PomZ^{D90A}-mCh, similarly to PomZ^{WT}-mCh, perfectly colocalized with the nucleoid while PomZ-mCh variants carrying the K66Q, G62V or K268E substitutions displayed diffuse localization, filling the nucleoid-free areas with fluorescent signal (Fig. S6D). We conclude that ATP-bound dimeric PomZ binds the nucleoid nonspecifically whereas monomeric PomZ does not. The observation that PomZ^{WT} colocalizes with the *E. coli* nucleoid also strongly suggests that PomZ^{WT} spontaneously binds ATP and dimerizes.

Importantly, none of the PomZ variants fused to mCh and expressed at native levels in *M. xanthus* (Fig. S6EF) complemented the cell division defect of the Δ*pomZ* mutant (Fig. 5D). Notably, all three variants unable to bind DNA failed to form clusters and displayed diffuse localization (Fig. S6E), demonstrating that they are unable to interact with PomXY to form a cluster. PomZ^{D90A}-mCh formed a single cluster somewhere on the nucleoid (Fig. S6E). Most of PomZ^{D90A}-mCh localized to this cluster. The PomZ^{D90A}-mCh cluster colocalized with PomY-eYFP demonstrating that it is associated with the PomXY complex (Fig. S6G). Consistently, PomZ^{D90A}-mCh cluster formation absolutely depended on PomX (Fig. S6H). Finally, we characterized cluster dynamics in the presence of PomZ^{D90A}. As shown in Fig. 5EF, the clusters showed little motion as in the Δ*pomZ* mutant (Cf. Fig. 4BC). Altogether, these data demonstrate that the conformation of PomZ that binds to the nucleoid, recruits the PomXY cluster to the nucleoid, and interacts with PomXY to generate the PomZ cluster, is the dimeric ATP-bound form. Moreover, ATP hydrolysis by PomZ is essential for PomXYZ cluster motion.

PomZ is rapidly turned over in the PomXYZ cluster and highly dynamic on the nucleoid

ATP-bound dimeric PomZ bound to the nucleoid interacts with the PomXY complex *in vivo*. However, PomXY strongly stimulates ATP hydrolysis by PomZ when PomZ binds to DNA *in vitro*. If this stimulation also occurs *in vivo*, then the prediction is that PomZ rapidly turns over in the PomXYZ cluster. To test this prediction, we performed fluorescence recovery after photobleaching (FRAP) experiments. After short 60 msec laser pulses were applied to bleach PomZ-mCh clusters, their fluorescence was restored within 9 sec with half maximal recovery ($t_{1/2}$) of 1.2±0.2 sec (n=20) (Fig. 6A). During the 60 msec laser pulse, the PomZ-mCh signal on the nucleoid outside of the cluster was also bleached (Fig. 6A) suggesting that PomZ is not only rapidly turned over in the cluster but also highly dynamic on the nucleoid. To this end, we bleached PomZ-mCh in a small region on the nucleoid outside of a cluster for 60 msec. During this short laser pulse, the entire PomZ-mCh signal on the bleached side of the nucleoid relative to the PomZ-mCh cluster was reduced (Fig. 6A).

Quantitative analyses showed that concurrent with the fast recovery of fluorescence signal on the bleached side of the nucleoid ($t_{1/2}$=1.7±0.4 sec; n=18), the signals in the cluster and on the unbleached side of the nucleoid lost intensity restoring a pre-bleach situation within 9 sec (Fig. 6A). Thus, unbleached PomZ-mCh in the cluster and on the unbleached side rapidly exchange with proteins on the bleached side.
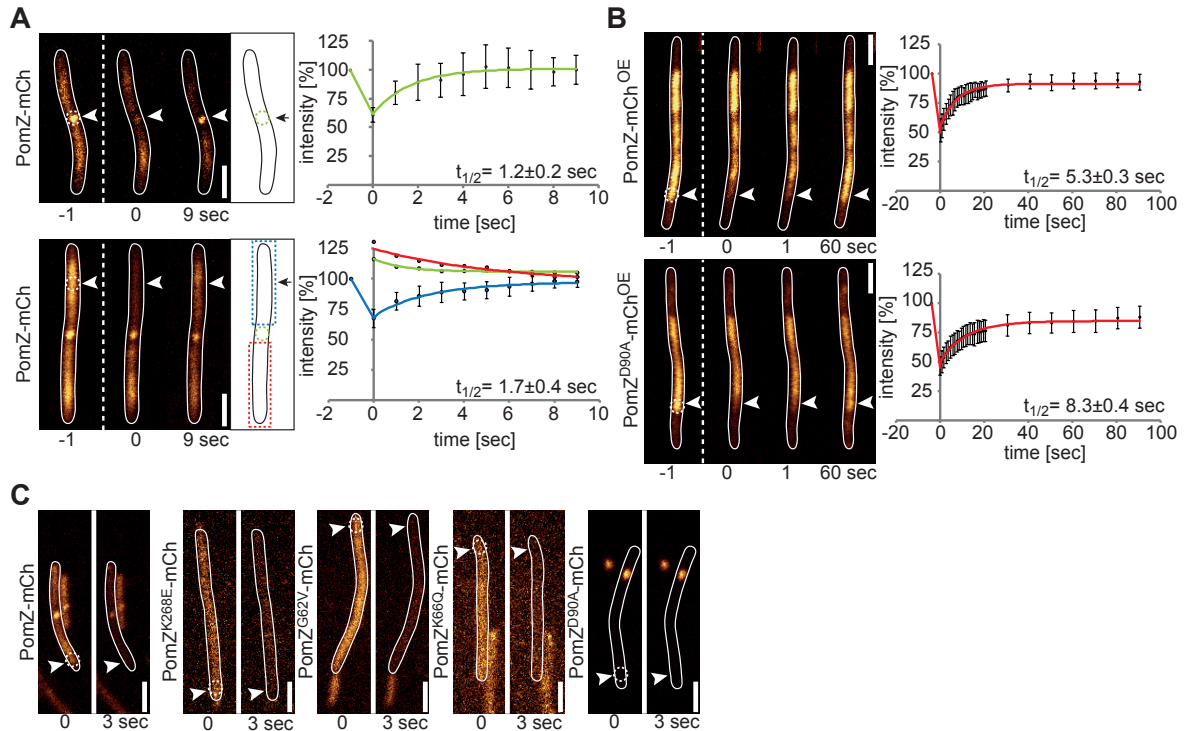

Figure 6: PomZ is rapidly exchanged in the PomXYZ cluster and diffuses rapidly on the nucleoid.

A. FRAP analysis of PomZ-mCh. A 5 pixel region (stippled circles) on the PomZ-mCh cluster (upper panel) or on the nucleoid outside of the cluster (lower panel) was photo-bleached, and recovery followed. Images were recorded every second. White arrows indicate regions of interest before and after bleaching. Scale bar, 2μm. Stippled lines indicate photo-bleaching event. Cartoons show areas used for recovery measurements in stippled colored lines and graphs show average relative integrated intensities in these areas as a function of time. Recovery half-time ($t_{1/2}$) was determined by fitting the mean data to a single-exponential function (n=20).

B. FRAP analysis on overexpressed PomZ-mCh variants. Cells overexpressing (OE) PomZ-mCh or PomZ^{D90A}-mCh were subjected to photo-bleaching in a 5 pixel region (stippled circles), and recovery followed. Stippled lines indicate photo-bleaching event. Images were acquired every 300 msec for 20 sec and then every 5 sec. Graphs represent average relative integrated intensities of the bleached region as a function of time. Recovery half-time ($t_{1/2}$) calculated as in A (n=20). White arrows as in A. Scale bar, 2μm. Strains used from top to bottom: SA7011, SA4799.

C. Photo-bleaching experiments with PomZ-mCh variants. Cells expressing PomZ-mCh variants were photo-bleached for 3 sec in a 5 pixel region (stippled circles) on the nucleoid outside of the cluster in the case of PomZ^{WT} and PomZ^{D90A} and on the nucleoid in the case of the three remaining strains. White arrows are as in A. Scale bar, 2μm. Strains used from left to right: SA3131, SA5837, SA5000, SA5001, SA3146.

To analyze if ATP-bound PomZ dimers undergo diffusion on the nucleoid, we bleached a small region on the nucleoid in strains overexpressing PomZ^{WT}-mCh or PomZ^{D90A}-mCh >50-fold (Fig. S1G; 6B). In these two strains, the fusion proteins create an intense signal colocalizing with the nucleoid and a cluster is not visible (Fig. 6B). A 160 msec laser pulse resulted in bleaching of the signal on the nucleoid outside of the bleached region. The signal in the bleached region recovered within 30 sec with a half-maximal recovery of 5.3±0.3 sec (PomZ^{WT}) and 8.3±0.4 sec (PomZ^{D90A}). Because PomZ^{D90A}-mCh is locked in the ATP-bound dimeric form that binds to the nucleoid, this signal recovery is the result of diffusion of the protein on the nucleoid and not the result of rebinding to the nucleoid of PomZ dimers generated from a pool of monomers after ATP hydrolysis. As PomZ^{WT}-mCh and PomZ^{D90A}-mCh show the same overall recovery kinetics these data imply that dimeric ATP-bound PomZ^{WT} diffuses rapidly on the nucleoid generating a diffusive PomZ flux on the nucleoid and that this flux contributes to signal recovery in the PomZ cluster and on the nucleoid.

To determine if the fast turnover of PomZ in the cluster depends on ATP hydrolysis, we analyzed cells expressing PomZ^{D90A}-mCh at native levels. Because most of PomZ^{D90A}-mCh is in the PomXYZ cluster, we adopted a bleaching approach in which a laser pulse was applied for 3 sec to the nucleoid outside of the cluster. After this pulse, the PomZ^{D90A}-mCh signal was unaffected (Fig. 6C). By contrast, the total cellular PomZ^{WT}-mCh signal was strongly decreased after the 3 sec laser pulse demonstrating that most PomZ^{WT} molecules had passed through the bleached area within 3 sec and confirming that PomZ^{WT}-mCh is highly dynamic. As expected, the signals from the diffusely localized PomZ^{K268E}, PomZ^{K66Q} and PomZ^{G62V}-variants were also almost completely bleached during the 3 sec bleach (Fig. 6C). We conclude that ATP hydrolysis is essential for the fast turnover of PomZ in the cluster.

A computational model for PomZ-dependent translocation and positioning of the PomXYZ complex

To understand the emergent properties of the Pom system, i.e. how the local protein/protein/DNA interactions in the PomXYZ complex are converted into a global cellular positioning system that is able to "sense" cluster position within cellular space and adjusts cluster motion accordingly, we searched for an experimentally-based mechanism that would give rise to a biased random walk of the PomXYZ complex to midnucleoid and constrained motion at midnucleoid at midcell (Fig. 7A). Three models have been suggested for ParA-dependent ParB/parS translocation. However, none of these are compatible with the experimental findings on the motion of the PomXYZ complex (STAR*Methods). Instead, to explain the intracellular patterning of the Pom proteins, we propose a PomZ flux-based mechanism that builds on the mechanism recently proposed for equi-positioning of plasmids (Ietswaart et al., 2014).
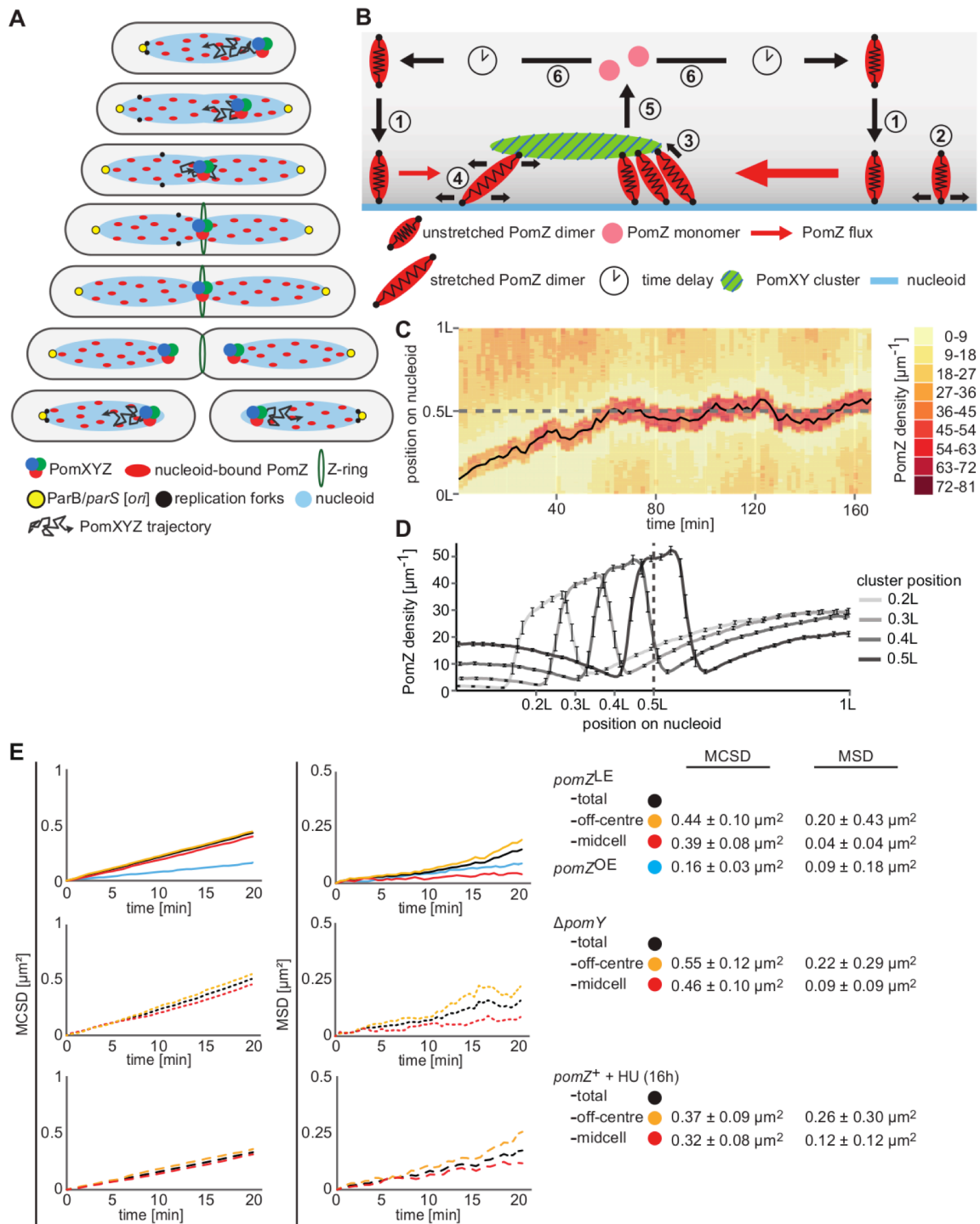
Figure 7: A PomZ flux-based mechanism for midcell positioning of the PomXYZ complex.

A. PomXYZ complex is dynamically localized on the nucleoid. Schematic illustrates localization of the complex starting with a cell immediately after division (top). Trajectories indicate the imminent biased random motion of off-centre complexes towards midcell and constrained motion at midcell.

B. Schematic of the PomZ flux-based model. Structures are not drawn to scale. See main text for details.

C. Kymograph showing representative simulation of PomZ localization on the nucleoid. The parameters listed in Table S2 were used in the simulation. The PomZ distribution is averaged over time in intervals of about 100 sec and plotted against time. Here, the equilibrium positions of the PomZ

dimers are used. Right, color code for PomZ density. Black line shows the trajectory of the midpoint of the cluster. Nucleoid length is denoted by L and dashed grey line indicates midnucleoid.

D. Average density of PomZ on the nucleoid for different cluster positions. PomZ density profile on the nucleoid (as shown in C over time for one run) were averaged when the cluster passed 0.2L, 0.3L, 0.4L and 0.5L (midnucleoid, dashed grey line) for the first time using 100 runs of the stochastic simulation. Error bars indicate 95% confidence intervals and are shown for ~5% of the average density values.

E. Quantification of PomY-mCh and mCh-PomX cluster translocation. Cluster centroids were tracked (n >50 per strain) and used to calculate MCSD and MSD. To quantify PomY-mCh cluster dynamics at low PomZ levels ($pomZ^{LE}$) $pomZ$ expression was induced using 3µM vanillate for 48 hrs. Cells were exposed to HU for 16 hrs before microscopy. Strains used from top to bottom: SA7070, SA7022, SA7008, SA4746.

See also Fig. S7 and S8.

In this model (STAR*Methods), the PomXY cluster is an object with a fixed composition of PomX and PomY molecules and with a molecular weight of ~15 MDa. Hence, we reduce the system to a model consisting of the PomXY cluster, the nucleoid, and PomZ. For simplicity, the nucleoid and the PomXY cluster are modeled as one-dimensional lattices on which PomZ dimers can diffuse. In this model (Fig. 7B; S7A), ATP-bound PomZ dimers use the nucleoid as a scaffold to which they attach (1) and rapidly diffuse on (2). When bound to the nucleoid, PomZ dimers can also bind to and interact with the PomXY cluster (3). PomZ dimers that are doubly bound to the nucleoid and PomXY can diffuse relative to both (4). ATPase activity of PomZ is stimulated when in contact with both the nucleoid and PomXY; after ATP hydrolysis, ADP-bound PomZ monomers are released (5) and undergo fast diffusion in the cytosol (6). Importantly, before PomZ can reattach to the nucleoid, the monomers have to undergo nucleotide exchange and dimerize giving rise to a time delay (clock symbol). In this model, the PomXY cluster acts as a sink for PomZ dimers diffusing on the nucleoid but the cluster is not an absolute barrier for PomZ, i.e. PomZ dimers can pass below the cluster without binding to it. Because PomZ dimers diffuse rapidly on the nucleoid (and much faster than the cluster moves) and the PomXY cluster acts as a sink for diffusing PomZ dimers on the nucleoid, the difference in the PomZ flux into the cluster from the two sides along the long cell axis depends on the position of the cluster (Ietswaart et al., 2014).In the case of an off-centre cluster (Fig. 7B), more PomZ dimers arrive at the cluster from the side with the longer distance to the nucleoid end (i.e., from the right in Fig. 7B). This flux difference translates into an asymmetric concentration profile of PomZ dimers bound to the cluster, i.e. a local PomZ concentration gradient across the cluster, with the highest concentration on the side facing most of the nucleoid (Fig. 7CD). In the case of a cluster at midnucleoid, the PomZ fluxes into the cluster from the two sides equalize and the concentration profile of PomZ over the cluster is essentially symmetric (Fig. 7CD).

It is not known how PomZ dimers generate the force to move the cluster. However, the chromosome has elastic properties (Wiggins et al., 2010; Lim et al., 2014) that can be harnessed to relay a ParB/parS complex across the steep gradient of nucleoid-bound ParA dimers (Lim et al., 2014). Proteins may also act as elastic force bearing structures (Dietz and Rief, 2008). In our model, we effectively account for both sources of elasticity by modelling PomZ dimers as springs. Therefore, this aspect of our model is similar to the DNA-relay mechanism (Lim et al., 2014) (STAR*Methods). In this scenario, there is a tug of war between PomZ dimers arriving from the left and right into the cluster: Some of the PomZ

dimers arriving at the cluster from the right will bind to the cluster in a stretched conformation and generate a mechanical force that points to the right. Similarly, PomZ dimers arriving from the left will generate a force pointing to the left. Therefore, any flux imbalance leads to a net force in the direction of the higher PomZ flux. In the case of off-centre clusters, this force points towards midnucleoid. In the case of clusters at midnucleoid, the PomZ flux from both sides equalizes, and, therefore, no net force is exerted on the cluster. Therefore, as long as the PomXY cluster preferentially moves in the direction of the highest PomZ flux, the proposed mechanism will result in biased random motion towards midnucleoid for off-centre clusters and constrained motion for clusters at midnucleoid, independently of the precise molecular mechanism giving rise to the forces resulting in cluster motion. Remarkably, this model reproduces off-centre to midnucleoid relocalization as well as constrained motion at midnucleoid of the PomXYZ cluster for physiological relevant parameters (STAR*Methods; Table S1, S2) with a timing similar to that observed *in vivo* (Fig. 7C and S7BC; Cf. 4A).

The time delay between detachment of ADP-bound PomZ monomers from the cluster and subsequent reattachment of ATP-bound PomZ dimers to the nucleoid is important to guarantee that a PomZ flux imbalance into the cluster correlates with the asymmetry of the cluster position on the nucleoid. If PomZ monomers would regain the ability to bind DNA quickly, they would preferentially bind to the nucleoid in close proximity to the cluster resulting in a decrease in the flux difference of PomZ dimers into the cluster from the two sides.

Testing the model experimentally
The model predicts that reduced as well as increased PomZ levels would reduce cluster motion (STAR*Methods; Fig. S7D). Indeed, if the PomZ level is reduced two-fold *in vivo* (Fig. S7E), we observe less motion of the clusters compared to WT but still with an overall bias towards midnucleoid for off-centre clusters and constrained motion for clusters at midnucleoid (Fig. 7E; S7F; Cf. 4BC). Moreover, after >50-fold overexpression of PomZ-mCh PomXYZ cluster motion was significantly reduced and similar to that in the Δ*pomZ* mutant (Fig. 7E; S7F; Cf. 4BC). The model further predicts that reduced PomZ ATPase activity would reduce the bias of cluster motion towards midcell (STAR*Methods; Fig. S7G). Indeed, in the presence of PomZ[D90A] *in vivo*, cluster motion is strongly reduced (Fig. 5EF). In the absence of a PomZ variant with an intermediate ATPase activity, we took advantage of the synergistic stimulation of PomZ ATPase activity *in vitro* by PomX and PomY. To this end, we analyzed the dynamics of PomX clusters in the absence of PomY. Off-centre as well as midcell clusters showed motion (Fig. S7H); importantly, MCSD for both cluster populations and MSD for off-centre clusters were significantly lower than in WT but still higher than in the PomZ[D90A] mutant (Fig. 7E; Cf. 4BC and 5EF). With the caveats that PomX clusters in the absence of PomY are differently shaped than in the presence of PomY and may not all contain PomZ (Cf. Fig. 2C), these data are in agreement with the prediction that reduced ATPase activity reduces cluster motion towards midcell and the mobility of the cluster in general.

We also predicted that perturbing the nucleoid structure would interfere with proper translocation. In *M. xanthus* cells treated for 16 hrs with 50mM hydroxyurea (HU) the nucleoid had condensed; however, PomY still formed off-centre and midcell clusters as in

untreated cells (Fig. S7IJ). Importantly, both cluster populations were less motile than in untreated cells and with significantly reduced MCSD and MSD (Fig. 7E; S7K).

Discussion

Here, we uncover a mechanism used by bacteria to regulate cell division. We show that PomX and PomY function together with the ParA/MinD ATPase PomZ to stimulate and position the site of cell division in *M. xanthus* by stimulating Z-ring formation as well as positioning at midcell. Several lines of evidence support the notion that the PomXYZ complex directly recruits FtsZ to the division site. First, fewer Z-rings are formed in the absence of any of the three Pom proteins and the few Z-rings formed are localized along the cell length. Second, the PomXYZ complex localizes to the future division site at midcell before and in the absence of FtsZ [here; (Treuner-Lange et al., 2013)]. Third, all three Pom proteins in the PomXYZ complex colocalize with FtsZ at the division site [here; (Treuner-Lange et al., 2013)]. Fourth, PomY and PomZ interact directly with FtsZ. Based on these observations, we conclude that the PomXYZ proteins constitute a system for regulation of bacterial cell division and function to mark the incipient division site, recruit FtsZ to this site and stimulate Z-ring formation.

PomZ shares characteristics with other ParA ATPases of the ParA/MinD superfamily. First, PomZ has a low intrinsic ATPase activity. Second, a mutational analysis supports that PomZ dimerizes and binds DNA nonspecifically upon ATP binding, is monomeric in the ADP-bound form and in the apo-form, and spontaneously undergoes ADP-to-ATP nucleotide exchange. Third, ATPase activity is stimulated by nonspecific DNA binding and by AAPs. PomX and PomY independently stimulate ATP hydrolysis by DNA-bound PomZ equally well; however, they function synergistically to stimulate ATP hydrolysis by DNA-bound PomZ suggesting that PomX and PomY may interact differently with PomZ. To our knowledge, PomZ is the first ParA/MinD ATPase with two distinct AAPs. Interestingly, PomX, PomY, ParB and MinE are all non-homologous.

Genetic analyses in *M. xanthus* together with heterologous expression experiments in *E. coli* demonstrated that the three Pom proteins are not only required but also sufficient for the formation of the ~15 MDa nucleoid-associated PomXYZ complex. The Pom proteins have distinct functions in this complex. In a co-factor independent manner, PomX assembles into filaments *in vitro* and PomY bundles these filaments. In the absence of PomY in *M. xanthus*, PomX assembles into ovoid clusters suggesting that PomX also self-assembles *in vivo*. In the presence of PomY, the PomX clusters become more round suggesting that PomY also *in vivo* modulates the structural arrangement of self-assembled PomX. *In vivo* this PomXY complex is not associated with the nucleoid, and is stalled randomly in cells. ATP and nucleoid-bound PomZ dimers interact with the PomXY complex and tether it to the nucleoid giving rise to the complex in which PomXYZ colocalize. The nucleoid-associated PomXY complex is highly dynamic and translocates across the nucleoid to the midnucleoid at midcell in a biased random walk and undergoes constrained motion at the midnucleoid at midcell. Both types of motion depend on PomXY stimulated ATP hydrolysis by PomZ.

To understand how the interactions between the Pom proteins and the nucleoid results in localization of the PomXYZ cluszer at midcell, we developed a mathematical model that recapitulates the *in vivo* behavior of the PomXYZ system. A key aspect in this model is that the diffusive flux of nucleoid-bound PomZ into the PomXYZ cluster from either side of the cluster scales with the length of the nucleoid to the left or right side of the cluster. A difference between the two PomZ fluxes into the cluster results in a local PomZ concentration gradient across the cluster, with the highest concentration on the side facing most of the nucleoid. As long as the cluster preferentially moves in the direction of the highest PomZ flux, then off-centre PomXYZ clusters will have a bias for translocation in the direction facing most of the nucleoid. If the cluster is at midnucleoid, which coincides with midcell until the chromosomes have segregated, the PomZ flux from the two sides equalizes, and, therefore, PomZ has an almost symmetric distribution over the cluster and cluster motion, as observed experimentally, is constrained to midcell. Of note, should the cluster overshoot in one direction and leave the midcell area, then the system is self-correcting and will eventually bring the cluster back to the midnucleoid at midcell. Thus, in this model, the difference between the two diffusive PomZ fluxes into the cluster is a proxy for PomXYZ cluster asymmetry on the nucleoid and converts the global intracellular asymmetry of the PomXYZ complex into a local PomZ concentration gradient over the cluster. ParA/MinD ATPases together with their AAP(s) can self-organize giving rise to different patterns within cells using the membrane or the nucleoid as a scaffold. We suggest that tuning of the interactions between a ParA/MinD ATPase, its cognate AAP(s) and scaffold ultimately results in different patterns formed including pole-to-pole oscillations, bipolar gradients and, as shown here, a biased random walk to midnucleoid and constrained motion at midnucleoid.

Systems that regulate Z-ring positioning and in that way cell division generally couple chromosome replication and segregation to cell division to ensure that each daughter cell receives the correct chromosome complement. In the case of the PomXYZ system, our data suggest that PomY as well as PomZ in the PomXYZ complex directly interact with FtsZ to stimulate Z-ring formation and positioning. However, the PomXYZ complex colocalizes over the midnucleoid at midcell with the Z-ring for several hours before replication and segregation are complete and cell constriction initiates. As in other bacteria, the precise cue that triggers the cytokinetic machinery including FtsZ to initiate constriction in *M. xanthus* is not known. Similarly, we do not know why the PomXYZ complex only recruits FtsZ at the midnucleoid at midcell and not during the translocation from an off-centre position to the midnucleoid. These questions will be addressed in future experiments.

Author contributions
Conceived and designed experiments: DS, LS-A
Developed theoretical concepts and models: EF, SB
Performed experiments: AH, DS, JV
Analyzed data: DS, EF, LS-A, SB
Contributed reagents/materials/analysis tools: SH
Wrote paper: DS, EF, LS-A, SB

References

Ah-Seng, Y., Lopez, F., Pasta, F., Lane, D. and Bouet, J.-Y. (2009) Dual role of DNA in regulating ATP hydrolysis by the SopA partition protein. J Biol Chem *284*, 30067-30075.

Barillà, D., Carmelo, E. and Hayes, F. (2007) The tail of the ParG DNA segregation protein remodels ParF polymers and enhances ATP hydrolysis via an arginine finger-like motif. Proc Natl Acad Sci USA *104*, 1811-1816.

Bi, E.F. and Lutkenhaus, J. (1991) FtsZ ring structure associated with division in *Escherichia coli*. Nature *354*, 161-164.

Bulyha, I., Schmidt, C., Lenz, P., Jakovljevic, V., Höne, A., Maier, B., Hoppert, M. and Søgaard-Andersen, L. (2009) Regulation of the type IV pili molecular machine by dynamic localization of two motor proteins. Mol Microbiol *74*, 691–706.

Dietz, H. and Rief, M. (2008) Elastic bond network model for protein unfolding mechanics. Phys Rev Lett *100*, 098101.

Easter, J. and Gober, J.W. (2002) ParB-stimulated nucleotide exchange regulates a switch in functionally distinct ParA activities. Mol Cell *10*, 427-434.

Fange, D. and Elf, J. (2006) Noise-induced Min phenotypes in *E. coli*. PLoS Comput Biol *2*, e80.

Gillespie, D.T. (1976) A general method for numerically simulating the stochastic time evolution of coupled chemical reactions. J Comp Physics *22*, 403-434.

Gillespie, D.T. (1977) Exact stochastic simulation of coupled chemical reactions. J Phys Chem *81*, 2340-2361.

Gómez-Santos, N., Treuner-Lange, A., Moraleda-Muñoz, A., García-Bravo, E., García-Hernández, R., Martínez-Cayuela, M., Pérez, J., Søgaard-Andersen, L. and Muñoz-Dorado, J. (2012) Comprehensive set of integrative plasmid vectors for copper-inducible gene expression in *Myxococcus xanthus*. Appl Environ Microbiol *78*, 2515-2521.

Halatek, J. and Frey, E. (2012) Highly canalized MinD transfer and MinE sequestration explain the origin of robust MinCDE-protein dynamics. Cell Rep *1*, 741-752.

Harms, A., Treuner-Lange, A., Schumacher, D. and Søgaard-Andersen, L. (2013) Tracking of chromosome and replisome dynamics in *Myxococcus xanthus* reveals a novel chromosome arrangement. PLoS Genet *9*, e1003802.

Hester, C.M. and Lutkenhaus, J. (2007) Soj (ParA) DNA binding is mediated by conserved arginines and is essential for plasmid segregation. Proc Natl Acad Sci U S A *104*, 20326-20331.

Hodgkin, J. and Kaiser, D. (1977) Cell-to-cell stimulation of movement in nonmotile mutants of *Myxococcus*. Proc Natl Acad Sci USA *74*, 2938-2942.

Howard, M., Rutenberg, A.D. and de Vet, S. (2001) Dynamic compartmentalization of bacteria: accurate division in *E. coli*. Phys Rev Lett *87*, 278102.

Hu, L., Vecchiarelli, A.G., Mizuuchi, K., Neuman, K.C. and Liu, J. (2015) Directed and persistent movement arises from mechanochemistry of the ParA/ParB system. . Proc Natl Acad Sci USA *112*, E7055-E7064.

Hu, Z., Gogol, E.P. and Lutkenhaus, J. (2002) Dynamic assembly of MinD on phospholipid vesicles regulated by ATP and MinE. Proc Natl Acad Sci USA *99*, 6761-6766.

Hu, Z. and Lutkenhaus, J. (1999) Topological regulation of cell division in *Escherichia coli* involves rapid pole to pole oscillation of the division inhibitor MinC under the control of MinD and MinE. Mol Microbiol *34*, 82-90.

Hu, Z. and Lutkenhaus, J. (2001) Topological regulation of cell division in *E. coli*. spatiotemporal oscillation of MinD requires stimulation of its ATPase by MinE and phospholipid. Mol Cell *7*, 1337-1343.

Hu, Z., Mukherjee, A., Pichoff, S. and Lutkenhaus, J. (1999) The MinC component of the division site selection system in *Escherichia coli* interacts with FtsZ to prevent polymerization. Proc Natl Acad Sci U S A *96*, 14819-14824.

Huang, K.C., Meir, Y. and Wingreen, N.S. (2003) Dynamic structures in *Escherichia coli*: Spontaneous formation of MinE rings and MinD polar zones. Proc Natl Acad Sci USA *100*, 12724-12728.

Huntley, S., Hamann, N., Wegener-Feldbrügge, S., Treuner-Lange, A., Kube, M., Reinhardt, R., Klages, S., Müller, R., Ronning, C.M., Nierman, W.C. and Søgaard-Andersen, L. (2011) Comparative genomic analysis of fruiting body formation in Myxococcales. Mol Biol Evol *28*, 1083-1097.

Ietswaart, R., Szardenings, F., Gerdes, K. and Howard, M. (2014) Competing ParA structures space bacterial plasmids equally over the nucleoid. PLoS Comput Biol *10*, e1004009.

Iniesta, A.A., García-Heras, F., Abellón-Ruiz, J., Gallego-García, A. and Elías-Arnanz, M. (2012) Two systems for conditional gene expression in *Myxococcus xanthus* inducible by isopropyl-β-d-thiogalactopyranoside or vanillate. J Bacteriol *194*, 5875-5885.

James, P., Halladay, J. and Craig, E.A. (1996) Genomic libraries and a host strain designed for highly efficient two-hybrid selection in yeast. Genetics *144*, 1425-1436.

Kaiser, D. (1979) Social gliding is correlated with the presence of pili in *Myxococcus xanthus*. Proc Natl Acad Sci USA *76*, 5952-5956.

Kruse, K. (2002) A dynamic model for determining the middle of *Escherichia coli*. Biophys J *82*, 618-627.

Lackner, L.L., Raskin, D.M. and de Boer, P.A.J. (2003) ATP-dependent interactions between *Escherichia coli* Min proteins and the phospholipid membrane *in vitro*. J Bacteriol *185*, 735-749.

Lansky, Z., Braun, M., Lüdecke, A., Schlierf, M., ten Wolde, P.R., Janson, M.E. and Diez, S. (2015) Diffusible crosslinkers generate directed forces in microtubule networks. Cell *160*, 1159-1168.

Leonard, T.A., Butler, P.J. and Löwe, J. (2005) Bacterial chromosome segregation: structure and DNA binding of the Soj dimer--a conserved biological switch. EMBO J *24*, 270-282.

Letunic, I., Doerks, T. and Bork, P. (2015) SMART: recent updates, new developments and status in 2015. Nucl Acids Res *43*, D257-D260.

Li, W., Cowley, A., Uludag, M., Gur, T., McWilliam, H., Squizzato, S., Park, Y.M., Buso, N. and Lopez, R. (2015) The EMBL-EBI bioinformatics web and programmatic tools framework. Nucl Acids Res *43*, W580-W584.

Lim, H.C., Surovtsev, I.V., Beltran, B.G., Huang, F., Bewersdorf, J. and Jacobs-Wagner, C. (2014) Evidence for a DNA-relay mechanism in ParABS-mediated chromosome segregation. Elife *3*, e02758.

Loose, M., Fischer-Friedrich, E., Ries, J., Kruse, K. and Schwille, P. (2008) Spatial regulators for bacterial cell division self-organize into surface waves *in vitro*. Science *320*, 789-792.

Lutkenhaus, J. (2012) The ParA/MinD family puts things in their place. Trends Microbiol *20*, 411-418.

Lutkenhaus, J., Pichoff, S. and Du, S. (2012) Bacterial cytokinesis: From Z ring to divisome. Cytoskeleton (Hoboken) *69*, 778-790.

Meinhardt, H. and de Boer, P.A.J. (2001) Pattern formation in *Escherichia coli*: A model for the pole-to-pole oscillations of Min proteins and the localization of the division site. Proc Natl Acad Sci USA *98*, 14202-14207.

Miertzschke, M., Koerner, C., Vetter, I.R., Keilberg, D., Hot, E., Leonardy, S., Søgaard-Andersen, L. and Wittinghofer, A. (2011) Structural analysis of the Ras-like G protein MglA and its cognate GAP MglB and implications for bacterial polarity. EMBO J *30*, 4185-4197.

Ptacin, J.L., Lee, S.F., Garner, E.C., Toro, E., Eckart, M., Comolli, L.R., Moerner, W.E. and Shapiro, L. (2010) A spindle-like apparatus guides bacterial chromosome segregation. Nat Cell Biol *12*, 791-798.

Raskin, D.M. and de Boer, P.A.J. (1999) Rapid pole-to-pole oscillation of a protein required for directing division to the middle of *Escherichia coli*. Proc Natl Acad Sci USA *96*, 4971-4976.

Ringgaard, S., van Zon, J., Howard, M. and Gerdes, K. (2009) Movement and equipositioning of plasmids by ParA filament disassembly. Proc Natl Acad Sci U S A *106*, 19369-19374.

Sambrook, J. and Russell, D.W. (2001). Molecular cloning: a laboratory manual, 3rd edn (Cold Spring Harbor, N.Y.: Cold Spring Harbor Laboratory Press).

Schindelin, J., Arganda-Carreras, I., Frise, E., Kaynig, V., Longair, M., Pietzsch, T., Preibisch, S., Rueden, C., Saalfeld, S., Schmid, B., Tinevez, J.Y., White, D.J., Hartenstein, V., Eliceiri, K., Tomancak, P. and Cardona, A. (2012) Fiji: an open-source platform for biological-image analysis. Nat Methods *9*, 676-682.

Schofield, W.B., Lim, H.C. and Jacobs-Wagner, C. (2010) Cell cycle coordination and regulation of bacterial chromosome segregation dynamics by polarly localized proteins. EMBO J *29*, 3068-3081.

Scholefield, G., Whiting, R., Errington, J. and Murray, H. (2011) Spo0J regulates the oligomeric state of Soj to trigger its switch from an activator to an inhibitor of DNA replication initiation. Mol Microbiol *79*, 1089-1100.

Shi, X., Wegener-Feldbrügge, S., Huntley, S., Hamann, N., Hedderich, R. and Søgaard-Andersen, L. (2008) Bioinformatics and experimental analysis of proteins of two-component systems in *Myxococcus xanthus*. J Bacteriol *190*, 613-624.

Thanbichler, M. and Shapiro, L. (2006) MipZ, a spatial regulator coordinating chromosome segregation with cell division in *Caulobacter*. Cell *126*, 147-162.

Touhami, A., Jericho, M. and Rutenberg, A.D. (2006) Temperature dependence of MinD oscillation in *Escherichia coli*: Running hot and fast. J Bacteriol *188*, 7661-7667.

Treuner-Lange, A., Aguiluz, K., van der Does, C., Gomez-Santos, N., Harms, A., Schumacher, D., Lenz, P., Hoppert, M., Kahnt, J., Munoz-Dorado, J. and Søgaard-Andersen, L. (2013) PomZ, a ParA-like protein, regulates Z-ring formation and cell division in *Myxococcus xanthus*. Mol Microbiol *87*, 235-253.

Vecchiarelli, A.G., Hwang, L.C. and Mizuuchi, K. (2013) Cell-free study of F plasmid partition provides evidence for cargo transport by a diffusion-ratchet mechanism. Proc Natl Acad Sci U S A *110*, E1390-1397.

Vecchiarelli, A.G., Neuman, K.C. and Mizuuchi, K. (2014) A propagating ATPase gradient drives transport of surface-confined cellular cargo. Proc Natl Acad Sci U S A *111*, 4880-4885.

Wiggins, P.A., Cheveralls, K.C., Martin, J.S., Lintner, R. and Kondev, J. (2010) Strong intranucleoid interactions organize the *Escherichia coli* chromosome into a nucleoid filament. Proc Natl Acad Sci USA *107*, 4991-4995.

CONTACT FOR REAGENT AND RESOURCE SHARING

EXPERIMENTAL MODEL AND SUBJECT DETAILS

Cell growth of *M. xanthus* strains
DK1622 was used as WT *M. xanthus* strain and all strains are derivatives of DK1622 unless otherwise noted. In-frame deletions were generated as described (Shi et al., 2008). *M. xanthus* was grown at 32°C in 1% CTT medium (Hodgkin and Kaiser, 1977) or on 1.5% agar supplemented with 1% CTT and kanamycin (50µg/ml), oxytetracycline (10µg/ml) or gentamycin (10µg/ml) if appropriate. To induce the expression of genes from P$_{cuoA}$ in *M. xanthus* (Gómez-Santos et al., 2012), the growth medium was supplemented with copper sulfate as indicated in the text. Similarly, to induce the expression of genes from P$_{van}$ in *M. xanthus* (Iniesta et al., 2012) growth media were supplemented with vanillate at indicated concentrations. Plasmids were integrated by site specific recombination into the Mx8 *attB* site or by homologous recombination at the native site, the *cuoA* locus or at the *mxan18-19* intergenic region in the case of vanillate inducible contructs. All in-frame deletions and plasmid integrations were verified by PCR (Sambrook and Russell, 2001).

Cell growth of *E. coli* strains
E. coli was grown in LB or 2xYT medium (Sambrook and Russell, 2001). Plasmids were propagated in *E. coli* TOP10 (F- *mcr*A, Δ(*mrr-hsd*RMS-*mcr*BC), Φ80*lac*ZΔM15, Δ*lac*X74, *deo*R, *rec*A1).To induce expression of genes in *E. coli* for protein localization BL21 (DE3) (*fhuA2 lon ompT gal (λDE3) dcm ΔhsdS λDE3=λsBamHIo ΔEcoRI-B int::(lacI::PlacUV5::T7gene1) i21 Δnin5) was used at 37°C*. Isopropyl-β-D-thiogalactopyranoside (IPTG) or arabinose was added as indicated. Cells were grown in LB medium containing 0.2% glucose.

METHOD DETAILS
Flux-based model for PomXYZ cluster positioning
We searched computationally for mechanisms that could give rise to a biased random walk of the PomXYZ complex to midnucleoid and constrained motion over the midnucleoid. Three models have been suggested for ParA-dependent ParB/*parS* translocation. However, none of these are compatible with the experimental findings on the motion of the PomXYZ complex: In the diffusion-ratchet model, the ParB/*parS* complex motion is slowed down by the interaction with DNA-bound ParA (Vecchiarelli et al., 2013; Vecchiarelli et al., 2014).

However, we observe that PomZ drives motion of the PomXYZ complex (Fig. 4BC). A second model is based on the notion that ParA forms nucleoid-associated filaments (Ringgaard et al., 2009; Ietswaart et al., 2014); however, we have no evidence supporting filament formation by PomZ (Treuner-Lange et al., 2013). The DNA-relay model incorporates that DNA-bound ParA wiggles around due to the elastic properties of DNA (Lim et al., 2014). Because ParA is highly asymmetrically localized forming a steep gradient across the entire nucleoid, this effectively leads to a net force exerted on the ParB/*parS* complex towards a higher ParA concentration and ParB/*parS* translocating up the gradient of nucleoid-bound ParA. However, we observe that PomZ is almost symmetrically distributed on the nucleoid around the PomXYZ cluster.

We propose a model that is based on the following experimental observations and inferences:

1. PomX, PomY and PomZ are required and sufficient for nucleoid-associated cluster formation (Fig. 5A). PomX nucleates the formation of this cluster and PomX and PomY independently of PomZ assemble to form a cluster (Fig. 2C, S3E).

2. PomZ in its ATP-bound dimeric form binds nonspecifically to the nucleoid (Fig. 5A, S6DE), interacts with the PomXY complex and recruits it to the nucleoid (Fig. S3DE).

3. Only nucleoid-bound dimeric PomZ interacts with the PomXY complex (Fig. S6EG).

4. PomZ alone whether bound to DNA or not has a low ATP turnover rate (Fig. 5C). PomX and PomY synergistically stimulate PomZ ATPase activity in the presence of DNA (Fig. 5C) suggesting that PomZ can simultaneously interact with PomXY and DNA.

5. Detachment of a PomZ dimer from the nucleoid depends on ATP hydrolysis (Fig. 6BC). Therefore, detachment of PomZ from the nucleoid occurs primarily at the PomXYZ cluster and PomZ in the PomXYZ cluster exchanges rapidly in an ATP hydrolysis-dependent manner (Fig. 6AC). After ATP hydrolysis, ADP-bound PomZ monomers detach from the nucleoid and the cluster. Before PomZ molecules can rebind to the nucleoid, they undergo ADP-to-ATP exchange and form dimers (Fig. S6BE).

6. PomZ bound to the nucleoid undergoes fast diffusion on the nucleoid, giving rise to a diffusive PomZ flux on the nucleoid (Fig. 6A-C).

7. PomZ undergoes fast diffusion in the cytosol (Fig. 6C).

8. The PomXY cluster acts as a sink for diffusing PomZ dimers on the nucleoid but PomZ dimers are not hindered from diffusing past the cluster (Fig. 6A).

9. Based on quantitative western blot analysis (Fig. S8), *M. xanthus* cells contain ~200 PomX molecules, 850 PomY molecules and ~200 PomZ molecules. Based on fluorescence microscopy, ~45% of PomX, and ~15% of PomY are present in the PomXY cluster resulting in an estimated molecular weight of this complex of ~15 MDa. ~10% of PomZ molecules are in the PomXYZ complex at any one time and the remaining PomZ is bound to the nucleoid on either side of the cluster or is in the cytosol.

Description of computational model

Here, we describe the details of our computational model. Fig. S7A illustrates our model with an emphasis on the numerical implementation. We model the nucleoid and the cluster as one-dimensional lattices of length L and $L_{cluster}$, respectively (the lattice spacing we denote by a, resulting in a total of M lattice sites) with reflecting boundaries at both ends of the nucleoid and the cluster. We assume that PomZ dimers can attach to every site on the nucleoid with the same probability. After ATP hydrolysis and detachment from the nucleoid and the cluster, PomZ molecules undergo nucleotide exchange and dimerization before they can reattach to the nucleoid. This delay between detachment and reattachment to the nucleoid together with fast diffusion of PomZ in the cytosol justifies our assumption of a constant attachment rate k_{on}/M along the nucleoid. Diffusion of PomZ dimers on the nucleoid is modelled on the one-dimensional lattice as hopping between neighbouring lattice sites. The rate with which a PomZ dimer at site n hops to the left or right (site $n-1$ or $n+1$) is set to $k_{hop}^0 = D/a^2$, because this results in a diffusive process with a diffusion constant D in the continuum limit. Since the time the cluster takes to move to midcell is only about $\frac{1}{4}$ of the doubling time of the cell, we assume that the number of PomZ molecules in the cell is constant over the course of the simulation. The simultaneous interactions of PomZ dimers with the PomXY cluster and the nucleoid are implemented similarly to a model introduced by Lansky et al. for crosslinker proteins bound between microtubules (Lansky et al., 2015). As discussed in the main text, we model the PomZ dimers as springs with a spring constant k. We take the rates for attachment of nucleoid-bound PomZ dimers to the cluster in a stretched state as the rate for attachment in the unstretched state, k_a^0, weighted by a Boltzmann factor:

$$k_a = k_a^0 \exp\left[-\frac{1}{2}\frac{k}{k_B T}\left(x_i^{cluster} - x_i^{nucleoid}\right)^2\right].$$

In the above equation, k_B is the Boltzmann constant, T the temperature and $x_i^{cluster}$, $x_i^{nucleoid}$ are the positions of the binding sites of the i-th PomZ dimer to the cluster and the nucleoid, respectively. Furthermore, a PomZ dimer bound to the nucleoid and the cluster is allowed to hop to the left or right lattice site with the rate (Lansky et al., 2015):

$$k_{hop} = k_{hop}^0 \exp\left[-\frac{1}{4}\frac{k}{k_B T}\left(\left(x_i^{cluster,to} - x_i^{nucleoid,to}\right)^2 - \left(x_i^{cluster,from} - x_i^{nucleoid,from}\right)^2\right)\right],$$

with $x_i^{cluster,from}$, $x_i^{nucleoid,from}$ and $x_i^{cluster,to}$, $x_i^{nucleoid,to}$ signifying the positions of the binding sites of the i-th PomZ dimer to the cluster and nucleoid before and after hopping, respectively. We assume that for the hopping events detailed balance holds. Hence, the ratio of the hopping rates from one site to a neighbouring one and back to the original site is weighted by a Boltzmann factor and the hopping rates are only determined up to a constant factor. We chose this factor such that the rate for hopping to a neighboring site and the rate for hopping back are the inverse of each other (Lansky et al., 2015). Note that we neglect the vertical distance between the nucleoid and the cluster when calculating the energy of a loaded spring. We introduce a rate k_h for a PomZ dimer doubly bound to the cluster and the nucleoid to detach completely from the cluster and the nucleoid. This rate is assumed to be constant, i.e. it does not depend on the degree of stretching of the spring. Note that we do not model ATP-binding and dimerization of PomZ molecules in the cytosol explicitly. The

time delay between detachment of ADP-bound PomZ monomers and reattachment of ATP-bound PomZ dimers is taken into account by choosing a constant attachment rate to each lattice site of the nucleoid in the model. Furthermore, we neglect detachment of PomZ dimers, which are bound to the nucleoid but not to the cluster, into the cytosol because the ATP turnover rate of PomZ in contact with DNA is negligible compared to the turnover rate of PomZ in contact with DNA and PomX/PomY (Fig. 5C).

The cluster movement is described by a force balance equation

$$\gamma \frac{dx}{dt} = -\sum_{i=1}^{N} k\left(x_i^{cluster} - x_i^{nucleoid}\right),$$

stating that the frictional force exerted on the cluster, given by the friction coefficient γ times the cluster velocity, balances the sum of all spring forces exerted on the cluster by the doubly bound PomZ dimers; the sum extends over all PomZ dimers bound to the cluster and the nucleoid (in total N).

In WT, approximately 10% of the 200 PomZ molecules are in the cluster. By contrast, PomZ^{D90A}-mCh, which cannot undergo ATP hydrolysis, is mostly in the cluster if expressed at native levels (Fig. S6E; 6C) suggesting that in WT cells the concentration of PomZ dimers bound to the cluster is below its saturation limit. In cells overexpressing PomZ^{D90A}-mCh > 50-fold, the fusion protein is also bound to the nucleoid away from the cluster (Fig. 6B). We conclude that the PomXY cluster has a limited number of binding sites but at least binding sites for 100 PomZ dimers. To include the limited number of binding sites on the cluster and on the nucleoid in our model, we implemented a maximal density of binding sites on the cluster and the nucleoid, $c_{cluster}$ and $c_{nucleoid}$, respectively. When all binding sites of a lattice site are occupied, no further PomZ dimer can attach to this site from the cytosol or from the neighbouring lattice sites.

We implemented the model as a Gillespie algorithm (Gillespie, 1976; Gillespie, 1977; Lansky et al., 2015). Since the position of the cluster changes with time, the rates k_a and k_{hop} are time-dependent. For the parameters we consider here, the simulation results show that this time-dependence can be neglected and hence we assume that the rates are constant. We chose the initial PomZ distribution such that all PomZ dimers are in the cytosol and let the simulation run for 600 sec while keeping the cluster fixed to allow the PomZ dynamics to approach the steady state distribution. The initial position of the midpoint of the cluster, p, was at 7% of the nucleoid length, which corresponds to the leftmost position of the cluster while still fully overlapping with the nucleoid.

Simulation results
At present, detailed experimental information about several of the molecular parameters of our computational model is lacking. Therefore, the focus of our mathematical analysis is mainly on the qualitative behaviour, and not a quantitative comparison between the results of the mathematical model and the experimental data. For some parameters it is possible to obtain an estimate from our experimental data and some parameters are estimated from the corresponding values from plasmid and chromosome segregation systems. The parameter estimates and sources are listed in Table S1. The detachment rate of PomZ dimers doubly

bound to the cluster and the nucleoid can be estimated from the measurement of the ATP turnover rate, because we assume that ATP hydrolysis is the rate-limiting step. The stiffness of the springs mimicking the elasticity of the PomZ dimers and the chromosome is set to a value obtained from a model for an *in vitro* reconstituted ParAB*S* system (Hu et al., 2015).

For the diffusion constant of PomZ on the nucleoid, we chose a value similar to the experimentally determined values in plasmid and chromosome segregation systems. We chose the value of the friction coefficient from the related ParB/*parS* systems, relating the diffusion constant of the ParB/*parS* complex to its friction coefficient by the Stokes-Einstein equation, $D_{cluster} = k_B T / \gamma$. Increasing the friction of the PomXY cluster in the cytosol leads to a longer mean time for the cluster to reach midnucleoid. The value used in the simulations (Table S2) is the value that results in cluster trajectories where the cluster typically reaches midnucleoid in approximately the same time as observed experimentally. With the full set of parameters listed in Table S2, the model reproduces midnucleoid localization of the PomXYZ cluster with the same timing as observed experimentally in *M. xanthus* cells (Fig. 7C, S7BC, 4A). The simulation results are largely insensitive to changes of the attachment rate of PomZ dimers to the nucleoid and to changes of the binding rate of nucleoid-bound PomZ dimers to the cluster. We tested both parameters over several orders of magnitudes without noticeable deviations in the simulation results (Table S2). The density profile of PomZ dimers on the nucleoid is different for different cluster positions (Fig. 7D). Importantly, the concentration of PomZ is always highest, where the cluster is located (Fig. 7D). The total amount of PomZ in the Pom cluster increases, when the cluster moves from an off-centre position towards midcell. This is because the average distance that a PomZ dimer travels on the nucleoid until it reaches the cluster gets smaller the closer the cluster is located to midnucleoid. Importantly, if the cluster is positioned at an off-centre position, the density profile is asymmetric over the cluster and with the highest density of PomZ on the side of the cluster facing the more distant pole of the nucleoid. By contrast, if the cluster is at midnucleoid, PomZ has an almost symmetric distribution over the cluster (Fig. 7D). The same holds true for the density of PomZ dimers over the entire nucleoid: it is asymmetric if the cluster is located off-centre, with a higher density on the side with the longer cluster-to-nucleoid end distance, and becomes symmetric around the cluster, if the cluster is at midnucleoid (Fig. 7D). These predictions are in overall agreement with our experimental data in which we found that even though the patchy PomZ signal over the nucleoid is almost symmetrically distributed around the cluster, it is slightly but significantly more asymmetric in the case of cells with an off-centre cluster and with the highest intensity on the side of the cluster containing most of the nucleoid. However, there are several reasons why a direct quantitative comparison between the asymmetry values obtained from the simulations and the fluorescence microscopy images is not possible. First, these images show the combined PomZ intensity in the cytosol, in the nucleoid and on the surface of the nucleoid. Therefore, the PomZ asymmetry on the nucleoid surface is likely underestimated. Second, our model is mainly conceptual. In particular, it reduces the system to one spatial dimension. This assumption contributes to an overestimation of the asymmetry value. Third, the asymmetry value of the PomZ distribution in the simulations depends on the parameter choice and not all parameters are measured experimentally.

Our simulation results predict that the mechanism of midnucleoid positioning of the PomXYZ cluster would be disturbed if PomZ is present at a reduced level, is overexpressed or if PomZ ATP hydrolysis is perturbed. If the number of PomZ molecules is reduced two-fold, the simulations predict movement of the clusters towards midnucleoid (Fig. S7D), but on a longer time scale. This prediction is in agreement with our experimental findings (Fig. 7E; S7EF). If the number of PomZ molecules is increased in our simulations, the movement of the cluster is less biased towards midnucleoid (Fig. S7D). For twice the number of PomZ molecules, the clusters behave as for the WT case, for four-fold the PomZ molecule number the bias towards midcell is reduced, and for six-fold the PomZ molecule number the cluster is stalled at its initial position and moves only slightly. These predictions can be explained as follows: If the number of PomZ dimers is high, exclusion effects on the nucleoid and at the cluster become important and cluster motion is reduced in two ways: First, PomZ dimers often cannot bind to the cluster because all cluster binding sites are occupied. This leads to a reduced bias of the cluster movement towards midnucleoid. Second, crowding of PomZ dimers locally at the cluster impedes the mobility of PomZ dimers bound to the cluster and hence reduces cluster motion. These predictions agree with our experimental observations, i.e. the PomXY cluster shows no directed movement towards midnucleoid and little motion in cells overexpressing PomZ-mCh > 50-fold (Fig. 7E; S7F). Note that exclusion effects on the nucleoid also decrease the flux difference of PomZ dimers on the nucleoid into the cluster, but because of the low occupancy of PomZ dimers on the nucleoid away from the cluster, this is a minor effect.

Cluster movement is also decreased for small ATP hydrolysis rates. ATP hydrolysis is necessary for the PomZ molecules to cycle between the cluster-bound and the cytosolic state. If the ATPase activity of PomZ is reduced, the number of PomZ dimers bound to the nucleoid is increased and ultimately, in the complete absence of ATP hydrolysis, all PomZ molecules become attached to the cluster because they cannot escape from the cluster once they are bound. Due to particle conservation in the cell, this leads to a decreased amount of PomZ molecules in the cytosol. Hence, the flux from the cytosol to the nucleoid becomes smaller and, therefore, the flux of nucleoid-bound PomZ into the cluster also decreases. This results in cluster trajectories that are less and less biased towards midcell for decreasing hydrolysis rates (Fig. S7G). Moreover, the higher PomZ dimer density at the cluster for smaller ATP hydrolysis rates leads to similar crowding effects as in the case for PomZ overexpression. Again, the mobility of the PomZ dimers bound to the cluster is reduced and therefore the cluster movement is reduced. These predictions are in perfect agreement with our experimental observations with the ATP hydrolysis deficient variant PomZ[D90A] (Fig. 5EF). Importantly, if the ATP hydrolysis rate is decreased approximately 10-fold, the cluster typically undergoes a biased random motion towards midnucleoid, however, the simulations suggest that this translocation occurs more slowly (Fig. S7G). These predictions are in agreement with our experimental observations on PomX cluster dynamics in the absence of PomY (Fig. 7E; S7H).

Note that there is an initial bias of cluster movement towards midcell also in the case of large PomZ dimer numbers and small or zero ATP hydrolysis rates in the simulations (Fig. S7DG). This has two reasons: First, if the PomXY cluster is located at the leftmost possible position on the nucleoid (such that it still fully overlaps with the nucleoid) there is only a PomZ dimer

flux from the right. Hence, if there is a force due to nucleoid-bound PomZ dimers attaching to the cluster, it typically drags the cluster to the right initially. Second, the reflecting boundary condition leads to a movement of the cluster towards midnucleoid as cluster-bound PomZ dimers can only hop to the right if they are on the first lattice site of the nucleoid.

Protein purification

Soluble His_6-PomZ was purified from *E. coli* as described (Treuner-Lange et al., 2013). To overexpress MalE-tagged PomZ or PomZ^{D90A}, plasmids pAH131 or pAH133 were propagated in *E.coli* Rosetta2(DE3). Cells were grown at 37°C in 2xYT medium to an OD_{600} of 0.6–0.7 and expression of MalE-PomZ and MalE-PomZ^{D90A} was induced with 0.3mM IPTG for 2 hrs at 37°C. Cells were harvested and washed in MalE lysis buffer 1 (20mM Tris/HCl; 200mM NaCl; 1mM EDTA; 1mM β-mercaptoethanol; pH 7.4) and resuspend in MalE lysis buffer 2 (MalE lysis buffer 1 with 100µg/ml PMSF; 1 x complete protease inhibitor (Roche Diagnostics GmbH); 10U/ml DNase 1. Cells were lysed by 3 rounds of sonication for 5min with a Branson Sonifier (Duty cycle 4; output control 40%) (Heinemann) on ice. Cell debris was removed by centrifugation 4700rpm for 20 min at 4°C and additional filtration with a 0.45µm sterile filter (Millipore Merck) and MalE-PomZ and MalE-PomZ^{D90A} were affinity purified with amylose resin (NEB) pre-loaded onto an empty column, equilibrated in MalE lysis buffer 1. Proteins were eluted with MalE elution buffer (MalE lysis buffer 1 supplemented with 10mM maltose). Elution fractions containing MalE-PomZ and MalE-PomZ^{D90A} were loaded onto a HiLoad 16/600 Superdex 200 pg column that was equilibrated with dialysis buffer (50mM Hepes/NaOH pH 7.2; 50mM KCl; 0.1mM EDTA; 1mM β-mercaptoethanol; 10% (v/v) glycerol). Collected MalE-PomZ after gel filtration was pooled. In case of MalE-PomZ^{D90A} protein was pooled and concentrated with a 5ml HiTrap Q HP column, equilibrated with dialysis buffer. MalE-PomZ^{D90A} was eluted from the column with cation-exchange buffer (dialysis buffer with 2000mM KCl) using a 50mM to 500mM KCl gradient. Elution fractions from the ion-exchange chromatography were dialyzed against dialysis buffer at 4°C. To overexpress His_6-tagged PomY, plasmid pDS3 was propagated in *E. coli* ArcticExpress(DE3)RP cells (Agilent Technologies). Cells were grown at 30°C in LB medium to an OD_{600} of 0.6–0.7. Cultures were pre-cooled and shifted to 18°C prior to induction of *pomY-His$_6$* expression with 1mM IPTG. Cells were incubated overnight at 18°C shaking at 230rpm. Cells were washed in lysis buffer 1 (50mM NaH_2PO_4; 300mM NaCl; 10mM imidazole; pH 8.0 (adjusted with NaOH)), and then lysed in 50ml lysis buffer 2 (lysis buffer 1; 0.1mM EDTA; 1mM β-mercaptoethanol; 100µg/ml PMSF; 1 x complete protease inhibitor (Roche Diagnostics GmbH); 10U/ml DNase 1; 0.1% Triton X-100) by 3 rounds of sonication for 5min with a Branson Sonifier (Duty cycle 4; output control 40%) (Heinemann) on ice. Cell debris was removed by centrifugation 4700rpm for 20 min at 4°C and additional filtration with a 0.45µm sterile filter (Millipore Merck). PomY-His_6 was purified with a 5ml HiTrap Chelating HP column, preloaded with $NiSO_4$ and equilibrated with lysis buffer 1. Proteins were eluted with elution buffer (lysis buffer 1 supplemented with 500mM imidazole). Elution fractions containing PomY-His_6 were loaded onto a HiLoad 16/600 Superdex 200 pg column that was equilibrated with dialysis buffer. Collected PomY-His_6 after gel filtration was pooled and concentrated with a 5ml HiTrap SP HP column, equilibrated with dialysis buffer. PomY-His_6 was eluted from the column with cation-exchange buffer using a 50mM to 2000mM KCl gradient. Elution fractions from the ion-exchange chromatography were dialyzed against dialysis buffer at 4°C. To purify PomX-His_6 plasmid pEMR3 was propagated in *E. coli* NiCo21(DE3) cells (NEB). Cells were grown in LB medium with 50µg/ml kanamycin

at 30°C to an OD_{600} of 0.6 – 0.7. Protein accumulation was induced with 0.5mM IPTG for 16 hrs at 18°C. Cells were washed in lysis buffer 1 and lysed in 50ml lysis buffer 2 without Triton X-100 by sonication as described before. Cell debris was removed by centrifugation at 20000g for 20 min a 4°C and PomX-His$_6$ was affinity purified with Protino® Ni-NTA resin (Macherey-Nagel) from batch, equilibrated in Lysis buffer 1. PomX-His$_6$ was eluted from the resin by washing 1 x with 5ml elution buffer 1 (lysis buffer 1 with 50mM imidazole) and 3 x with 5ml elution buffer 2 (lysis buffer 1; 250mM imidazole). Purified PomX-His$_6$ was dialyzed against dialysis buffer. To purify native FtsZ plasmid pKA70 was propagated in Rosetta2(DE3) cells (Novagen). Cells were grown in 2xYT medium with 50µg/ml ampicillin at 37°C to an OD_{600} of 0.6 – 0.7. Expression of *ftsZ* was induced with 0.5mM IPTG for 3 hrs at 37°C. Cells were washed in FtsZ lysis buffer 1 (50mM Tris-HCl pH 7.9; 50mM KCl; 1mM EDTA; 1mM β-mercaptoethanol; 10% (v/v) glycerol) and lysed in FtsZ lysis buffer 2 (lysis buffer 1, 1 x complete protease inhibitor (Roche Diagnostics GmbH); 10U/ml DNase 1) by sonication as described above. Cell debris was removed by centrifugation at 20000g for 20 min at 4°C and the soluble fraction was applied to ammonium sulfate precipitated by adding ammonium sulfate in small steps to 33% of saturation at 4°C to precipitate native FtsZ. Precipitate was dissolved in lysis buffer 1 and loaded onto a 5ml HiTrap Q HP column, equilibrated in lysis buffer 1. Proteins were eluted with FtsZ elution buffer (FtsZ lysis buffer 1; 1000mM KCl). Fractions containing FtsZ were pooled and diluted 1:5 with dilution buffer (lysis buffer 1 without KCl) and loaded onto a 5ml HiTrap Q HP column, equilibrated with lysis buffer 1. Proteins were eluted again with FtsZ elution buffer as described before along a short gradient of 4 column volumes.

Protein sedimentation assay

Before sedimentation assays, a clearing spin was performed for proteins to be analyzed at 20,000g for 10min at 4°C. Purified proteins at a final concentration of 3µM in a total volume of 25µl were mixed and incubated at for 2-10min at 32°C in buffer (50mM Hepes/NaOH, pH 7.2, 50mM KCl, 1mM ß-mercaptoethanol, 10mM $MgCl_2$). Subsequently, samples were separated into soluble and insoluble fractions by centrifugation (160,000g, 60 min, 25°C). Insoluble and soluble fractions were separated. Equivalent volumes of soluble and the insoluble fractions were separated by SDS-PAGE and stained with Instant Blue™ (expedeon) for 10 min.

ATPase assay

A colorimetric ATPase assay was performed as described (Treuner-Lange et al., 2013). Briefly, MalE-PomZ and MalE-PomZ^{D90A} alone or with PomY-His$_6$, PomX-His$_6$ or both at final concentrations of 2µM were mixed in a 96-well plate (Greiner Bio-One) in triplicate in buffer A (50mM Hepes/NaOH pH 7.2, 50mM KCl, 10mM $MgCl_2$, 1mM β-mercaptoethanol, 1mM ATP). Reactions were incubated for 30 min at 37°C. Reactions were mixed with 250µl Malachite-green reagent (Sigma-Aldrich) incubated for 5 min and stopped with 50µl of 34% (v/v) citric acid. After 15 min, the developed color was measured with an Infinite M200 Pro plate-reader at 660nm (Tecan). If nonspecific DNA was added, pUC18 plasmid DNA in 50mM Hepes/NaOH pH 7.2; 50mM KCl; 0.1mM EDTA; 1mM β-mercaptoethanol; 10% (v/v) glycerol was used at a final concentration of 5nM.

Negative stain transmission electron microscopy

For fixation and negative stain of protein samples, 10µl of a protein sample of interest (concentration before applying: PomX-His$_6$ and PomY-His$_6$, 3µM and 3µM) were applied on one side of the EM grid (Plano) and incubated for 1min at room temperature. Liquid was blotted through the grid by applying the unused side of the grid on Whatman paper. The grid was washed twice with double-distilled H$_2$O and once with a 1% uranyl acetate solution with the same technique. Then uranyl acetate was applied on the grid for 20 sec and dried by blotting the liquid through the grid with a Whatman paper. In case of FtsZ, 3µM protein was pre-incubated at room temperature for 2 min before GTP was added at a final concentration of 2.5mM. After additional incubation for 10 min, protein was applied to the grid and grids were handled as described above. Finished grids were stored in a grid holder for several months at room temperature. Electron microscopy was done with a CM120 elcetron microscope (FEI) at 120kV.

Right angle light scattering
Right angle light scattering was performed with 10µM FtsZ at pH 6.5 (50mM MES/NaOH, 50mM KCl, 10mM MgCl$_2$, 1mM β-mercaptoethanol) on a temperature-controlled ISS PC1 spectrofluorometer with a cooled photomultiplier with excitation and emission wavelength set to 350nm. FtsZ was preincubated for 2 min at 8°C and experiment was subsequently started. After 100 sec GTP at a final concentration of 2.5mM was added to initiate filament formation. Light scattering was followed for 900 sec. FtsZ without addition of GTP served as negative control.

Immunoblot analysis
Polyclonal α-PomX and α-PomY antibodies were raised by immunization of rabbits with the purified His$_6$-tagged proteins (Eurogentec). Immunoblot analysis was performed as described (Sambrook and Russell, 2001), using α-PomX, α-PomY, α-PomZ (Treuner-Lange et al., 2013), α-FtsZ (Treuner-Lange et al., 2013) or α-PilC (Bulyha et al., 2009) together with horseradish-conjugated goat anti-rabbit immunoglobulin G as recommended by the manufacturer (Sigma) as secondary antibody. For detection of mCh-tagged proteins monoclonal rabbit α-mCh antibodies were used as described by the manufacturer (BioVision) together with the peroxidase-conjugated goat α-rabbit immunoglobulin G secondary antibodies. Blots were developed using Luminata Forte chemiluminescence reagent (Millipore).

Quantitative immunoblot analysis
An estimation of the number of molecules of PomX, PomY and PomZ was determined using a quantitative immunoblot analysis. For this 2ml of two independent WT cultures of an OD$_{550}$ of 0.6 were spun down and used to make cell lysates for immunoblot analysis. Equal amounts of cell lysates were separated on a 10% SDS-Page, proteins were transferred to a 0.2µm PVDF membrane that was probed with specific α-PomX (1:15000), α-PomY (1:15000) or α-PomZ (1:10000) antibodies and a 1:25000 dilution of anti-rabbit IgG-peroxidase conjugated secondary antibody (Sigma-Aldrich). Signals were developed with Luminata Forte chemiluminescence reagent (Millipore). Signal intensities of the bands were quantified using Fiji and compared against a standard curve generated from known amounts of PomX-His$_6$, PomY-His$_6$ or His$_6$-PomZ on the same Immunoblot. Knowing the cell number of cultures that were used to make the WT cell lysates from counting cells with a Multisizer™ 3 Coulter

Counter (Beckmann-Coulter) molecule number was determined in at least three independent biological replicates.

Fluorescent microscopy and live cell imaging

In all experiments, cells from exponentially growing cultures were transferred to slides containing a thin pad of 1% SeaKem LE agarose (Cambrex) with TPM buffer (10mM Tris-HCl pH 7.6, 1mM KH_2PO_4 pH 7.6, 8mM $MgSO_4$), covered with a coverslip and imaged with a temperature-controlled Leica DMI6000B microscope with adaptive focus control, a motorized stage (Prior) and a HCX PL APO 100x/1.47 oil Corr TIRF objective at 32°C with a Hamamatsu Orca Flash 4.0 using Leica MM AF software. Image processing and data analysis was performed using Metamorph® v 7.5 (Molecular Devices). For DAPI staining, cells were incubated with 1µg/ml DAPI for 10 min at 32°C prior to microscopy. For time-lapse recordings, cells were placed on a TPM-buffered agarose pad containing 0.2% CTT medium containing TetraSpeck™ 0.5µm fluorescently labelled beads (Molecular Probes™) for image alignment and analysis of cluster dynamics. Automated picture alignment and semi-automated cluster tracking was done using Metamorph® v 7.5. For tracking cluster dynamics, the maximum identity method was used with a minimal identity of 60% and a maximal displacement of 25 pixels. Kymographs were generated using Metamorph® v 7.5.

Fluorescence recovery after photobleaching

Fluorescence recovery after photobleaching (FRAP) experiments were performed with a temperature controlled Nikon Ti-E microscope with Perfect Focus System and a CFI PL APO 100x/1.45 Lambda oil objective at 32°C with a Hamamatsu Orca Flash 4.0 camera using NIS Elements AR 2.30 software (Nikon). For photobleaching a 651nm laser beam was focused on the on the central part of the image plane. After acquisition of an initial pre-bleach picture, cells of interest were bleached using a single 5 × 5 pixel circular shaped region. Photobleaching of SA3131 was performed with 1 laser pulse with 5% laser power and a dwelling time of 500 µsec. For strains SA7011 and SA4799, FRAP was performed with 10 consecutive laser pulses with 10% laser power using the same dwelling time. Images were recorded every 1 sec in case of SA3131 and every 300 msec in case of SA7011 and SA4799. For every image, total integrated cellular fluorescence in a region of interest (ROI) within the outline of the cell was measured together with total integrated background fluorescence of a ROI of the same size placed outside of the cell. Additionally, fluorescence intensity was measured in the bleached region together with background fluorescence or a ROI of same size placed on the background. After background correction, corrected fluorescence intensity of the bleached area (or area of interest) was divided by total corrected cellular fluorescence, which in term corrects for bleaching effects during picture acquisition. This relative fluorescence was correlated to the initial fluorescence in the bleached area (or area of interest). The mean relative fluorescence of several cells was plotted as function of time [sec]. To determine the recovery rate for the tested fluorescent protein (t_1), the plotted data was fitted to a single exponential equation ($y = y_0 + A * e^{-x/t}$) using Sigma Plot v 12.5. Half-maximal recovery ($t_{1/2}$) was calculated from the recovery rate (t_1) by $t_{1/2} = \ln(2) * t_1$.

PomZ asymmetry measurement

For PomZ asymmetry analysis, PomZ-mCh in SA3131 was imaged with an acquisition time of 1 sec. To calculate the asymmetry index the integrated and background-corrected patchy

PomZ-mCh signal on either side of a cluster was divided by the fluorescent area on either side of the cluster, giving the intensity values I_{left} and I_{right}, left and right of the PomZ-mCh cluster (Fig. S3B). The asymmetry index was calculated as $(I_{left}-I_{right}) / (I_{left}+I_{right})$ independently for off-centre and midcell clusters. The normalized asymmetry value for the nucleoid on either side of the cluster was calculated similarly using Pico green stained nucleoids (Harms et al., 2013) in cells of SA3131.

GAL4-based yeast two hybrid assay
Yeast two hybrid assays were performed as described by the manufacturer (Clontech). Briefly, genes of interest were fused to the GAL4-AD fragment (activation domain) or the GAL4-BD fragment (DNA-binding domain). Plasmids were co-transformed into yeast strain AH109. Transformants were selected on SD/-Leu/-Trp agar for inheritance of both plasmids. Four independent clones were resuspended in SD/-Leu/-Trp medium and grown for 3 doubling times at 30°C. OD was adjusted to 0.5 and 3µl cells were placed on SD/-Leu/-Trp/-His (medium stringency) selective agar. Plates were incubated at 30°C for 120 hrs. Growth on medium stringency selective agar was classified as a positive interaction. Additionally each plasmid containing a gene of interest was co-transformed with an empty vector only expressing the GAL4-AD or BD fragment, respectively. In an experiment, all strains were spotted with all the controls on the same selective agar plates. The data shown is a representative agar plate of two independent transformation experiments.

Plasmid construction
All DNA fragments generated by PCR were verified by sequencing. All oligonucleotides used are listed in Table S3.
Plasmids pDS1, pDS12, pDS16, pMAT12, pAH27: For pDS1 up- ("KA-371/Mxan_0634-5") and downstream fragment ("KA-373/KA-374") were amplified from genomic *M. xanthus* DNA and digested EcoRI+XbaI and XbaI+HindIII, respectively. Fragments were cloned separately into pBJ114 and sequenced. For pAH27 up- ("KA-224/Mxan_0636-1") and downstream fragment ("Mxan_0636-2/Mxan_0636-3") were amplified from genomic *M. xanthus* DNA and digested EcoRI+XbaI and XbaI+HindIII, respectively. Fragments were cloned separately into pBJ114 and sequenced. pMAT12 is a derivative of pAH27. Upstream fragment ("KA-200/Mxan_0635-3") was amplified from genomic DNA, digested with EcoRI+XbaI and cloned into pAH27 that was digested EcoRI+XbaI before. pDS12 is a derivative of pDS1. For construction of pDS12, pAH27 was digested XbaI+HindIII and downstream fragment was cloned into pDS1 that was digested with the same enzymes before. pDS16 is a derivative of pDS1 in which the downstream fragment (XbaI+HindIII) was replaced with another downstream fragment ("Mxan_0635-1/Mxan_0635-2") that was digested in the same way.

Plasmid pDS3 and pEMR3: For pDS3 *pomY* was amplified with "Mxan_0634-11" and "Mxan_0634-12" from genomic DNA and cloned into pET24b+ (EcoRI and HindIII). For pEMR3, *pomX* was amplified with primer "NdeI-pomX fwd" and "pomX c-term His rev" and cloned into pET24b+ using NdeI and HindIII.

Plasmids pDS81, pDS82: For both plasmids *pomY* was amplified from genomic *M. xanthus* DNA using the primers "Mxan_0634 fwd EcoRI" and "Mxan_0634 rev stop BglII" and cloned into pGAD424 and pGBT9.

Plasmids pDS83, pDS84: For pDS83 *pomZ* was amplified from genomic *M. xanthus* DNA using the primers "Mxan_0635 fwd SalI linker" and "Mxan_0635 rev stop BglII" and cloned into pGAD424. For pDS84 *pomZ* was amplified using the primers "Mxan_0635 fwd BamHI linker" and "Mxan_0635 rev stop PstI" To be translated in the correct frame *pomZ* contains one additional amino acid at the beginning which additionally serves as a part of the linker for both GAL4-AD and GAL4 DNA-BD fragment fusions.

Plasmids pDS85, pDS86: For both plasmids *pomX* was amplified from genomic *M. xanthus* DNA using the primers "Mxan_0636 fwd EcoRI" and "Mxan_0636 rev stop BamHI" and cloned into pGAD424 and pGBT9.

Plasmids pDS87, pDS88: For both plasmids *ftsZ* was amplified from genomic *M. xanthus* DNA using the primers "Mxan_5597 fwd EcoRI" and "Mxan_5597 rev stop BamHI" and cloned into pGAD424 and pGBT9.

Plasmids pDS7, pDS8, pDS18 and pDS19: For pDS8 *pomY* with its native promoter was amplified from genomic DNA with primers "KA-371" and "Mxan_0634-4" and cloned with EcoRI and BglII into pKA28 (Treuner-Lange et al., 2013). For pDS7 *pomY-mCh* was amplified from pDS8 with "Mxan_0634-6" and "mCherry stop rev HindIII" and cloned into pSW105 with XbaI and HindIII. For pDS18 *eyfp* was amplified from pAH7 with "KA-396" and "KA-397" and cloned with BamHI and HindIII into pSWU30. *pomY* was amplified with "KA-371" and "Mxan_0634-4" from genomic DNA and cloned into the resulting plasmid with EcoRI and BglII. P*pilA*pomY-mCh* was excised from pDS7 with EcoRI and HindIII and ligated into pSWU30 resulting in pDS19.

Plasmids pKA46, pAH35, pAH52, pAH53 and pAH96: For pKA46 the native *pomX* promoter was amplified with "KA-382" and "KA-383" from genomic DNA and cloned with EcoRI and KpnI into pSWU30. *mCh* was amplified with "KA-302" and "KA-303" from pKA28 and cloned into the same plasmid using KpnI and BamHI. For the third fragment *pomX* was amplified with "KA-384" and "KA-348" from genomic DNA and cloned into the vector with BamHI and HindIII. For pAH35 *mCh-pomX* was amplified from pKA46 with primers "mCherry fwd XbaI" and "KA-348" and cloned into pSW105 using XbaI and HindIII as restriction sites. The same strategy was used for pAH52 but *mCh-pomX* was cloned into pMAT11 with XbaI and HindIII. Plasmid pAH53 is a derivative of pAH35 in which the *pilA* promoter is replaced by the native *pomZ* promoter that was amplified with "KA-200" and "pomZ prom rev XbaI" and cloned into pAH35 with EcoRI and XbaI. For pAH96 P*pomZ*mCh-pomX* was excised from pAH53 with EcoRI and HindIII and cloned into pSWU30.

Plasmids pDS21 and pDS22: For pDS21 *pomY-mCh* was excised from pDS7 with XbaI and HindIII and cloned into pMAT11. For pDS22 *pomY-eyfp* was amplified from pDS18 with primers "KA-397" and "Mxan_0634-6" and ligated XbaI-HindIII into pMAT11.

Plasmids pEB16, pKA55 and pAH100: All three plasmids are derivatives of pKA28 and constructed by site directed mutagenesis using the Quickchange II XL site directed

mutagenesis kit (Agilent) as described by the manufacturer's instructions. For pEB16 point mutation for $pomZ^{G62V}$ was introduced with primers "KA-413" and "KA-414". For pKA55 point mutation for $pomZ^{K66Q}$ was introduced with primers "KA-417" and "KA-418". For pAH100 point mutation for $pomZ^{K268E}$ was introduced with primers "AH-91" and "AH-92".

Plasmid pKA45 and pEB13: For pKA45 *pomZ-mCh* was amplified from pKA28 with "KA-288" and "KA-293" and cloned XbaI-HindIII into pSW105. pEB13 was constructed in the same way by using pKA43 as template for PCR fragment.

Plasmid pAH83: A fragment downstream of *ssb* (*MXAN_1071*) was amplified with primers "EB-7" and "EB-8" from chromosomal DNA and cloned BamHI and EcoRI into pBJ114. Then *eyfp* was amplified from pAH7 with primers "EB-11" and "EB-12" and cloned into the same plasmid with BamHI and XbaI. Finally, a fragment upstream of *ssb* was amplified with primers "EB-5" and "EB-6" and also cloned into the same plasmid using XbaI and HindIII, resulting in pAH83.

Plasmid pDS74, pDS75 and pDS80: For pDS74 $P_{pilA}pomZ$ was excised from pKA19 with EcoRI and HindIII and cloned into pSWU30 digested with the same enzymes. pDS75 is a derivative of pDS74. For pDS75 the Mx8 *attB* locus was excised from pDS74 using BsrDI and BlpI. This was replaced by the *MXAN18-19* intergenic region amplified from pMR3691 using the primers "Mxan18-19 fwd BsrDI" and "Mxan18-19 rev BlpI". To create pDS80, P_{nat} $pomZ^{D90A}$ together with a short part of the vector backbone was excised from pKA43 with NdeI and HindIII. This fragment was cloned into pDS75 to replace P_{pilA} *pomZ*, which was digested with the same enzymes before.

Plasmid pDS37, pDS43 and pDS46: pDS37, pDS43 and pDS46 are derivatives of pRSFDuet-1. To construct pDS37 *mCh-pomX* was amplified from pAH53 with "mCherry BspHI fwd" and "Mxan_0636-3 HindIII rev stop" and cloned into pRSFDuet-1 multiple cloning site 1 (MCS1) with BspHI and HindIII. For pDS43 *pomZ-mCh* was amplified from pKA28 with primers "Mxan_0635 BspHI fwd" and "KA-478" and cloned into pRSFDuet-1 in the same way. For pDS46 *pomY-eyfp* was amplified from pDS18 using "Mxan_0634-18" and "Mxan_0634-15" and cloned into pRSFDuet-1 as described before.

Plasmid pDS68: To construct pDS68, *pomZ-mCh* was amplified from pKA28 with "Mxan_0635 start NdeI" and "mCherry stop PacI" and cloned into MCS2 of pDS46 using the indicated restriction enzymes.

Plasmids pDS38 and pDS45: For pDS38 *pomX* was amplified from genomic DNA using the primers "Mxan_0636 BspHI fwd" and "Mxan_0636-3 HindIII rev stop" and cloned into pBAD24 using the indicated restriction sites. To construct pDS45, *pomY-eyfp* was amplified from pDS18 with primers "Mxan_0634-18" and "Mxan_0634-15" and ligated into pBAD24 using BspHI and HindIII restriction sites.

Plasmid pDoB12: For pDoB12 *ftsK* was amplified with the primers "*ftsK* start XbaI" and "*ftsK* nostop BamHI rev" from genomic DNA and cloned with the indicated enzymes into pKA45.

Plasmid pMAT112: For pMAT112 the *aadA* gene was amplified with "pIJ778 SacI down" and "pIJ778 BglII Pst up" from pIJ778 and ligated into pMAT76 that was amplified with "pMAT76 BglII" and "pMAT76 SacI". For pMAT76, the multiple cloning site of pMR3691 was changed. pMR3691 was opened with NdeI and KpnI and ligated with an annealed primer double strand consisting of "Cla-Sca linker+" and "Cla-Sca linker –", resulting in pMAT56. This vector was opened with ClaI and KpnI and ligated with *tetR-eyfp* that was amplified from pMAT6 with "TetR-YFP-ClaI" and TetR-YFP-KpnI.

Plasmid pDS157: For pDS157 *pomZ* was amplified with primers "Mxan0635 NdeI fwd" and "Mxan0635 KpnI rev stop" from genomic DK1622 DNA and cloned with the indicated enzymes into pMR3691.

Plasmid pAH131 and pAH133: For pAH131 *pomZ* was amplified from genomic DK1622 DNA with primers "AH120" and "KA207", digested with HindIII and phosphorylated with T4 polynucleotid kinase (NEB) and ligated into pMAL-c2X that was digested with XmaI and HindIII before. pAH133 was cloned the same way as pAH131 but *pomZ*^{D90A} was amplified from pEB13 using the same primers.

QUANTIFICATION AND STATISTICAL ANALYSIS
Statistical details
n-values for number of cells analyzed are listed in the main text or in figure legends.

t-test/F-test
We performed two-sample t-tests to determine if two population means were significantly different. Based on the results of an F-test for equality of two variances, we used an equal or an unequal variance t-test (using the built-in functions of Excel).

Two one-sided test
To statistically test for equivalence of midnucleoid and ParB positions in mutants compared to WT, we performed two one-sided test equivalence tests using R. We assumed an equivalence margin of 10% of cell length based on the average standard deviation of the midnucleoid/ParB positions WT of 7.27% cell length. We found statistical significance for equivalence of the population means ($p<0.05$; assuming an equivalence margin of 10%) in all but one case (ParB cluster position in cells containing one ParB cluster, when comparing the *pomX* mutant to WT). In this case, which had fewer data points than the other samples, we found statistically significant evidence for equivalence using an equivalence margin of 22%.
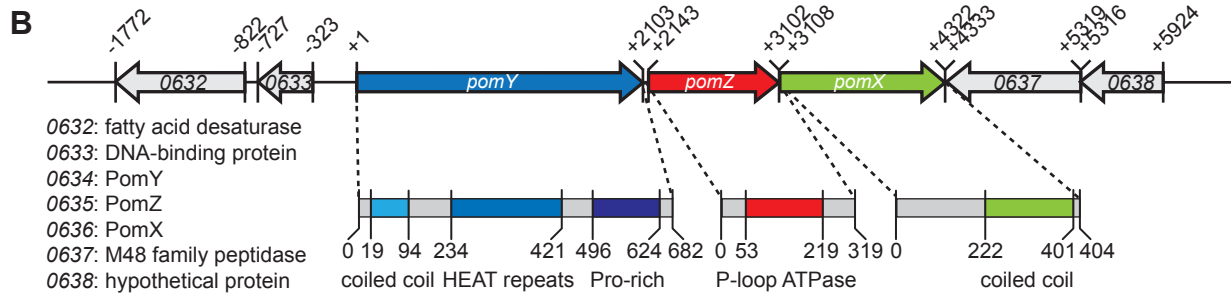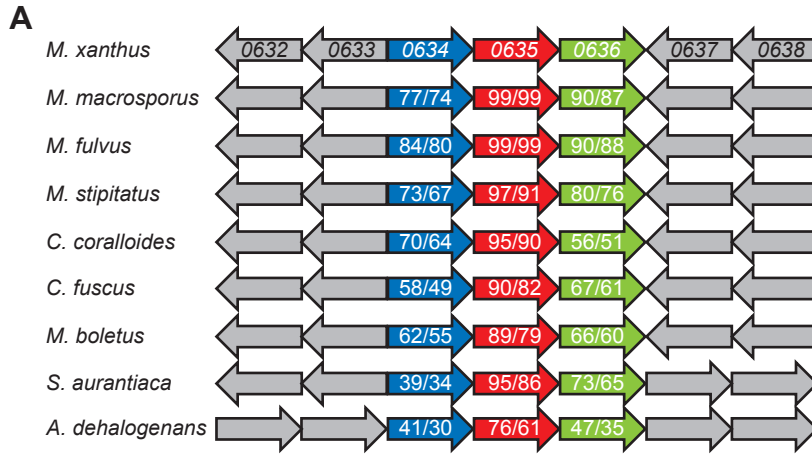
Calculation of MCSD and MSD
To calculate mean cumulative squared distance (MCSD) of a PomXYZ cluster the distance a cluster moved between two frames of a time-lapse series was measured, squared and then averaged over all measured cells in the time-lapse series and the same time interval. The squared distances per time interval were then summed over time and plotted as function of

time. To calculate mean squared displacement (MSD) of a PomXYZ cluster its distance to the original position at t=0 was determined for every time interval. Distance was squared and then plotted as function of time. Clusters were divided into off-centre and midcell clusters for both quantifications as indicated.

Quantification of cell length

The cell length of strains of indicated genotypes is shown in box plots. Boxes enclose the 25th and 75th percentile with red lines representing the mean cell length and whiskers the 10th and 90th percentile. All outliers are shown as black dots if not mentioned differently. Box plots were produced using Sigma Plot v 12.5.

A — Comparative genomic organization of the pom gene cluster across *M. xanthus*, *M. macrosporus*, *M. fulvus*, *M. stipitatus*, *C. coralloides*, *C. fuscus*, *M. boletus*, *S. aurantiaca*, and *A. dehalogenans*.

B — Genetic locus and domain organization:

0632: fatty acid desaturase
0633: DNA-binding protein
0634: PomY
0635: PomZ
0636: PomX
0637: M48 family peptidase
0638: hypothetical protein

coiled coil   HEAT repeats   Pro-rich   P-loop ATPase   coiled coil

C

strain	mean cell length	constrictions	anuc. cells	length anuc. cells
WT	7.7 ± 1.9	7%	0%	
ΔpomX	15.4 ± 9.5	3%	5.9%	2.8 ± 1.5
ΔpomX/mCh-pomX	8.4 ± 2.6	6%		
ΔpomX/mCh-pomX^OE	7.8 ± 1.8	8%		
ΔpomY	16.2 ± 11.2	4%	7.4%	3.2 ± 1.3
ΔpomY/pomY-mCh	8.0 ± 1.8	10%		
ΔpomY/pomY-mCh^OE	8.5 ± 2.2	7%		
ΔpomZ	10.4 ± 7.1	3%	12.4%	3.2 ± 1.5
ΔpomYZ	15.5 ± 8.5	4%		
ΔpomXY	17.2 ± 11.8	1%		
ΔpomXZ	13.6 ± 7.8	2%		
ΔpomXYZ	10.4 ± 5.6	1%		

D — DIC and DAPI images of ΔpomX and ΔpomY

E — α-PomX and α-PomY immunoblots

F — α-PomY immunoblot of ΔpomY/P_cuoA pomY-mCh with CuSO_4 [μM]
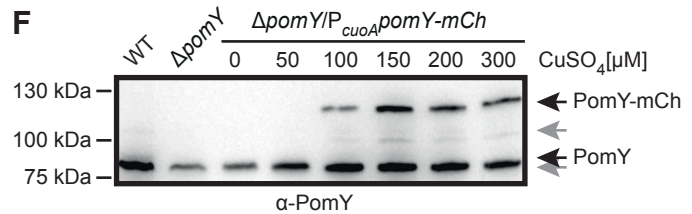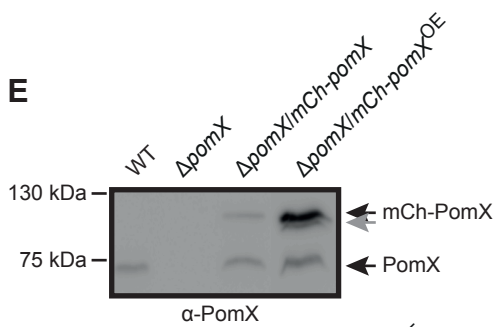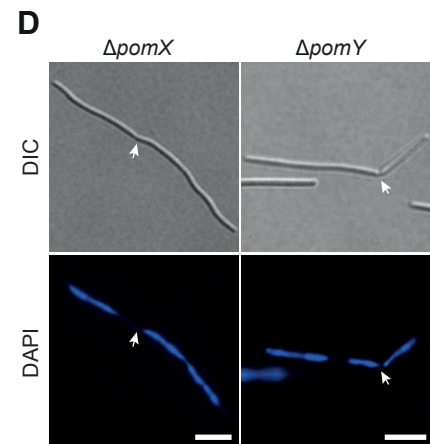
G — α-PomZ immunoblot

Figure S1, related to Figure 1. *pomX*, *pomY* and *pomZ* are encoded in a gene cluster present in other Myxobacteria

A. Conservation of the *pomXYZ* locus in Myxobacteria. Transcription direction is indicated by the orientation of arrows. PomX, PomY and PomZ homologs were identified with reciprocal BLASTP analysis (Huntley et al., 2011). % of similarity/identity between homologs is indicated by numbers in the arrows and were calculated using EMBOSS Needle software (pairwise sequence alignment) (Li et al., 2015).

B. *pomX*, *pomY* and *pomZ* gene cluster in *M. xanthus*. Start and stop codons are indicated. Domain structures were predicted by SMART analysis (Letunic et al., 2015). Transcription direction is indicated by arrows.

C. Quantification of average cell length, constriction frequency and anucleate cells of the indicated genotypes. The strains expressing mCh-PomX^{OE} and PomY-mCh^{OE} overexpress the two proteins (see also S1E). Strains used from top to bottom: DK1622, SA4223, SA4229, SA4252, SA4703, SA4713, SA4712, SA3108, SA4743, SA6130, SA4254, SA4722. n>250 cells for each strain.

D. Cell divisions in Δ*pomX* and Δ*pomY* mutants. Cell division position was analyzed in DAPI-stained cells of the indicated genotypes. White arrows indicate cell division constrictions. n>45 constrictions for each strain. Scale bar 2µm.

E. Accumulation of PomX, PomY and their fluorescent fusions in strains of indicated genotypes. Equal amounts of protein were loaded per lane. Western blots were probed with α-PomX and α-PomY antibodies. The strains labelled mCh-PomX^{OE} and PomY-mCh^{OE} overexpress the two proteins. Strains used in upper blot from left to right: DK1622, SA4223, SA4229, SA4252, and in the lower blot: DK1622, SA4703, SA4713, SA4712.

F. Immunoblot analysis of PomY and PomY-mCh accumulation in cells of indicated genotypes grown in media supplemented with indicated concentrations of CuSO$_4$. From left to right: DK1622, SA4703, SA4734. Equal amounts of protein were loaded per lane and the blots were probed with specific α-PomY antibodies as indicated.

G. Immunoblot analysis of PomZ, PomZ-mCh and PomZ^{D90A}-mCh accumulation after overexpression (OE). Equal amounts of protein were loaded per lane and the blots were probed with specific α-PomZ antibodies. Black arrow indicate PomZ and PomZ-mCh, grey arrows indicate PomZ-mCh degradation products. Strains used from left to right: DK1622, SA3108, SA3147, SA5006.
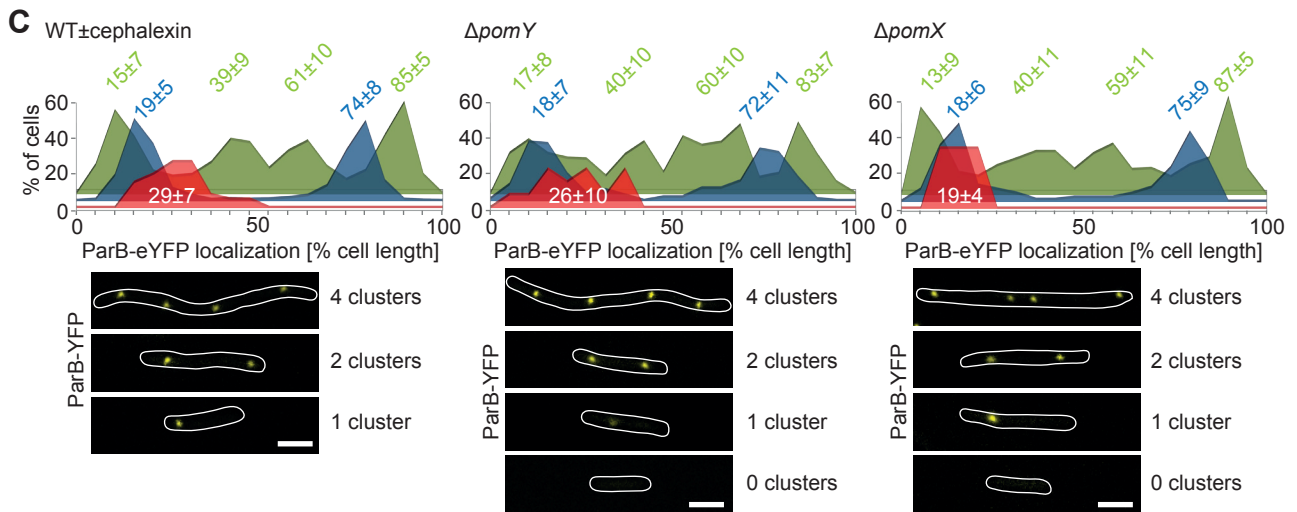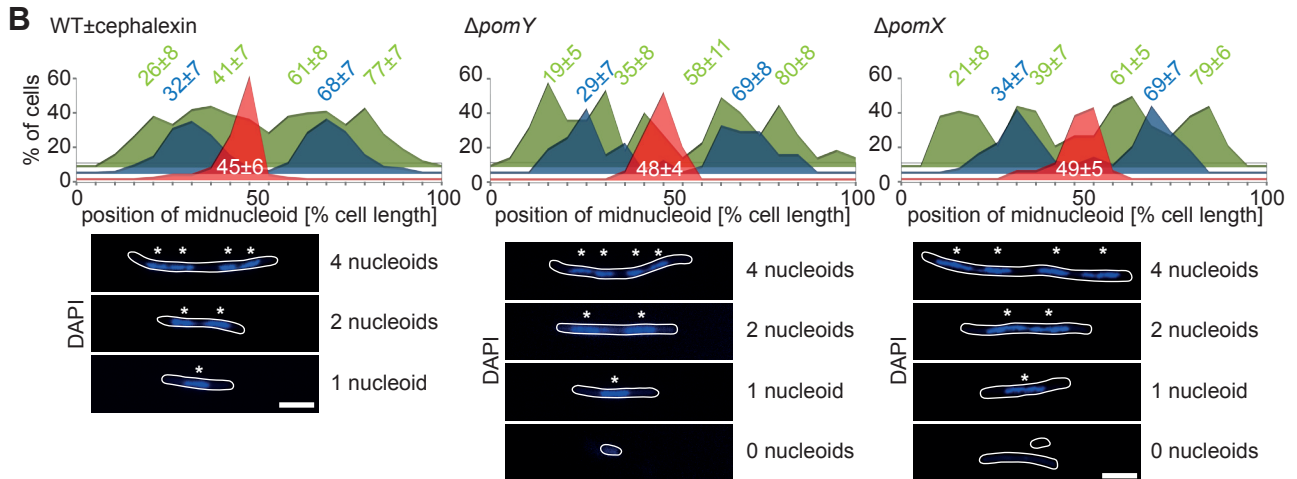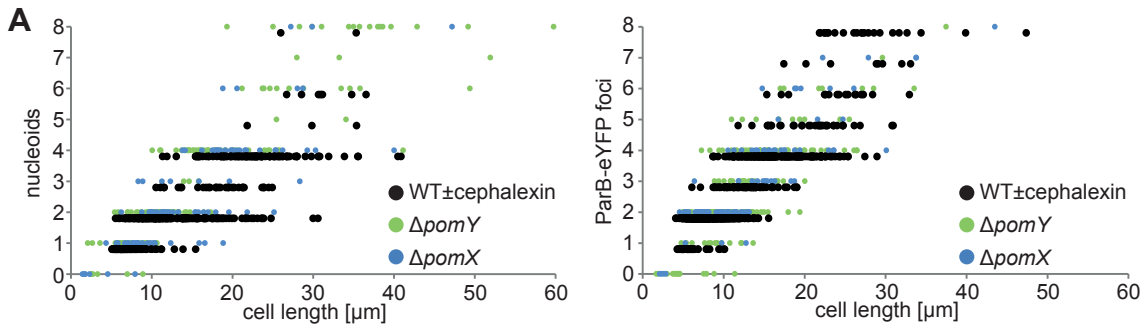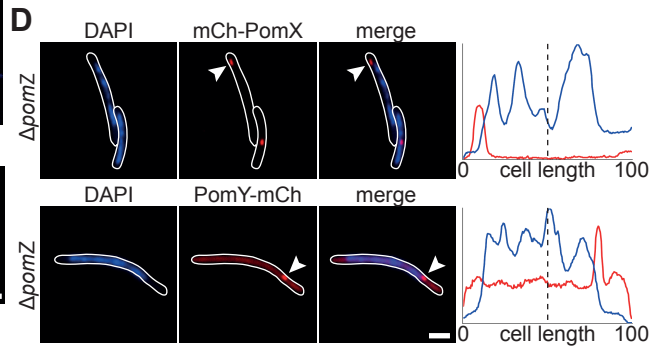
A

nucleoids vs cell length [µm] — WT±cephalexin, ΔpomY, ΔpomX

ParB-eYFP foci vs cell length [µm] — WT±cephalexin, ΔpomY, ΔpomX

B

WT±cephalexin

26±8 32±7 41±7 61±8 68±7 77±7

45±6

% of cells vs position of midnucleoid [% cell length]

DAPI: 4 nucleoids, 2 nucleoids, 1 nucleoid

ΔpomY

19±5 29±7 35±8 58±11 69±8 80±8

48±4

% of cells vs position of midnucleoid [% cell length]

DAPI: 4 nucleoids, 2 nucleoids, 1 nucleoid, 0 nucleoids

ΔpomX

21±8 34±7 39±7 61±5 69±7 79±6

49±5

% of cells vs position of midnucleoid [% cell length]

DAPI: 4 nucleoids, 2 nucleoids, 1 nucleoid, 0 nucleoids

C

WT±cephalexin

15±7 19±5 39±9 61±10 74±8 85±5

29±7

% of cells vs ParB-eYFP localization [% cell length]

ParB-YFP: 4 clusters, 2 clusters, 1 cluster

ΔpomY

17±8 18±7 40±10 60±10 72±11 83±7

26±10

% of cells vs ParB-eYFP localization [% cell length]

ParB-YFP: 4 clusters, 2 clusters, 1 cluster, 0 clusters

ΔpomX

13±9 18±6 40±11 59±11 75±9 87±5

19±4

% of cells vs ParB-eYFP localization [% cell length]

ParB-YFP: 4 clusters, 2 clusters, 1 cluster, 0 clusters
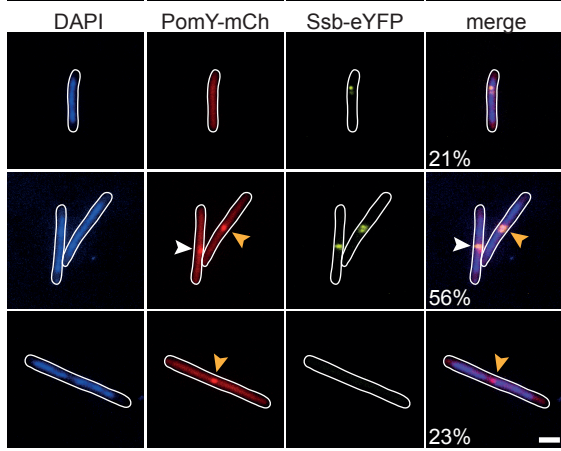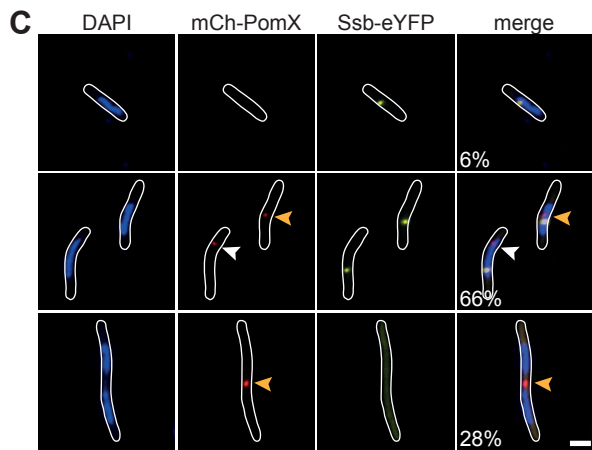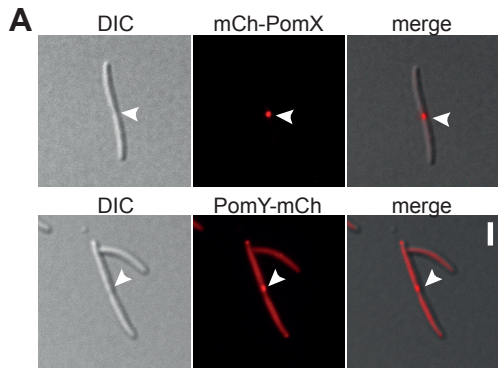
Figure S2, related to Figure 1. Δ*pomX* and Δ*pomY* mutants are unaffected in nucleoid localization and numbers

A. Quantification of chromosome number and number of origins of replication in WT, Δ*pomX* and Δ*pomY* cells. For nucleoid number analysis cells were stained with DAPI and in the case of WT additionally incubated with cephalexin for 8 and 12 hrs before visualization by DIC and fluorescence microscopy. The number of nucleoids was tracked and plotted as function of cell length. n>200 cells each strain. Strains used for quantification of nucleoids: DK1622, SA4223, SA4703. ParB-eYFP foci analyzed in SA4202, SA4219, SA4709.

B, C. Replication and chromosome segregation is unaffected by lack of PomX and PomY. The localization of nucleoid midpoints and ParB-eYFP were analyzed from the same cells as in A and plotted as a function of % of cell length. Histograms show the localization of midnucleoid and ParB-eYFP foci in cells with 1 (red), 2 (blue) and 4 (green) chromosomes or ParB-eYFP foci. Numbers display the mean position ± SD in percent of cell length. Scale bar, 2μm.

A

DIC | mCh-PomX | merge

DIC | PomY-mCh | merge

B

DAPI | PomZ-mCh | linescan

patchy

off-centre

midcell

midcell

cell length 0 — 100

I_{left} | I_{right}

I_{left} | I_{right}

asymmetry

off-centre | midcell | nucleoid (Pico Green)

C

DAPI | mCh-PomX | Ssb-eYFP | merge

6%

66%

28%

DAPI | PomY-mCh | Ssb-eYFP | merge

21%

56%

23%

D

DAPI | mCh-PomX | merge

Δ*pomZ*

cell length 0 — 100

DAPI | PomY-mCh | merge

Δ*pomZ*

cell length 0 — 100
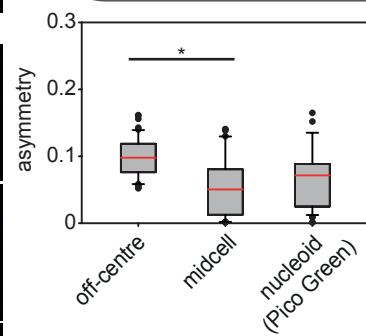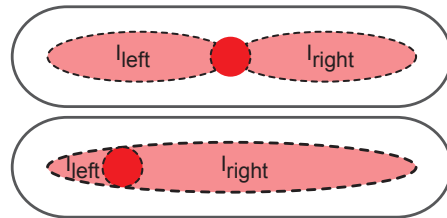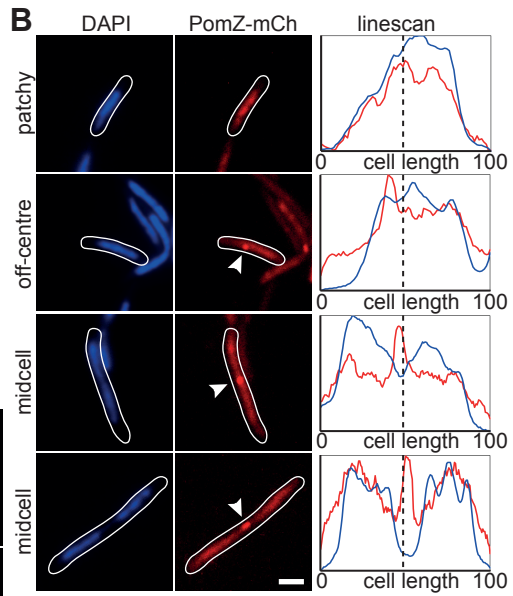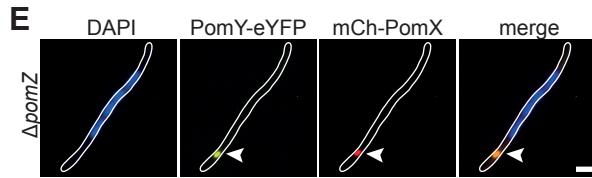
	PomY-mCh		mCh-PomX	
	+	-	+	-	*pomZ*
on nucleoid/midcell	82	57	94	54
subpolar	0	8	0	37
diffuse	18	35	6	9

E

DAPI | PomY-eYFP | mCh-PomX | merge

Δ*pomZ*

<u>Figure S3, related to Figure 2. PomX and PomY localize at midcell before the end of replication</u>

A. PomX and PomY colocalize with cell division constrictions. White arrows indicate constrictions in SA4229 (upper panel) and SA4713 (lower panel). Scale bar, 2µm.

B. PomZ-mCh localization in DAPI-stained cells. Linescans display fluorescence intensity of PomZ-mCh signal (red) and DAPI signal (blue) along the long cell axes of the indicated cells. Scale bar, 2µm. Schematic PomZ-mCh localization illustrates the values I_{left} and I_{right} used for calculation of the asymmetry value for the patchy PomZ-mCh signal over the nucleoid. Box plot shows quantification of PomZ-mCh asymmetry for cells with off-centre or midcell PomZ-mCh cluster and Pico Green stained nucleoids. * indicates that the two distributions are significantly different (t-test, p<0.01). Strain used: SA3131.

C. PomX and PomY localize to midcell before completion of replication. Δ*pomX* and Δ*pomY* cells expressing mCh-PomX and PomY-mCh together with Ssb-eYFP were DAPI stained and analyzed. Numbers display percentages with cells of that localization pattern (n=200 for each strain). Scale bar, 2µm. White arrows display off-centre clusters and orange arrows display midcell clusters of mCh-PomX and PomY-mCh. Strains used from top to bottom: SA7042, SA7043.

D. PomZ recruits PomX and PomY clusters to the nucleoid. Linescans as in B with DAPI (blue) and mCh-PomX or PomY-mCh (red). White arrows indicate clusters that do not colocalize with the nucleoid. The table lists % of cells with the localization on the left in the presence or absence of PomZ (n>200). Scale bar, 2µm. Strains used: SA4712, SA4720, SA4252, SA5821.

E. PomX and PomY colocalize in the absence of PomZ. White arrow indicates off-centre cluster of PomY-eYFP and mCh-PomX. Scale bar, 2µm. PomY-eYFP was expressed in presence of 150µM Cu^{2+}. Strain used: SA5839.
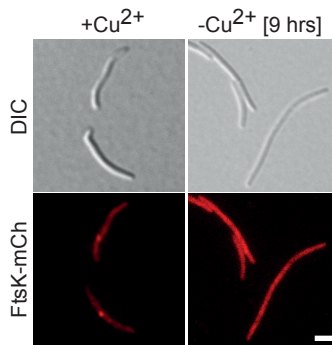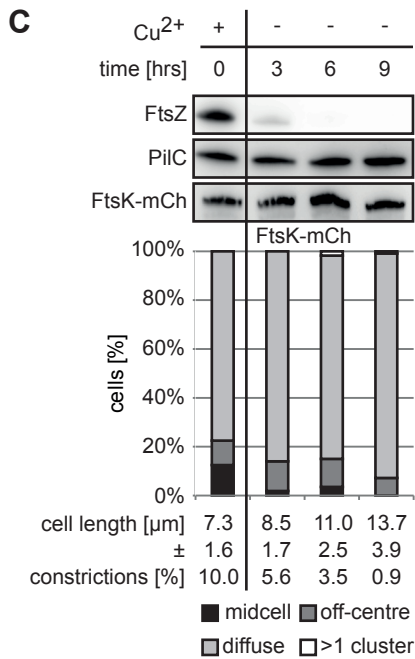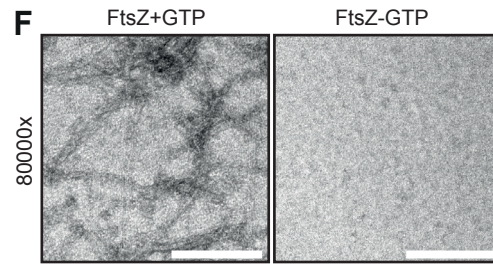
A

	mCh-PomX	merge	PomY-mCh
+Cu²⁺			
-Cu²⁺ [9 hrs]			

B

	mCh-PomX				PomY-mCh			
cephalexin	-	+	+	+	-	+	+	+
time [hrs]	0	3	6	9	0	3	6	9
cell length [µm]	7.9	9.9	14.3	18.4	8.3	11.2	13.7	16.9
±	1.9	2.3	3.5	6.2	2.0	3.9	3.9	5.3
constrictions [%]	8.2	23.0	39.4	53,5	3.0	9.4	10.4	25.3

■ midcell ■ off-centre □ >1 cluster ■ diffuse

C

Cu²⁺	+	-	-	-
time [hrs]	0	3	6	9
FtsZ				
PilC				
FtsK-mCh				

FtsK-mCh

cell length [µm]	7.3	8.5	11.0	13.7
±	1.6	1.7	2.5	3.9
constrictions [%]	10.0	5.6	3.5	0.9

■ midcell ■ off-centre
■ diffuse □ >1 cluster

	+Cu²⁺	-Cu²⁺ [9 hrs]
DIC		
FtsK-mCh		

D

PomX-His6, PomY-His6, His6-PomZ, FtsZ

130 kDa, 100 kDa, 70 kDa, 55 kDa, 35 kDa, 25 kDa, 15 kDa

MalE-PomZ^D90A, MalE-PomZ

130 kDa, 100 kDa, 55 kDa, 35 kDa, 25 kDa, 15 kDa, 10 kDa

E

10µM FtsZ
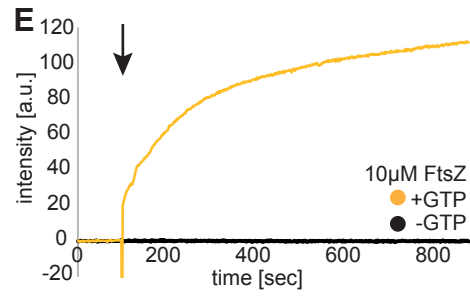● +GTP
● -GTP

F

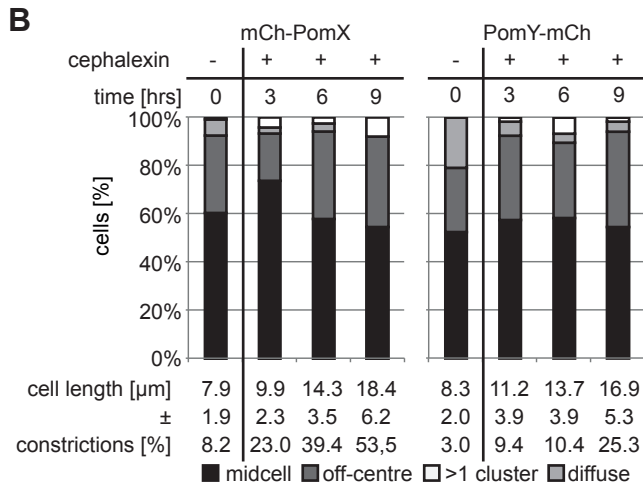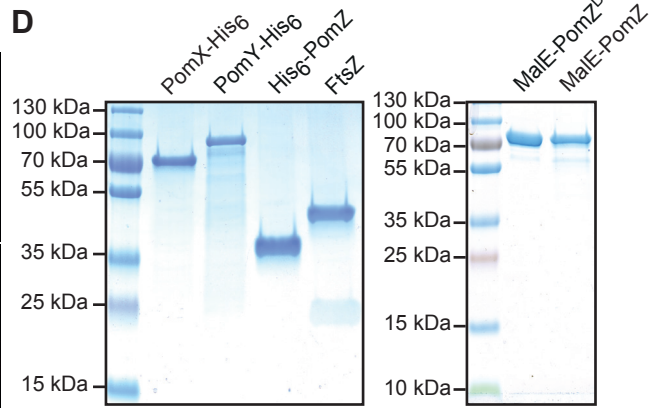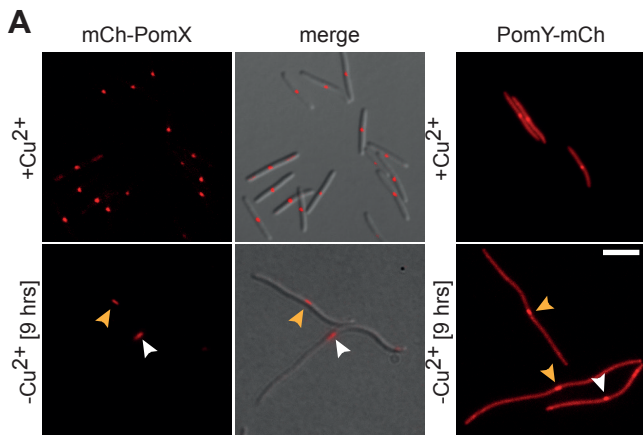| FtsZ+GTP	FtsZ-GTP

80000x

<u>Figure S4, related to Figure 3. PomX and PomY localize at midcell in the absence of FtsZ</u>

A. Localization of mCh-PomX and PomY-mCh in FtsZ-depleted cells. Cells of strain SA5809 (left) and SA4718 (right) were treated as described in Fig. 3B and images acquired before and 9 hrs after removal of Cu^{2+} from the growth media. White arrows indicate off-centre clusters and orange arrows indicate midcell clusters of mCh-PomX and PomY-mCh, respectively. Scale bar, 5µm.

B. Localization of PomY-mCh and mCh-PomX in cephalexin treated cells. Cells of strain SA4712 and SA4252 were treated with cephalexin for 9 hrs, stained with DAPI and analyzed by fluorescence microcopy. Mean cell length ± SD as well as constriction frequency were calculated (n>100 cells per time point and strain) together with PomY-mCh and mCh-PomX localization pattern at each time point. Pattern abundance is displayed in the histograms as % of total cells analyzed.

C. FtsK cluster formation depends on FtsZ. FtsK-mCh localization was followed during an FtsZ-depletion experiment as in A at indicated time points using strain SA4169. Upper panel, FtsZ level during the depletion experiment. Middle panel, accumulation of the loading control PilC in the same cells. Lower panel, accumulation of FtsK-mCh in the same cells. Cells were washed twice with copper-free medium and transferred to copper-free medium at t= 0 hrs. For each time point n>150 cells were analyzed to quantify average cell length ± SD, constriction frequency and pattern of FtsK-mCh localization. Pattern abundance is displayed in the histograms as % of total cells analyzed. Representative cells are shown in the panels on the right. Scale bar, 2µm.

D. SDS-PAGE analysis of purified proteins used in this study. Proteins were applied to SDS-PAGE on a 10% SDS-gel and stained with Instant Blue™. Molecular size markers are shown on the left. The calculated molecular mass of PomX-His$_6$ is 45.4kDa, of PomY-His$_6$ is 72.3kDa, of His$_6$-PomZ 37.7kDa of FtsZ is 44.7kDa, of MalE-PomZ is 77.7kDa and of MalE-PomZ^{D90A} is 77.6kDa. Note that in SDS-PAGE PomX-His$_6$ has a mobility larger than the monomer.

E. FtsZ forms GTP-dependent filaments in right angle light scattering. Experiments were performed with 10µM FtsZ at 8°C at pH 6.5. GTP at a final concentration of 2.5mM was added

at 100 sec as indicated by the black arrow. The graphs show mean values from two independent experiments.

F. Negative stain electron microscopy of FtsZ filaments. 3μM FtsZ at pH 6.5 were applied to a grid and negatively stained after incubation with or without 2.5mM GTP for 10 min at room temperature. Scale bar, 100nm.
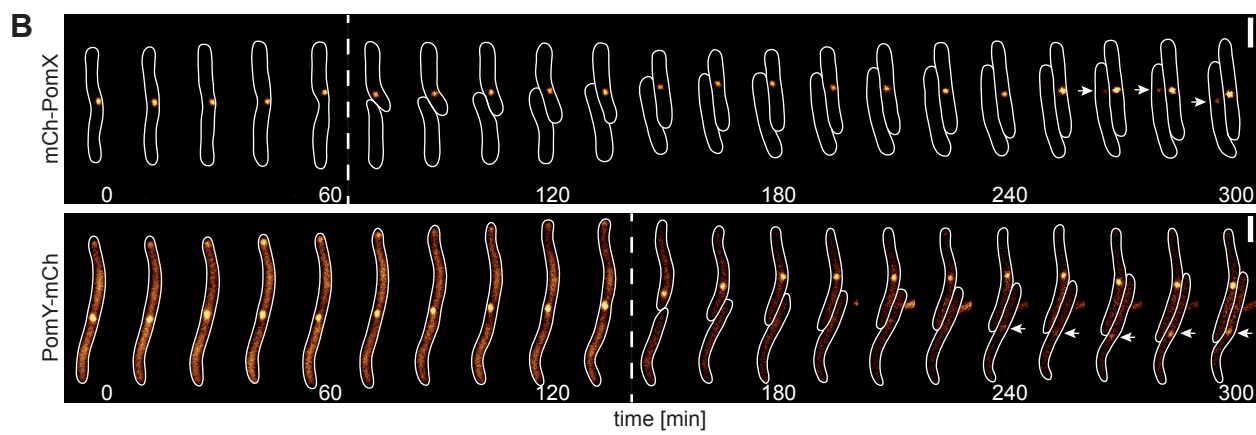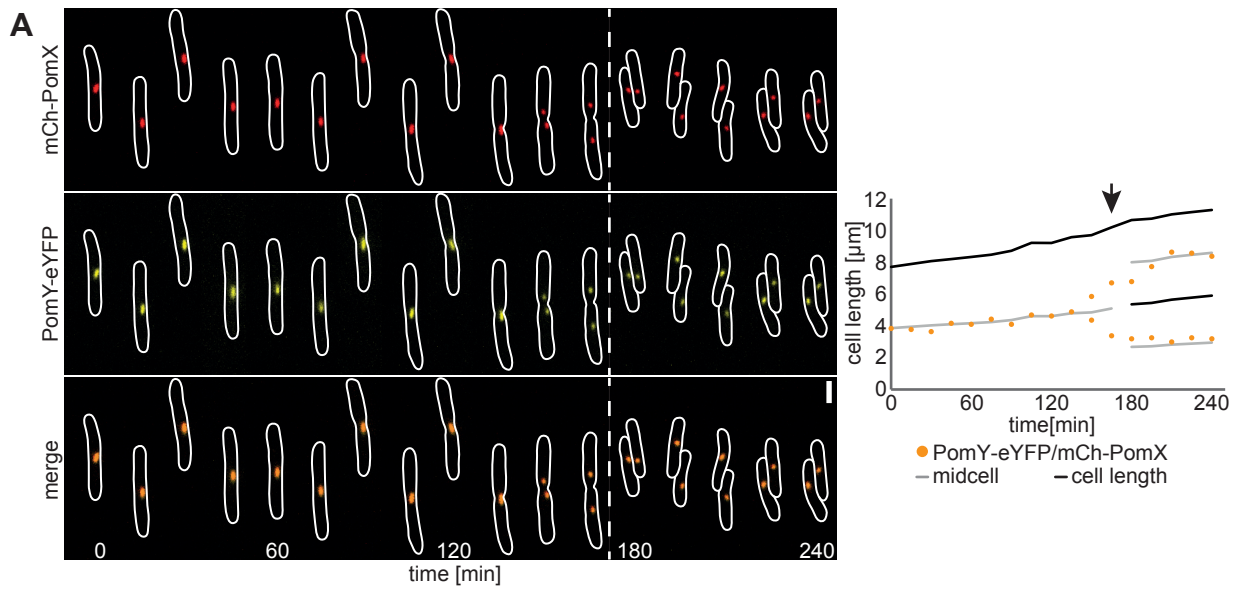
A

mCh-PomX

PomY-eYFP

merge

time [min]

0   60   120   180   240

PomY-eYFP/mCh-PomX
— midcell
— cell length

B

mCh-PomX

0   60   120   180   240   300

PomY-mCh

0   60   120   180   240   300

time [min]

<u>Figure S5, related to Figure 4. PomX and PomY are dynamically localized</u>

A. PomX and PomY colocalize during translocation to midcell and at midcell. Cells of strain SA7041 were recorded for 4 hrs on an agar pad containing 0.2% CTT growth medium at 32°C. Images were acquired every 15 min. PomY-eYFP was expressed in presence of 150µM Cu^{2+}. The white stippled line indicates a cell division event. Scale bar, 2µm. Right, schematic illustrate cluster localization in the cell on the left. The black arrow indicates the cell division event.

B. PomX and PomY are occasionally asymmetrically distributed to daughter cells during cell division. Cells expressing mCh-PomX (SA4797) or PomY-mCh (SA7000) were followed for 4 hrs on an agarose pad containing 0.2% CTT growth medium at 32°C. Images were recorded every 15 min. The depicted cells are representative for an asymmetric distribution of mCh-PomX and PomY-mCh during cell division. White stippled lines indicate cell divisions. White arrows indicate mCh-PomX and PomY-mCh in an emerging cluster. Scale bar, 2µm.
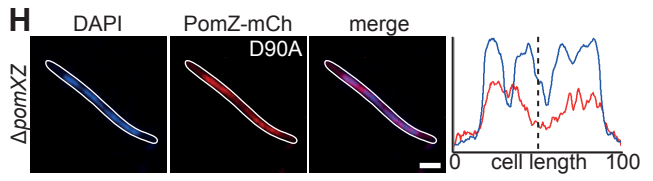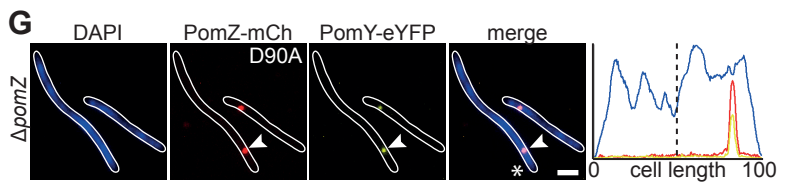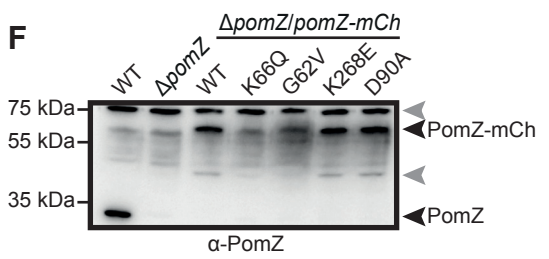
A

PomX-His₆ / PomY-His₆ rows with S/P lanes, 100 kDa and 70 kDa markers.

B

ATP binding [K66Q], dimerization [G62V], DNA binding [K268E], ATP hydrolysis [D90A], 2 ATP, 2 ADP, 2 Pi cycle diagram.

C

Sequence alignment, positions 56–107 and 265–311. G62, K66, D90, K268 highlighted.

	56	G62	K66	D90	107
PomZ_-_Mxanthus					
ParA1_-_Vcholerae					
ParA_-_Paeruginosa					
Soj_-_Bsubtilis					
ParA_-_Mxanthus					
ParA_-_Ccrescentus					
ParA_-_Mtuberculosis					
ParA_-_Cglutamicum					
ParA_-_Scoelicolor					
PpfA_-_Rsphaeroides					
ParA2_-_Vcholerae					

D

E.coli — DAPI, PomZ-mCh, merge panels: WT, K66Q, G62V, K268E, D90A

E

DAPI, PomZ-mCh, merge panels: WT, K66Q, G62V, K268E, D90A

F

ΔpomZ/pomZ-mCh. Lanes: WT, ΔpomZ, WT, K66Q, G62V, K268E, D90A. Markers 75, 55, 35 kDa. PomZ-mCh, PomZ. α-PomZ

G

ΔpomZ — DAPI, PomZ-mCh, PomY-eYFP, merge, D90A; profile plot cell length 0–100

H

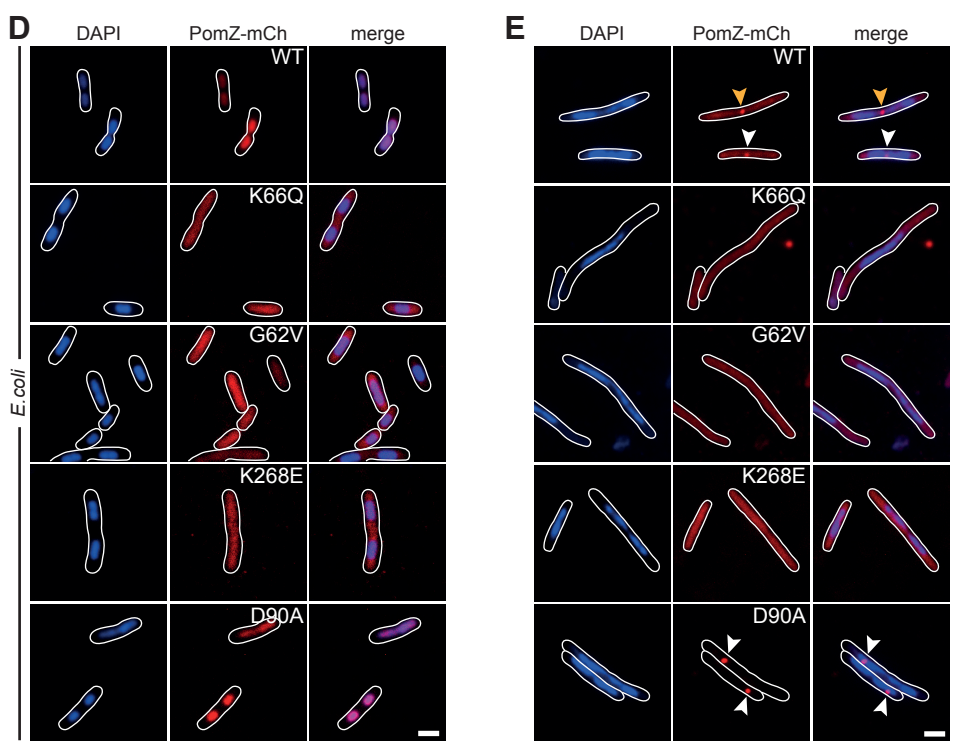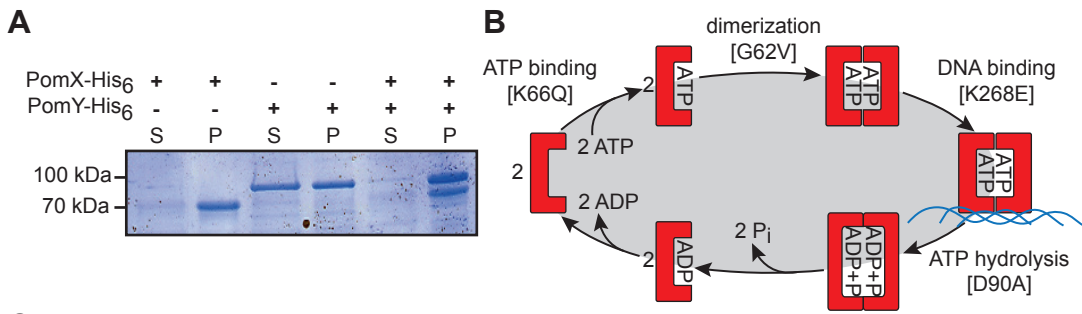ΔpomXZ — DAPI, PomZ-mCh, merge, D90A; profile plot cell length 0–100

Figure S6, related to Figure 5 and Figure 6. PomZ ATPase activity and DNA-binding are important for PomZ function and localization

A. PomX and PomY cosediment *in vitro.* Instant Blue™-stained SDS-PAGE of sedimentation-reactions of 3μM of PomX-His$_6$ and PomY-His$_6$ alone and in combination. Protein content of supernatant (S) and pellet fraction (P) was separated after high speed centrifugation. Molecular size markers are shown on the left.

B. Schematic of canonical ParA ATPase cycle. Amino acid substitutions refer to the numbering of PomZ residues (Cf. C).

C. Alignment of PomZ with other ParA ATPases. PomZ was aligned with other ParA ATPases using the MAFFT algorithm. Orange, brown, red and purple boxes indicate residues Gly62, Lys66, Asp90 and Lys268, respectively in PomZ. PomZ^{K66Q} and PomZ^{G62V} are predicted monomeric variants, PomZ^{K268E}, is predicted to be blocked in DNA binding, and PomZ^{D90A}, is strongly reduced in ATP hydrolysis and is predicted to be locked in the ATP-bound dimeric form that binds DNA nonspecifically (Leonard et al., 2005; Hester and Lutkenhaus, 2007; Ptacin et al., 2010; Schofield et al., 2010; Kiekebusch et al., 2012). Note that only the parts of the alignment that include these four residues are shown. Protein sequences used for the alignment: *B. subtilis* Soj (gi|586852); *V. cholerae* ParA1 (gi|15642766); *V. cholera* ParA2 (gi|15601863); *P. aeruginosa* ParA (gi|15600756); *M. xanthus* ParA (gi|108467427); *C. crescentus* ParA (gi|239977514); *M. tuberculosis* ParA (gi|923109897); *C. glutamicum* ParA (gi|41223089); *S. coelicolor* ParA (gi|75489208); *R. sphaeroides* PpfA (gi|332276184); *M. xanthus* PomZ (gi|108460931).

D. Subcellular localization of PomZ-mCh variants in *E. coli. E. coli* BL21 DE3 was treated and analyzed as described in Fig. 5A. Scale bar, 2μm.

E. Subcellular localization of PomZ-mCh variants in *M. xanthus. ΔpomZ* cells expressing PomZ, PomZ^{K66Q}, PomZ^{G62V}, PomZ^{K268E} or PomZ^{D90A} fused to mCh were DAPI stained. White and orange arrows indicate off-centre and midcell clusters. Scale bar, 2μm. Strains used top to bottom: SA3131, SA5001, SA5000, SA5837, SA3146.

F. Immunoblot analysis of PomZ and PomZ-mCh accumulation and its variants in cells of indicated genotypes. Strains used left to right: DK1622, SA3108, SA3131, SA5001, SA5000, SA5837, SA3146. Equal amounts of protein were loaded per lane and the blots were probed with α-PomZ antibodies.

G. PomZ^{D90A} colocalizes with PomY clusters on the nucleoid. White arrow indicates colocalizing PomY-eYFP and PomZ^{D90A}-mCh cluster in a cell for which the linescan is shown on the right; linescan was done as in Fig. 2A with DAPI (blue), PomZ-mCh (red) and PomY-eYFP (yellow). Scale bar, 2µm. PomY-eYFP was expressed with 150µM Cu^{2+} (Cf. Fig. S1F). Strain used: SA4758.

H. PomZ^{D90A} cluster formation depends on PomX. Linescan is as in Fig. 2A with DAPI (blue) and PomZ^{D90A}-mCh (red). Scale bar, 2µm. Strain used: SA7014.
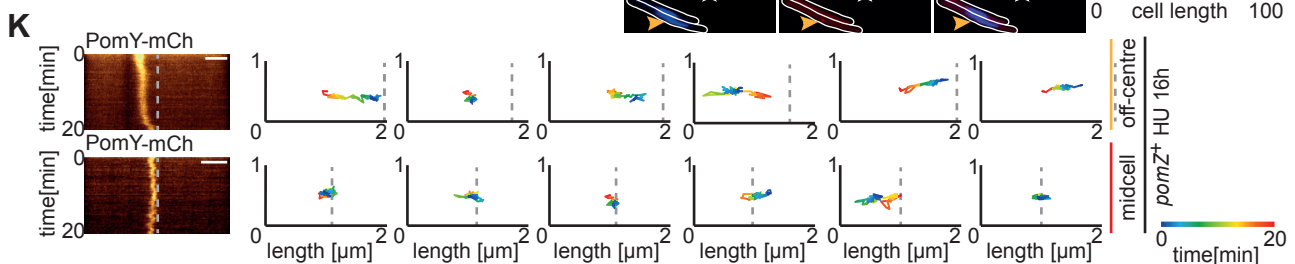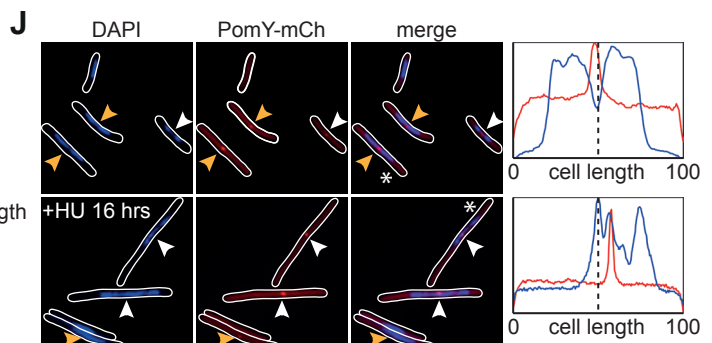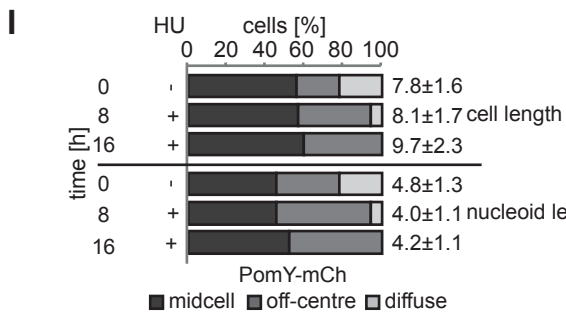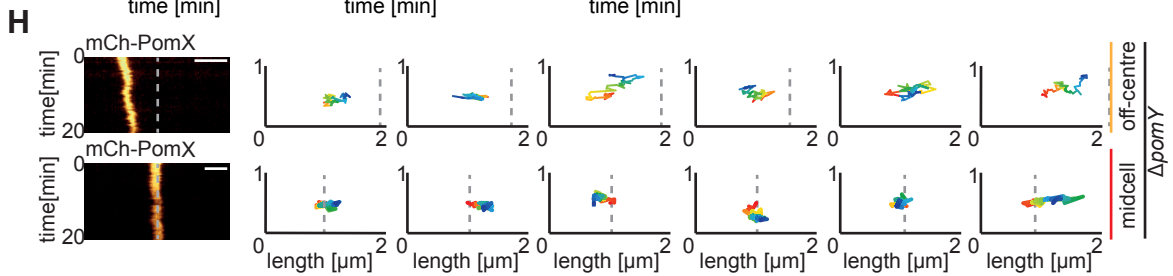
A PomXY X k_h

k_a^0 k_a k_a $\dfrac{k_{on}}{M}$ k_{hop}^0

nucleoid · attachment to PomXY cluster · hopping of cluster-bound PomZ dimers · ATP-hydrolysis & detachment · attachment to nucleoid · hopping · reflecting boundary condition

unstretched ATP-bound PomZ dimer
stretched ATP-bound PomZ dimer
X cluster position on nucleoid
M number of lattice sites on the nucleoid

B $k_h = 0.01$ sec^{-1}, $n_{total} = 100$

C 84 ± 32 min (n=99)

E WT ΔpomZ ΔpomZ/P_van pomZ
0µM 3µM Van
α-PomZ

D $n_{total} = 50$ | $n_{total} = 200$ | $n_{total} = 400$ | $n_{total} = 600$

F PomY-mCh / PomY-mCh / mCh-PomX
off-centre — pomZ^LE
midcell
pomZ^OE
length [µm]

G $k_h = 0.1$ sec^{-1} | $k_h = 0.001$ sec^{-1} | $k_h = 0$ sec^{-1}

H mCh-PomX
off-centre — ΔpomY
midcell
length [µm]

I HU cells [%]
time [h]		
0	-	7.8±1.6
8	+	8.1±1.7 cell length
16	+	9.7±2.3
0	-	4.8±1.3
8	+	4.0±1.1 nucleoid length
16	+	4.2±1.1

■ midcell ■ off-centre ■ diffuse
PomY-mCh

J DAPI PomY-mCh merge
+HU 16 hrs
cell length

K PomY-mCh
off-centre — pomZ^+ HU 16h
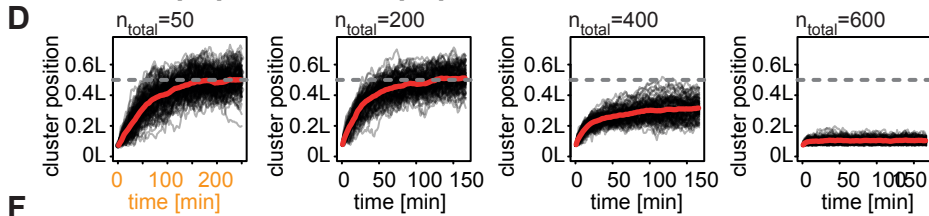midcell
length [µm]
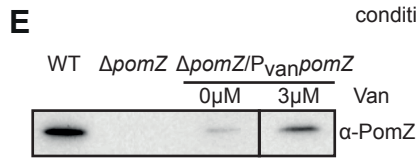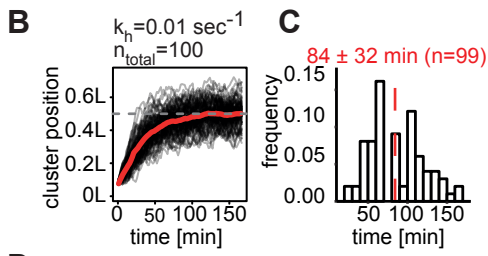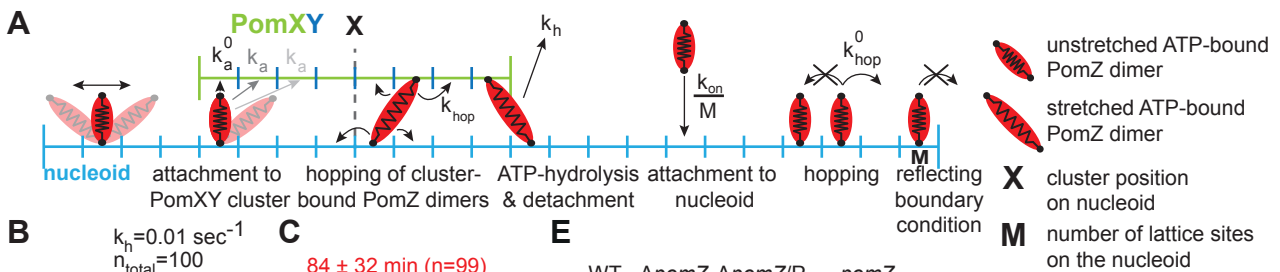time[min] 0 — 20

<u>Figure S7, related to Figure 7 and STAR*Methods. A PomZ flux-based model for midcell</u>

<u>positioning of the PomXYZ complex</u>

A. Schematic illustration of the mathematical model. The nucleoid and the cluster are modeled as one-dimensional lattices with reflecting boundaries. A PomZ dimer in the cytosol can attach to a single lattice site of the nucleoid with rate k_{on}/M (M is the total number of lattice sites of the nucleoid). PomZ dimers bound to the nucleoid can hop to a neighboring lattice site with rate k_{hop}^0, if the maximal number of binding sites is not reached for this lattice site (we chose the parameters such that only one dimer can bind per lattice site, Table S2). Due to thermal fluctuations nucleoid-associated PomZ dimers can spontaneously switch from a stretched to an unstretched conformation (indicated by transparent PomZ dimers). PomZ dimers on the nucleoid can bind to the cluster with a rate k_a^0, which decreases according to a Boltzmann factor if the PomZ dimer attaches to the cluster in a stretched state (rate k_a, the decreasing intensity of the arrows indicates a decrease in the attachment rate the further the PomZ dimer has to be stretched in order to attach to this site). Moreover, doubly-bound PomZ dimers can hop on the cluster and the nucleoid with rate k_{hop} and hydrolyze ATP with rate k_h and subsequently detach from the nucleoid and the cluster into the cytosol. The position of the midpoint of the cluster on the nucleoid is denoted by x.

B. Simulated trajectories of the PomXY cluster for the parameters summarized in Table S2. The position of the midpoint of the cluster on the nucleoid over time is shown for 100 runs of the stochastic simulation in black. The data was divided with respect to time into 90 time intervals of the same size and the cluster positions were averaged per time interval (shown in red). The horizontal dashed grey line indicates midnucleoid.

C. Histogram of the time the cluster needs to reach midcell (same data as in B). Time is recorded until the midpoint of the cluster first reaches midnucleoid. Note that the average time a cluster needs to reach midcell is not equivalent to the time, when the average trajectory of all cluster movements reaches midcell. In red the mean ± SD of the distribution is shown.

D. Simulated trajectories of the PomXYZ cluster as described in B for 0.5-, 2-, 4- and 6-fold the number of PomZ dimers.

E. Accumulation of PomZ under regulation of a vanillate inducible promoter. Cells of strain SA7070 were grown exponentially in the presence of vanillate (Van) at the indicated concentrations for 48 hrs and subjected to western blot analysis using specific α-PomZ antibodies. Same amount of total cell extracts were loaded per lane.

F. Kymographs and two-dimensional trajectories of PomY-mCh and mCh-PomX translocation at different PomZ levels. Kymographs and trajectories are as in Fig. 4B. For cluster translocation at low levels of PomZ ($pomZ^{LE}$) $pomZ$ expression was induced with 3µM vanillate in exponentially growing cells of strain SA7070 for 48 hrs before fluorescence microscopy (Cf. E). Note that $pomZ^{OE}$ cells rarely had midcell clusters of mCh-PomX and the clusters were not divided into off-centre and midcell. Strains used: SA7070 (upper two panels), SA7022 (lower panel). Scale bar, 2µm.

G. Simulated trajectories of the PomXYZ cluster as described in B for different ATP hydrolysis rates of PomZ dimers interacting with the PomXY cluster ($k_h = 0.1\ sec^{-1}, 0.001\ sec^{-1}, 0\ sec^{-1}$).

H. Kymographs and two-dimensional trajectories of mCh-PomX translocation in cells lacking PomY in strain SA7008. Kymographs and trajectories are as in Fig. 4B. Scale bar, 2µm.

I. Effect of hydroxyurea (HU) on PomY-mCh localization. Exponentially growing cells of strain SA4712 (Δ$pomY$/P$_{pilA}pomY$-mCh) were supplemented with 50mM HU for 16 hrs. Cells were treated with DAPI and imaged before treatment and then every 8 hrs after addition of HU. For each time point >100 cells were analyzed. To correlate PomY-mCh cluster localization with chromosome length, the long axis of the DAPI stained nucleoid was measured.

J. Images of PomY-mCh in HU-treated and untreated cells. Nucleoids were stained with DAPI. White arrows indicate off-centre clusters of PomY-mCh and orange arrows indicate midcell clusters. Cells marked with white * were used for linescans (right). Linescans show fluorescence intensity of DAPI stained nucleoids (blue) and PomY-mCh signals (red) along the long axes of the cell.

K. Kymographs and two-dimensional trajectories of PomY-mCh in HU-treated cells. Kymographs and trajectories are as in Fig. 4B. Exponentially growing cells of strain SA4746 were supplemented with 50mM HU for 16 hrs before fluorescence microscopy. Scale bar, 2µm.

WT			PomX-His$_6$				
		0.6	1.1	2.2	3.3	4.4	ng

α-PomX

WT			PomY-His$_6$			
		5.7	11.4	22.8	45.6	ng

α-PomY

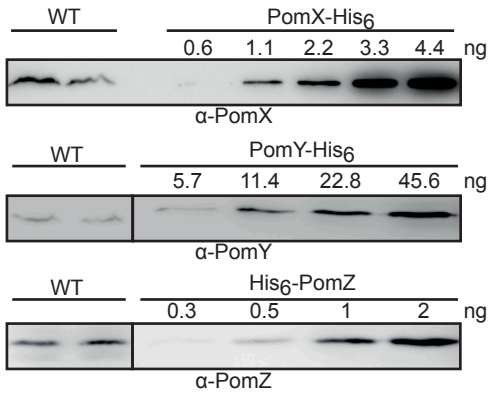| WT			His$_6$-PomZ			
		0.3	0.5	1	2	ng

α-PomZ

Figure S8, related to Figure 7 and STAR*Methods. Quantification of PomX, PomY and PomZ molecules per cell

Cell extracts from a known number of WT cells were probed in duplicate with specific antibodies for the presence of PomX (upper row) PomY (second from top), and PomZ (third from top) in parallel with different amounts of the corresponding purified His_6-tagged protein (Cf. Fig. S4D). Molecule number was calculated from the intensity of the band in WT lysates compared to a standard curve prepared from the dilution series of known protein amounts on the same western blot.

Table S1, related to STAR*Methods. Parameters of relevance for the Pom system from experiments and/or literature on related systems

Parameter	Value	Source/Comment
Number of PomZ molecules per cell	200	Western blot analysis (Fig. S8)
Length of *M. xanthus* nucleoid	$4.8 \pm 1.3 \, \mu m$	Measured
Diameter of Pom cluster (along long and short axis)	$0.71 \pm 0.15 \, \mu m$ $0.63 \pm 0.09 \, \mu m$	Measured
Attachment rate of ParA to nucleoid	$50 \, sec^{-1}$ $0.03 \, sec^{-1}$	(Ietswaart et al., 2014) (Lim et al., 2014)
Diffusion constant of ParA on nucleoid	$(0.01 - 1) \, \mu m^2 sec^{-1}$ $0.01 \, \mu m^2 sec^{-1}$	(Ietswaart et al., 2014) (Lim et al., 2014)
ATP-hydrolysis rate of PomZ in contact with PomXY and DNA	$34 \, ATP/h \times \frac{1}{2} \approx 0.01 \, sec^{-1}$	Measured
Diffusion constant ParB/*parS* complex in cytosol	$0.0003 \, \mu m^2 sec^{-1}$ $0.0001 \, \mu m^2 sec^{-1}$	(Ietswaart et al., 2014) (Lim et al., 2014)
Spring constant of ParA-ParB bond	$5 \times 10^{-2} \, pN/nm$ $\approx 10^4 \, k_B T/\mu m^2$	(Hu et al., 2015)
Generation time	$5h = 18000 \, sec$	(Treuner-Lange et al., 2013)
Time the cluster needs to move to midcell	$(82 \pm 51) \, min$ (PomY) $(81 \pm 53) \, min$ (PomX)	Measured

Table S2, related to STAR*Methods. Parameters used in the simulations

Parameter	Symbol	Value	Tested parameter space where model functions
Number of PomZ dimers	n_{total}	100	
Length of nucleoid	L	5 μm	
Diameter of PomXY cluster	$L_{cluster}$	0.7 μm	
Maximal density of PomZ binding sites on PomXY cluster	$c_{cluster}$	$1/0.007$ $μm^{-1}$	
Maximal density of PomZ binding sites on nucleoid	$c_{nucleoid}$	$1/0.007$ $μm^{-1}$	
Lattice spacing	a	0.007 μm	
Attachment rate of PomZ to nucleoid	k_{on}	0.1 s^{-1}	$(0.01 - 10)$ s^{-1}
Diffusion constant of PomZ on nucleoid	D	0.01 $μm^2 sec^{-1}$	
ATP-hydrolysis rate of PomZ bound to nucleoid and cluster	k_h	0.01 sec^{-1}	
Diffusion constant PomXY cluster in cytosol → $\gamma = k_B T/D_{cluster}$	$D_{cluster}$	0.0002 $μm^2 sec^{-1}$	
Spring constant of PomZ dimer	k	10^4 $k_B T/$ $μm^2$	
Attachment rate of PomZ dimer to cluster in unstretched state (per lattice site)	k_a^0	5 sec^{-1}	$(5 - 500)$ sec^{-1}
Initial position of PomXY cluster	p	0.35 μm $= 0.07$ L	

Chapter 4

Regulation of Pom cluster dynamics in *M. xanthus*

Abstract

Precise positioning of the cell division site is essential for the correct segregation of the genetic material into the two daughter cells. In the bacterium *Myxococcus xanthus*, the proteins PomX and PomY form a cluster on the chromosome that performs a biased random walk to midcell and positively regulates cell division there. PomZ, an ATPase, is necessary for tethering of the cluster to the nucleoid and regulates its movement towards midcell. It has remained unclear how the cluster dynamics change when the biochemical parameters, such as the attachment rates of PomZ to the nucleoid and the cluster, the ATP hydrolysis rate of PomZ or the mobility of PomZ dimers interacting with the nucleoid and cluster, are varied. To answer these questions, we investigate a one-dimensional model that includes the nucleoid, the Pom cluster and the PomZ protein. We find that a mechanism based on the diffusive PomZ fluxes on the nucleoid into the cluster can explain the latter's midnucleoid localization for a broad parameter range. Furthermore, there is an ATP hydrolysis rate that minimizes the time the cluster needs to reach midnucleoid. If the dynamics of PomZ dimers on the nucleoid is slow relative to the cluster's velocity, we observe oscillatory cluster movements around midnucleoid. To understand midnucleoid localization, we developed a semi-analytical approach that dissects the net movement of the cluster into its components: the difference in PomZ fluxes into the cluster from either side, the force exerted by a single PomZ dimer on the cluster and the effective friction coefficient of the cluster. Importantly, we predict that the Pom cluster oscillates around midnucleoid if the diffusivity of PomZ on the nucleoid is reduced. A similar approach to that applied here may also prove useful for cargo localization in ParABS systems.

Summary

In order for the rod-shaped bacterium *M. xanthus* to reproduce, its genetic content must be duplicated, distributed equally to the two cell halves and then the cell must divide precisely at midcell. Three proteins, called PomX, PomY and PomZ, are important for the localization of the cell division site at midcell. PomX and PomY form a cluster and PomZ tethers this cluster to the bacterial DNA or nucleoid (complex of chromosomal

DNA and proteins) and is important for the movement of the cluster from the nucleoid pole towards midcell. We are interested in the question how the cluster trajectories change when the PomZ dynamics is varied. To address this question we investigate a previously developed mathematical model that incorporates the nucleoid, the cluster and the PomZ dimers. We simulated the cluster trajectories for different model parameters, such as different diffusion constants of PomZ on the nucleoid. Interestingly, when the PomZ dimers diffuse slowly on the nucleoid, we observed oscillatory cluster movements around midcell. Our results provide general insights into intracellular positioning of proteins.

4.1 Introduction

The formation of protein patterns and the intracellular positioning of proteins is a major prerequisite for many important processes in bacterial cells, such as cell division. In order to maintain the genetic content of the bacterial cell, the chromosome (nucleoid) is duplicated during the cell cycle and must be segregated into the two cell halves prior to cell division. The future division site is defined by the FtsZ ring, which forms at midcell and recruits the cytokinetic machinery. Interestingly, FtsZ is highly conserved in bacteria, while the protein systems responsible for the positioning of the FtsZ ring, and with it the cell division site, are not [7–9].

Recently, Schumacher et al. identified a set of proteins, called PomX, PomY and PomZ, in *Myxococcus xanthus* cells that are important for midcell localization and formation of the FtsZ ring [1, 2, 101]. PomZ is an ATPase, which belongs to the family of ParA/MinD ATPases. It binds non-specifically to DNA in its dimeric, ATP-bound state, and its activity is stimulated by interactions with PomX, PomY and DNA. PomX and PomY form a single cluster, which is tethered to the nucleoid via PomZ dimers bound to the chromosome. Starting from an off-center position near one nucleoid pole, the cluster moves towards midnucleoid, coinciding with midcell [2]. When the cluster has reached midcell, the FtsZ ring forms there and the cell divides. During cell division, the cluster splits into two halves, such that each half is located at one pole of the nucleoids in the daughter cells, and the same cycle repeats. Notably, the Pom proteins localize to midcell before FtsZ and also in the absence of FtsZ [1, 2].

Midcell localization of the FtsZ ring has been well studied in *Escherichia coli* cells [36, 41–43, 45–49, 51–54, 56]. Here, Min proteins (MinC, MinD and MinE) guide the formation of the FtsZ ring at midcell. Both systems contain an ATPase (PomZ and MinD, respectively) and perform the same task in the cell, i.e. midcell sensing. Nevertheless, the two systems differ in various ways: First, the scaffold to which the ATP-bound ATPase binds is different: MinD binds to the cell membrane and PomZ to the bacterial nucleoid in the cytoplasm. Second, MinD-bound MinC inhibits [24], whereas the Pom cluster promotes FtsZ ring formation at midcell [2]. Finally, the observed protein patterns differ: the Pom proteins colocalize in a cluster that moves towards midcell, while the Min proteins, which do not form a cluster, oscillate from pole to pole [24, 25]. The oscillatory pole-to-pole movement of the Min proteins results

in a minimal Min protein concentration at midcell on average over time. Since FtsZ ring formation is negatively regulated by MinC, this restricts the ring to midcell. From a mechanistic point of view, the Pom system is closer to plasmid and chromosome segregation systems that involve a ParABS system than to the Min system.

Like the Pom system, plasmid and chromosome segregation systems make use of an ATPase that shuttles one or several cargoes (such as a plasmid, a partition complex or a protein cluster) along the nucleoid. Low-copy-number plasmids need to be actively segregated to ensure that both daughter cells inherit a copy of the plasmid. To ensure their equal distribution to the daughter cells, the plasmids are tethered to the nucleoid and positioned at equal distances along the nucleoid by ParABS systems [10, 13, 15]. A ParABS system consists of the proteins ParA and ParB, and a DNA sequence, *parS*. ParA proteins are ATPases, which bind non-specifically to DNA as ATP-bound dimers [34, 65, 66]. Their ATPase activity is stimulated in the presence of ParB [67–69], which binds to the *parS* sequence on the chromosome (to form the partition complex) or on the plasmid [9]. Besides plasmid and chromosome segregation [28], ParABS systems are also important for the positioning of cellular components (e.g. chemotactic clusters or carboxysomes) [17, 60]. Several different cargo dynamics involving ParABS systems have been observed. For one cargo these localization patterns include, among others, midcell localization [3, 14, 15], oscillatory movement of ParA and its cargo [10, 13, 72] as well as movement from one cell pole to the other [6]. Multiple cargoes are found to equidistantly position along the nucleoid [3, 10, 13–15].

To account for the dynamics observed in Par systems, various mechanisms have been proposed. Some models rely on ParA filament formation [10, 28, 67, 73, 80, 81, 95]; others challenge this assumption in *in vivo* systems [6, 12, 97]. A diffusion-ratchet mechanism for the movement of ParB-coated beads *in vitro* and DNA segregation *in vivo* has been introduced [69, 76, 79, 97, 98, 115]. Based on the observation that DNA has elastic properties [5, 6], a DNA relay mechanism for the movement of the partition complex was proposed [6, 100]. Here, the force exerted on the cargo is attributed to the elastic properties of the chromosome. Ietswaart et al. observed that if a plasmid is located off-center on the nucleoid, the ParA flux from the left and right sides of the plasmid differ [3]. Based on this idea, they proposed a model that produces equal plasmid spacing over the nucleoid as long as the plasmid moves in the direction of the higher ParA concentration [3]. Additionally, models based on reaction-diffusion equations for Par protein dynamics, have been introduced [16, 74, 75, 85].

In order to account for the experimental observations in *M. xanthus* cells, we have proposed a model for midcell localization [2] that includes the elasticity of the nucleoid and the PomZ proteins [6, 105]. Our model suggests a positioning mechanism that relies on the biasing of fluxes of PomZ dimers on the nucleoid, similar to the equipositioning mechanism proposed by Ietswaart et al. [3]. With this model we were able to reproduce midnucleoid localization with physiologically relevant parameters [2], but it remained unclear how the movement of the cluster changes when the rates of the key biological processes involved are varied.

Here, we investigate Pom cluster dynamics when the attachment rate of PomZ dimers to the nucleoid, the binding rate of PomZ dimers to the cluster, the ATP

hydrolysis rate of PomZ dimers and the diffusivity of PomZ dimers on the nucleoid and cluster are each varied over a broad parameter range. Interestingly, we observed that there exists an intermediate ATP hydrolysis rate that minimizes the time the clusters need to reach midnucleoid. Furthermore, we found that fast diffusion of PomZ dimers on the cluster accelerates the movement of the cluster towards midnucleoid. To gain a better understanding of the cluster dynamics observed in the *in silico* parameter sweeps, we investigated how PomZ dimers generate a net force on the cluster in our model. For the case where the PomZ gradient builds up faster than the velocity of cluster movement, we derived a semi-analytical approximation for the average cluster trajectory, which dissects the generation of a net force into two parts: the difference between the diffusive PomZ fluxes into the cluster from either side, and the force exerted by a single PomZ dimer during its interaction with the cluster. This net force can account for the movement of the cluster to midnucleoid. In contrast, when the PomZ dimers diffuse slowly on the nucleoid, we observed oscillatory cluster movement.

4.2 Stochastic model

Previously, we developed a stochastic lattice gas model to understand the dynamics of the PomXY cluster, i.e. the cluster consisting of PomX and PomY proteins, in *M. xanthus* bacterial cells [2]. In this model, both the nucleoid and the PomXY cluster are reduced to one-dimensional lattices of length L and L_c, respectively (Fig. 4.1). Note, that we regard the PomXY cluster composition as static in our model. The PomZ dimer dynamics is modeled as follows: ATP-bound PomZ dimers can bind to the nucleoid with rate k_{on} (Fig. 4.1A(1)), except where the PomXY cluster is located, and diffuse on the nucleoid with diffusion coefficient D_{nuc} (Fig. 4.1A(2)). We model the PomZ dimers effectively as springs with spring stiffness k to account for the elastic properties of the chromosome and the PomZ dimers. We expect the PomZ dimers to be stiffer than the chromosome, such that the elasticity of the nucleoid is the main contribution (see also [6, 115]). A PomZ dimer has two binding sites, and attaches to the nucleoid via the first. Because of thermal fluctuations, the relative position of the second binding site, which enables PomZ to bind to the PomXY cluster, is distributed according to a Boltzmann distribution with the energy of the spring. Therefore, PomZ dimers can attach to the PomXY cluster even if their nucleoid binding sites are not directly below the cluster (Fig. 4.1A(3) and 4.1B). We include this factor in the model by multiplying the rate of attachment, k_a^0, by the Boltzmann factor corresponding to the energy of the spring (as in [105]):

$$k_a = k_a^0 \exp\left[-\frac{1}{2}\frac{k}{k_B T}(x_i^{\mathrm{clu}} - x_i^{\mathrm{nuc}})^2 \right]. \tag{4.1}$$

The positions of the cluster and nucleoid binding sites of the i-th PomZ dimer bound to the nucleoid and the PomXY cluster are given as x_i^{clu} and x_i^{nuc}, respectively (see Fig. 4.1B).
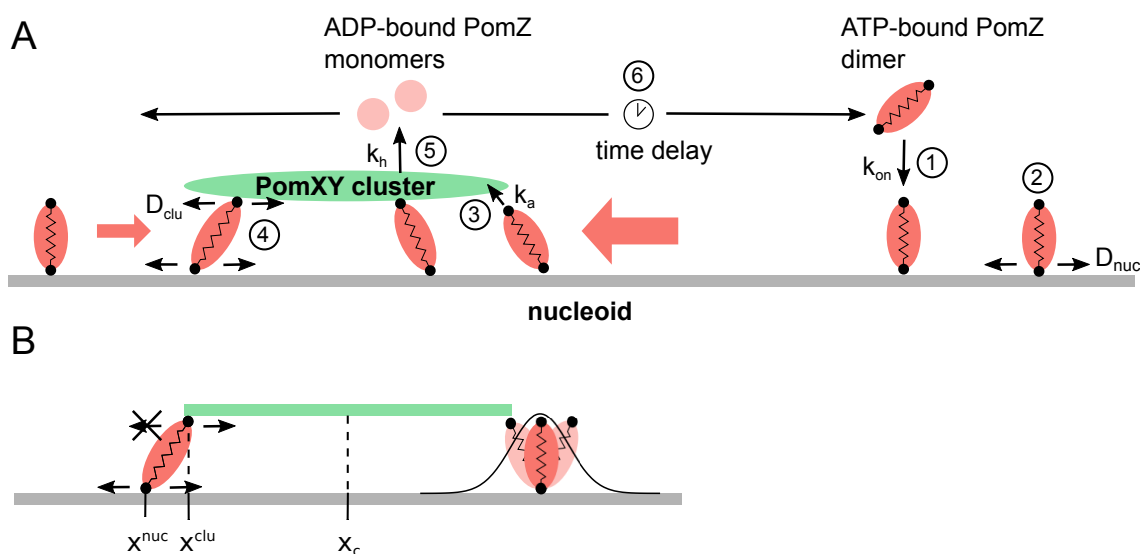
Figure 4.1 Flux-based model for midnucleoid positioning. (A) In our mathematical model, ATP-bound PomZ dimers can attach to the nucleoid (1) and then diffuse along it (2). The elasticity of the chromosome and the PomZ dimers is effectively included by modeling the PomZ dimers as springs. A nucleoid-bound PomZ dimer has a free binding site available to bind to the PomXY cluster (3). When also bound to the PomXY cluster, a PomZ dimer can diffuse both on the cluster and on the nucleoid (4). The interaction of PomZ with the PomXY cluster (and DNA) leads to a stimulation of the ATPase activity of PomZ, which in turn causes a conformational change in the ATP-bound PomZ dimer and the release of two ADP-bound monomers into the cytosol (5). ADP-bound PomZ monomers must exchange ADP for ATP and form dimers before they can bind to the nucleoid again (these processes are not explicitly included in the model). Hence, there is a delay between release of the inactive, ADP-bound form and reconstitution of the active, ATP-bound form (6). (B) Details of the PomZ interactions with the PomXY cluster. Not only PomZ dimers with a nucleoid binding site below the PomXY cluster, but also PomZ dimers outside of the cluster region can attach to the cluster, in a stretched configuration. The edges of the PomXY cluster are reflecting boundary conditions for the movement of PomZ's cluster binding site (indicated by the crossed arrow).

PomZ dimers bound to the PomXY cluster and the nucleoid are assumed to diffuse on both scaffolds (Fig. 4.1A(4)). This assumption is motivated by two experimental observations. First, fluorescently tagged PomZ brightly stains the entire cluster in fluorescence micrographs [2]. Second, in a mutant with PomZ dimers that cannot bind to DNA, PomZ is homogeneously distributed inside the cell, which suggests that PomZ dimers only bind to the PomXY cluster when they are nucleoid-bound [2]. Based on these two experimental findings it seems reasonable that PomZ dimers are also mobile on the PomXY cluster as otherwise the concentration of PomZ would be rather concentrated at the cluster edges. We allow for different diffusivities of the PomZ

dimers on the PomXY cluster and the nucleoid. The hopping rates of the nucleoid and cluster binding sites are $\epsilon_{\text{hop, nuc}}^0 = D_{\text{nuc}}/a^2$ and $\epsilon_{\text{hop, clu}}^0 = D_{\text{clu}}/a^2$, with the lattice spacing a, respectively, being weighted by a Boltzmann factor that accounts for the energy change of the spring due to the movement:

$$\epsilon_{\text{hop}} = \epsilon_{\text{hop}}^0 \exp\left[-\frac{1}{4}\frac{k}{k_B T}\left((x_i^{\text{clu, to}} - x_i^{\text{nuc, to}})^2 - (x_i^{\text{clu, from}} - x_i^{\text{nuc, from}})^2\right)\right]. \qquad (4.2)$$

Here, $x_i^{\text{clu, from}}, x_i^{\text{nuc, from}}$ and $x_i^{\text{clu, to}}, x_i^{\text{nuc, to}}$ signify the position of the binding sites of the i-th PomZ dimer to the cluster and nucleoid before and after hopping, respectively. The additional factor of $1/2$ in the exponent is chosen such that detailed balance holds for the hopping events and the rates for hopping to a neighboring site and hopping back are the inverse of each other (see [105]). Because of the exponential factor in Eq. 4.2 a PomZ dimer is most likely to move in the direction that relaxes the spring. We chose reflecting boundary conditions for diffusion of PomZ on both the nucleoid and the PomXY cluster. PomX, PomY and DNA stimulate the ATPase activity of PomZ, which leads to a conformational change and finally to detachment of two ADP-bound PomZ monomers from the nucleoid [2]. In our model, we combine the processes of nucleotide hydrolysis and detachment into one rate by assuming that nucleoid- and cluster-bound PomZ dimers are released into the cytosol with hydrolysis rate k_h (Fig. 4.1A(5)). The ADP-bound PomZ monomers must then exchange ADP for ATP and dimerize before they can rebind to the nucleoid. This leads to a delay between detachment from and reattachment to the nucleoid (Fig. 4.1A(6)). The delay and the rapid diffusion of PomZ in the cytosol [2] lead to an essentially homogeneous distribution of ATP-bound, dimeric PomZ in the cytosol. Hence, our assumption of a homogeneous attachment rate of cytosolic ATP-bound PomZ dimers to the nucleoid is justified. Note that we do not include ADP-bound PomZ and PomZ monomers explicitly in our model, but only consider PomZ proteins in the ATP-bound dimeric state. The total number of PomZ dimers is assumed to be constant and is denoted by N_{total}.

So far we have described the stochastic dynamics of the PomZ dimers. The interactions of PomZ dimers with the PomXY cluster result in forces being exerted on the cluster, which cause it to move on the nucleoid. The observable of interest is the PomXY cluster position, x_c, over time. We approximate the PomXY cluster dynamics as overdamped, such that the equation of motion for the cluster position is given by the following force balance equation

$$\gamma_c \partial_t x_c = -k \sum_{i=1}^{N} (x_i^{\text{clu}} - x_i^{\text{nuc}}), \qquad (4.3)$$

with γ_c being the friction coefficient of the PomXY cluster in the cytosol and N the total number of cluster-bound PomZ dimers. Experiments show that the Pom cluster displays very little motion in *M. xanthus* cells that lack PomZ, whereas its mobility is increased if PomZ is present [2]. Based on this observation, we disregard movements of

the cluster due to thermal noise and focus on the stochasticity in the interactions of PomZ dimers with the PomXY cluster, which in turn lead to stochastic forces acting on the cluster. Therefore, we do not include a Langevin noise term in Eq. 4.3.

4.3 *In silico* parameter analysis

With physiologically relevant parameters (Table S4.1, for the discussion of the parameters see A.1), the stochastic simulations show midnucleoid positioning of the PomXY cluster (Fig. 4.2, data shown in black). The underlying mechanism for midnucleoid localization is based on the flux of PomZ on the nucleoid, which can be described as follows. If the PomXY cluster is located to the left of midnucleoid, the average flux of PomZ dimers into the cluster from the right is larger than that from the left [3] (red arrows in Fig. 4.1A). Particles that attach to the cluster typically exert a net force in the direction from which they reached the cluster. Thus the flux imbalance leads to a net force towards the right, i.e. towards midnucleoid. If the cluster overshoots midnucleoid or is already positioned to the right of midnucleoid, the asymmetry in the fluxes is reversed and the cluster moves back towards midnucleoid. Overall, this leads to a self-regulating process that positions the PomXY cluster at midnucleoid.

Wild-type cells contain a total PomZ dimer number of $N_{\text{total}} \approx 100$ [2], which results in a low density of PomZ dimers on the nucleoid, and hence exclusion effects can be neglected. Here, we focus on the low PomZ density regime, which reflects the wild-type situation, and therefore we do not limit the PomZ dimer density on the nucleoid. We performed parameter sweeps by varying the attachment rate of PomZ dimers to the nucleoid, k_{on}, the binding rate of nucleoid-bound PomZ dimers to the PomXY cluster, k_a^0, the ATP hydrolysis rate of PomZ dimers, k_h, and the mobility of PomZ dimers on the nucleoid, D_{nuc}, and on the PomXY cluster, D_{clu}, over a broad range (Fig. 4.2).

The parameter sweeps show that increasing the attachment rate to the nucleoid, k_{on}, or the binding rate to the PomXY cluster, k_a^0, decreases the time the cluster needs to reach midnucleoid (Fig. 4.2A and 4.2B). In both cases, the trajectories become independent of the particular parameter when its value exceeds a certain threshold. We conclude that increasing the rate of attachment of PomZ to the nucleoid or the binding of PomZ to the PomXY cluster speeds up the positioning process until an optimum is reached.

Next, we consider the effects of varying the rate of ATP hydrolysis by PomZ dimers associated with the PomXY cluster, which is important to maintain the cyclic flux of PomZ dimers between cytosolic and DNA-bound states. This rate also sets the time scale for the interaction of PomZ dimers with the PomXY cluster. The simulations show that decreasing the hydrolysis rate ($k_h = 0.01\,\text{s}^{-1}$) reduces the velocity of the average PomXY cluster trajectory towards midnucleoid (Fig. 4.2C). Qualitatively, large hydrolysis rates ($k_h = 10\,\text{s}^{-1}$) have essentially the same effect (Fig. 4.2C). Hence, there is a hydrolysis rate k_h that minimizes the time the PomXY cluster needs to reach midnucleoid. Although the average PomXY cluster trajectory behaves similarly for large and small hydrolysis rates, we observe that the variance of the cluster distribution
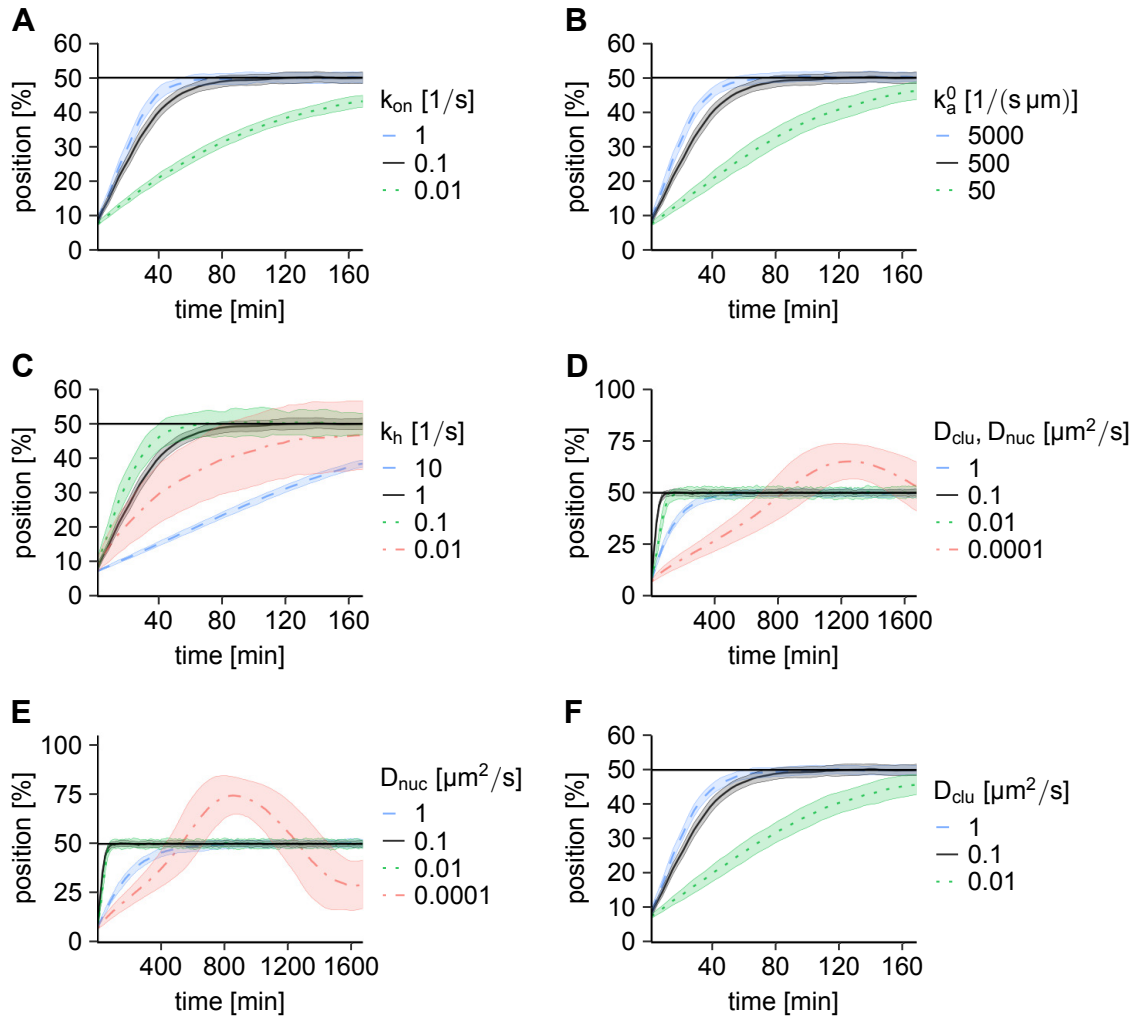
Figure 4.2 Exploring the parameter space. (A-F) Stochastic simulations show different qualitative behavior of the PomXY cluster trajectories when the model parameters are altered. We performed stochastic simulations using the parameter set given in Table S4.1, with one of the parameters varied as indicated. In D, the diffusion constants of PomZ on the nucleoid and on the PomXY cluster are set to the same value. The result for the parameter set given in Table S4.1 is always shown in black for comparison purposes. The average cluster trajectories are shown as unbroken or dashed lines and the shaded regions indicate the region of $\pm$ one standard deviation. In the simulations, the initial position of the PomXY cluster is chosen such that the left edge of the cluster coincides with the left edge of the nucleoid (for more details see Materials and methods section). For the calculation of the mean and standard deviations the cluster positions are grouped into time intervals of $3.33\,\mathrm{min}$. For each parameter set we simulated at least 100 trajectories.

over time decreases with increasing hydrolysis rate (Fig. 4.2C).

Apart from the ATP hydrolysis rate, we expect the diffusivity of PomZ on the nucleoid to be a crucial parameter for cluster movement, because it determines the time needed for PomZ dimers to explore the nucleoid to the left or right of the cluster. Interestingly, when we reduce the diffusivity of PomZ on the nucleoid in the simulations, the clusters begin to oscillate around the midnucleoid position (Fig. 4.2D, 4.2E and Fig. S4.1). For values of D_{nuc} large enough such that midnucleoid localization is obtained, we observe that there exists an optimal value that minimizes the time the clusters need to reach midcell, similar to the observation for the ATP hydrolysis rate. Finally, we also decreased the diffusion constant of PomZ dimers on the PomXY cluster, while keeping the diffusion constant on the nucleoid fixed. In this case, the clusters take longer to reach midcell (Fig. 4.2F).

In addition to the parameter sweeps shown in Fig. 4.2, we also considered the PomXY cluster trajectories when the spring stiffness k and the total PomZ dimer number N_{total} are varied. In short, the cluster trajectories do not change remarkably when the spring stiffness is altered over one order of magnitude, and an increase in the particle number increases the velocity of cluster movement towards midcell (Fig. S4.2).

We also investigated the cluster trajectories in a model identical to the one discussed so far, but which also includes detachment of PomZ dimers that are bound to the nucleoid only. The simulation results (Fig. S4.3) show that the larger the detachment rate, k_{off}, the longer the clusters need to reach midcell and for very large rates the cluster does not reach midcell at all. We expect that if the typical length a PomZ dimer diffuses on the nucleoid before it detaches, $L_{\text{diff}} = \sqrt{2D_{\text{nuc}}/k_{\text{off}}}$, is larger than $(L-L_c)/2$, the cluster is positioned at midcell. This condition implies that the detachment rate, k_{off}, needs to be smaller than $8D_{\text{nuc}}/(L-L_c)^2 \approx 0.04\,\text{s}^{-1}$ for midnucleoid positioning. Indeed, our simulation results show midcell localization for detachment rates below this threshold. Even for detachment rates above the threshold, $k_{\text{off}} = 0.1\,\text{s}^{-1}$, midcell localization of the cluster is obtained (Fig. S4.3). How the detachment rate influences the cluster dynamics can be understood in more detail by considering the flux difference of PomZ dimers into the cluster, which decreases with an increasing detachment rate (Fig. S4.3). For very large detachment rates the flux difference of PomZ dimers into the cluster vanishes already before the cluster is at midcell, leading to the stalling of the cluster at an off-center position observed in the simulations (Fig. S4.3).

To summarize, we observed that there exists an ATP hydrolysis rate that minimizes the time taken to reach midnucleoid. The diffusion constant of PomZ on the nucleoid determines whether the PomXY cluster moves towards or oscillates around midnucleoid. Moreover, the clusters move faster towards midcell if PomZ dimers diffuse faster on the PomXY cluster.

4.4 A deterministic approximation for the average cluster trajectory

In order to account for the features revealed by our *in silico* parameter sweeps, we need to take a closer look at how forces are generated in the system. PomZ dimers generate forces by interacting with the PomXY cluster due to the elastic properties of the chromosome and the proteins themselves. However, fluctuations of PomZ dimers around their equilibrium positions do not produce a net force. So how is the net force that leads to the bias in cluster movement actually produced? In order to answer this question, we first note that detailed balance is broken in the model. In this non-equilibrium system, we have a cyclic flow of PomZ dimers: PomZ dimers attach to the nucleoid in their active state (as ATP-bound PomZ dimers), diffuse on the nucleoid and are released into the cytosol in their inactive state (ADP-bound PomZ monomers) at some point after encountering the PomXY cluster. This cyclic flow can lead to a net force exerted on the cluster as we describe in the following.

When the PomZ dynamics is fast compared to the PomXY cluster dynamics, as suggested by the experimental data for wild-type *M. xanthus* cells [2], we can make an adiabatic assumption, i.e. the time scales for the PomXY cluster and PomZ movements can be separated. More specifically, on the time scale of PomZ dynamics, the cluster position can be regarded as constant. Here, and in the rest of this section, we assume that the adiabatic assumption holds true, and approximate the system by a stationary model, i.e. a system with a fixed PomXY cluster position. As we neglect exclusion effects on the nucleoid, PomZ dimers can only interact with each other via the PomXY cluster. However, when the cluster is stationary, no interaction between the cluster-bound PomZ dimers is possible, and thus there are no correlations between the movements of different PomZ proteins. Therefore, we can consider the interactions of PomZ dimers with the PomXY cluster as independent, which yields the following deterministic approximation for the total net force, F, acting on a cluster at position x_c

$$F(x_c) = (N_R(x_c) - N_L(x_c))f, \tag{4.4}$$

with f being the time-averaged force exerted by a single PomZ dimer that attaches to the nucleoid on the right side of the cluster. For symmetry reasons, a PomZ dimer coming from the left then exerts a time-averaged force $-f$. N_R and N_L denote the numbers of PomZ dimers that are bound to the PomXY cluster and had originally attached to the nucleoid to the right and left of the cluster, respectively. These two numbers increase with the diffusive flux of nucleoid-bound PomZ dimers reaching the cluster region from the right and left side, $j_{R/L}$, respectively, and decrease with the ATP hydrolysis rate, k_h, as long as the attachment rate to the PomXY cluster is non-zero. Hence, we obtain

$$N_{R/L}(x_c) = \frac{j_{R/L}(x_c)}{k_h} \tag{4.5}$$

in the steady-state. Inserting this into Eq. 4.4, yields

$$F(x_c) = \frac{j_R(x_c) - j_L(x_c)}{k_h} f = \frac{f}{k_h} j_{\text{diff}}(x_c) \equiv C j_{\text{diff}}(x_c). \tag{4.6}$$

We conclude that the net force is proportional to the flux difference of PomZ dimers at the cluster, j_{diff}, and the proportionality constant is given by $C = f/k_h$. Importantly, simulation results with a fixed PomXY cluster position confirm the observation that the total force exerted on the PomXY cluster is proportional to the PomZ flux difference (Fig. S4.4).

Next, we investigate how the net force exerted on the PomXY cluster results in movement of the cluster. Notably, the PomZ dimers interacting with the PomXY cluster not only produce a net force on the cluster, they also reduce the mobility of the cluster by tethering it to the nucleoid. We assume that these two processes can be considered independently. When we simulate the movement of a PomXY cluster with a fixed number of PomZ dimers bound to it (the ATP hydrolysis rate k_h is set to zero) and apply forces of different magnitudes to the cluster, we observe a linear increase in the steady-state velocity of the cluster with the force (Fig. S4.5). This suggests that the force exerted on the cluster is balanced by a frictional force. The average velocity of the PomXY cluster is then determined by the flux difference of PomZ dimers into the cluster, the proportionality constant C and the effective friction coefficient $\gamma(x_c)$ of the cluster

$$v(x_c) = \frac{F(x_c)}{\gamma(x_c)} = \frac{C j_{\text{diff}}(x_c)}{\gamma(x_c)}, \tag{4.7}$$

which is the central equation in our analysis. Note that the friction coefficient depends on the position of the PomXY cluster, because the number of PomZ dimers attached to the cluster changes with the cluster position. To obtain the average cluster trajectory, we need to integrate Eq. 4.7 over time. Hence, we need expressions for the flux difference into the cluster, the constant C and the effective friction coefficient of the PomXY cluster.

4.4.1 Analytical expression for the PomZ flux difference

To derive an analytical expression for the difference in PomZ flux into the cluster in the adiabatic limit, we introduce a reaction-diffusion (RD) model which closely resembles that investigated in the stochastic simulation. The nucleoid is modeled as a one-dimensional line of length L and the PomXY cluster is a finite interval on this line, $I_c = [x_c - L_c/2, x_c + L_c/2]$. Let $c(x, t)$ denote the concentration of PomZ dimers bound to the nucleoid only, $c_b(x, t)$ the concentration of PomZ dimers bound to the nucleoid and cluster, and N_{cyto} the number of PomZ dimers in the cytosol. The nucleoid and the PomXY cluster are assumed to have reflecting boundary conditions for the nucleoid-bound and cluster-bound PomZ dimers, respectively. In accordance with the stochastic model, PomZ dimers attach to the nucleoid left and right of the cluster with rate k_{on} and diffuse on the nucleoid with diffusion constant D_{nuc}. In the RD model we

simplify the interactions of PomZ dimers with the PomXY cluster: nucleoid-bound PomZ in the cluster region, I_c, can bind to the cluster with a rate k_a^{total}, neglecting the elasticity of the PomZ dimers and the chromosome included in our stochastic model. To obtain an expression for k_a^{total} that resembles attachment in the stochastic model, we need to integrate the rate of attachment of PomZ dimers positioned at x on the nucleoid to position y on the PomXY cluster over all cluster positions:

$$k_a^{\text{total}}(x) = \int_{x_c - L_c/2}^{x_c + L_c/2} k_a^0 e^{-\frac{1}{2}\frac{k}{k_B T}(y-x)^2} dy. \tag{4.8}$$

Since we expect the physiological value of the spring stiffness k to be large (Table S4.1, [115]), the Boltzmann factor decays quickly, and hence we can neglect boundary effects of the PomXY cluster ($L_c \to \infty$):

$$k_a^{\text{total}} = \begin{cases} k_a^0 \sqrt{\frac{2\pi k_B T}{k}}, & x \in I_c, \\ 0, & \text{otherwise.} \end{cases} \tag{4.9}$$

We assume that PomZ dimers bound to the PomXY cluster and the nucleoid diffuse with a diffusion constant D_{b}. How does this value depend on the diffusion constants of PomZ on the nucleoid and on the PomXY cluster, D_{nuc} and D_{clu}, and on the spring stiffness, k, in the lattice gas model? If the diffusion constants on the cluster and the nucleoid are the same, $D_{\text{clu}} = D_{\text{nuc}} \equiv D$, the center of mass of the PomZ dimer diffuses with $D_{\text{b}} = 0.5D$, independently of the spring stiffness. This result is known from the Rouse model, which models polymers as n beads coupled by springs. Here, the diffusion constant of the center of mass of the polymer decreases with the number of beads as $1/n$ [116]. For a stiff spring coupling the nucleoid and cluster binding sites, the diffusion constant of the two binding sites can be considered as equal and equivalent to that for the center of mass.

Finally, PomZ dimers bound to the cluster and nucleoid can hydrolyze ATP and subsequently detach into the cytosol with rate k_h. With these model assumptions we obtain the following reaction-diffusion equations to describe the PomZ dynamics, respecting particle number conservation:

$$\partial_t c(x,t) = D_{\text{nuc}}\partial_x^2 c(x,t) + \frac{k_{\text{on}} N_{\text{cyto}}(t)}{L}, \qquad (x \notin I_c) \tag{4.10}$$

$$\partial_t c(x,t) = D_{\text{nuc}}\partial_x^2 c(x,t) - k_a^{\text{total}} c(x,t), \qquad (x \in I_c) \tag{4.11}$$

$$\partial_t c_b(x,t) = D_{\text{b}}\partial_x^2 c_b(x,t) + k_a^{\text{total}} c(x,t) - k_h c_b(x,t), \qquad (x \in I_c) \tag{4.12}$$

$$\partial_t N_{\text{cyto}}(t) = k_h \int_{x_c - L_c/2}^{x_c + L_c/2} dx\, c_b(x,t) - k_{\text{on}}\frac{L - L_c}{L} N_{\text{cyto}}(t), \tag{4.13}$$

with the following no-flux boundary conditions at the nucleoid and PomXY cluster edges:

$$\partial_x c(x,t)|_{x=0} = 0 = \partial_x c(x,t)|_{x=L}, \tag{4.14}$$

$$\partial_x c_b(x,t)|_{x=x_c-L_c/2} = 0 = \partial_x c_b(x,t)|_{x=x_c+L_c/2}. \tag{4.15}$$

We solved the stationary state of the reaction-diffusion system analytically using *Mathematica* [117] (for details see A.2). The results obtained from the RD equations for the PomZ density and flux on the nucleoid, as well as the flux difference into the cluster, agree with the stochastic simulation results for the parameter values given in Table S4.1 (Fig. 4.3). A large spring stiffness is necessary for the good agreement between the two different models, because in the RD model we do not include the elasticity of the PomZ dimers, which is best reflected by a large spring stiffness. We observe that the density and the flux profiles are asymmetric for off-center clusters, and become more and more symmetric as the cluster approaches midnucleoid (Fig. 4.3A and 4.3B). This leads to a diffusive flux difference into the cluster that decreases towards midnucleoid (Fig. 4.3C). Note that the flux difference decreases slightly for clusters close to the nucleoid pole, which is due to total particle number conservation in the system.
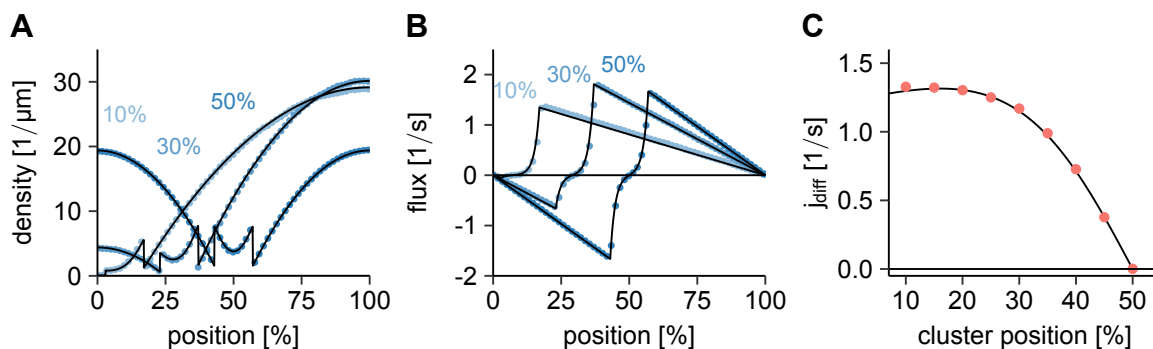

Figure 4.3 Comparison of the RD with the stochastic model. (A, B) Density and flux of PomZ dimers along the nucleoid for PomXY clusters at $10\%, 30\%$ and 50% nucleoid length. For the PomZ density we use the nucleoid binding site as the PomZ dimer position if PomZ is nucleoid-bound only and the cluster binding site if PomZ is bound to the cluster. Regarding the flux, only PomZ dimers bound to the nucleoid, but not the PomXY cluster, are considered. The analytical result obtained from the RD equations is shown in black and the results from the stochastic simulations in blue. (C) PomZ flux difference into the cluster as a function of the cluster position. The black line indicates the result from the RD equation, the red points are results from the stochastic simulations. For the data shown in this Figure we simulated 100 cluster trajectories with parameters as in Table S4.1. See the Materials and methods section for more details.

4.4.2 Force exerted by a single PomZ dimer

Next, we investigate the force exerted by a single PomZ dimer on the PomXY cluster. How can the interaction of a PomZ dimer with the PomXY cluster lead to a net force? First, PomZ dimers can exert a net force by attaching to the PomXY cluster in a stretched configuration: a particle to the left/right of the cluster can bind to the cluster from a position beyond either end (Fig. 4.1B). Second, PomZ dimers interacting with the PomXY cluster can diffuse on both the nucleoid and cluster. When they reach the edge of the PomXY cluster they can impart a force to the cluster, because the cluster binding site is restricted in its movement, in contrast to the nucleoid binding site (Fig. 4.1B). In principle, PomZ dimers can also generate a net force at the nucleoid ends, which moves the PomXY cluster towards midnucleoid, but since PomZ dimers rarely encounter the nucleoid ends, this can only represent a minor contribution. To investigate the force generated by a single PomZ dimer, we performed stochastic simulations with a stationary PomXY cluster and only one PomZ dimer in the system, which can attach to the nucleoid at a site so far away from the cluster that no interaction between the particle and the cluster is possible. Once bound to the nucleoid, the PomZ dimer can diffuse along it, interact with the PomXY cluster and detach. We record the positions of the PomZ dimer binding site on the nucleoid and on the PomXY cluster when the particle attaches to the cluster. Furthermore, we record the time-averaged and time-integrated force exerted by a PomZ dimer on the PomXY cluster. Note that the position of the cluster relative to the nucleoid is irrelevant as long as the cluster is not positioned close to a nucleoid boundary. We only consider particles that attach to the nucleoid at the right side of the cluster. For PomZ dimers that attach to the left side only the sign of the forces changes due to a left-right symmetry of the system.

Importantly, the ensemble average of the time-integrated forces of PomZ dimers attaching from the right is greater than zero, $f_{\text{int}} = (5.92 \pm 0.02) \times 10^{-3}\,\text{pN}\,\text{s}$ (the error denotes the standard error of the mean), showing that a particle coming from the right indeed, on average, exerts a force directed to the right and vice versa (Fig. S4.6, parameters as in Table S4.1). The average distance between nucleoid and cluster binding sites when the particle attaches to the PomXY cluster is $\Delta x_0 = 0.0011\,\mu\text{m}$, which is less than one lattice spacing, $a = 0.01\,\mu\text{m}$. With this initial distance between the two binding sites, we can estimate how much force is produced by the binding of a PomZ dimer to the PomXY cluster in a stretched configuration. Let us assume that the cluster binding site is fixed. Then the movement of the nucleoid binding site can be considered as an Ornstein-Uhlenbeck process, i.e. a particle diffusing in a potential given by the energy of the spring. This leads to the following estimate for the time-integrated force

$$f_{\text{int}}^{\text{OU}} = \int_0^{1/k_h} k\Delta x_0 e^{-\beta k D_{\text{nuc}}t}dt \approx \frac{\Delta x_0}{\beta D_{\text{nuc}}} \approx 4.4 \times 10^{-5}\,\text{pN}\,\text{s}, \qquad (4.16)$$

which is two orders of magnitudes smaller than the time-integrated force obtained from the simulations. Note that the time scale for relaxation in the Ornstein-Uhlenbeck

process $\tau_{\mathrm{OU}} = 1/(\beta k D_{\mathrm{nuc}}) = 0.001\,\mathrm{s}$ is much less than the time for which a PomZ dimer is typically attached to the PomXY cluster $\tau = 1/k_h = 1\,\mathrm{s}$ for the parameter set in Table S4.1. Hence, we conclude that the force produced due to the initial deflection of the PomZ dimer is not the main contribution to the time-integrated force for the parameters considered here. This suggests that the force exerted by a PomZ dimer when it encounters the PomXY cluster's edge is an important contribution to the net force generated.

The constant C in Eq. 4.7 is given by the time-averaged one-particle force f divided by the ATP hydrolysis rate k_h. In our simulation, we determined the ensemble average of the time-averaged forces using the interaction times as weights, which results in a constant $C = 0.0059\,\mathrm{pN\,s}$ for the parameters as in Table S4.1 (see Materials and methods for details). Note that this value for C matches with the proportionality constant between the total force exerted on the PomXY cluster and the PomZ flux difference for a stationary cluster, $C = 0.0059\,\mathrm{pN\,s}$ (Fig. S4.4). We now have approximations for the flux difference into the cluster (results from Eq. 4.10-4.15) and the proportionality constant between the force and the flux difference (Eq. 4.6). The only parameter yet to be estimated is the effective friction coefficient of the PomXY cluster, which we consider next.

4.4.3 Effective friction coefficient of the PomXY cluster

We derived an analytical expression for the effective friction coefficient by assuming that the PomXY cluster and the nucleoid boundaries can be disregarded (see A.3). We find that the effective friction coefficient of the PomXY cluster is given by the cytosolic friction coefficient plus a term that increases linearly with the number, N, of PomZ dimers bound to the cluster:

$$\gamma(x_c) = \gamma_c + \frac{k_B T N(x_c)}{D_{\mathrm{clu}} + D_{\mathrm{nuc}}}. \tag{4.17}$$

The increase with N is due to the fact that the more PomZ dimers tether the cluster to the nucleoid, the more restricted it is in its movement. Furthermore, we find that the larger the diffusion constant of PomZ dimers on the nucleoid and the cluster, the smaller the additional contribution to the friction coefficient γ_c. This can be attributed to the fact that the PomZ dimers restrict the cluster's movement less strongly the more mobile they are. Our analytical result agrees with the simulation results for an infinitely extended cluster and nucleoid and a constant number N of PomZ dimers bound to the cluster (Fig. S4.7, for details see Materials and methods section). In general, an approximation for the number of cluster-bound PomZ dimers can be obtained from the stationary solution of the RD model (see A.2). With the friction coefficient of the PomXY cluster we now have estimates for all factors that contribute to the velocity of the PomXY cluster (Eq. 4.7) and hence determine the average cluster trajectory.

4.4.4 Semi-analytical approach explains observed simulation results

Using the analytical values for the PomZ flux difference at the cluster boundaries, the effective friction coefficient of the PomXY cluster, and the simulated values for the force exerted by a single particle on the PomXY cluster, we can obtain an estimate for the average cluster velocity. The single particle force, and thus the constant C, does not change with the cluster position. Hence the dependence of the velocity on the position of the cluster is given by an analytical expression, which can be integrated numerically. For most of the parameters, the simulated average cluster trajectory and the approximation from our semi-analytical approach are in good agreement (Fig. 4.4A-4.4F, Fig. S4.8). In some cases, e.g. for $k_h = 0.01\,\mathrm{s}^{-1}$, our approximation lies above the simulation results. This is probably due to the fact that the dynamics of the PomXY cluster and the PomZ dimers cannot really be separated in these cases, as assumed in our approximation. If PomZ dimers remain attached to the PomXY cluster for a long time, which is the case for low ATP hydrolysis rates, the cluster can move a certain distance before the PomZ dimers hydrolyze ATP and detach from the cluster and the nucleoid. If the cluster is to the left of midnucleoid and moves to the right, the cluster-bound PomZ dimers move on average to the left and accumulate at the left boundary of the cluster. This leads to an increase in the force exerted by the PomZ dimers on the left edge of the cluster, and hence reduces the velocity of the cluster's movement towards midnucleoid. When the PomZ dynamics is slow compared to the PomXY cluster dynamics, as is the case for small D_{nuc}, the adiabatic assumption breaks down, and our semi-analytical approach fails to reproduce the simulated cluster trajectories (Fig. 4.4D and 4.4E).

With the semi-analytical approach we get further mechanistic insights into the regulation of the cluster dynamics by PomZ dimers. The good agreement between the simulated cluster trajectories and our estimates from this approach, for most of the parameters (Fig. 4.4), shows that the average cluster dynamics can be described solely by the PomZ flux difference into the cluster, the force a single PomZ dimer exerts on the cluster and the effective friction coefficient. Now we use this approach to get further insights into the cluster dynamics when the ATP hydrolysis rate and the diffusion constant of PomZ on the PomXY cluster are varied, two parameters that showed interesting behavior in the parameter sweeps (Fig. 4.2C and 4.2F). In the first case, there is an optimal hydrolysis rate that minimizes the time required for the cluster to reach midnucleoid. In the second case, movement of the cluster becomes less directed towards midnucleoid when the mobility on the PomXY cluster is decreased.

Fig. 4.5 gives an overview of the different contributions to the cluster's velocity when the ATP hydrolysis rate, k_h, or the diffusion constant of PomZ on the PomXY cluster, D_{clu}, is varied (for further parameters see Fig. S4.9 and Fig. S4.10). The flux difference of PomZ dimers into the cluster "measures" the position of the cluster on the nucleoid (first row). Interactions of PomZ dimers with the PomXY cluster lead to forces that are exerted on the cluster. Cluster-bound PomZ dimers exert a net force upon encountering the PomXY cluster's edge and they increase the friction of the
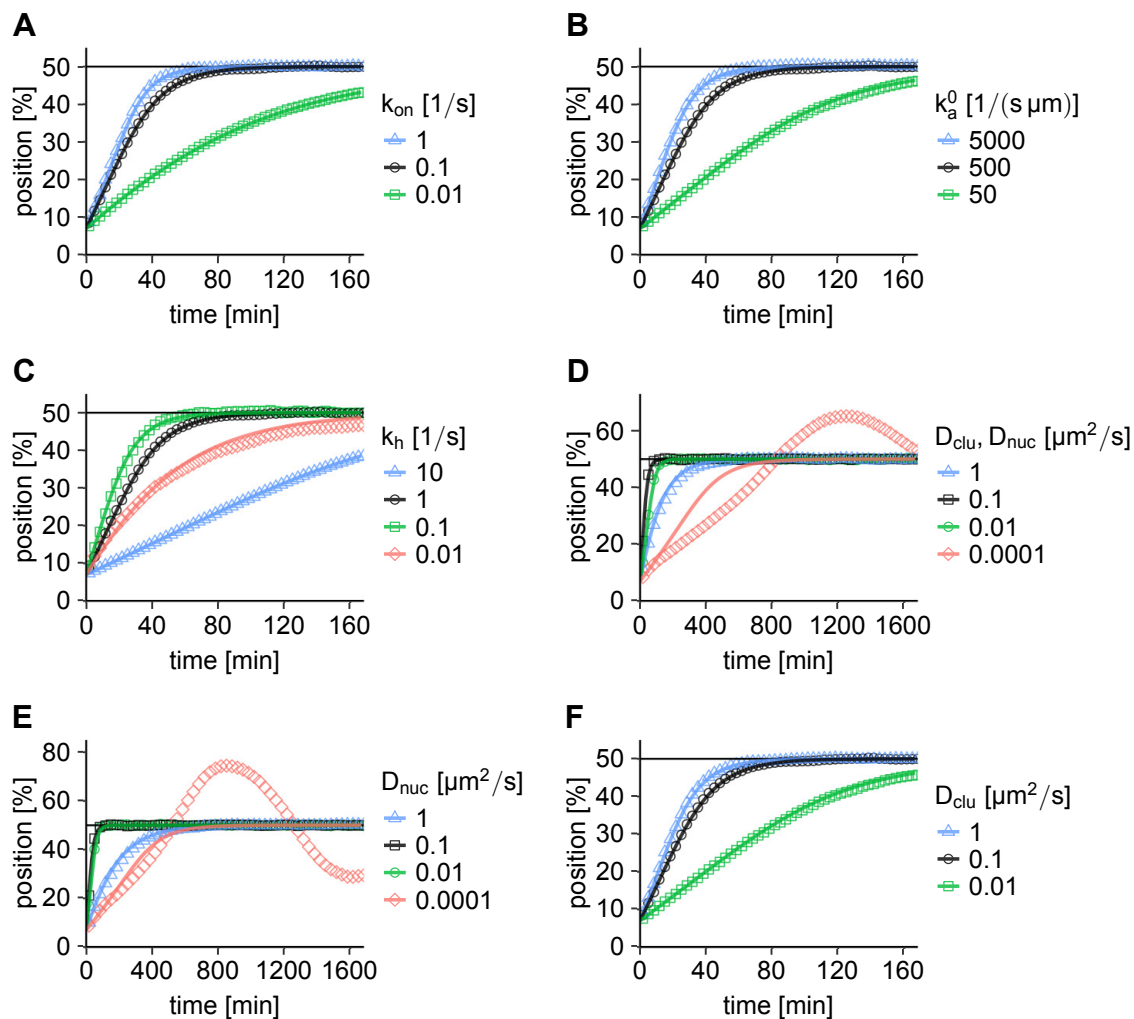
Figure 4.4 Comparison of the average cluster trajectory from simulations with our semi-analytical approximation. (A-F) The cluster trajectories obtained from integrating the equation of motion of the PomXY cluster, Eq. 4.7, (solid lines) agree with the simulation results for most parameters (points of different shape, same data as shown in Fig. 4.2). In the semi-analytical approximation we use the theoretical values for the flux difference and the friction coefficient together with the simulated value for C. For the parameters for which the cluster overshoots midcell (small D_{nuc}), our semi-analytical theory does not match the simulation results. This is expected, because we make the assumption that the PomZ dimer dynamics is faster than PomXY cluster movement (adiabatic assumption). If not explicitly given in the Figure, the parameters are as in Table S4.1.

PomXY cluster by tethering it to the nucleoid (second and third row). Taken together, a difference in the PomZ fluxes onto the ends of the cluster and local force generation by PomZ dimers at the PomXY cluster boundaries impart a velocity to the cluster that leads to a net movement towards midnucleoid (fourth row).
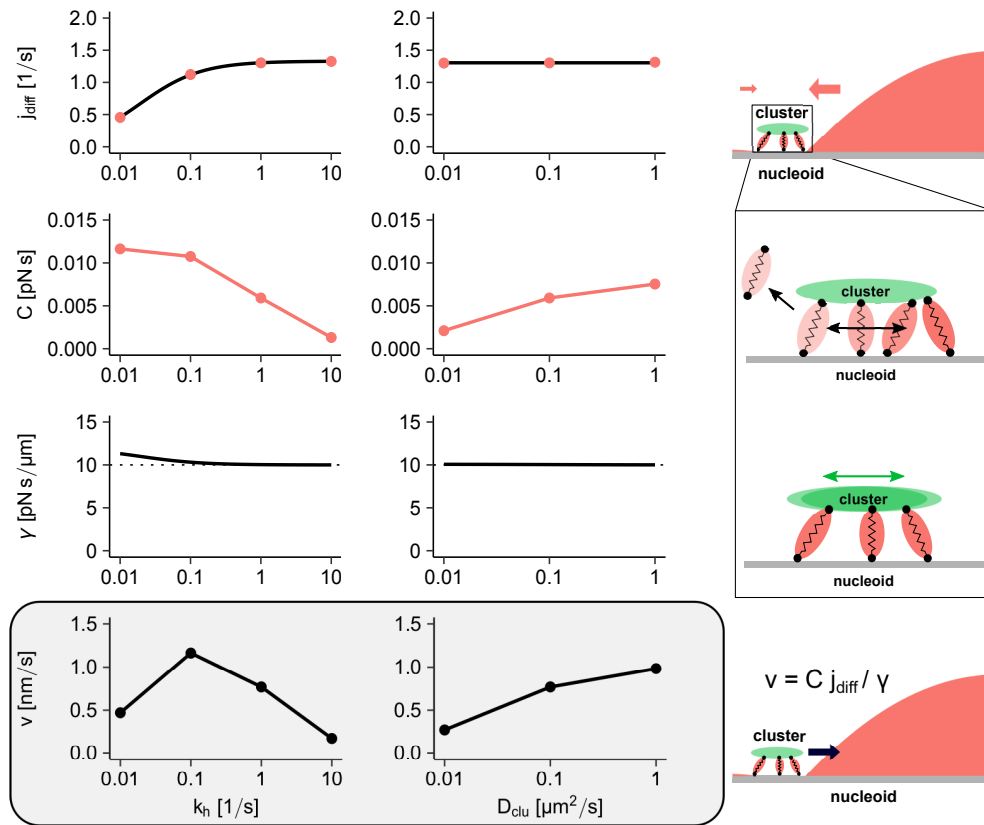
Figure 4.5 Force generation in the flux-based model. The average velocity of the cluster is approximated by the difference in flux of PomZ dimers into the cluster region from either side, j_{diff}, the constant C, which describes the force exerted by a single PomZ dimer on the PomXY cluster, and the effective friction coefficient of the PomXY cluster, γ. Here, the impact of varying the hydrolysis rate k_h (first column) or the diffusion constant of PomZ dimers on the PomXY cluster, D_{clu} (second column) is shown. The first row shows the PomZ flux difference at the cluster when the cluster is at 20% nucleoid length. The result from the RD equations (black line) matches the stochastic simulation results (red points). The second row shows the proportionality constant C determined from one-particle simulations (more than 40 000 PomZ dimer-cluster interactions are simulated). The points are connected by lines to guide the eye. The third row shows the analytical curves for the effective friction coefficient of the PomXY cluster at 20% nucleoid length obtained from Eq. 4.17. An increase in the number of PomZ dimers bound to the PomXY cluster (e.g. for low k_h values) leads to effective friction coefficients larger than the cytosolic friction coefficient (dotted horizontal line). Finally, the average velocity of the cluster can be calculated based on the flux difference, the constant C and the friction coefficient using Eq. 4.7. The velocity obtained using the theoretical values for both the flux difference and the friction coefficient, and the simulated values for C, is shown in the last row (grey box). The points are connected by lines to guide the eye. If not explicitly given in the Figure, the parameters are as in Table S4.1. See the Materials and methods section for more details.

Increasing the hydrolysis rate increases the flux difference, because the ATP hydrolysis rate determines the rate of PomZ dimer release from the nucleoid, and hence is important for the flux of PomZ dimers through the system (Fig. 4.5). To understand the dependence of $C = f/k_h$ on k_h, we first consider the dependence of the time-averaged force f on k_h. When a PomZ dimer attaches to the PomXY cluster, it typically binds close to the PomXY cluster's edge (Fig. S4.6). The probability density of the particle flattens over time because the PomZ dimer diffuses on the PomXY cluster and the nucleoid. For very long times, the average PomZ dimer position is the center of the PomXY cluster. Hence a particle is more likely to impart a net force to the PomXY cluster early in the interaction period than late. We conclude that the ensemble average of the time-averaged forces of a single PomZ dimer increases with k_h, which we indeed observe in the simulations (Fig. S4.11). Nevertheless, this increase is less than linear in k_h, such that $C = f/k_h$ decreases with k_h (Fig. 4.5). The effective friction coefficient also decreases with increasing k_h, because the number of PomZ dimers bound to the PomXY cluster decreases. The increasing flux difference, the decreasing constant C, and a decrease in friction together result in a maximal velocity, v, of the cluster for intermediate k_h values (Fig. 4.5). This explains why there exists a hydrolysis rate for which the cluster trajectory reaches midnucleoid in a minimal time. Furthermore, we observed that the variance in the cluster position decreases with increasing k_h. Since an increase in the hydrolysis rate increases the flux of PomZ dimers through the system and decreases the interaction time of PomZ dimers with the PomXY cluster, we expect a less stochastic movement of the cluster for larger hydrolysis rates, as observed.

Furthermore, we considered the case where the PomZ diffusion constant on the PomXY cluster is reduced while keeping the diffusion constant on the nucleoid fixed. Since diffusion on the PomXY cluster only affects the PomZ dynamics locally at the PomXY cluster, changing this rate does not change the flux difference of PomZ into the cluster (Fig. 4.5), but it does alter the magnitude of force generation at the cluster. We find that the time-averaged one-particle force decreases with decreasing diffusion constant (Fig. 4.5), which explains the increase in the time required for a cluster to reach midnucleoid for small diffusion constants (Fig. 4.2F). Why the force decreases when the diffusion constant on the PomXY cluster is reduced can be understood intuitively as follows: Our findings indicate that the main contribution to the net force generated by the PomZ dimers is the force they exert when they encounter the PomXY cluster's edge. When the diffusion constant of PomZ on the PomXY cluster, D_{clu}, is zero, the nucleoid binding site of a cluster-bound PomZ dimer equilibrates and fluctuates around this equilibrium position without producing a net force. Hence, in this case only the attachment of PomZ dimers to the PomXY cluster in a stretched state results in a net force. Note that for a non-zero diffusion constant on the PomXY cluster two opposing effects play a role for the number of times the PomZ dimers reach the PomXY cluster's edge: The smaller D_{clu}, the higher the probability of finding the cluster binding site close to the cluster's edge, but the lower the chance that the cluster binding site will hop to the cluster's edge, or indeed will hop at all.

To summarize, with our semi-analytical approach we can get new mechanistic insights into the cluster dynamics. In this approach we separate the global asymmetry,

i.e. a cluster located at an off-center position, which results in different diffusive PomZ fluxes into the cluster, from the forces locally exerted on the cluster. In particular, we can identify the different contributions to the velocity of the cluster and thereby understand why there is an ATP hydrolysis rate that results in a minimal time the clusters need to reach midcell and why diffusion of PomZ dimers on the PomXY cluster matters in our model.

4.5 Oscillatory behavior vs. midnucleoid localization of the cluster

We observe a marked discrepancy between the simulated average cluster trajectory and our approximation when the diffusion constant of PomZ on the nucleoid is reduced and the cluster oscillates around midnucleoid (Fig. 4.4D and 4.4E). Deviations from our theoretical predictions are to be expected in this situation, because we make an adiabatic assumption in our semi-analytical approach, i.e. we assume that the PomZ dimer dynamics on the nucleoid is fast compared to the cluster movement. This assumption no longer holds when PomZ dimers diffuse slowly on the nucleoid. In this case, the distribution of PomZ density along the nucleoid determined from simulations with a dynamic cluster deviates drastically from its steady-state distribution (Fig. S4.12). If the cluster initially lies to the left of midnucleoid and approaches midnucleoid from that side, our theory predicts a symmetric PomZ density, whereas the simulations show a higher density in front of the cluster. The flux difference also deviates from the stationary case: it increases as the cluster moves towards midnucleoid instead of vanishing at midnucleoid (Fig. S4.12). Both the asymmetric density and the non-zero flux difference at midnucleoid are in accordance with the observed oscillatory behavior.

The switch between cluster localization at midnucleoid and oscillatory movement around midnucleoid is regulated by the relative time scales of PomZ dynamics and cluster dynamics: If the PomXY cluster is moving slowly or the PomZ dimers move fast, the latter have time to adjust to a change in the PomXY cluster position. On the other hand, if the PomXY cluster moves fast or the PomZ dimers move slowly, the PomZ dimer distribution deviates from the stationary case. The delay between the movement of the PomXY cluster and the build-up of the PomZ gradient, which in turn biases the movement of the cluster, leads to oscillations: the longer the delay, the larger the amplitudes of the oscillations. To investigate the oscillatory case further, we performed additional simulations in which the diffusion constant of the PomZ dimers and that of the PomXY cluster in the cytosol - which is inversely proportional to the friction coefficient, γ_c, according to the Stokes-Einstein relation - were varied. As expected, we find oscillatory behavior of the clusters for low diffusion constants of PomZ on the nucleoid and PomXY cluster (Fig. 4.6). In the oscillatory regime we find both bimodal and monomodal cluster position distributions (Fig. 4.6).

As mentioned above, the onset of oscillations depends on the time scales of PomZ gradient formation and cluster movement. In order to understand how the parameters
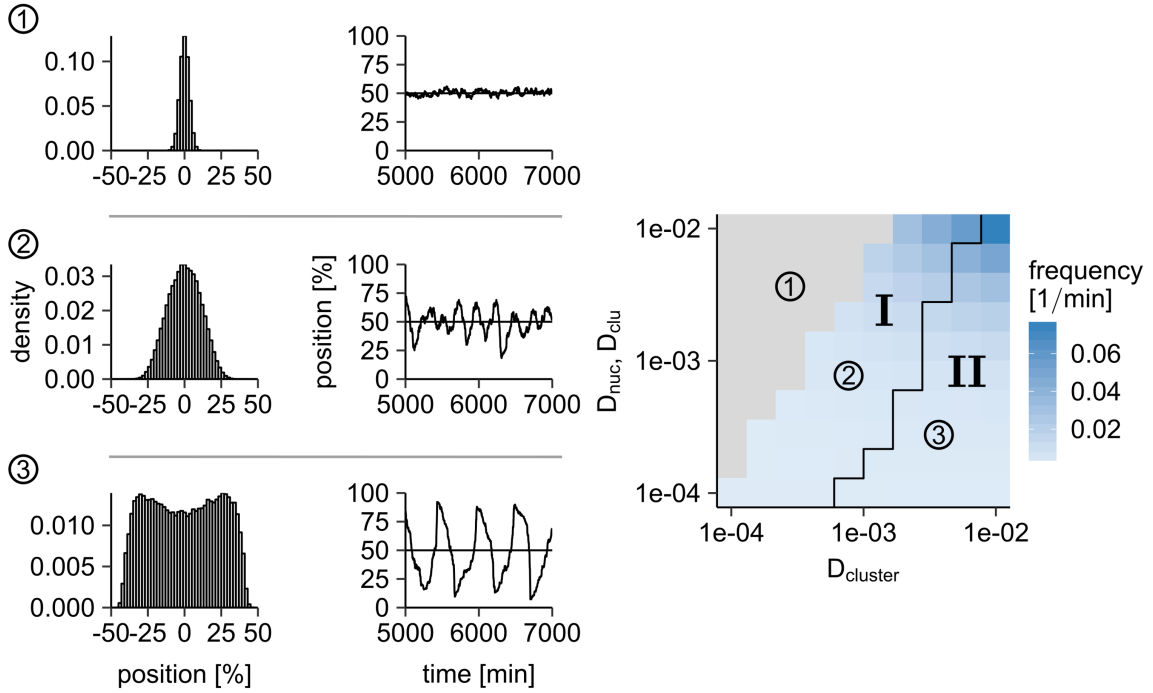
Figure 4.6 Oscillatory cluster movement occurs if PomZ dynamics is slower than PomXY cluster dynamics. We varied the diffusion constant of the PomXY cluster, $D_{\mathrm{cluster}} = k_B T/\gamma_c$, and the diffusion constant of PomZ on the nucleoid and PomXY cluster (D_{clu} and D_{nuc}, are set to the same value). The other parameters are as in Table S4.1. The clusters localize at midnucleoid for high PomZ diffusion constants and low diffusion constants of the PomXY cluster D_{cluster} (grey region). If the diffusion constant of PomZ is decreased from $0.01\,\mu\mathrm{m}^2/\mathrm{s}$, the clusters begin to oscillate, because the time scales of the PomZ dimer dynamics and the PomXY cluster dynamics become comparable (region I). The average frequency of oscillation is shown in blue (100 runs per parameter set are considered). In this parameter regime, the distribution of cluster positions is peaked around midnucleoid (see histograms on the left for the parameters marked in the phase diagram). For even lower PomZ diffusion constants and relatively large diffusion constants of the PomXY cluster (region II) the cluster positions are bimodally distributed. In the simulations, the clusters begin at midnucleoid and are recorded for $10\,000\,\mathrm{min}$. The black line in the frequency plot indicates a threshold. Below the curve the cluster distribution is bimodal, above it the distribution has only one peak. For details of the data analysis see the Materials and methods section.

change the behavior of the cluster trajectory, i.e. lead to oscillatory movement or midcell positioning, we assume that the cluster is located at midnucleoid and search for a stability condition that distinguishes the two behaviors. The diffusion time for a PomZ dimer to explore a nucleoid of size L is given by

$$t_{\mathrm{PomZ}} = \frac{L^2}{D_{\mathrm{nuc}}}. \tag{4.18}$$

In theory, the velocity of a cluster that starts from midnucleoid should be zero, because there should be no difference between the fluxes of PomZ dimers from both sides. However, due to stochastic effects, more particles may attach to the cluster from the right than from the left side, which will displace the cluster to the right. For our time scale argument, we consider an extreme case: we assume that PomZ dimers only arrive from one side, which we choose to be the right side without loss of generality. The time required for a cluster to move the length of the nucleoid is then given by

$$t_{\text{cluster}} = \frac{L}{v} \approx \frac{L\gamma(0.5L)}{Cj_{\text{right}}(0.5L)}, \tag{4.19}$$

with j_{right} being the flux of PomZ dimers into the cluster from the right. Here, we approximate the velocity of the cluster by its effective description, Eq. 4.7, using $x_c = 0.5L$, and replace the flux difference with the flux from the right only. According to Eq. 4.19, the condition for stable positioning of the cluster at midnucleoid

$$t_{\text{PomZ}} \ll t_{\text{cluster}} \tag{4.20}$$

yields

$$\frac{D_{\text{nuc}}}{L} \gg \frac{Cj_{\text{right}}(0.5L)}{\gamma(0.5L)} = \frac{Cj_{\text{right}}(0.5L)}{\gamma_c + (k_B T N(0.5L))/(D_{\text{clu}} + D_{\text{nuc}})}. \tag{4.21}$$

For the parameter sweeps considered before (Fig. 4.2 and Fig. S4.2), we find $t_{\text{cluster}} \gg t_{\text{PomZ}}$ for all cases except for small diffusion constants of PomZ on the nucleoid.

With our time-scale argument, Eq. 4.21, we can make further predictions as to which parameters should result in oscillations. First, we consider a change in the total particle number, N_{total}. Both j_{right} as well as the number of cluster-bound proteins, N, are proportional to N_{total}, and C does not depend on N_{total}. Therefore, the right-hand side of Eq. 4.21 is proportional to N_{total} for small values of N_{total} and converges to a constant for large values. From this we expect that oscillatory behavior may occur for large particle numbers. Simulations with 500 PomZ dimers and a smaller diffusion constant of PomZ on the nucleoid and the PomXY cluster compared to the parameters in Table S4.1 ($D_{\text{nuc}} = D_{\text{clu}} = 0.01\,\mu\text{m}^2/\text{s}$) indeed show oscillatory behavior, whereas simulations with the same parameters, but 100 PomZ dimers show midnucleoid localization (Fig. S4.13). However, for very large PomZ dimer numbers we expect exclusion effects, which are not considered here, to have an impact that will also affect the cluster dynamics.

Second, we investigate the effects on cluster dynamics of changing the nucleoid length L. Again, the constant C, which represents the force exerted by a single PomZ dimer on the PomXY cluster, does not depend on L. The number of cluster-bound proteins decreases with L, because the total PomZ dimer number in the system is constant. The flux j_{right} also decreases with L, because on longer nucleoids the PomZ dimers must diffuse, on average, a longer distance from their initial attachment point on the nucleoid until they reach the cluster. Bringing all terms in Eq. 4.21 that depend

on L to the right hand side yields a curve that first increases with L, then reaches a maximum and decreases again for large L. Hence, we expect no oscillations for small and large nucleoid lengths and oscillations might occur for intermediate lengths. Simulations with intermediate and large nucleoid lengths L indeed show this behavior (Fig. S4.13).

4.6 Discussion

We analyzed how the cluster movement changes when the rates for the key biological processes are varied over a broad range. We found that there exists an optimal ATP hydrolysis rate of PomZ such that the time the cluster needs to move to midnucleoid is minimized. A parameter sweep of the diffusion constant of PomZ on the PomXY cluster shows that the mobility of PomZ dimers on the PomXY cluster is important for cluster movement towards midnucleoid. Qualitative changes in the cluster trajectories are observed when the diffusion constant of PomZ on the nucleoid is reduced: midnucleoid positioning of the cluster switches to oscillatory behavior of the cluster around midnucleoid. Hence, we conclude that positioning of the cluster in the flux-based model critically depends on the time scale for the cluster dynamics in comparison to the one for the PomZ dimer dynamics on the nucleoid. If the latter is slow compared to the PomXY cluster dynamics, the cluster will oscillate around midnucleoid. In contrast, fast PomZ dynamics on the nucleoid leads to midnucleoid localization of the cluster. In the latter case, we find that the average velocity of the PomXY cluster can be described by the PomZ flux difference into the cluster, which measures how far away the cluster is from midnucleoid, the force exerted by a single PomZ dimer on the cluster, and the effective friction coefficient of the cluster, which depends on the number of PomZ dimers bound to it (semi-analytical approach). This approach allows for further mechanistic insights into the cluster movement by PomZ dimer interactions. With it we can explain the dependence of the cluster dynamics on the model parameters as observed in our simulations.

The mechanism we propose for midcell localization of the Pom cluster in *M. xanthus* is based on a flux-balance argument, which was previously proposed for positioning by the Par system [3] and also for self-organized positioning of protein clusters that dynamically form on the nucleoid [16]. In the model by Ietswaart et al. [3] and the model we present here, the cargo is a fixed structure, whereas Murray and Sourjik [16] consider a reaction-diffusion model for a protein that can form dynamic clusters on the nucleoid, which are positioned by the same protein due to a flux-balance argument. Necessary conditions for flux-based positioning are that the ATPase diffuses on the nucleoid (faster than the cargo) and cycles between a nucleoid-bound and cytosolic state [2, 3, 16]. Furthermore, the typical length an ATPase diffuses on the nucleoid before it detaches into the cytosol (without a preceded interaction with the cargo) has to be sufficiently large compared to the nucleoid length to ensure positioning of a cargo at midcell (see Fig. S4.3) [16, 77].

How the forces are generated by the ParA-like ATPase to move the cargo (plasmid, partition complex or protein cluster) is still under debate. Lim et al. proposed that forces are generated due to the elasticity of the nucleoid [6], which we also assume here. Alternatively, net movement of the cargo due to a chemophoresis force has been suggested [74–77]. The previously proposed models that include the elasticity of the nucleoid [6, 78, 100, 115] assume that the ParA dimers are less mobile on the nucleoid than the cargo. However, PomZ is found to diffuse rapidly on the nucleoid [2] compared to the very slowly diffusing Pom cluster (in the absence of PomZ), which is crucial for midcell sensing [2, 3]. This explains the different cargo dynamics observed for the DNA-relay model (oscillations on the nucleoid) and our model for the Pom system (midnucleoid localization). Importantly, when we chose small diffusion constants of PomZ on the nucleoid, we also see oscillatory movements of the Pom cluster. Hence, our flux-based model for midcell positioning of the Pom cluster, which includes the elasticity of the nucleoid and fast diffusion of PomZ on the nucleoid, differs from previously proposed models for the Par system.

Interestingly, the density of PomZ is high at the PomXY cluster [2]. Here, the Pom system deviates from observations for some Par systems for plasmid and chromosome segregation that show a low ParA density at the plasmids / partition complexes [10, 76]. However, there are also positioning systems that show an accumulation of the ATPase at the cargo [60, 99], which resembles the observations for the Pom system. Motivated by experimental observations [2], we make two important model assumptions that affect the density profile of PomZ at the cluster: First, we assume that cluster-bound PomZ dimers can only detach from the cluster via ATP hydrolysis, such that the dimers are captured at the cluster until they are released into the cytosol. Second, based on fluorescence microscopy images that show a high PomZ density over the entire PomXY cluster [2], we assume that cluster-bound PomZ dimers can diffuse on both the cluster and the nucleoid.

These assumptions have important implications on how forces are generated at the cluster in our model. We find that the PomZ dimers, which are modeled as springs to account for the elasticity of the nucleoid, not only exert forces when they attach to the cluster in a stretched configuration (as in the DNA-relay model, [6]), but instead forces can be generated every time a cluster-bound PomZ dimer encounters the cluster's edge. This explains how a net force can be exerted on the cluster by the PomZ dimers together with a high density of PomZ over the entire cluster. The PomZ dimers that interact with the cluster are not only responsible for the net force, they also decrease the mobility of the cluster due to the tethering. We find that the cluster-bound PomZ dimers decrease the effective friction coefficient of the cluster, for which we derive an analytic expression, Eq. 4.17 (similar to the derivation in [105]).

Another important observation for the Pom system in *M. xanthus* is that the cluster is relatively large (0.7 μm in length, [2]) compared to plasmids / partition complexes (about 0.1 μm in length, [6]), which explains the very low mobility of the Pom cluster if PomZ is not present in the cell [2]. In contrast to the slow diffusion of the Pom cluster, the PomZ dimers diffuse quickly on the nucleoid [2]. These observations explain the lack of a clear depletion zone in PomZ in the wake of the cluster for the

parameters mimicking the wild type situation (Fig. 4.3A) and thereby also rule out a Brownian ratchet mechanism [76, 78, 115] for the positioning of the Pom cluster. The experimental observation that the mobility of the Pom cluster is larger in wild type cells compared to mutants that lack PomZ [2], also speaks against such a mechanism.

Our model prediction of an oscillatory cluster movement when the dynamics of the PomZ dimers is slow compared to the dynamics of the PomXY cluster is in agreement with findings for the Par system [75, 115], despite differences between their models and ours. Similar to our finding that an intermediate ATP hydrolysis rate of PomZ minimizes the time the cluster needs to reach midcell, Hu et al. observed that an intermediate detachment rate of the ATPase from the cargo leads to the most persistent movement of the cargo [78]. However, their model differs from our model as they consider the movement of a fast diffusing cargo on a two-dimensional DNA-carpet to mimic an *in vitro* Par system [76]. In contrast, our model for the *in vivo* Pom system accounts for the nucleoid as an object of finite size. Since the Pom cluster diffuses slowly compared to the PomZ dimers, the diffusive fluxes of PomZ into the cluster need to be accounted for when determining the dependence of the cluster dynamics on the ATP hydrolysis rate (Fig. 4.5).

The model we present here is based on experimental findings for the Pom proteins in *M. xanthus* cells [2]. Apart from the spring stiffness, which is an effective constant to account for the elasticity of the chromosome, all model parameters relate to a biological process or a combination of processes. This is advantageous also for a quantitative description of the Pom system, which will be an aim for future research. Measurements of the biological rates, such as the nucleoid attachment rate, the diffusion constants, the cluster binding rate and the ATP hydrolysis rate of ATP-bound PomZ dimers *in vivo*, would help to convert the model into a quantitative one. Another limitation of our current model is that it is one-dimensional, i.e. we do not include geometric effects due to the three-dimensional nature of the cell, the nucleoid and the Pom cluster. Since the Pom cluster is relatively large, we do not expect that it can penetrate into the nucleoid volume as observed for plasmids and partitioning complexes [12]. How the cluster dynamics changes in a three-dimensional geometry is an interesting question for further research. Furthermore, in the current model we do not account for the PomXY cluster formation, but consider the cluster as a fixed structure. This is motivated by the experimental finding that PomX forms filaments *in vitro* and a high fraction of all PomX is in the cluster *in vivo* [2]. However, it remains unclear how the cluster is formed *in vivo* and how the size of the cluster is maintained from one cell generation to the next.

Our model for the Pom cluster positioning makes three important predictions, which would be interesting to test experimentally: First, the cluster starts to oscillate if PomZ dimers diffuse slowly on the nucleoid. We hypothesize that this might be tested experimentally by increasing the binding affinity of PomZ dimers to the DNA and in this way decreasing the mobility of PomZ on the nucleoid. Second, we predict that there is an optimal ATP hydrolysis rate to minimize the time the cluster takes to reach midnucleoid. Decreasing the rate of ATP hydrolysis by PomZ dimers associated with the PomXY cluster in experiments reduced the velocity of cluster movement

towards midcell [2]. It would be interesting to test whether the velocity of the cluster is also reduced for an enhanced ATP hydrolysis rate in *in vivo* experiments. Finally, we predict that the mobility of the PomZ dimers on the Pom cluster can increase the velocity of the cluster movement. To test this model prediction, experiments to uncover the dynamics of PomZ dimers bound to the cluster are needed.

The research presented here gives insights into the dynamics of the Pom cluster in *M. xanthus*, which is determined by its interactions with the nucleoid-bound PomZ dimers. With our semi-analytical approach we gain a better mechanistic understanding of the net force generation in our model. This approach might also prove to be useful for the related ParABS systems or other stochastic, out of equilibrium systems to position intracellular cargoes. Determining experimentally how forces are generated by the ParA-like ATPases in the biological systems, including the Pom and Par system, is an important task for further research. Chemophoresis forces can explain the net movement of catalytic particles in the direction of an increasing or decreasing concentration of a solute [77] and have also been applied to positioning by the Par system [74–77, 85]. To what extent a chemophoresis force and / or the elasticity of the nucleoid lead to the net force that moves the cargoes remains to be investigated.

4.7 Materials and methods

The mathematical model is implemented using a Gillespie algorithm [112], a stochastic simulation algorithm. In short, this algorithm works as follows: In each simulation step, all possible actions with their corresponding rates are determined. If the rates are constant in time, the time until any of these actions happens is exponentially distributed with the sum of all rates as rate parameter. To perform one simulation step, a uniformly distributed random number $\xi \in (0, 1]$ is drawn, which results in a time step

$$\Delta t = -\frac{\ln \xi}{\alpha}, \tag{4.22}$$

where α is the sum over all rates. Then a uniformly distributed random number is drawn to determine which of the possible actions happens. This is done by weighting the different actions according to their rates.

Two different kinds of simulations are performed: In the first, the PomZ dynamics and the PomXY cluster dynamics are simulated ("dynamic cluster simulations"). In the second, the PomXY cluster position is kept fixed and only the PomZ dynamics is considered ("stationary cluster simulations"). In the latter case, all rates in the model are constant and the time step for the Gillespie algorithm can be calculated as described above, Eq. 4.22. In contrast, if the PomXY cluster is dynamic, the rates for attachment of a nucleoid-bound PomZ dimer to the PomXY cluster and the hopping rates on the nucleoid, or cluster for cluster-bound PomZ dimers, depend on the cluster position, which is itself time-dependent. The time that elapses before the next action

is now given by

$$\int_t^{t+\Delta t} \alpha(t')dt' = -\ln(\xi), \tag{4.23}$$

which must be solved for Δt. Since an analytical integration of the time-dependent rates is not feasible, the expression needs to be solved numerically, which is computationally costly. However, if the PomXY cluster moves only a small distance between two Gillespie steps, the time-dependent rates also change only slightly. We tested the importance of the time dependence of the rates by approximating the time-dependent rates with their rate at time t, and added a rate to the simulation that has no effect, except that the time step preceding the next action is decreased on average. The results obtained when this rate was set to a high value were very similar to those found in its absence. Hence for the parameters we consider in this work, the time dependence of the rates can be ignored.

Dynamic cluster simulations

In the simulations to determine the cluster dynamics, all PomZ dimers are initially in the cytosol. The PomXY cluster position is kept fixed for $t_{\min} = 10$ min with all possible actions of the PomZ dimers allowed. As a result, the initial condition resembles the stationary distribution of PomZ dimers. The initial position of the cluster is such that the left edge of the cluster and the nucleoid coincide.

To derive PomZ flux and density profiles at specific PomXY cluster positions, the simulated fluxes and densities are recorded only if the PomXY cluster is within a certain distance of a predefined position of interest. For example, to get the PomZ flux / density for clusters at 20% nucleoid length, recording begins when the PomXY cluster is in the region $20 \pm 0.2\%$ and stops if it leaves the region $20 \pm 1\%$. Averaging is performed over all times at which the PomXY cluster resides within the specific region, weighting each density or flux profile with the corresponding time spent by the PomXY cluster in that specific region. To estimate the difference in PomZ flux into the PomXY cluster from either side, the maximal and minimal flux values in the average flux profile of PomZ dimers bound to the nucleoid, but not the PomXY cluster, are determined. These values are typically found a short distance from the edge of the PomXY cluster region, because PomZ dimers can attach to the PomXY cluster in a stretched configuration. The two extreme flux values of opposite sign are added together to get the average flux difference of PomZ dimers into the cluster.

Analysis of friction coefficient

In the simulations to measure the effective friction coefficient of the PomXY cluster, all PomZ dimers in the system are bound to the PomXY cluster and they cannot detach from it ($k_h = 0$) such that the number of cluster-bound PomZ dimers is constant. An external force is applied to the cluster and the force-velocity curve is recorded. More specifically, at least three different forces (0.005 pN, 0.01 pN, 0.02 pN) are applied, and the average steady-state cluster velocity is calculated based on 100 trajectories.

Plotting the force against the velocity yields a linear dependence, and the friction coefficient can be obtained from the slope. In these simulations an infinitely extended PomXY cluster and nucleoid is considered, i.e. boundaries are neglected. This is done because otherwise the PomZ dimers would accumulate at one of the cluster ends.

Analysis of oscillatory properties

In the simulations set up to study the oscillatory behavior of the cluster, the PomXY cluster starts at midnucleoid and its position is recorded over a long time (at least 1000 min). Initially, all PomZ dimers are in the cytosol, but the cluster movement only starts after $t_{min} = 10$ min, such that the PomZ dynamics can approach its stationary distribution. Two observables are of interest: the cluster position distribution and the Fourier spectrum of the cluster trajectories. In the case of the first, the histogram depicting the cluster positions of all runs is smoothed using a Gaussian moving average and peaks are identified in the smoothed profile, which are local maxima or minima. Depending on the parameters chosen, there might be no local minima. In this case, the cluster position distribution has a monomodal shape. If there is a minimum and the difference between the maximal and minimal peak is larger than 2% of the maximal count and the maximum is further away from the midnucleoid position than the minimum, the profile is classified as bimodal.

To determine if the cluster trajectories are oscillatory or not and to estimate the frequencies of cluster oscillations, the procedure used is as follows: For each run, the temporal average of the cluster position is subtracted from the cluster trajectory and a fast Fourier transform of the resulting data is performed. The modulus of the Fourier-transformed cluster position for each run is summed, and the resulting spectrum is smoothed using a moving average with Gaussian weights. Then the largest peak is identified in the smoothed data with a minimal peak height 20% higher than the value corresponding to the smallest frequency, $f_{min} = 1/T_{max}$, in the smoothed data set (T_{max} is the duration of the signal considered in the Fourier transformation). If there is a peak, the cluster trajectory is oscillatory with the frequency determined by the peak in the Fourier spectrum. On the other hand, if no peak is found, the trajectories are classified as "non-oscillatory".

Stationary cluster simulations

Simulations with a fixed position of the PomXY cluster are performed to measure the force exerted by a single PomZ dimer on the cluster ("one-particle simulations") or to measure the PomZ dimer flux into the cluster and the forces exerted on the cluster for an arbitrary number of PomZ dimers in the system. In these simulations, the PomZ dimer(s) are initially in the cytosol. When the adiabatic assumption holds true, the results from the stationary cluster simulations can be used as approximations for the PomZ dynamics in the dynamic cluster simulations.

One-particle simulations

To determine the force typically exerted by a single PomZ dimer on the PomXY cluster, simulations with only one PomZ dimer in the system are performed. Here, the PomXY cluster is located far away from the nucleoid boundaries (at midnucleoid) and the PomZ dimer attaches to a lattice site on the right side of the cluster that is so far away from the cluster that no interaction with the cluster is possible. In the simulations, we record the nucleoid and cluster binding site positions when the PomZ dimer attaches to the PomXY cluster, and the force exerted on the PomXY cluster integrated over time and averaged over time for a number, N_{runs}, of PomZ dimers interacting with the PomXY cluster. To obtain the constant $C = f/k_h$, the ensemble average of the time-averaged force, f, needs to be determined. This quantity is calculated as follows:

$$f = \frac{\sum_i f_i t_i}{\sum_i t_i} = \frac{\sum_i f_i^{\mathrm{int}}}{\sum_i t_i},$$

with f_i and f_i^{int} the time-averaged and time-integrated force exerted by a single PomZ dimer interacting with the PomXY cluster and t_i the corresponding time of interaction. In this definition of f, each time-averaged force is weighted by the time the particle remains attached to the PomXY cluster when calculating the mean. Note that the constant C can also be expressed in terms of the ensemble average of the time-integrated force, f^{int}:

$$C = \frac{f}{k_h} = \frac{\sum_i f_i^{\mathrm{int}}}{k_h \sum_i t_i} \approx \frac{\sum_i f_i^{\mathrm{int}}}{N_{\mathrm{runs}}} = f^{\mathrm{int}},$$

because $\frac{1}{N_{\mathrm{runs}}} \sum_i t_i = \frac{1}{k_h}$ for large N_{runs}.

Acknowledgments

4.8 Expression for the initial force a PomZ dimer exerts when binding to the cluster

We found that the force a single particles exerts on the cluster is an important factor for the bias in the cluster movement (section 4.4). Forces are exerted when PomZ binds to the cluster in a stretched configuration and every time it encounters the cluster's edge while bound to the cluster. To investigate the former contribution further, we considered the probability distributions of the binding sites of PomZ on the nucleoid and the cluster when PomZ binds to the cluster, for which we were able to derive analytical expressions. With those distributions we also get an analytical expression for

the average force a PomZ dimer exerts on the cluster due to attachment in a stretched configuration.

To get the probability of PomZ to bind from site x on the nucleoid to the cluster, we consider the following model. We incorporate the nucleoid as a one-dimensional interval $[0, L]$ and the cluster is located at the left edge of the nucleoid, $I_c = [0, L_c]$, an assumption we make for convenience only. PomZ dimers can be either in the cytosol (with probability $p_{\text{cyto}}(t)$), bound to the nucleoid, but not to the cluster ($p(x, t)$), and bound to both the nucleoid and the cluster ($p_b(x, t)$). Cytosolic PomZ binds to the nucleoid on which it diffuses (see RD equations in section 4.4.1). However, the model we present here, differs from the previous continuum models considered, as follows: When nucleoid-bound PomZ attaches to the cluster it does not move anymore until it is released into the cytosol upon ATP hydrolysis. This is because we are interested in the probability distribution at the moment when PomZ binds to the cluster. The probabilities evolve in time according to the following partial differential equations (the total probability is one):

$$\partial_t p(x, t) = D_{\text{nuc}} \partial_x^2 p(x, t) - k_a^{\text{total}}(x) p(x, t) + \frac{k_{\text{on}}}{L} p_{\text{cyto}}(t) \Theta(x - L_c), \tag{4.24}$$

$$\partial_t p_b(x, t) = k_a^{\text{total}}(x) p(x, t) - k_h p_b(x, t), \tag{4.25}$$

$$\partial_t p_{\text{cyto}}(t) = \int_0^L k_h p_b(x, t) \, \mathrm{d}x - k_{\text{on}} \frac{L - L_c}{L} p_{\text{cyto}}(t), \tag{4.26}$$

with the no-flux boundary conditions

$$\partial_x p(x, t)|_{x=0} = 0 = \partial_x p(x, t)|_{x=L}. \tag{4.27}$$

Nucleoid-bound PomZ dimers attach from position x on the nucleoid to any position on the cluster with rate $k_a^{\text{total}}(x)$, which was defined as (section 4.4.1):

$$k_a^{\text{total}}(x) = \int_0^{L_c} k_a^0 e^{-\beta \frac{k}{2}(y-x)^2} \, \mathrm{d}y. \tag{4.28}$$

The integral can be solved analytically, but involves error functions:

$$k_a^{\text{total}}(x) = k_a^0 \sqrt{\frac{\pi k_B T}{2k}} \left[\text{erf}\left(\sqrt{\frac{k}{2k_B T}}(L_c - x) \right) + \text{erf}\left(\sqrt{\frac{k}{2k_B T}} x \right) \right]. \tag{4.29}$$

For a high spring stiffness of the PomZ dimers, k, the function $k_a^{\text{total}}(x)$ can be approximated by a Heaviside step function that is non-zero only in the cluster region, $\hat{k}_a^{\text{total}} \Theta(L_c - x)$ (see Fig. 4.7A), as done previously (Eq. 4.9). Here, $\hat{k}_a^{\text{total}}$ refers to the maximal value of $k_a^{\text{total}}(x)$, which is given by

$$\hat{k}_a^{\text{total}} = k_a^0 \sqrt{\frac{2\pi k_B T}{k}}. \tag{4.30}$$
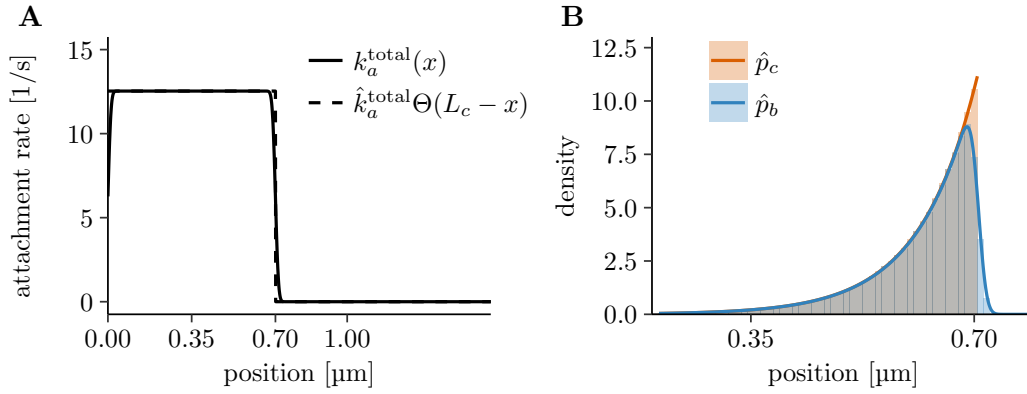
Figure 4.7 Distributions for the nucleoid and cluster binding site positions when PomZ binds to the cluster. (A) The attachment rate $k_a^{\text{total}}(x)$, which depends on the position of PomZ on the nucleoid (solid line), can be approximated by a step function, $\hat{k}_a^{\text{total}}\Theta(L_c - x)$ (dashed line), for the parameters we consider (Table S4.1). (B) The analytical results for the probability distribution of the nucleoid (blue) and cluster (orange) binding sites when PomZ binds to the PomXY cluster are shown. The results from solving the above RD equations (solid lines) match those from our stochastic simulations (histograms shown in partially transparent colors). The data from the stochastic simulations is the same as shown in Fig. S4.6 using the parameters in Table S4.1.

However, since we want to derive an expression for the probability distribution of the PomZ dimer binding site on the nucleoid when PomZ attaches to the cluster, we need to incorporate attachment of PomZ to the cluster from positions x outside of the cluster region. It turns out that if we make the approximation mentioned above in Eq. 4.24, but not in Eq. 4.25, we can get analytical solutions for the binding site distributions that agree with the results from the stochastic simulations. With this approximation, Eq. 4.24 becomes:

$$\partial_t p(x,t) = D_{\text{nuc}}\partial_x^2 p(x,t) - \hat{k}_a^{\text{total}}p(x,t), \quad \text{(in the cluster region),} \tag{4.31}$$

$$\partial_t p(x,t) = D_{\text{nuc}}\partial_x^2 p(x,t) + \frac{k_{\text{on}}}{L}p_{\text{cyto}}(t), \quad \text{(away from the cluster).} \tag{4.32}$$

We solved these PDEs with the no-flux boundary condition (Eq. 4.27) in the steady state using *Mathematica* [117]. At the right edge of the cluster, $x = L_c$, the solutions for $p(x)$ in the cluster region and outside as well as their derivative have to be continuous

$$\lim_{x \to L_c^-} p(x) = \lim_{x \to L_c^+} p(x), \tag{4.33}$$

$$\lim_{x \to L_c^-} \partial_x p(x) = \lim_{x \to L_c^+} \partial_x p(x). \tag{4.34}$$

Next, we use this solution to get $p_b(x)$. From Eq. 4.25 we obtain, in the steady state

$$p_b(x) = \frac{k_a^{\text{total}}(x)}{k_h}p(x). \tag{4.35}$$

We are interested in the probability for binding from position x on the nucleoid if binding occurs:

$$\hat{p}_b(x) \equiv p(x_{\text{nuc}} = x|\text{binding}) = \frac{p(x_{\text{nuc}} = x, \text{binding})}{p(\text{binding})} = \frac{p_b(x)}{\int_0^L p_b(x')\mathrm{d}x'}. \tag{4.36}$$

Our result for $\hat{p}_b(x)$ matches the distribution of binding sites on the nucleoid from the stochastic simulations (Fig. 4.7B).

PomZ attaches to the cluster according to a Boltzmann distribution. To obtain the probability for a dimer to bind to position y on the cluster, $\hat{p}_c(y)$, we need to integrate the probability to bind from position x times the conditional probability for a PomZ dimer at position x to bind to position y on the cluster, over all x positions:

$$\hat{p}_c(y) = p(x_{\text{clu}} = y|\text{binding}) \tag{4.37}$$

$$= \int_0^L p(x_{\text{nuc}} = x, x_{\text{clu}} = y|\text{binding})\,\mathrm{d}x \tag{4.38}$$

$$= \int_0^L p(x_{\text{nuc}} = x|\text{binding})p(x_{\text{clu}} = y|x_{\text{nuc}} = x, \text{binding})\,\mathrm{d}x \tag{4.39}$$

$$= \int_0^L \hat{p}_b(x)\frac{e^{-\beta\frac{k}{2}(y-x)^2}}{\int_0^{L_c} e^{-\beta\frac{k}{2}(z-x)^2}\mathrm{d}z}\,\mathrm{d}x. \tag{4.40}$$

This result also agrees with the corresponding distribution of cluster binding sites from the stochastic simulations (Fig. 4.7B). With this finding, an expression for the average initial stretching of a PomZ dimer can be obtained

$$\langle x - y \rangle = \int_0^L \mathrm{d}x \int_0^{L_c} \mathrm{d}y (x-y)p(x_{\text{nuc}} = x, x_{\text{clu}} = y|\text{binding}) \tag{4.41}$$

$$= \int_0^L \mathrm{d}x \int_0^{L_c} \mathrm{d}y (x-y)\hat{p}_b(x)\frac{e^{-\beta\frac{k}{2}(y-x)^2}}{\int_0^{L_c} e^{-\beta\frac{k}{2}(z-x)^2}\mathrm{d}z}. \tag{4.42}$$

We obtain $\langle x - y \rangle \approx 0.0011\,\mu\text{m}$ for the parameters in Table S4.1, in agreement with the result from the stochastic simulations (see Fig. S4.6). Hence, the average force a PomZ dimer exerts on the cluster just upon binding is given by $-k\langle y - x \rangle \approx 0.044\,\text{pN}$. However, we found in section 4.4.2 that this force is quickly reduced due to the relaxation of the spring. Hence, for the parameters we considered (Table S4.1), the initial force is only a minor contribution to the average force exerted by a single PomZ dimer on the cluster. So far, we have determined this average force exerted while PomZ is bound to the cluster from simulations. Deriving an analytical expression for this force is the first step to derive a purely analytical expression for the average cluster trajectory.

4.9 A minimal model for the Pom cluster dynamics

To further investigate the oscillatory cluster movements we considered a model that is based on our effective description of the Pom cluster dynamics (semi-analytical approach) discussed in section 4.4. It reduces the system even further and hence we refer to it as "minimal model", in the following. We found that the average velocity of the cluster is given by $v(x_c) = Cj_{\text{diff}}(x_c)/\gamma(x_c)$, i.e. proportional to the force a single PomZ dimer exerts on the cluster, C, and the flux difference of nucleoid-bound PomZ into the cluster, $j_{\text{diff}}(x_c)$, as well as inversely proportional to the effective friction coefficient of the cluster $\gamma(x_c)$. The latter depends on the position of the cluster, x_c, as the number of PomZ dimers bound to the cluster depends on x_c. However, this dependence is typically only weak and hence we can approximate the friction coefficient by its average value

$$\tilde{\gamma} = \frac{1}{L} \int_0^L \gamma(x_c) \, \mathrm{d}x_c. \tag{4.43}$$

With this approximation, the average velocity of the cluster is given by

$$v(x_c) \approx \frac{C}{\tilde{\gamma}} j_{\text{diff}}(x_c) \equiv \lambda j_{\text{diff}}(x_c). \tag{4.44}$$

Though λ does not depend on x_c, it does depend on the model parameters.

The effective description of the cluster dynamics we discussed before (section 4.4) is only valid if the cluster dynamics is a lot slower than the PomZ dynamics (adiabatic assumption). However, we expect that the velocity of the cluster can still be approximated to be proportional to the flux difference into the cluster, when the adiabatic assumption does not hold true. In this section, we consider a minimal model where we assume that Eq. 4.44 is valid in general.

4.9.1 Definition of the minimal model

We consider the coupled dynamics of the PomZ density, $c(x, t)$, and the position of the cluster, $x_c(t)$, and assume that the velocity of the cluster is proportional to the flux difference in PomZ into the cluster. In contrast to the continuum model in section 4.4, here, we do not explicitly incorporate cluster-bound PomZ dimers and model the cluster as a point:

$$\partial_t c(x,t) = D_{\text{nuc}} \partial_x^2 c(x,t) + \frac{k_{\text{on}}}{L} N_{\text{cyto}}(t) - \sigma_0 k_h c(x,t) \delta(x - x_c(t)), \tag{4.45}$$

$$\partial_t x_c(t) = \lambda j_{\text{diff}}(x_c, t) = \lambda(D_{\text{nuc}} \partial_x c(x,t)|_{x \to x_c^-} + D_{\text{nuc}} \partial_x c(x,t)|_{x \to x_c^+}), \tag{4.46}$$

$$\partial_t N_{\text{cyto}}(t) = -k_{\text{on}} N_{\text{cyto}}(t) + k_h \sigma_0 c(x_c(t), t), \tag{4.47}$$

with the no-flux boundary conditions

$$\partial_x c(x,t)|_{x=0} = 0 = \partial_x c(x,t)|_{x=L}. \tag{4.48}$$

The total PomZ dimer number is conserved:

$$\int_0^L c(x,t)\mathrm{d}x + N_{\text{cyto}}(t) = N_{\text{total}}. \tag{4.49}$$

The parameter λ in Eq. 4.44 depends on other model parameters, such as D_{nuc}. However, for simplicity we neglect this dependence and treat λ as constant.

   We start by considering the adiabatic regime, when the PomZ dynamics is fast compared to the cluster dynamics. In this case, the cluster can be regarded as stationary on the time scale of the cluster dynamics. We solved Eq. 4.45 in the steady state (as in [3]):

$$c_{\text{left}}(x) = \frac{k_{\text{on}}N_{\text{cyto}}}{2LD_{\text{nuc}}}(x_c^2 - x^2) + c(x_c), \tag{4.50}$$

$$c_{\text{right}}(x) = \frac{k_{\text{on}}N_{\text{cyto}}}{2LD_{\text{nuc}}}(x_c^2 - x^2) + \frac{k_{\text{on}}N_{\text{cyto}}}{D_{\text{nuc}}}(x - x_c) + c(x_c). \tag{4.51}$$

The constants $c(x_c)$ and N_{cyto} are determined by particle conservation and the flux balance at the cluster (flux into and out of the cluster are equal):

$$N_{\text{cyto}} = \frac{N_{\text{total}}}{1 + \frac{k_{\text{on}}}{k_h}\frac{L}{\sigma_0} + \frac{k_{\text{on}}}{3D_{\text{nuc}}}L^2 + \frac{k_{\text{on}}}{D_{\text{nuc}}}x_c(x_c - L)},$$

$$c(x_c) = N_{\text{cyto}}\frac{k_{\text{on}}}{k_h\sigma_0}.$$

With the steady state solution of the PomZ density, $c(x)$, which depends on x_c, we get the following equation of motion for the cluster dynamics in the adiabatic regime:

$$\partial_t x_c(t) = \lambda k_{\text{on}}N_{\text{cyto}}\left(1 - \frac{2}{L}x_c(t)\right). \tag{4.52}$$

Not only the term in brackets, but also N_{cyto} depends on x_c. We find that midcell, $x_c = L/2$, is a fixed point for the cluster dynamics. The fixed point is stable, because $\lambda k_{\text{on}}N_{\text{cyto}}$ is always greater or equal than zero and hence the velocity of x_c changes its sign from positive to negative when increasing the value of x_c [118]. Hence, the cluster moves towards and stably localizes at midcell, independent of its starting position.

4.9.2 Numerical solution of the minimal model and results

Next, we considered the non-adiabatic regime. In this case, an analytical solution of the coupled differential equations, Eq. 4.45 –4.48, was not feasible and hence we integrated the equations numerically. However, also a numerical integration of the equations is not straightforward as we couple ODEs with a PDE (see also Supplementary Information of [75]).

   We used an explicit method with the _forward time centered space_ (FTCS) scheme for the diffusive part and an Euler forward scheme for the cluster position and the

number of PomZ in the cytosol [119]. We discretize space and time

$$x_j = x_0 + j\Delta x, \quad j \in \{0, \dots, J\}, \tag{4.53}$$

$$t_n = t_0 + n\Delta t, \quad n \in \{0, \dots, N\}, \tag{4.54}$$

and denote $c(x_j, t_n), x_c(t_n)$ and $N_{\text{cyto}}(t_n)$ as c_j^n, x_c^n and N_{cyto}^n, respectively. The cluster position, x_c^n is a real number. In the following we denote by m the integer such that x_m is the lattice site closest to the cluster position. The difference equations for the PomZ concentration on the nucleoid then read ($\forall n \in \{0, \dots, N\}$):

$$\frac{c_j^{n+1} - c_j^n}{\Delta t} = D_{\text{nuc}} \frac{c_{j+1}^n + c_{j-1}^n - 2c_j^n}{\Delta x^2} + \frac{k_{\text{on}} N_{\text{cyto}}}{L} - k_h c_j^n \delta_{j,m}, \quad j \in \{1, J-1\}, \tag{4.55}$$

$$\frac{c_0^{n+1} - c_0^n}{\Delta t} = D_{\text{nuc}} \frac{c_1^n - c_0^n}{\Delta x^2} + \frac{k_{\text{on}} N_{\text{cyto}}}{2L} - k_h c_0^n \delta_{0,m}, \tag{4.56}$$

$$\frac{c_J^{n+1} - c_J^n}{\Delta t} = D_{\text{nuc}} \frac{c_{J-1}^n - c_J^n}{\Delta x^2} + \frac{k_{\text{on}} N_{\text{cyto}}}{2L} - k_h c_J^n \delta_{J,m}. \tag{4.57}$$

For the cluster position and N_{cyto} we use the following difference equations

$$\frac{x_c^{n+1} - x_c^n}{\Delta t} = \lambda D_{\text{nuc}} \frac{c_{m+1}^n - c_{m-1}^n}{\Delta x}, \tag{4.58}$$

$$\frac{N_{\text{cyto}}^{n+1} - N_{\text{cyto}}^n}{\Delta t} = -k_{\text{on}} N_{\text{cyto}}^n + k_h \Delta x \, c_m^n. \tag{4.59}$$

Next, we use the difference equations above to obtain numerical solutions for the PomZ concentration along the nucleoid and the cluster position over time. The nucleoid is represented by an interval of length, $l_{\text{nuc}} = 5\,\mu\text{m}$, and we discretize space using a lattice spacing of $\Delta x = 0.05\,\mu\text{m}$. Initially, all PomZ proteins are in the cytosol, $N_{\text{cyto}}^0 = N_{\text{total}} = 100$. We simulate the PomZ dynamics for a time $t_{\text{min}} = 10\,\text{s}$ and only after this time the cluster starts moving. The total time of the simulations is $t_{\text{max}} = 100\,\text{s}$. For the time step Δt we chose a value that satisfies

$$\Delta t \leq \frac{\Delta x^2}{2D_{\text{nuc}}}. \tag{4.60}$$

This condition ensures numerical stability of the diffusion equation (setting k_{on} and k_h to zero in Eq. 4.55). It can be obtained by a von Neumann stability analysis [119]. However, here, we do not have periodic boundary conditions (as assumed in the von Neumann stability analysis) and we also have additional on- and off-dynamics of PomZ. Hence, this upper bound for the time step might not be sufficient to ensure numerical stability. Eq. 4.60 implies that for large diffusion constants the time step has to be chosen very small, which is costly in terms of computation time. This could be improved by using an implicit method (e.g. Crank-Nicolson method), which involves solving an equation in each time step, but yields stable solutions for larger, or even an arbitrary step size [119].

To test the validity of our numerical integration scheme, we compared our results from this scheme with the analytical results obtained for the steady state PomZ density on the nucleoid and the cluster dynamics, Eq. 4.50 – 4.52. We find that both results agree nicely (Fig. 4.8A,B), which indicates that our numerical integration scheme is sound. Here, we did not fit parameters to experiments, so time scales do not match those of other sections.
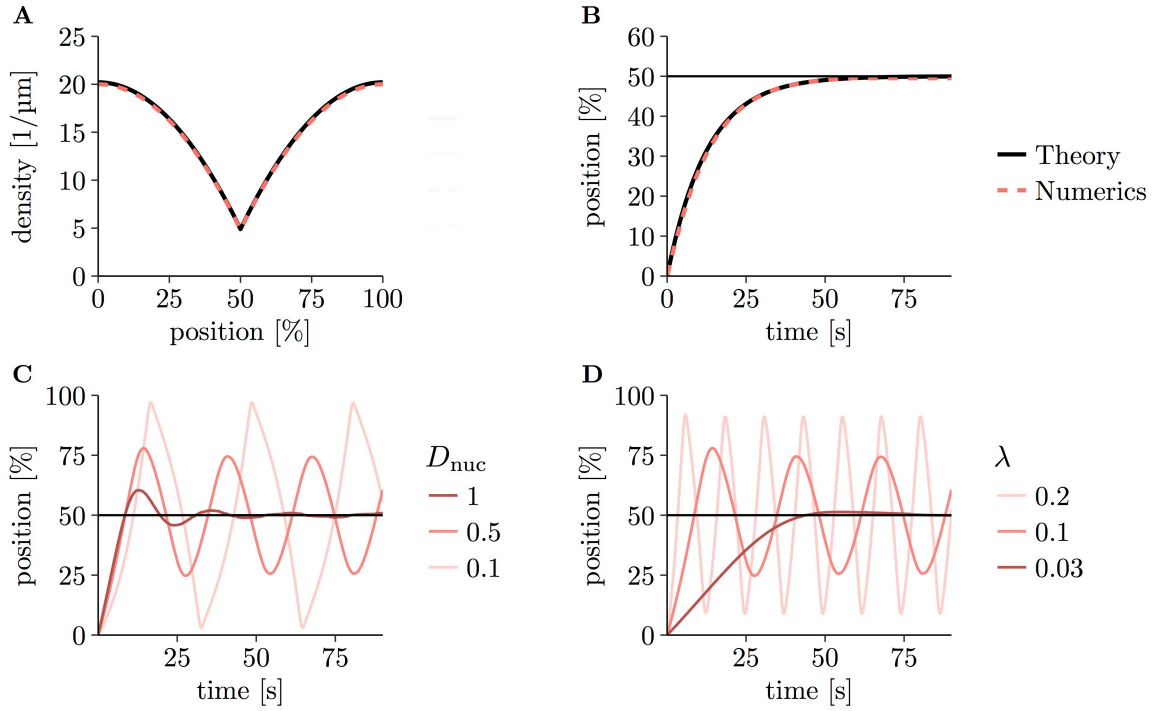

Figure 4.8 The minimal model shows oscillatory cluster dynamics for small D_{nuc} and large λ. (A, B) The results from numerically integrating Eq. 4.45 – 4.48 (red dashed lines) match our analytical results for the adiabatic limit, Eq. 4.50 – 4.52 (solid black lines). In (A) the density of PomZ along the nucleoid length for a cluster at midnucleoid and in (B) the cluster position over time is shown. In the latter case, we chose an initial position of the cluster of $x_c^0 = 0$. We integrated the equation of motion for the cluster position (Eq. 4.52) numerically to obtain the cluster trajectory. The parameter σ_0 we set to the lattice spacing Δx, in order to match the PomZ fluxes from the nucleoid into the cytosol for the analytical and numerical approach. (C, D) Cluster trajectories for different values of D_{nuc} (C), and λ (D). We used the following parameters if not explicitly stated otherwise: $k_{\text{on}} = 0.1\,\text{s}^{-1}$ and $k_h = 10\,\text{s}^{-1}$. The parameters λ and D_{nuc} were chosen to be $\lambda = 0\,\mu\text{m}, D_{\text{nuc}} = 0.1\,\mu\text{m}^2/\text{s}$ in (A), $\lambda = 0.04\,\mu\text{m}, D_{\text{nuc}} = 20\,\mu\text{m}^2/\text{s}$ in (B) and $\lambda = 0.1\,\mu\text{m}, D_{\text{nuc}} = 0.5\,\mu\text{m}^2/\text{s}$ in (C, D).

As a next step we numerically solved the cluster trajectories for parameters that might be outside of the adiabatic regime. In the stochastic, particle-based model we observed oscillatory cluster dynamics for small diffusion constants of PomZ on the nucleoid, D_{nuc}, and small friction coefficients of the Pom cluster (section 4.5). Small

friction coefficients can be related to large diffusion constants, via the Stokes-Einstein relation. Based on this observation, we studied the cluster dynamics in the minimal model when the parameters D_{nuc} and λ were varied. We find that the clusters start to oscillate when D_{nuc} is decreased. The oscillations increase in amplitude and decrease in frequency, when D_{nuc} is decreased further (Fig. 4.8C). This observation agrees with our previous findings from the stochastic model, also regarding the change in frequency and amplitude (Fig. 4.6).

The parameter λ couples the PomZ dynamics with the movement of the cluster. The larger it is, the more the cluster position changes due to a flux difference in nucleoid-bound PomZ. Varying this parameter leads to oscillatory cluster movements for large values of λ (Fig. 4.8D). In this case, both the frequency and the amplitude increase with λ. This observation is in contrast to our finding when D_{nuc} is varied: when the parameter is changed such that the cluster dynamics deviates more and more from midcell localization (increasing amplitude), the frequency of oscillations is either increased (for λ), or decreased (for D_{nuc}). Interestingly, we also observe an increase in the oscillation frequency, when the diffusion constant of the cluster, D_{cluster}, is increased in the stochastic simulations (Fig. 4.6). Both, D_{cluster} and λ increase the dynamics of the cluster, which could explain the similar behavior observed.

With the minimal model we could reproduce the oscillatory behavior of the cluster found in the stochastic simulations, when the Pom dynamics is slow compared to the cluster dynamics. Cluster trajectories for parameters in the non-adiabatic regime can be calculated by our numerical solution of the coupled system of partial and ordinary differential equations, Eq. 4.45 – 4.48. The minimal model presented here is an effective description of the stochastic model. However, the results from both models cannot be directly compared, because the minimal model does not include the dependence of λ on other parameters. Another limitation of the minimal model is that the concentration of nucleoid-bound PomZ is not differentiable at the cluster position due to the Dirac delta function in Eq. 4.45. Replacing the delta by a strongly peaked Gaussian function ensures that the solutions are differentiable. However, to get analytical solutions, e.g. for the onset of the fluctuations, is still challenging and so far only done using approximations (see e.g. [75]).

A Supporting information

A.1 Discussion of the parameters used in the simulations

So far, not all parameters we use in our model are determined experimentally in *M. xanthus*. To nevertheless get an estimate for the physiological values, we approximated the values that are not experimentally determined by the corresponding ones from the related Par system, where possible. Varying the parameters over a broad range, as done in this study, also helps to ensure that the physiological parameter values are included. Importantly, several parameters can be varied without a remarkable change in the cluster dynamics (Fig. 4.2).

The values for the total number of PomZ dimers, N_{total}, the length of the nucleoid and the cluster, L and L_c, are determined from experiments in *M. xanthus* cells [2]. The rate k_h in our model combines several processes, such as ATP hydrolysis and the conformational change of the PomZ dimer that finally leads to the detachment of PomZ from the nucleoid and the cluster. This rate can be estimated from FRAP experiments in *M. xanthus*. If PomZ is bleached at the position of the PomXY cluster, PomZ dimers recover with a recovery half-time of $(1.2 \pm 0.2)\,\text{s}$ [2]. Based on this time scale for the turnover of PomZ at the cluster, we use $k_h = 1\,\text{s}^{-1}$ in our simulations.

Moreover, the FRAP experiments in [2] indicate that PomZ diffuses quickly on the nucleoid, which can explain the experimentally observed high PomZ density at the cluster although the turnover of cluster-bound PomZ dimers is fast. Based on this observation we chose the diffusion constant of PomZ on the nucleoid to $D_{\text{nuc}} = 0.1\,\text{µm}^2/\text{s}$, which is in the upper range of values reported in the literature for ParA dimer diffusion on the nucleoid (from $0.001\,\text{µm}^2/\text{s}$ [115] to $1\,\text{µm}^2/\text{s}$ [3, 69]). Since the dynamics of PomZ dimers bound to the cluster is not measured yet, we set the diffusion constant of PomZ dimers on the PomXY cluster, D_{clu}, to the same value as D_{nuc}.

The attachment rate of PomZ to the nucleoid, k_{on}, combines several biochemical processes: Before PomZ that was just released at the cluster can rebind to the nucleoid, it needs to exchange ADP for ATP, dimerize and regain the ability to bind non-specific DNA [2, 97]. *In vitro* measurements of the DNA binding rate of ParA that can bind non-specifically to DNA [97] suggest a binding rate of about $50\,\text{s}^{-1}$. Since it takes long for ParA to regain the DNA binding ability compared to the binding itself [97] and they have to reach the nucleoid before they can bind to it, this value can be regarded as an upper bound. In previous models for the ParA positioning system, the rate for ParA to rebind the nucleoid has been chosen between $0.01\,\text{s}^{-1}$ to $50\,\text{s}^{-1}$ [3, 6, 100, 115]. We used a value in this range, $k_{\text{on}} = 0.1\,\text{s}^{-1}$, and varied the rate two orders of magnitude in our simulations. We find that above a certain value of k_{on} the trajectories do not change remarkably if the rate is increased even more (Fig. 4.2). The same holds true for the attachment rate of PomZ dimers to the PomXY cluster, k_a^0. We chose the attachment rate of PomZ to the cluster such that the cluster dynamics does not change remarkably if k_a^0 is increased.

The friction coefficient of the cluster, $\gamma_c = k_B T / D_{\text{cluster}}$, we used as a fit parameter to obtain the experimentally observed time scale for the clusters to reach midcell of

Parameter	Symbol	Value
Number of PomZ dimers	N_{total}	100*
Length of nucleoid	L	$5\,\mu\text{m}$*
Length of cluster	L_c	$0.7\,\mu\text{m}$
Attachment rate PomZ to nucleoid	k_{on}	$0.1\,\text{s}^{-1}$
Attachment rate PomZ to PomXY cluster (unstretched)	k_a^0	$500\,\text{s}^{-1}\,\mu\text{m}^{-1}$
Diffusion constant PomZ on nucleoid	D_{nuc}	$0.1\,\mu\text{m}^2/\text{s}$
Diffusion constant PomZ on PomXY cluster	D_{clu}	$0.1\,\mu\text{m}^2/\text{s}$
ATP hydrolysis rate PomZ bound to PomXY cluster	k_h	$1\,\text{s}^{-1}$
Diffusion constant PomXY cluster in cytosol	$D_{\text{cluster}} = k_B T/\gamma_c$	$0.0004\,\mu\text{m}^2/\text{s}$
Spring constant PomZ dimers	k	$10^4\,\text{k}_\text{B}\text{T}/\mu\text{m}^2$
Lattice spacing	a	$0.01\,\mu\text{m}$

* In the one-particle simulations, the total number of PomZ dimers, N_{total}, is one and the nucleoid length is chosen to be $L = 2.1\,\mu\text{m}$ to decrease computation time.

Table S4.1 Parameters used in the simulations. If not explicitly stated otherwise the values for the model parameters shown here are those used in the simulations. For a discussion of the parameters see A.1.

about 80 min, in our simulations. The fit result, $D_{\text{cluster}} \approx 0.0004\,\mu\text{m}^2/\text{s}$, is comparable to literature values for plasmids ($0.001\,\mu\text{m}^2/\text{s}$ [3, 100]), though a bit smaller. A smaller diffusion constant of the Pom cluster compared to plasmids is expected because of the large size of the cluster. The effective spring stiffness, k, which accounts for the elasticity of the nucleoid and the PomZ dimers, is approximated by the value for the stiffness of a bond between the plasmid and the nucleoid via ParA dimers used in [115]. To test our choice of the lattice spacing, we also performed simulations using the parameters as in Table S4.1, but with $a = 0.005\,\mu\text{m}$. We did not observe remarkable changes in the cluster dynamics compared to our results with $a = 0.01\,\mu\text{m}$.

A.2 Stationary solution of the RD model

To get analytical expressions for the flux difference of PomZ dimers into the cluster and the number of PomZ dimers bound to the PomXY cluster, we described the PomZ dynamics in terms of reaction-diffusion equations (Eq. 10-15 in the main text). We are interested in the steady-state solutions. Eq. 10 and 11 is solved by imposing no flux boundary conditions at $x = 0$ and $x = L$ and setting the values for the concentration, $c(x, t)$, and its derivative, $\partial_x c(x, t)$, inside and outside of the PomXY cluster region equal at the cluster boundaries, $x = x_c \pm L_c/2$. The second condition, an equivalence

of the first derivative of the concentration, is due to balance of diffusive fluxes at $x = x_c \pm L_c/2$. Since the diffusion constants of PomZ dimers bound to the nucleoid, but not bound to the PomXY cluster, are the same below the PomXY cluster and away from it, the first derivative has to be set equal at $x = x_c \pm L_c/2$. The resulting expression for $c(x, t)$ can be used to solve Eq. 12 in the steady state. For the cluster-bound PomZ dimers, $c_b(x, t)$, no-flux boundary conditions hold at the PomXY cluster's edges. The last unknown is N_{cyto}, which is determined by mass conservation,

$$\int_0^L c(x)\, dx + \int_{x_c - L_c/2}^{x_c + L_c/2} c_b(x)\, dx + N_{\text{cyto}} = N_{\text{total}}$$

or equivalently by solving Eq. 13 in the steady state. The solutions for $c(x), c_b(x)$ and N_{cyto} are obtained with _Mathematica_. They are quite lengthy and hence not written out here explicitly. The flux difference of PomZ dimers into the cluster can then be calculated as follows:

$$j_{\text{diff}} = D_{\text{nuc}}\partial_x c(x)|_{x_c + L_c/2} + D_{\text{nuc}}\partial_x c(x)|_{x_c - L_c/2}.$$

We chose the sign of the flux difference to be positive if more PomZ dimers arrive from the right than from the left side. The number of PomZ dimers bound to the PomXY cluster is given by:

$$N(x_c) = \int_{x_c - L_c/2}^{x_c + L_c/2} c_b(x)\, dx.$$

A.3 Derivation of the effective friction coefficient of the PomXY cluster

Our aim is to get an analytical expression for the effective friction coefficient of the PomXY cluster, i.e. the friction coefficient when the cluster is tethered to the nucleoid by N PomZ dimers. We consider an infinitely extended PomXY cluster and nucleoid to exclude boundary effects. Note that the absolute positions of the PomZ dimers do not matter, only the difference between the positions of the nucleoid and cluster binding sites matters. Hence, all PomZ dimers can be moved to the same nucleoid position. The position of the cluster binding site then has a distribution that is peaked at the position of the nucleoid binding site if no force is exerted to the PomXY cluster and the peak of the distribution is shifted to the right if the PomXY cluster is pulled to the right by an external force. Let us denote the position of the cluster by $x(t)$. The position of the nucleoid binding site of all PomZ dimers is denoted $x^{\text{nuc}}(t)$, and the average position of the cluster binding sites $x(t) + \Delta x^{\text{clu}}(t)$. Then the following

equations hold

$$\partial_t x(t) = \frac{F}{\gamma_c} - N\frac{k}{\gamma_c}(x(t) + \Delta x^{\mathrm{clu}}(t) - x^{\mathrm{nuc}}(t)),$$

$$\partial_t \Delta x^{\mathrm{clu}}(t) = -\frac{k}{\gamma_{\mathrm{clu}}}(x(t) + \Delta x^{\mathrm{clu}}(t) - x^{\mathrm{nuc}}(t)),$$

$$\partial_t x^{\mathrm{nuc}}(t) = -\frac{k}{\gamma_{\mathrm{nuc}}}(-x(t) - \Delta x^{\mathrm{clu}}(t) + x^{\mathrm{nuc}}(t)),$$

with γ_{clu}, γ_{nuc} the friction coefficient of PomZ dimers on the PomXY cluster and the nucleoid, respectively. They are related to the diffusion constants of a PomZ dimer on the nucleoid and PomXY cluster via Stokes-Einstein, $D_{\mathrm{clu/nuc}} = k_B T/\gamma_{\mathrm{clu/nuc}}$. We solved the coupled ODE system above using *Mathematica*. Taking the time derivative of the position of the PomXY cluster, $x(t)$, and dividing F by this expression for the velocity of the cluster yields the effective friction coefficient of the PomXY cluster in dependence of N and the other model parameters:

$$\gamma(t, N) = \frac{e^{k(1/\gamma_{\mathrm{clu}} + 1/\gamma_{\mathrm{nuc}} + N/\gamma_c)t}\gamma_c(\gamma_c(\gamma_{\mathrm{clu}} + \gamma_{\mathrm{nuc}}) + \gamma_{\mathrm{clu}}\gamma_{\mathrm{nuc}}N)}{e^{k(1/\gamma_{\mathrm{clu}} + 1/\gamma_{\mathrm{nuc}} + N/\gamma_c)t}\gamma_c(\gamma_{\mathrm{clu}} + \gamma_{\mathrm{nuc}}) + \gamma_{\mathrm{clu}}\gamma_{\mathrm{nuc}}N}.$$

For large times ($t \to \infty$), this simplifies to

$$\gamma(N) = \gamma_c + \frac{\gamma_{\mathrm{clu}}\gamma_{\mathrm{nuc}}N}{\gamma_{\mathrm{clu}} + \gamma_{\mathrm{nuc}}}. \tag{S4.1}$$

We find that the effective friction coefficient of the cluster is given by the cytosolic friction plus an additional term that increases linearly with the number of PomZ dimers bound to the cluster, N. This expression is a generalization of the term derived by Lansky et al., [105] using a force-balance argument. The simulations fit well with this theoretical curve if we use an infinitely extended nucleoid and PomXY cluster, i.e. we neglect the boundary conditions (Fig. S4.7). If the nucleoid and PomXY cluster size is finite in the simulations, the measured effective friction coefficient is higher than the analytical result derived here, because the PomZ dimers move to the rear cluster's edge when the cluster is pulled forward and the reflecting boundary conditions of the cluster for the movement of PomZ's cluster binding site increase the friction. However, in the dynamic cluster simulations, i.e. simulations with a finite nucleoid and PomXY cluster, which is moved on the nucleoid by PomZ dimer interactions, cluster-bound PomZ dimers can detach into the cytosol with the ATP hydrolysis rate k_h. Hence, the effect of accumulation of PomZ dimers at the rear cluster's edge is diminished. In these simulations, the number of cluster-bound PomZ dimers depends on the position of the cluster on the nucleoid. In this case, we replace Eq. S4.1 with

$$\gamma(x_c) = \gamma_c + \frac{\gamma_{\mathrm{clu}}\gamma_{\mathrm{nuc}}N(x_c)}{\gamma_{\mathrm{clu}} + \gamma_{\mathrm{nuc}}}.$$
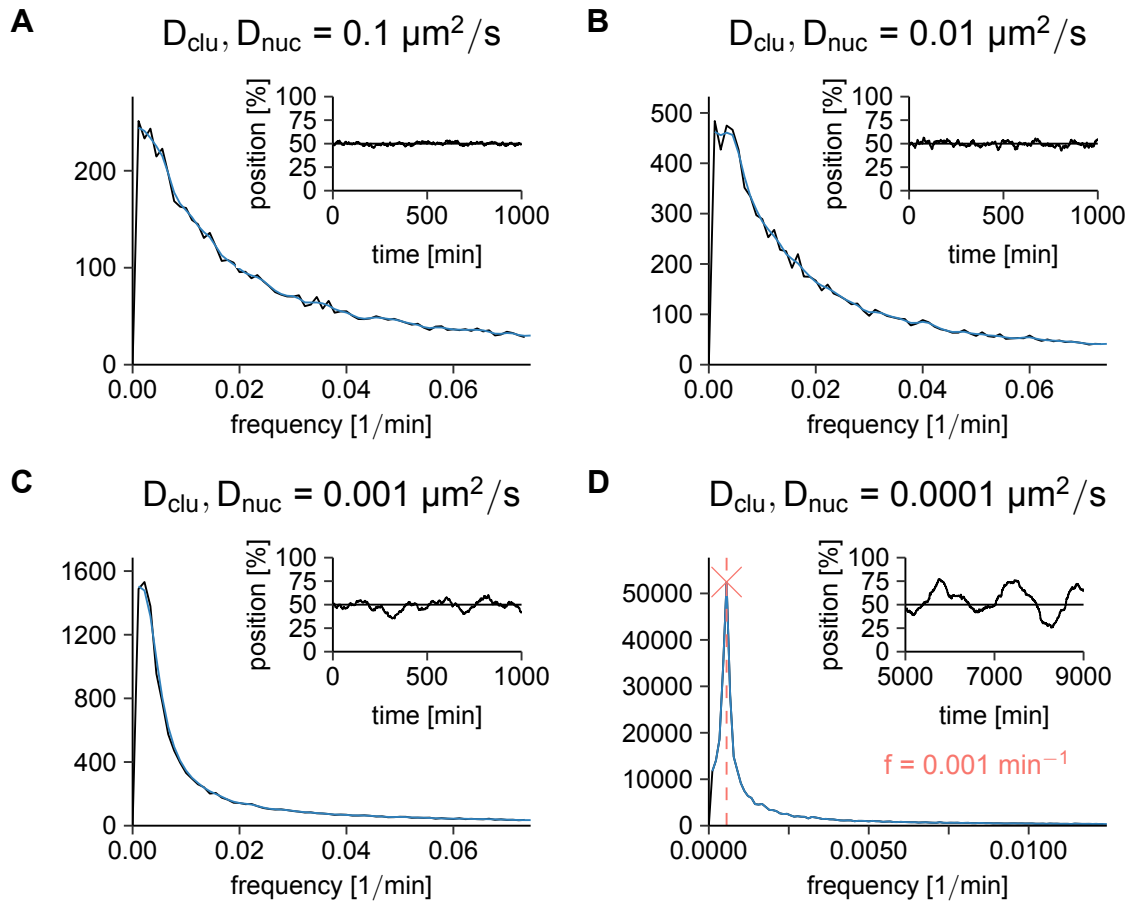
A.4 Supplementary Figures

Figure S4.1 Midnucleoid localization vs. oscillatory movements. (A-D) The average magnitude of the fast Fourier transform signal (black line) is smoothed using a moving average with Gaussian weights (blue line) to determine whether there is a peak in the Fourier spectrum or not (for details see Materials and methods). The insets show a cluster trajectory for one run. The diffusion constants of PomZ on the nucleoid and PomXY cluster are varied over three orders of magnitudes; the other parameters are chosen as in Table S4.1. For the Fourier analysis we performed 100 runs of the simulation for $\geq 1000\,\mathrm{min}$ with a cluster starting at midnucleoid.
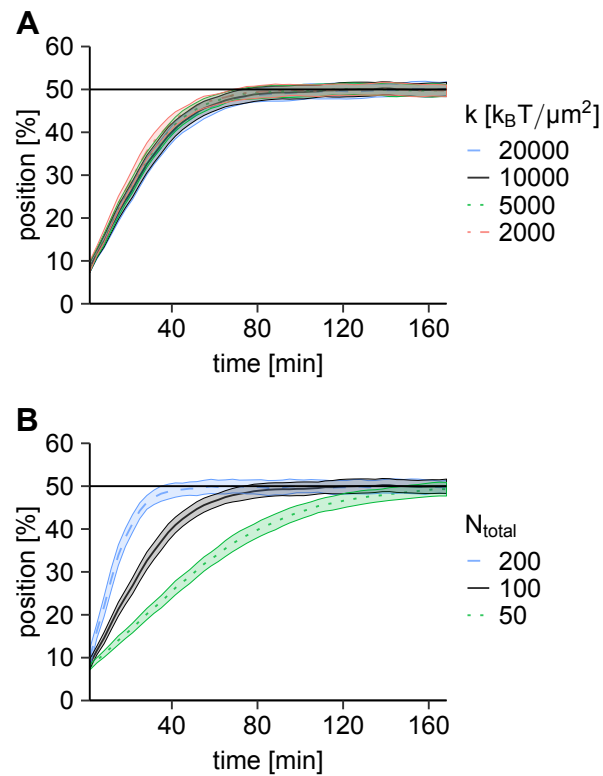
Figure S4.2 Additional parameter sweeps. Same as in Fig. 4.2, but here we vary the spring stiffness, k (A), and the total number of PomZ dimers, N_{total} (B). The spring stiffness can be changed over an order of magnitude without changing the cluster dynamics. However, note that the attachment rate of PomZ dimers to the PomXY cluster is defined in such a way that the total attachment rate to the cluster depends on k. The more PomZ dimers are in the system, the faster the clusters move towards midnucleoid.
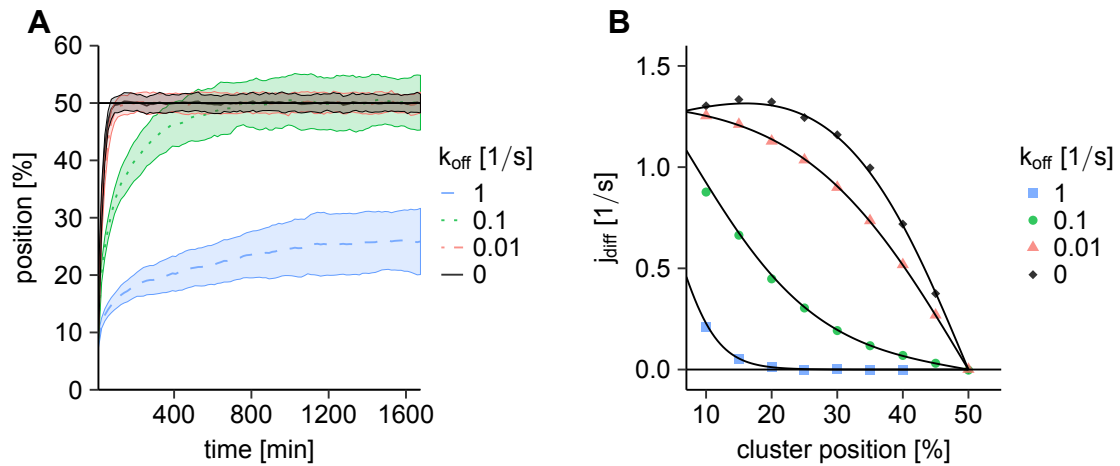
Figure S4.3 Cluster dynamics if nucleoid-bound PomZ dimers can also detach from the nucleoid when they are not bound to the cluster. (A) Same as in Fig. 4.2, but here we modified our model described in the main text by allowing PomZ dimers that are bound to the nucleoid to detach (with rate k_{off}) from the nucleoid into the cytosol also when they do not interact with the PomXY cluster. In black, the simulation results for the model described in the main text (PomZ dimers can only detach when they interact with the cluster) are shown, for comparison reasons. The larger the detachment rate, k_{off}, the longer it takes until the cluster reaches midnucleoid and for very large detachment rates, the cluster does not reach midnucleoid at all. (B) PomZ flux difference into the cluster as a function of the cluster position for the same detachment rates, k_{off}, as in A. The black lines indicate the results from the RD model. For the cases with $k_{off} \neq 0$, we extended the RD equations such that they include detachment of PomZ dimers bound to the nucleoid only. The results from the stochastic simulations (points of different shape and color) nicely agree with the theoretical values. For each parameter set we simulated 100 cluster trajectories.
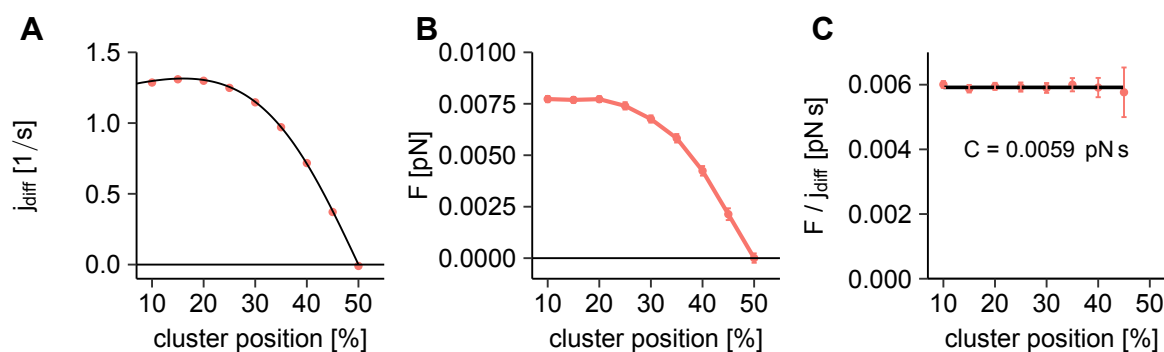
Figure S4.4 The net force is proportional to the flux difference for a stationary PomXY cluster. We simulated the PomZ dynamics for a cluster that is kept fixed at different positions on the nucleoid. (A) The PomZ flux difference into the cluster, j_{diff}, obtained from the simulations (in red) agrees nicely with the predicted flux difference from the RD model (black line). (B) In the simulations, the total force exerted by the PomZ dimers on the PomXY cluster averaged over time, F, also decreases towards zero when the cluster moves from an off-center position towards midnucleoid. (C) The ratio of the total force and the PomZ flux difference (red dots) does not change remarkably with the cluster position, as expected. We discard the value at 50% nucleoid length, because both the flux difference and the total force are supposed to be zero in this case. The black line is a fit of a constant curve to the data with fit parameter $C = F/j_{\text{diff}} = 0.0059\,\text{pN}\,\text{s}$. The 95% confidence interval of the fit is smaller than the width of the line. The simulated values for the flux difference and the total force are obtained by averaging over 10 realizations of the stochastic simulation per cluster position (the error bars show the 95% confidence interval). The simulation parameters are as in Table S4.1.
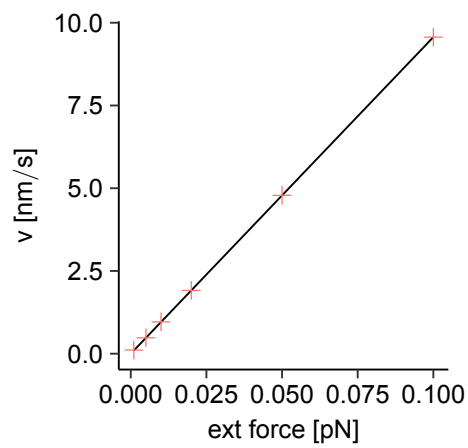
Figure S4.5 Force-velocity curve. The average velocity of the PomXY cluster increases linearly with the external force applied to the cluster. For different external force values we simulated 100 trajectories of a PomXY cluster and determined the average steady-state velocity of the cluster (red crosses). A linear fit to the data (black line) matches the simulation results well and yields the effective friction coefficient of the cluster, which is the inverse of the slope. In the simulations an infinitely extended cluster and nucleoid was used (for details see Materials and methods). We simulated $N_{\text{total}} = 20$ PomZ dimers, all bound to the PomXY cluster, and the ATP hydrolysis rate k_h was set to zero. The other parameters are as in Table S4.1.
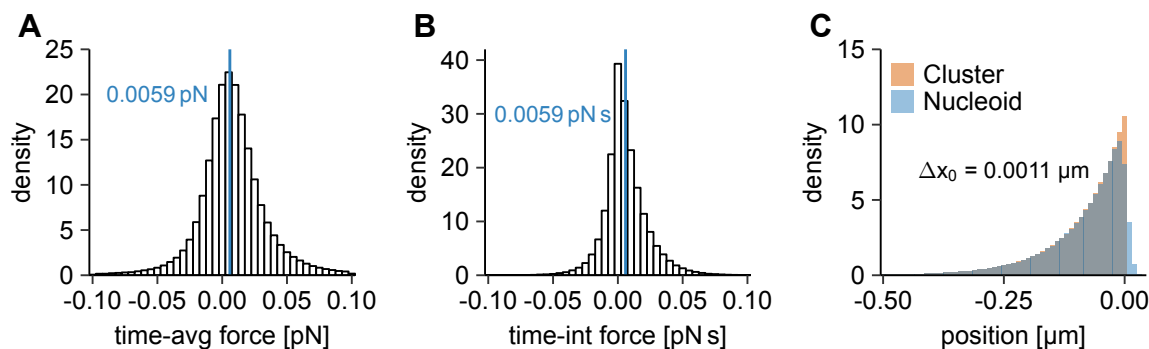
Figure S4.6 Single particle force generation. To determine the constant C, simulations with only one PomZ dimer and a fixed PomXY cluster position are performed (parameters as in Table S4.1). The PomZ dimer stochastically attaches to the rightmost side of the nucleoid, diffuses on the nucleoid, interacts with the PomXY cluster and then detaches from the PomXY cluster and the nucleoid. We simulated more than $400\,000$ particle-cluster interactions and recorded the distributions of time-averaged forces (A), time-integrated forces (B) and the distributions of the binding sites of the PomZ dimers on the nucleoid and cluster when attaching to the PomXY cluster (C). The ensemble average of the time-averaged force, weighting each time-averaged force with the corresponding time a PomZ dimer is attached to the cluster, is positive $f = (5.91 \pm 0.02) \times 10^{-3}\,\text{pN}$ (the error is the standard error of the mean). The same holds true for the mean time-integrated force $f_{\text{int}} = (5.92 \pm 0.02) \times 10^{-3}\,\text{pN\,s}$, which implies that a PomZ dimer arriving at the cluster from the right on average exerts a net force to the right. When attaching to the PomXY cluster, PomZ dimers are typically slightly stretched towards the PomXY cluster, which yields an average distance between the nucleoid and cluster binding site of $\Delta x_0 = 0.0011\,\mu\text{m}$.
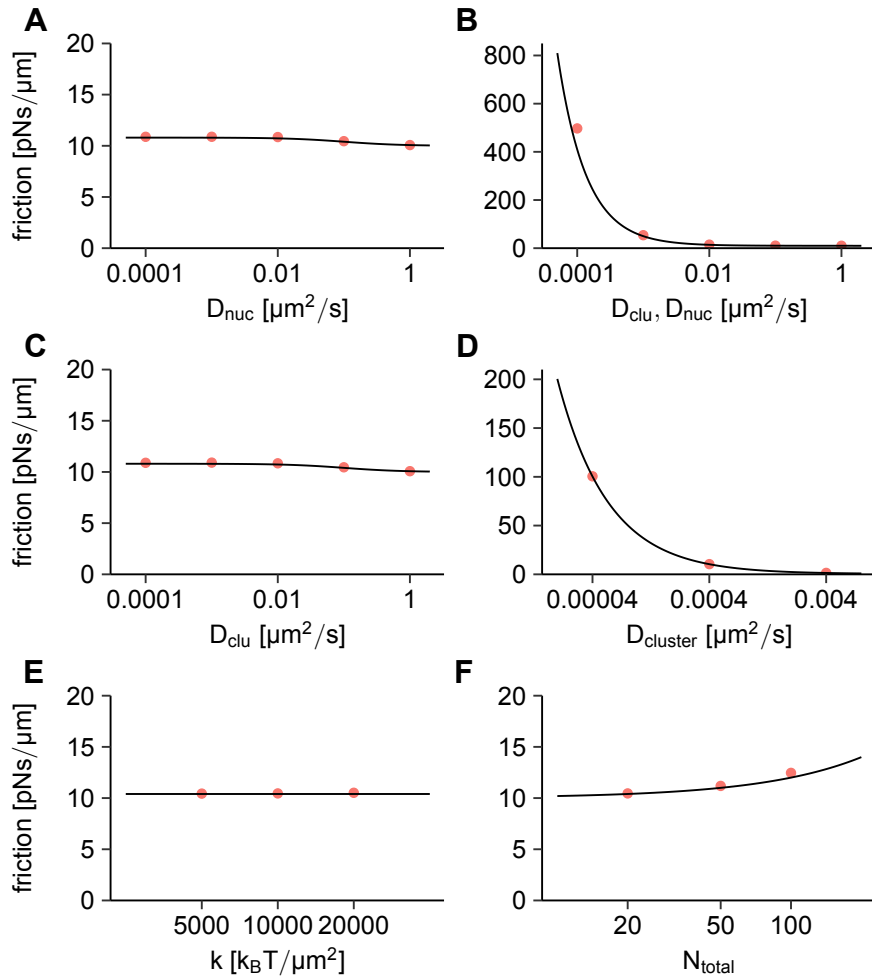
Figure S4.7 Friction coefficient of the PomXY cluster. (A-F) We determined the friction coefficient of the PomXY cluster with $N = 20$ PomZ dimers bound to it, when the diffusion constant of PomZ on the nucleoid and the PomXY cluster (A-C), the cytosolic diffusion constant of the PomXY cluster (D), and the spring stiffness of the PomZ dimers (E) is varied. Finally, we varied the PomZ dimer number bound to the PomXY cluster keeping all other parameters fixed (F). In all cases, the friction coefficients obtained from simulations (red dots) agree with the theoretical prediction (black line, Eq. 4.17). The effective friction coefficient of the PomXY cluster increases with an increasing friction of PomZ on the nucleoid and the PomXY cluster, an increasing cytosolic cluster friction and an increasing cluster-bound PomZ dimer number. It does not depend on the spring stiffness of the PomZ dimers for the parameter range considered. For more details see the Materials and methods section. In the simulations performed for this Figure, the nucleoid and PomXY cluster are infinitely extended, all PomZ dimers in the system are bound to the cluster, the ATP hydrolysis rate is set to zero and the other parameters are as in Table S4.1 if not explicitly given.
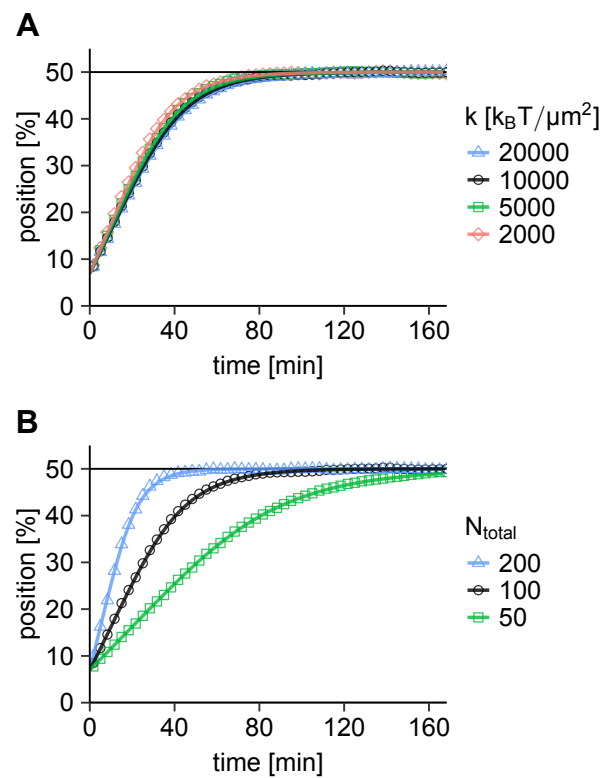
Figure S4.8 Comparison of the average cluster trajectory from simulations and our semi-analytical approximation for additional parameters. Same as in Fig. 4.4, when the spring stiffness k (A) and the total PomZ dimer number N_{total} (B) is varied. The average cluster trajectories are the same as shown in Fig. S4.2.
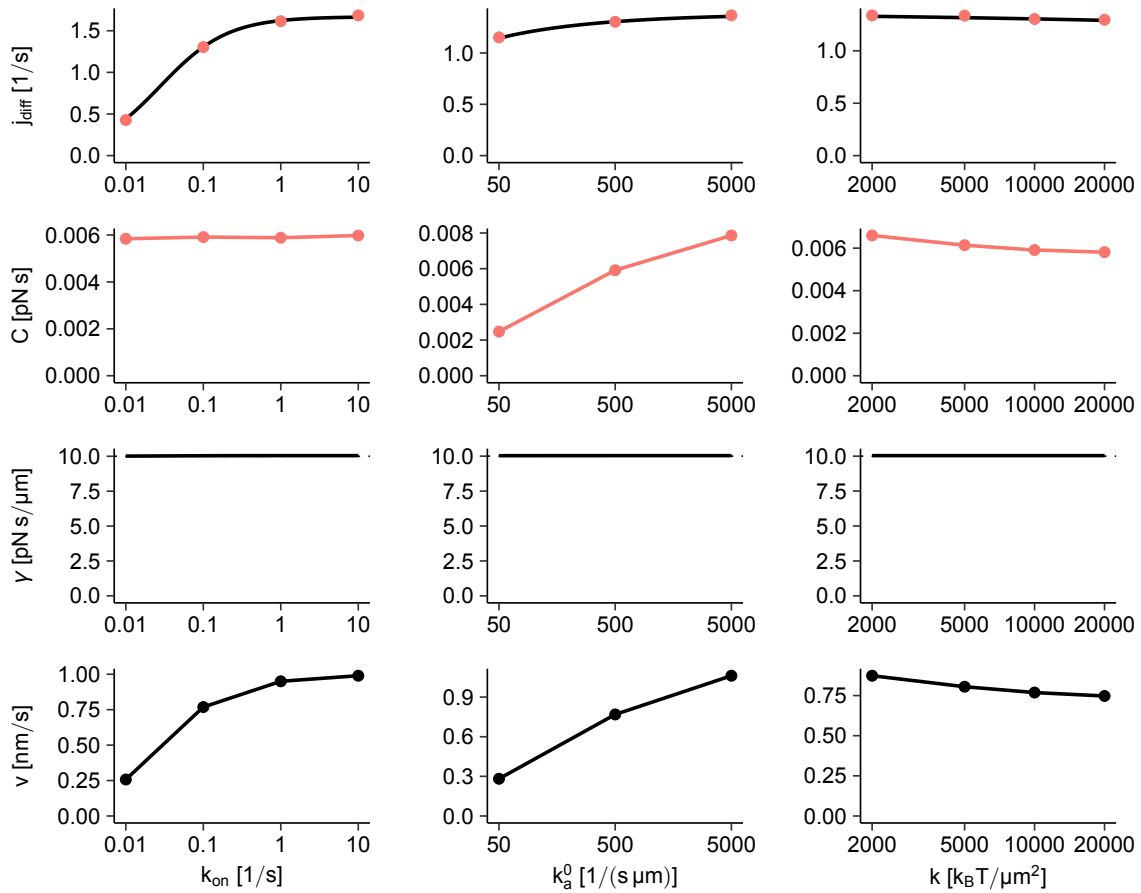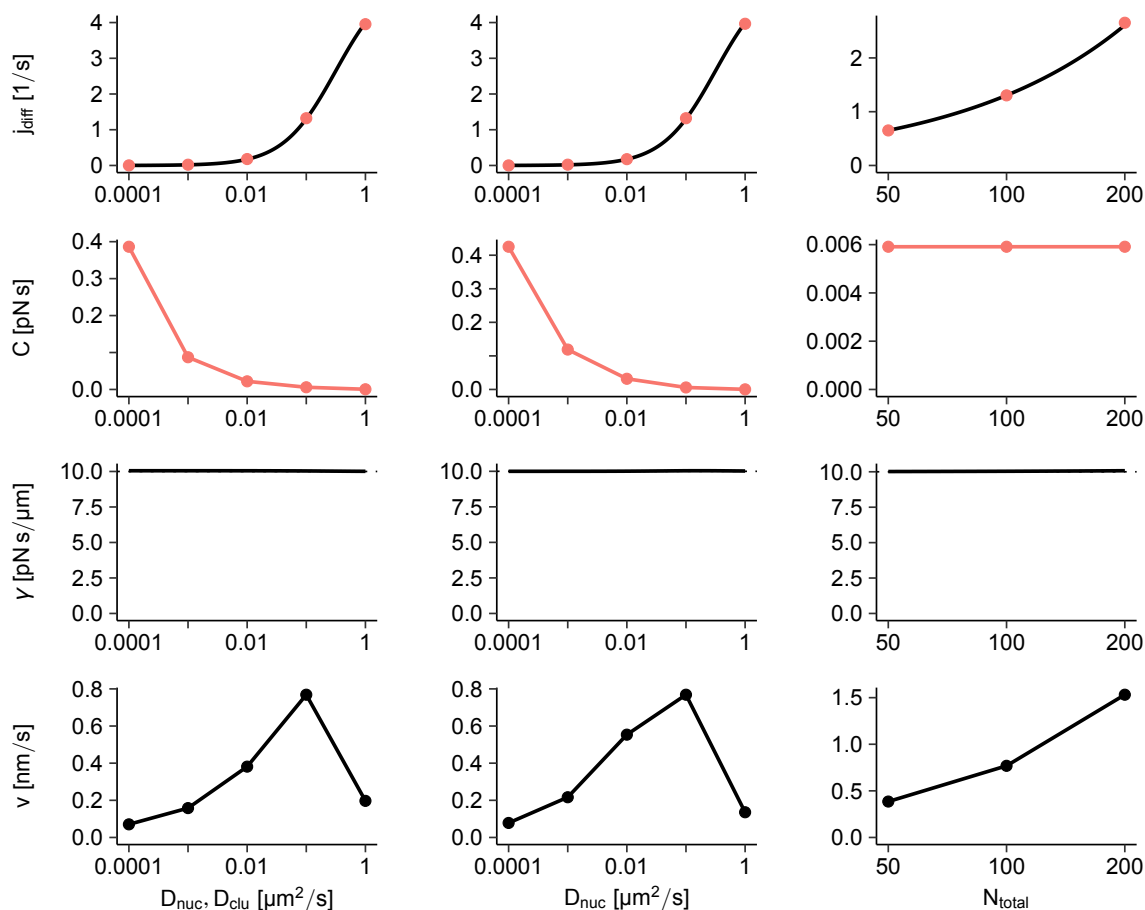
Figure S4.9 Force generation results for additional parameters. Same as in Fig. 4.5 for parameter sweeps varying the attachment rate to the nucleoid k_{on}, the attachment rate to the PomXY cluster k_a^0 and the spring stiffness k. An increase in k_{on} and k_a^0 increases the velocity of the cluster towards midnucleoid. An increase in k leads to stiffer springs and hence less stretched PomZ dimers, but on the other hand, the force, which is linear in k, is increased for the same deflection of the springs. This results in a more or less constant value for C and also a constant velocity of the cluster when varying k over one order of magnitude. Note that a change in the spring stiffness also changes the total attachment rate of PomZ dimers to the PomXY cluster.

Figure S4.10 Force generation results for additional parameters. Same as in Fig. 4.5 for parameter sweeps varying the diffusion constants of PomZ on the PomXY cluster and the nucleoid ($D_{\mathrm{nuc}} = D_{\mathrm{clu}}$), the diffusion constant of PomZ on the nucleoid, D_{nuc}, and the total PomZ dimer number, N_{total}. For very small diffusion constants of PomZ on the nucleoid our semi-analytical approach breaks down (see Fig. 4.4). Interestingly, the net velocity of the cluster is maximal for an intermediate diffusion constant of PomZ on the nucleoid and the PomXY cluster, $D_{\mathrm{nuc}} = D_{\mathrm{clu}} = 0.1\,\mu\mathrm{m}^2/\mathrm{s}$ (see also Fig. 4.4). An increase in the total PomZ dimer number increases the PomZ flux difference into the cluster, but does not change the constant C, since C is an observable for a single particle. Though the number of PomZ dimers bound to the cluster increases if the total number of PomZ dimers is increased, this does not lead to a significant increase of the friction coefficient of the cluster for the parameters we consider (Table S4.1). The velocity of the cluster, which is proportional to the flux difference, then increases with the PomZ dimer number.
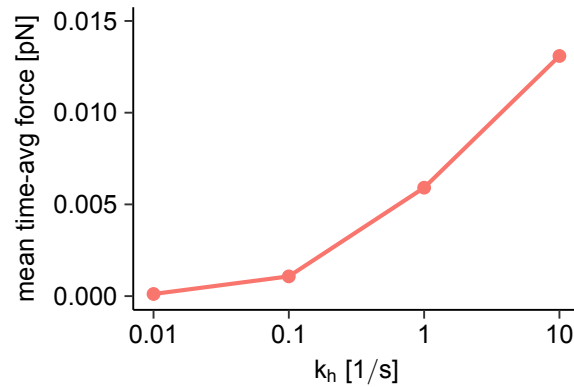
Figure S4.11 Mean time-averaged force for different k_h values. The ensemble average of the time-averaged force a single particle exerts on the PomXY cluster increases with the hydrolysis rate k_h. The larger the hydrolysis rate, the shorter the interaction time of the PomZ dimer with the PomXY cluster. Since the PomZ dimers typically attach close to the cluster's edge and over time diffuse towards the center of the cluster, the average force exerted by the particle decreases over time. Therefore, a shorter interaction time yields a larger time-averaged force. If not explicitly given in the Figure, the parameters are as in Table S4.1.
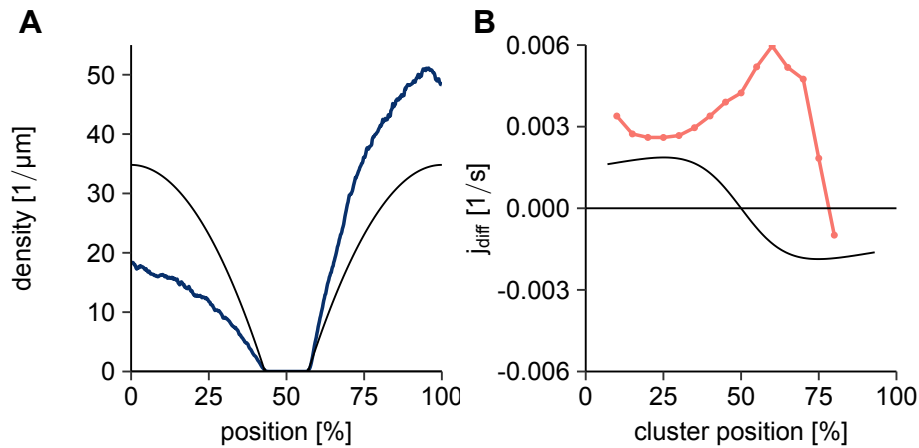
Figure S4.12 PomZ density and flux for an oscillatory cluster. PomZ density along the nucleoid (A) and PomZ flux difference into the cluster (B) as shown in Fig. 4.3 using the parameters in Table S4.1, but a reduced diffusion constant of PomZ on the nucleoid and PomXY cluster ($D_{nuc} = D_{clu} = 0.0001\,\mu\text{m}^2\,\text{s}^{-1}$).
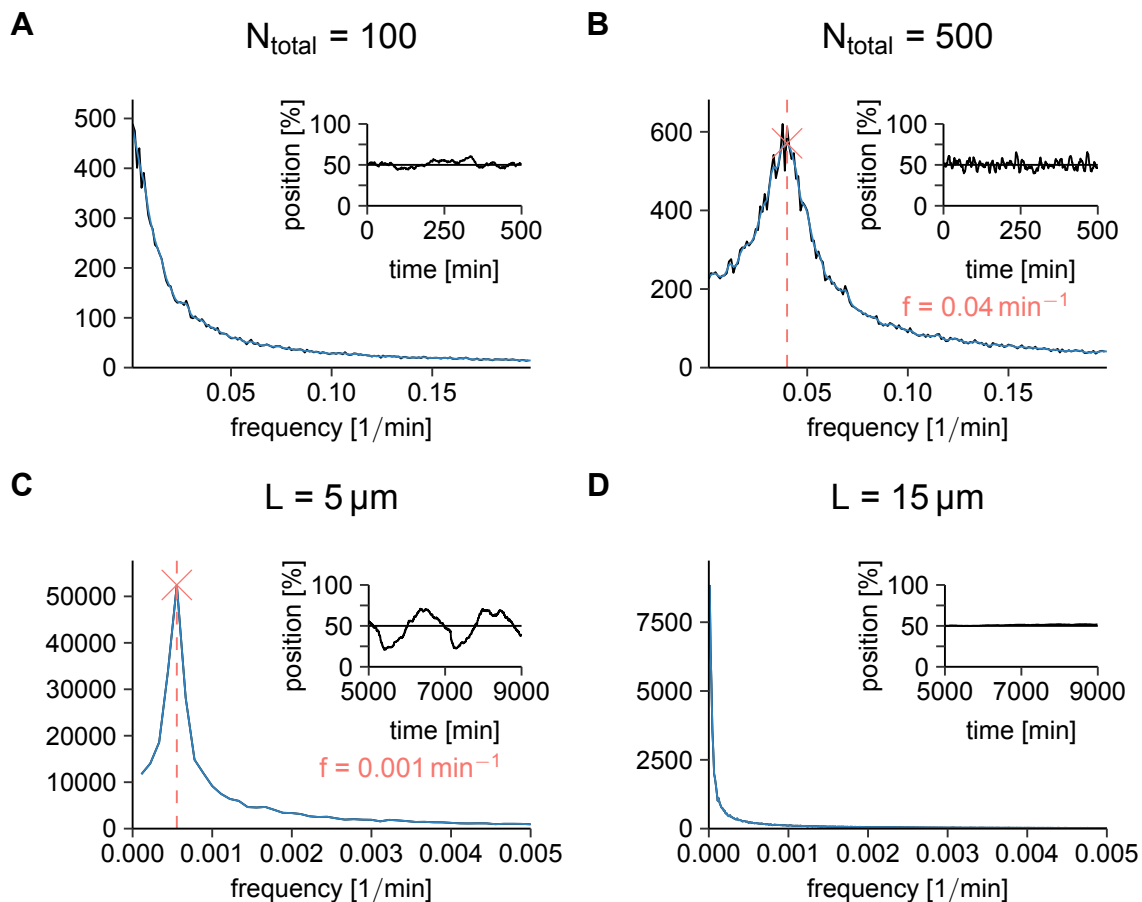
Figure S4.13 Frequency analysis of the cluster dynamics varying N_{total} and L.
The averaged fast Fourier transform of the cluster trajectories and a single trajectory (inset)
are shown (see Fig. S4.1 and Materials and methods for details). (A, B) When the total
PomZ dimer number is increased from $N_{\text{total}} = 100$ to $N_{\text{total}} = 500$, the cluster dynamics
change from fluctuating around midnucleoid to oscillatory with a frequency of $f = 0.04 \, \text{min}^{-1}$
($D_{\text{nuc}} = D_{\text{clu}} = 0.01 \, \mu\text{m}^2/\text{s}$, other parameters as in Table S4.1). For the Fourier analysis we
performed 100 runs of the simulation for 1000 min with a cluster starting at midnucleoid. (C,
D) When the nucleoid length, L, is increased from $L = 5 \, \mu\text{m}$ to $L = 15 \, \mu\text{m}$, the peak in the
Fourier spectrum, which indicates on average oscillations of the clusters with a frequency
$f = 0.001 \, \text{min}^{-1}$, disappears ($D_{\text{nuc}}, D_{\text{clu}} = 0.0001 \, \mu\text{m}^2/\text{s}$, other parameters as in Table S4.1).
We performed 100 runs of the simulation for at least 10 000 min with a cluster starting at
midnucleoid.

Chapter 5

Flux-based positioning of protein clusters in three-dimensional cell geometry

In this chapter, I present our analyses of the Pom system in the three-dimensional cell geometry. This project was motivated by the question whether a flux-based mechanism can lead to midcell or equidistant positioning also if the proteins (PomZ) can diffuse past the cargo (PomXY cluster). In the first part of this chapter, we approached this question by considering the cytosolic and nucleoid-bound PomZ dynamics for a stationary cluster in terms of reaction-diffusion (RD) equations. We solved the RD equations in different model geometries using the COMSOL Multiphysics® software (finite element solver) [11]. In the second part, I present our results from particle-based stochastic simulations to model the cluster dynamics in the three-dimensional cell geometry, which are currently prepared for publication (joint work with Matthias Kober). We generalized our stochastic model described previously (chapter 3 and 4) by incorporating the nucleoid as a cylinder and the cluster as a rectangular sheet, moving on the surface of the cylindrical nucleoid (for further details on the model see chapter 2).

5.1 Stationary PomZ distributions for different model geometries

First, we described the PomZ dynamics in terms of reaction-diffusion equations, which we then solved for different nucleoid and cell geometries. We assumed that PomZ can be in one of the following four states: i) ATP-bound in the cytosol (the concentration is denoted by c_T), ii) ADP-bound in the cytosol (c_D), iii) nucleoid-bound (c), or iv) nucleoid- and cluster-bound (c_b). This is a simplified scheme as we neglect the monomeric and dimeric forms of PomZ.

PomZ diffuses in the cytosol with diffusion constant D_{cyt} and exchanges ADP for ATP with nucleotide exchange rate k_{ne}. The rate k_{ne} is an effective rate that includes both dimerization, which we do not explicitly include here, and nucleotide exchange. ATP-bound cytosolic PomZ binds to the nucleoid, at all regions of the nucleoid apart from the location of the PomXY cluster, with rate $\tilde{k}_{\text{on}}$ and then diffuses on the nucleoid with diffusion constant D_{nuc}. Nucleoid-bound PomZ dimers in the cluster region attach to the cluster with rate k_a^{total}. In this state, they can still diffuse, but with a lower diffusion constant, $D_b = D_{\text{nuc}}/2$, to account for the reduced mobility of the PomZ

dimers when bound to the cluster. The PomZ dimers are trapped at the cluster, as they can only leave the cluster (as ADP-bound PomZ) upon ATP-hydrolysis with rate k_h.
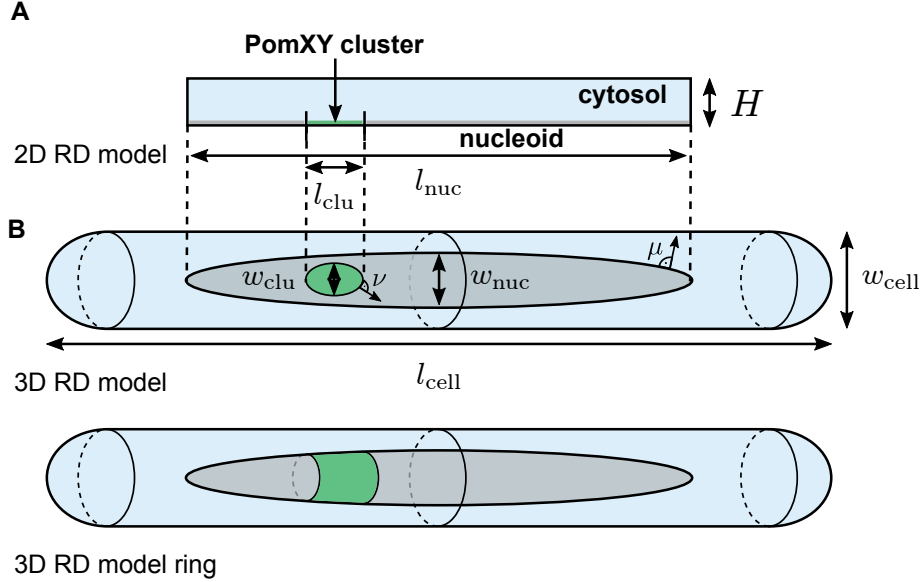

Figure 5.1 Different geometries for which we solved the RD equations. We considered two different model geometries, a two- ("2D RD model") and a three-dimensional one ("3D RD model"). (A) In the first model, the nucleoid is incorporated as a one-dimensional line. The PomXY cluster is defined by an interval on the nucleoid. The two-dimensional area above the nucleoid represents the cytosolic volume in the cell. (B) In the 3D RD model the cell is modeled as a rod-shaped object with an ellipsoidal nucleoid inside. The cluster is again a region of the nucleoid, either of elliptical shape (top) or ring-shaped (bottom). We assume that PomZ dimers only bind to the surface of the nucleoid, i.e. they do not penetrate into the nucleoid volume.

These processes can be described by the following reaction-diffusion equations conserving the total PomZ protein number:

$$\partial_t c_T = D_{\text{cyt}} \nabla^2 c_T + k_{\text{ne}} c_D, \tag{5.1}$$

$$\partial_t c_D = D_{\text{cyt}} \nabla^2 c_D - k_{\text{ne}} c_D, \tag{5.2}$$

$$\partial_t c = D_{\text{nuc}} \nabla^2 c + \tilde{k}_{\text{on}} c_T, \qquad \text{(away from the cluster)}, \tag{5.3}$$

$$\partial_t c = D_{\text{nuc}} \nabla^2 c - k_a^{\text{total}} c, \qquad \text{(in the cluster region)}, \tag{5.4}$$

$$\partial_t c_b = D_b \nabla^2 c_b + k_a^{\text{total}} c - k_h c_b, \tag{5.5}$$

with the reactive boundary conditions

$$D_{\text{cyt}}\nabla_\mu c_T|_{\mu=\mu_0} = -\tilde{k}_{\text{on}}c_T, \quad \text{(away from the cluster)}, \tag{5.6}$$

$$D_{\text{cyt}}\nabla_\mu c_D|_{\mu=\mu_0} = k_h c_b, \quad \text{(in the cluster region)}, \tag{5.7}$$

$$D_{\text{cyt}}\nabla_\mu c_D|_{\mu=\mu_0} = 0, \quad \text{(away from the cluster)}, \tag{5.8}$$

$$D_b\nabla_\nu c_b|_{\nu=\nu_0} = 0. \tag{5.9}$$

Here, μ denotes a normal vector to the nucleoid surface, and ν a normal vector tangential to the nucleoid surface and normal to the cluster's contour on the nucleoid (see Fig. 5.1B).

We consider two different cell geometries: either we model the cytosol as a rectangle with the lower edge mimicking the nucleoid ("2D RD model") or we account for the full three-dimensional geometry of the cell ("3D RD model") (see Fig. 5.1). In the later case, the cell is modeled as a rod-shaped object resembling the geometry of a *M. xanthus* cell, and the nucleoid is modeled as an ellipsoidal object inside the cell. The PomXY cluster is incorporated in our model as an object of either nearly elliptical or ring shape, which is always located on the nucleoid (see Fig. 5.1B). We assume that PomZ dimers only bind to and diffuse on the surface of the nucleoid.

Initially, all PomZ proteins are in the cytosol as ATP-bound PomZ and the concentration is homogeneously distributed. We calculated the solutions of the RD equations above until a maximal time of 1000 s. The time is chosen such that the concentration profiles have reached their steady state values, which we verified based on the observation that the results do not change anymore with time.

Parameter choice

The aim of this project is to investigate the influence of the model geometry on the PomZ density distributions and fluxes. Hence, we chose the same parameters as before in the one-dimensional stochastic model (Table S4.1), whenever possible. However, due to the differences between the stochastic and the RD models (different geometry, cytosolic PomZ distribution is included), some parameters still needed to be determined. We set the cytosolic diffusion constant of PomZ, D_{cyt}, to a value measured for cytosolic MinE [104]. For the effective nucleotide exchange rate we took as approximate value the exchange rate of MinD [104].

In our stochastic, particle-based model, we used an attachment rate of PomZ to the nucleoid, $k_{\text{on}} = 0.1\,\text{s}^{-1}$, which is the rate with which a PomZ dimer in the cytosol binds somewhere to the nucleoid. In order to compare our results from the RD models, where we explicitly include the cytosol, to the stochastic model we set the attachment rate to $\tilde{k}_{\text{on}} = k_{\text{on}}V_{\text{cyt}}/R_{\text{nuc}}$, with the cytosolic volume, V_{cyt}, and the surface area of the nucleoid, R_{nuc}. This formula can be derived as follows: We neglect that PomZ dimers do not attach to the nucleoid at the location of the cluster, and assume that PomZ attaches everywhere to the nucleoid. Integrating Eq. 5.3 over the nucleoid region, R_{nuc},

Parameter	Symbol	Value
Number of PomZ dimers	N_{total}	100
Length of nucleoid	l_{nuc}	$5\,\mu\text{m}$
Length of cluster	l_{clu}	$0.7\,\mu\text{m}$
Attachment rate PomZ to nucleoid	k_{on}	$0.1\,\text{s}^{-1}$
Total attachment rate PomZ to cluster	k_a^{total}	$12.5\,\text{s}^{-1}$
Diffusion constant PomZ on nucleoid	D_{nuc}	$0.1\,\mu\text{m}^2/\text{s}$
Diffusion constant cluster-bound PomZ	D_b	$0.05\,\mu\text{m}^2/\text{s}$
Diffusion constant PomZ in the cytosol	D_{cyt}	$10\,\mu\text{m}^2/\text{s}$
ATP hydrolysis rate PomZ bound to PomXY cluster	k_h	$1\,\text{s}^{-1}$
Nucleotide exchange rate	k_{ne}	$6\,\text{s}^{-1}$
2D Height of cytosolic volume	H	$0.5\,\mu\text{m}$
3D Width of nucleoid	w_{nuc}	$0.6\,\mu\text{m}$
Width of cluster	w_{clu}	$0.6\,\mu\text{m}$
Length of cell	l_{cell}	$7.7\,\mu\text{m}$
Width of cell	w_{cell}	$1\,\mu\text{m}$

Table 5.1 Parameters used in the RD models. We used these parameters in our RD model unless explicitly stated otherwise. Some parameters are specific for the two- or three-dimensional RD models (grouped by the double lines).

yields

$$\int_{R_{\text{nuc}}} \partial_t c \, d\sigma = \partial_t \int_{R_{\text{nuc}}} c \, d\sigma = \int_{R_{\text{nuc}}} D_{\text{nuc}} \nabla^2 c \, d\sigma + \int_{R_{\text{nuc}}} \tilde{k}_{\text{on}} c_T \, d\sigma = \tilde{k}_{\text{on}} \int_{R_{\text{nuc}}} c_T \, d\sigma. \tag{5.10}$$

The diffusion term vanishes as we integrate over the entire nucleoid surface. If we assume that the cytosolic PomZ-ATP distribution is homogeneous, it is given by $c_T = C_T/V_{\text{cyt}}$, with C_T the total number of PomZ-ATP in the cytosol. With the total number of PomZ bound to the nucleoid, $C = \int_{R_{\text{nuc}}} c \, d\sigma$, the above equation becomes

$$\partial_t C = \tilde{k}_{\text{on}} \int_{R_{\text{nuc}}} \frac{C_T}{V_{\text{cyt}}} \, d\sigma = \tilde{k}_{\text{on}} \frac{R_{\text{nuc}}}{V_{\text{cyt}}} C_T \overset{!}{=} k_{\text{on}} C_T. \tag{5.11}$$

For the rate $\tilde{k}_{\text{on}}$ to result in a rate k_{on} for cytosolic PomZ to attach to the nucleoid, we need to chose $\tilde{k}_{\text{on}} = k_{\text{on}} V_{\text{cyt}}/R_{\text{nuc}}$. The value for $\tilde{k}_{\text{on}}$ thus depends on the model geometry. In the two-dimensional geometry we have $\tilde{k}_{\text{on}} = k_{\text{on}} H = 0.05\,\mu\text{m}\,\text{s}^{-1}$ and in the three-dimensional one, $\tilde{k}_{\text{on}} = k_{\text{on}} V_{\text{cyt}}/R_{\text{nuc}} \approx 0.06\,\mu\text{m}\,\text{s}^{-1}$. For the attachment rate of PomZ to the cluster we use the total attachment rate k_a^{total}, which corresponds to

the rate with which a PomZ dimer in the stochastic model attaches to any site on the cluster (see section 4.4.1).

In the 2D RD model the height of the cytosolic bulk is a free parameter. It can be varied without a significant change of the results, as long as the cytosolic PomZ-ATP distribution is approximately homogeneous. If the cytosolic volume is chosen very large, this assumption does not hold true anymore, and so the results start to depend on H. The values for the width of the cluster and the cell length have been measured by experiments [2] and the values of the nucleoid and cell width are chosen such that the geometry resembles the one from *M. xanthus* cells.

Results

First, we compare our result obtained from the 2D RD model with the ones from the stochastic, particle-based model, in order to ensure that we chose the parameters such that the two models are comparable. We find that, the two different approaches indeed give very similar results with our choice of the parameters (Table 5.1), both for the PomZ density profile along the nucleoid and the PomZ flux difference into the cluster from either side, j_{diff} (see Fig. 5.2).
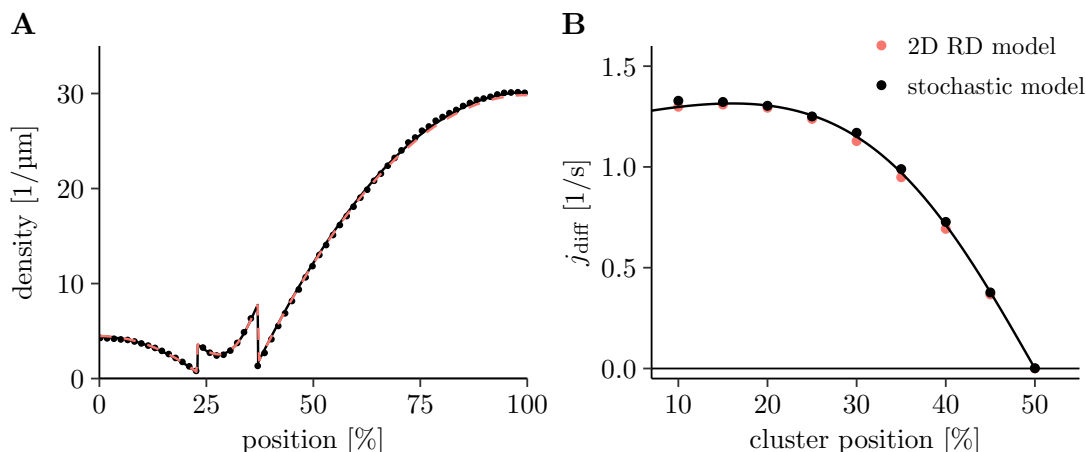
Figure 5.2 Comparison of RD model with stochastic, particle-based simulations. (A) PomZ density profile along the nucleoid obtained from the 2D RD model (red dashed line) and using our stochastic particle-based model (black dots). The black line shows the result from the continuum model described in section 4.4.1, which differs from the 2D RD model as the latter includes the cytosolic PomZ distribution. (B) The difference in the fluxes of nucleoid-bound PomZ into the cluster from either side, j_{diff}, is non-zero for an off-center located cluster and becomes zero when the cluster reaches midnucleoid. We find excellent agreement between the results from the 2D RD model, the stochastic model and the analytical solution from the continuum model (section 4.4.1). For the RD model we used the parameters as given in Table 5.1. The data from the stochastic simulations shown here is the same as in Fig. 4.3.

The RD model differs from the stochastic model, as we explicitly included the cytosolic PomZ distribution in the former. However, since PomZ dimers diffuse quickly in the cytosol and the binding rate to the nucleoid is rather slow ($k_{on} = 0.1\,\text{s}^{-1}$), the cytosolic PomZ-ATP density can be approximated to be homogeneous in the RD model, which explains the good agreement between the results. Note that the delay of PomZ between its inactive (ADP-bound monomers) and active (ATP-bound dimers able to bind DNA non-specifically) form is due to several processes including nucleotide exchange, dimerization and gaining the ability to bind DNA non-specifically. Not for all of these processes, the rates are experimentally determined yet. Here, we reduced the number of processes to two: relatively fast nucleotide exchange and slow attachment to the nucleoid.
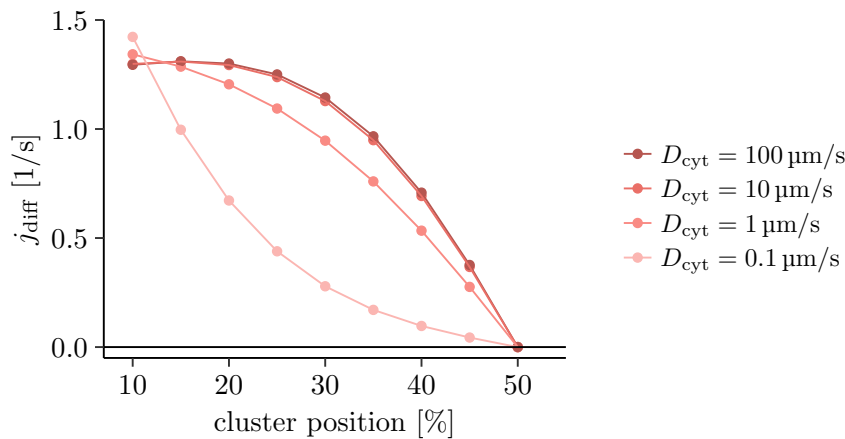
Figure 5.3 Flux difference of PomZ into the cluster in the 2D RD model with different cytosolic diffusion constants. We calculated the flux difference of nucleoid-bound PomZ into the cluster region from either side, j_{diff}, in the 2D RD model and varied the cytosolic diffusion constant of PomZ, D_{cyt}. Except for very small values of the cluster position, j_{diff} decreases with a decreasing diffusion constant and the shape of the curve changes from concave to convex. Thus, a flux-based mechanism should lead to midcell positioning faster for larger cytosolic diffusion constants.

To investigate the effect of the cytosolic PomZ-ATP distribution on the flux difference of nucleoid-bound PomZ into the cluster, j_{diff}, we varied the cytosolic diffusion constant D_{cyt} from $0.1\,\mu\text{m}^2/\text{s}$ to $100\,\mu\text{m}^2/\text{s}$. We find that overall j_{diff} decreases with decreasing D_{cyt} (Fig. 5.3). This decrease can be explained by the fact that PomZ is only locally redistributed in the cytosol when the diffusion constant is small, in contrast to a global redistribution for large diffusion constants. Only when PomZ is spatially redistributed over the whole cytosolic volume, the amount of PomZ attaching to the nucleoid left and right of the cluster scales with the length of these nucleoid regions. The larger values of j_{diff} for small D_{cyt} values observed for clusters close to the nucleoid end (at 10% of nucleoid length) can be attributed to the fact that if the redistribution of PomZ

occurs only in the cytosol region close to the cluster, PomZ dimers also likely attach to the nucleoid close by the cluster. Hence they reach the cluster faster than if they attach with equal likelihood along the nucleoid.

Next, we solved the RD equations in the three-dimensional model geometry (Fig. 5.1B). We either used a region of elliptical shape or a rotationally symmetric region ("ring-shaped" cluster) on the nucleoid to model the cluster. In the former case, PomZ dimers can diffuse past the cluster, which raised the question of whether an asymmetry in the fluxes — a necessary condition for a flux-based mechanism — can still be achieved in the steady state [3]. In Fig. 5.4 we compare our steady state results for the PomZ flux difference from all different RD models and the stochastic model. In the three-dimensional geometry the PomZ flux difference into the cluster still differs if the cluster is off-center and is zero at midcell (Fig. 5.4). The flux difference is reduced compared to the 2D RD model or our stochastic model, which agrees with our expectation that PomZ dimers can diffuse past the cluster and in this way reduce the asymmetry in the PomZ distribution on the nucleoid.
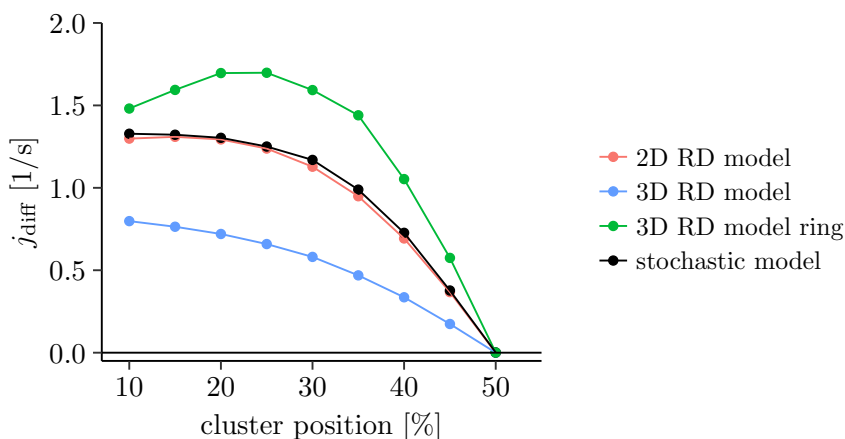

Figure 5.4 Flux difference of PomZ into the cluster for the different models considered. We calculated the flux difference of PomZ into the cluster for different cluster positions and models. The lines are plotted to guide the eye. The results from the stochastic simulations is shown in black (same data as shown in Fig. 4.3). For the numerical solutions of the RD models we used the parameters given in Table 5.1.

However, our investigations on different shapes of the clusters show that the flux past the cluster is not the only aspect that is different between the 2D and 3D RD models. In the case of a ring-shaped cluster, PomZ dimers cannot pass the cluster, which is similar to the 2D RD model. Nevertheless, we find larger values for j_{diff} as obtained for the 2D RD model. Hence, the flux of PomZ passing the cluster is not the only reason for the observed change in j_{diff} observed in the 3D RD model with an elliptical cluster. The two three-dimensional models differ from the two-dimensional model by the ratio of the areas of cluster to nucleoid, $r = R_{\text{clu}}/R_{\text{nuc}}$. If the cluster

region covers a larger region of the nucleoid, more PomZ dimers can detach into the cytosol and hence the flux through the system increases. For a cluster at midnucleoid, we have the following ratios: $r = 14\%$ (2D RD model and stochastic model), $r \approx 18\%$ (3D RD model with ring-shaped cluster) and $r = 4\%$ (3D RD model with elliptical cluster). In the 3D RD model, the value for r changes with the cluster position: it is largest at midnucleoid and smallest at the nucleoid poles. This changed area could explain the initial increase in j_{diff} observed for the 3D RD model with a ring-shaped cluster (Fig. 5.4). However, we also discuss another possible explanation in the next paragraph.

Another factor that changes the flux difference of PomZ at the cluster between the two- and three-dimensional models results from modeling the nucleoid as an elliptical object. In this case, the surface area of the nucleoid left and right of the cluster does not scale linearly with the respective lengths of these regions as in the 2D RD model. The area of the region with the larger cluster-to-nucleoid-end distance constitutes an even larger fraction of the nucleoid compared to the one-dimensional case, which leads to an increase in the flux difference. On the other hand, there are also factors that might decrease j_{diff}. For example, the bulk-to-boundary ratio is large at the nucleoid poles, which leads to a higher flux of PomZ-ATP attaching to the nucleoid poles compared to the nucleoid at midcell (see [56]). We expect that an increased attachment of PomZ at the nucleoid poles decreases the flux difference, as PomZ needs longer to reach the cluster compared to a homogeneous on-flux of PomZ to the nucleoid.

In this section we have focused on the steady state PomZ density and fluxes on the nucleoid for different model geometries. We found that spatial redistribution of PomZ in the cytosol is important for a flux-based mechanism as the flux difference, for clusters not at midcell, becomes larger. Furthermore, we found that a flux difference in PomZ can still be achieved in a three-dimensional geometry for which PomZ dimers can diffuse past the cluster. In the next section, we focus on the cluster dynamics.

5.2 Pom cluster dynamics in three-dimensional cell geometry

Abstract

Positioning of macromolecular structures in bacteria is vital for cell organization and division. In the bacterium *Myxococcus xanthus*, a large cluster of Pom proteins forms, which is tethered to the nucleoid by the ATPase PomZ and moves in a stochastic, but biased manner towards midcell. The cluster localizes at midcell and initiates cell division. Previously a positioning mechanism based on the flux of PomZ on the nucleoid was proposed. However, the Pom cluster dynamics was considered for a reduced, one-dimensional geometry of the nucleoid and the cluster, and therefore it remained unclear whether such a mechanism can lead to midcell positioning also for a biologically more realistic nucleoid geometry. Here we introduce a mathematical model, which accounts for the full three-dimensional shape of the nucleoid such that

nucleoid-bound PomZ dimers can diffuse past the Pom cluster. PomZ dimers can exert forces on the cluster due to the elastic properties of the nucleoid. Using stochastic simulations, we find that the cluster still moves towards and localizes at midcell on the three-dimensional nucleoid. Furthermore, we investigate the effect of the cytosolic PomZ distribution on the cluster dynamics and the dynamics of two clusters. In the latter case, we find localization at the one- and three-quarter positions along the nucleoid. We conclude that a flux-based mechanism allows for cluster positioning also in a biologically realistic three-dimensional cell geometry.

5.2.1 Introduction

Intracellular positioning of proteins is important for several bacterial processes including midcell localization of the cell division machinery as well as chromosome and plasmid segregation. The underlying positioning systems often involve P-loop ATPases such as ParA and MinD [9, 28]. These ATPases switch between an ATP- and ADP-bound state with different subcellular localizations depending on the nucleotide state: the ATP-bound form typically binds as dimer to the nucleoid or membrane and the ADP-bound form diffuses in the cytosol (see Fig. 5.5). ATPase activating proteins stimulate their ATPase activity, which results in detachment of the ATP-bound form from the respective scaffold. Intracellular patterns of these ParA-like ATPases depend on the binding properties of the ADP- and ATP-bound form, the localization of the stimulating proteins as well as the cell geometry [48, 52, 56].
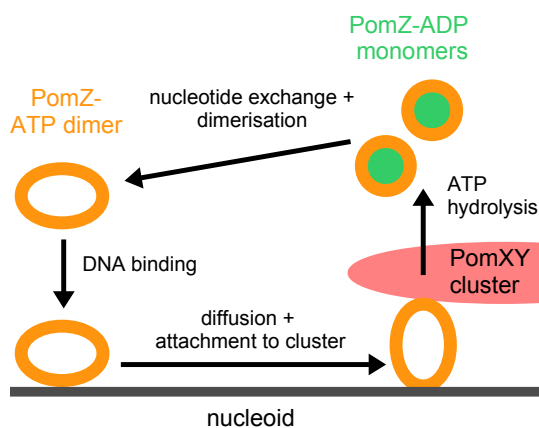

Figure 5.5 Schematic of the states and biochemical interactions of PomZ. Main steps of the ATPase cycle of PomZ based on experimental evidence [2]. Cytosolic PomZ-ATP dimers can attach to the nucleoid, on which they diffuse. Nucleoid-bound PomZ dimers can bind to the PomXY cluster. PomX, PomY and DNA stimulate the ATPase activity of PomZ, which results in a conformational change of the PomZ dimer and finally detachment of two ADP-bound monomers into the cytosol. The ADP-bound PomZ monomers have to replace ADP by ATP, dimerize and gain the competence for non-specific DNA-binding before they can again bind to the nucleoid as ATP-bound PomZ dimers.

In the bacterium *Myxococcus xanthus*, three proteins (PomX, PomY and PomZ) are required for the robust localization of the FtsZ ring at midcell [1, 2, 101]. The ParA-like ATPase PomZ switches between a cytosolic and a nucleoid bound state (see Fig. 5.5). It binds as an ATP-bound dimer non-specifically to DNA. PomX and PomY form a cluster, the PomXY cluster, which is tethered to the nucleoid via PomZ dimers. The cluster and DNA synergistically stimulate the ATPase activity of PomZ, which leads to a conformational change of PomZ and results in two ADP-bound PomZ monomers being released into the cytosol. Before they are able to rebind to the nucleoid, they need to exchange ADP for ATP, dimerize and gain the competence for non-specific DNA binding. Shortly after cell division, the cluster is located at one end of the nucleoid. While the chromosome is duplicated and segregated, the cluster moves from this off-centre position towards midnucleoid, which coincides with midcell, in a stochastic, but biased manner. At midnucleoid it positively regulates FtsZ ring formation [2]. Experiments with deletion mutants suggest that PomZ is crucial for the observed movement of the cluster [2]. Hence, midcell localization in *M. xanthus* relies on the ParA-like ATPase PomZ and proteins that stimulate its ATPase activity.

In *Escherichia coli* midcell localization of the cell division machinery is controlled by the Min system. The Min proteins cycle between a membrane-bound and a cytosolic state [36]. They undergo pole-to-pole oscillations and thereby ensure that the FtsZ ring is formed at midcell [25]. How such oscillatory protein patterns emerge is well-studied theoretically [41–43, 45–48, 51, 52, 55, 56]. Interestingly, cycling of a protein between two states and spatial redistribution of the proteins via the cytosol have been found to be important also in other pattern forming systems (e.g. cell polarization by Cdc42 in *Saccharomyces cerevisae* and PAR protein patterns in *Caenorhabditis elegans*), showing that these are generic principles for self-organized protein pattern formation [53, 54]. Though the Min proteins have the same biological function as the Pom proteins — to robustly position the FtsZ ring at midcell — these two systems differ in two key aspects: Pom proteins bind to the nucleoid instead of the membrane and PomX and PomY proteins form a cluster whose movement is determined by the interactions with nucleoid-bound PomZ. In this regard, the Pom system in *M. xanthus* is closer to the Par system for low copy number plasmid and chromosome segregation as well as systems to position chemotaxis protein clusters [60] or carboxysomes [17]. These systems also include an ATPase, like PomZ, that bind to the nucleoid to position a cargo (plasmids, partition complex or protein cluster).

ParAB*S* systems consist of an ATPase ParA, a DNA-binding protein ParB and a DNA sequence *parS*. ParA binds in its ATP-bound dimeric form non-specifically to DNA and the protein ParB binds specifically to the *parS* region on the chromosome or plasmids. The DNA-bound ParB proteins also bind to chromosome-bound ParA, which leads to an activation of ParA's ATPase activity and finally detachment of ADP-bound ParA monomers into the cytosol [9, 28]. To understand intracellular positioning by ParAB*S* systems, several models have been proposed [3, 6, 10, 16, 73–76, 78–81, 100, 115]. A mechanism for ParA-mediated cargo movement based on the elasticity of the chromosome [5] was suggested [6, 100]. Here, the elastic properties of the chromosome lead to a wiggling movement of the nucleoid-bound ParA dimers. When interacting

with a cargo (plasmid or partition complex), they 'relay' the cargo into the direction of a higher ParA concentration, on average. For equal plasmid partitioning upon cell division, a mechanism that incorporates the fluxes of the ATPase on the nucleoid was proposed: Ietswaart et al. [3] showed that the diffusive ParA fluxes at a plasmid from either side only equalize if the plasmids are at equally distant positions along the nucleoid. Hence, plasmids can be equally spaced on the nucleoid if they move into the direction from which more ParA proteins are arriving.

Previously, we introduced a one-dimensional mathematical model to study the PomXY cluster dynamics in *M. xanthus* [2, 120], which incorporates the elasticity of the nucleoid as in the DNA-relay model [6]. Based on this model, we proposed a mechanism that relies on the PomZ dimer fluxes on the nucleoid (similar to [3]) to generate the experimentally observed PomXY cluster dynamics, which is midcell localization. It remained unclear, however, whether such a flux-based mechanism can also localize midcell if the full three-dimensional geometry of the nucleoid is accounted for. The reason is that, in contrast to the one-dimensional case, PomZ dimers can now more easily pass the cluster without interacting with it. As a result, an asymmetry in the PomZ density and fluxes might be balanced.

Here, we introduce a mathematical model that incorporates the nucleoid, the PomXY cluster and PomZ dimers, which are either in the cytosol or bound to the nucleoid and, in the latter case, can interact with the PomXY cluster. In contrast to previous models [2, 3, 120], here we account for the biologically realistic three-dimensional geometry of the nucleoid by modeling it as a cylindrical object (Fig. 5.6a, bottom right). We find midnucleoid localization of the Pom cluster also in this geometry. Furthermore, we investigate the effect of the cytosolic PomZ distribution on the cluster dynamics, which has previously been assumed to be spatially homogeneous [2, 3, 120]. The simulation results indicate that the time for midcell localization of the cluster decreases with a decreasing cytosolic diffusion constant, which corresponds to an increasing deviation of the cytosolic PomZ distribution from a spatially homogeneous PomZ distribution. Inspired by plasmid equipartitioning [3, 10, 13–15], we further studied the dynamics of two clusters in our model. We find localization of the clusters at the one- and three-quarter positions along the nucleoid length.

Results

To investigate a flux-based mechanism for intracellular localization of protein clusters in a biologically realistic geometry, we first explain how the experimentally observed states of PomZ and its interactions with the nucleoid and the PomXY cluster (Fig. 5.5) are accounted for in our mathematical model. Previously, we introduced a model that reduces both the nucleoid and the PomXY cluster to one-dimensional objects. With this model we could explain midcell localization of a PomXY cluster in one dimension, but can we explain midcell localization also in a biologically realistic three-dimensional geometry? To answer this question, we investigated a model with the same biochemical reactions and states of PomZ as before, but replaced the one-dimensional geometry of the nucleoid and the PomXY cluster by a three-dimensional geometry. With this
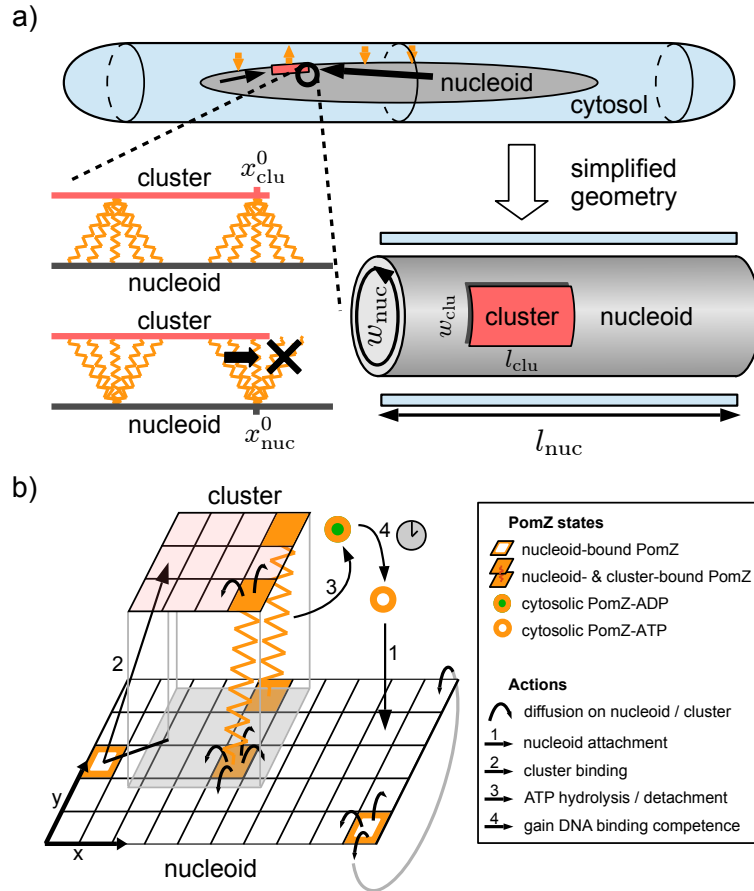
Figure 5.6 Mathematical model for PomXY cluster positioning accounting for the three-dimensional nucleoid geometry. (a) Schematic representation of the geometry used in our model. Top: Simplified sketch of the geometry of a *M. xanthus* cell. Cytosolic, ATP-bound PomZ binds to the nucleoid, and diffuses on the nucleoid. When bound to the PomXY cluster, PomZ hydrolyses ATP and in turn is released into the cytosol (the orange arrows indicate the on-/off-dynamics of PomZ). This leads to a net diffusive flux of PomZ on the nucleoid towards the cluster, which is larger from the side with the larger cluster to nucleoid end distance (black arrows) [3]. Bottom left: PomZ dimers are effectively modeled as springs connecting a nucleoid and cluster binding site. These two binding sites can diffuse on the nucleoid and cluster, respectively. For a particular cluster binding site x_{clu}^0, a symmetric distribution of the nucleoid binding site around x_{clu}^0 is possible and results in a zero net force exerted on the cluster. In contrast, for a particular nucleoid binding site position, x_{nuc}^0, the possible positions for the cluster binding site are limited if the PomZ dimer is located close to the cluster's edge (black cross). This asymmetry can result in a force exerted on the cluster (black arrow). Bottom right: The model geometry derived from the biologically realistic three-dimensional cell. The nucleoid is modeled as a cylinder and the cytosol is included effectively by modeling the cytosolic PomZ distribution along the long cell axis. (b) Schematic of the interactions of PomZ with the nucleoid and cluster considered in our model (see main text and SI text A.1 for details).

model at hand, we performed stochastic simulation using the Gillespie algorithm [112] to study the PomXY cluster dynamics (for details on the simulation see SI text A.5).

5.2.2 Flux-based mechanism for midcell localization

The PomXY cluster dynamics on the nucleoid crucially depends on the PomZ dynamics as the cluster is tethered to the nucleoid via PomZ dimers [2]. Based on the biochemical processes suggested by experiments [2] and depicted in Fig. 5.5, we model the PomZ dynamics as follows (see Fig. 5.6b and SI text A.1 for details): ATP-bound PomZ dimers can bind to the nucleoid with rate k_{on} (action 1 in Fig. 5.6b). On the nucleoid, they can diffuse with diffusion constant D_{nuc}. The PomZ dimers are modeled effectively as springs to account for the elasticity of the chromosome (as in [6]). We expect the PomZ proteins to be significantly stiffer than the chromosome, such that they relax faster, and hence the chromosome is likely to be the main contribution to the effective elasticity of a nucleoid-cluster connection mediated by PomZ. For simplicity we will refer to the PomZ dimers as springs in the following although the elasticity mainly stems from the nucleoid. A nucleoid-bound PomZ dimer can attach to the cluster with rate k_a, also in a stretched configuration (action 2 in Fig. 5.6b and SI text A.1). We assume that cluster-bound PomZ can diffuse on both the nucleoid and the PomXY cluster (as done previously, [120]). However, the movement of nucleoid- and cluster-bound PomZ is reduced due to the energy cost for stretching the spring (for details see SI text A.1). Cluster-bound PomZ dimers are released into the cytosol upon ATP hydrolysis, which is stimulated by PomX, PomY and DNA. ATP hydrolysis leads to a conformational change of the PomZ dimer and triggers the release of two ADP-bound PomZ monomers into the cytosol [2]. In our model, we combine these processes into one by using a single rate k_h for cluster-bound PomZ-ATP dimers to detach into the cytosol as monomers (action 3 in Fig. 5.6b). Before PomZ can rebind to the nucleoid, it has to gain the ability to bind non-specifically to DNA, which causes a time delay between detachment from and reattachment to the nucleoid and hence leads to spatial redistribution of the quickly diffusing cytosolic PomZ dimers in the cell (action 4 in Fig. 5.6b). The interactions of the PomZ dimers with the cluster result in mechanical forces being exerted on the cluster, which leads to movement of the cluster. But how does the described PomZ dynamics explain midcell localization of the cluster?

Previously we suggested a flux-based mechanism for midcell positioning in the one-dimensional model geometry [2, 120], which can be summarized as follows: PomZ dimers cycle between a cytosolic and a nucleoid-bound state by binding to the nucleoid and locally detaching from the nucleoid into the cytosol when interacting with the PomXY cluster. Detachment of PomZ at the cluster is triggered by ATP hydrolysis. This process consumes energy and breaks detailed balance. Hence, the system is out of thermal equilibrium and a steady mass flux of PomZ dimers can be maintained. In particular, this flux includes a diffusive flux of PomZ dimers on the nucleoid towards the cluster. For a cluster located away from midnucleoid, which we refer to as off-centre, the diffusive PomZ fluxes into the cluster from either side differ [3]. This can be explained heuristically as follows: Since, in wild-type *M. xanthus* cells, the cluster dynamics is

much slower than the PomZ dynamics [2], there is a clear time-scale separation and one may analyze the PomZ dynamics for a given stationary cluster position (adiabatic approximation). For a spatially uniform cytosolic PomZ distribution, the total amount of PomZ dimers attaching to the nucleoid left and right of the cluster scales with the lengths of these regions [3]. In the one-dimensional model geometry, the PomZ flux onto the nucleoid and the diffusive nucleoid-bound PomZ flux into the cluster are equal for the left and the right region separately because the total number of PomZ dimers bound to the nucleoid left and right of the cluster has to be constant in the steady-state [3]. Therefore, as long as the cluster is positioned off-centre and PomZ dimers only detach at the cluster, the diffusive fluxes of PomZ dimers into the cluster from either side are different.

These fluxes induce an asymmetric PomZ concentration profile along the nucleoid, which in turn leads to a concentration gradient of PomZ dimers bound to the cluster. The asymmetric PomZ distribution has important implications for the forces exerted by PomZ dimers on the PomXY cluster: Since PomZ dimers are modeled as effective springs, they can attach to the cluster in a stretched configuration and in this way exert forces on the cluster. In addition to the force generated due to the initial deflection of the spring, which relaxes over time, cluster-bound PomZ dimers can exert a force every time they encounter the cluster's edge since the movement of the cluster binding site is restricted to the cluster region (see Fig. 5.6a, bottom left): If the nucleoid-binding site of a PomZ dimer, x_{nuc}^0, is located close to the cluster's edge, the probability density for the position of the cluster-binding site is asymmetric with respect to x_{nuc}^0. Hence, the average force exerted on the cluster resulting from averaging over all possible cluster-binding sites points outwards of the cluster. Since the average forces exerted by PomZ dimers from the right and left side of the cluster point in opposite directions, the difference in the PomZ fluxes from each side determines the net force exerted on the cluster [120]. In total, this leads to a self-regulated midcell localization process as long as the PomZ dynamics is fast compared to the cluster dynamics and, if this is not the case, to oscillatory cluster movements along the nucleoid [120].

5.2.3 A three-dimensional model for midcell localization

To understand how the geometry of the nucleoid and the size of the PomXY cluster affect the cluster dynamics and thereby test if a flux-based mechanism is still feasible in a biologically realistic three-dimensional geometry, we investigated the mathematical model illustrated in Fig. 5.6. Here, the nucleoid and the PomXY cluster are approximated as a cylindrical object and a rectangular sheet, respectively. Since experiments in *M. xanthus* cells suggest that the PomXY cluster is large [2] we assume that the cluster tethered to the nucleoid via PomZ dimers moves on the nucleoid's surface and does not penetrate the bulk of the nucleoid. Moreover, we assume that PomZ dimers also bind to and diffuse on the nucleoid's surface only.

The cylindrical geometry of the nucleoid is mathematically implemented by a rectangular sheet with periodic boundary conditions for the PomZ movements along the short cell axis (*y*-direction) and reflecting boundary conditions along the long cell

axis (x-direction, Fig. 5.6b). We assume that PomZ dimers are captured at the PomXY cluster, until they leave the cluster by ATP hydrolysis induced detachment into the cytosol. The cluster is modeled as a rectangle with reflecting boundaries at its edges for the PomZ dimer movement. We refer to the extension of the cluster along the long and short cell axis as the cluster's length, l_{clu}, and width, w_{clu}, respectively (see Fig. 5.6a).

Besides the nucleoid and the cluster, the cytosol needs to be accounted for in our model as PomZ dimers cycle between a nucleoid-bound and cytosolic state. We expect the cytosolic diffusion constant of PomZ to be of the same order as that of MinD proteins in *E. coli* cells, $D_{\text{cyt}} \approx 10 \, \mu\text{m}^2\text{s}^{-1}$ [104]. For ParA ATPases involved in chromosome and plasmid segregation, a time-delay between ParA just released from the nucleoid into the cytosol and ParA that is competent for non-specific DNA binding is observed experimentally [97]. Upon ATP hydrolysis and release of two ADP-bound ParA monomers into the cytosol, ParA needs to bind ATP, dimerize and gain the competence for binding non-specifically to DNA before it can reattach to the nucleoid. The last step, a conformational change of the ATP-bound ParA dimers to gain competence for non-specific DNA binding, is the slowest process with a time scale of the order of minutes, $\tau \approx 5 \, \text{min}$ [97]. Since PomZ is ParA-like, we expect the PomZ ATPase cycle to be similar to the ParA cycle and therefore assume the corresponding reaction rates to be of the same order of magnitude. This amounts to the following estimate for the diffusive length of cytosolic PomZ, $L_{\text{diff}} = \sqrt{D_{\text{cyt}}\tau} \approx 55 \, \mu\text{m}$, which is significantly larger than the average cell length of a *M. xanthus* cell, $L_{\text{cell}} \approx 7.7 \, \mu\text{m}$ [2], suggesting that the assumption of a well-mixed PomZ density in the cytosol is justified [52, 56].

However, it is not known how the cytosolic PomZ distribution affects the cluster dynamics in our proposed flux-based mechanism. In particular, does a non-uniform distribution increase or reduce the speed of the cluster movement towards midcell? To obtain a qualitative answer to this question, we account for the cytosolic PomZ distribution in a simplified way by focusing on the variation in PomZ density along the long cell axis and approximating the density along the short cell axis as uniform (Fig. 5.6a). To obtain the cytosolic PomZ distribution along the long cell axis, we model the PomZ-ATP and PomZ-ADP densities as one-dimensional reaction-diffusion equations. In section 5.2.6 we discuss how the cluster dynamics is affected when reducing the cytosolic PomZ diffusion constant, which leads to deviations from the uniform PomZ distribution, but for now we assume a uniform distribution in the cytosol.

5.2.4 A flux-based model can explain midcell positioning in three dimensions

Our simulations of the three-dimensional model show that the PomXY cluster still localizes at midnucleoid (Fig. 5.7a,b). If the cluster's width does not cover the complete nucleoid circumference and the parameters match the ones used in the one-dimensional model where possible (see SI text A.4), the movement towards midcell takes longer
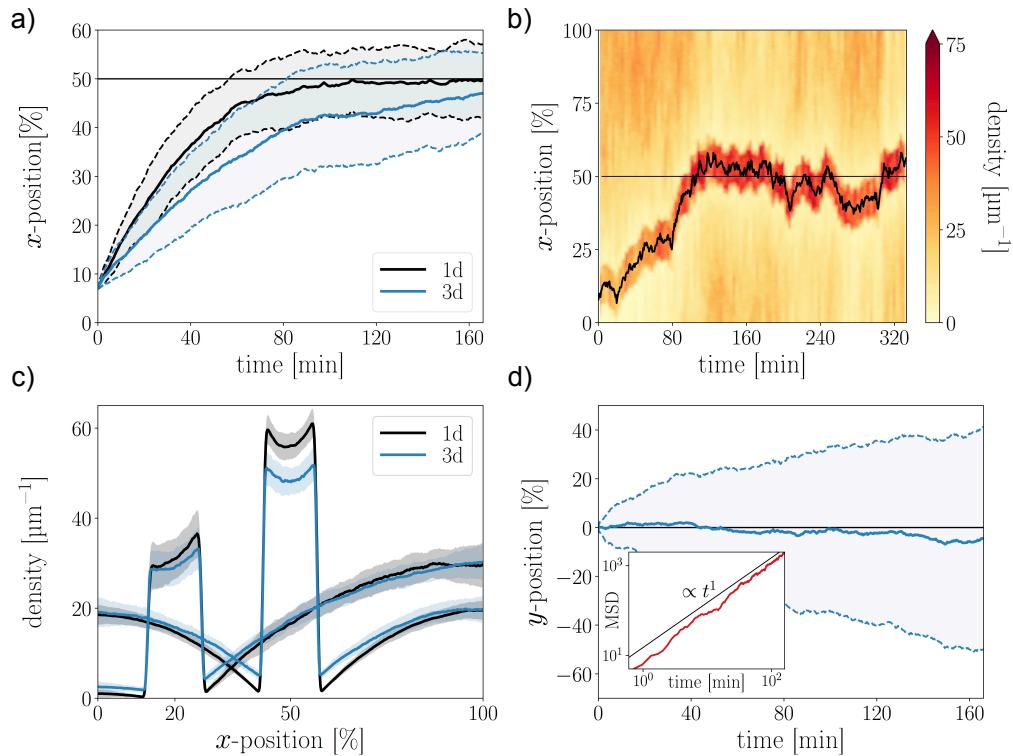
Figure 5.7 A flux-based mechanism can explain midcell localization in a three-dimensional geometry. (a) Comparison of the average PomXY cluster trajectories along the long cell axis direction obtained from the three-dimensional model and its one-dimensional counterpart studied previously [120]. We averaged over an ensemble of 100 simulations. The shaded regions depict one standard deviation around the mean density value. Initially, the clusters are positioned at the left edge of the nucleoid such that they still overlap entirely with the nucleoid (7% of nucleoid length). Midnucleoid is indicated by the horizontal black line. (b) Kymograph showing the nucleoid-bound PomZ density along the long cell axis direction (integrated over the nucleoid's circumference) over time. The trajectory of the PomXY cluster is shown as solid black line. The horizontal black line indicates midnucleoid. (c) Comparison between one- and three-dimensional average nucleoid- and cluster-bound PomZ density profile along the long cell axis for clusters at 20% and 50% of nucleoid length based on 100 simulations (the shaded region again denotes one standard deviation). (d) Average cluster trajectory in y-direction using an ensemble of 100 simulations (solid blue line). The shaded region indicates one standard deviation above and below the average trajectory. The inset shows the mean-square displacement, which increases linearly in time, indicating diffusive motion. The parameter values used in the simulations of the three-dimensional model are given in Table S5.1. For the simulations of the one-dimensional model we chose the parameters such that we account for the geometry differences between the two models (see SI text A.4). For details on the data analysis see SI text A.6.

than in the one-dimensional case (Fig. 5.7a). Since the dynamics of the cluster is determined by the PomZ dimer interactions with the cluster, we analyzed the average nucleoid-bound PomZ dimer density along the long cell axis for clusters located off-

centre and at midnucleoid (Fig. 5.7c). For both the one- and three-dimensional model we observe an asymmetric PomZ distribution along the nucleoid for an off-centre positioned cluster and a symmetric distribution for a cluster located at midnucleoid. The asymmetry implies a different diffusive flux of PomZ into the cluster from either side, which in turn results in an asymmetric distribution of cluster-bound PomZ dimers (Fig. 5.7c). An average flux difference resulting from the PomZ asymmetry on the nucleoid (the diffusive flux is proportional to the derivative of the concentration profile) only exists if the cluster is located away from midnucleoid and zero, if the cluster is located at midnucleoid. This suggests that midnucleoid localization of the PomXY cluster can be explained by the fluxes of the PomZ dimers on the nucleoid also in the three-dimensional model. In comparison to the one-dimensional case the flux difference at the cluster as well as the steepness of the density gradient of cluster-bound PomZ for clusters located off-centre is reduced (Fig. 5.7c), which explains the slower movement of the cluster towards midcell observed in our simulations (Fig. 5.7a).

In addition to the cluster dynamics along the long cell axis, we also considered the dynamics along the short cell axis. Because of the rotational symmetry the clusters do not have a preferred direction along this axis, on average. However, both diffusive and persistent, unidirectional motion is conceivable. We expect persistent movement if PomZ diffusion on the nucleoid is slow compared to the cluster dynamics, such that a depletion zone in nucleoid-bound PomZ forms in the rear of the cluster [76, 85, 98, 100, 120]. In this case, the initial direction of the cluster's movement along the nucleoid's circumference is chosen stochastically by the interactions of the PomZ dimers with the cluster. Once the cluster started to move in one direction, it is more likely to continue in this direction, because the amount of PomZ dimers interacting with the cluster from its rear is reduced due to the depletion zone. In contrast, for fast PomZ diffusion on the nucleoid, we expect an approximately symmetric PomZ distribution around the cluster, resulting in equal likelihood for the cluster to move in each direction, suggesting diffusive motion. For the parameter set we considered (Table S5.1) the clusters show diffusive behavior in y-direction as indicated by a mean-square displacement that grows linearly in time (Fig. 5.7d, inset).

5.2.5 Dependence of the dynamics of the cluster on its size

In this section we ask how the arrival time of the cluster at midnucleoid depends on the linear dimensions of the PomXY cluster. To obtain comparable results for clusters of different size, we used the same initial position of the cluster in our simulations (13% of nucleoid length), with the position of the cluster always referring to the midpoint of the cluster. The arrival time is then defined as the first passage time of the cluster to reach midnucleoid. Our numerical simulations show that the larger the cluster's length or width, the faster the cluster moves towards midcell (Fig. 5.8a). In the following we discuss how these two observations can be explained heuristically.

Since in the three-dimensional model we consider the same dynamics and interactions of PomZ dimers with the nucleoid and cluster as in the one-dimensional case, we expect that the cluster dynamics is determined by the same factors: the flux difference of
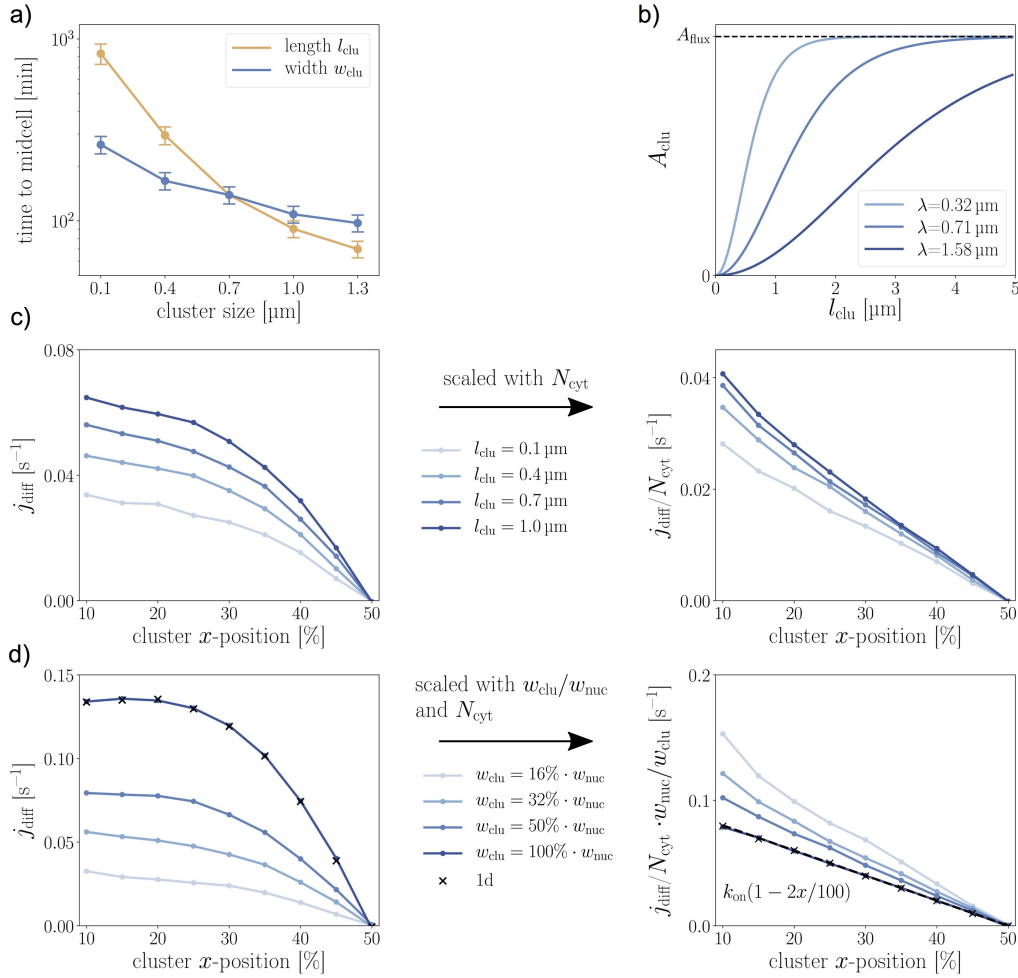
Figure 5.8 Dependence of the cluster dynamics on the size of the cluster. (a) Average first passage time of the PomXY cluster to reach midnucleoid for different cluster sizes. In all simulations the cluster starts at 13% of nucleoid length, which corresponds to the leftmost position possible such that for all cluster sizes considered a full overlap with the nucleoid is ensured. The error-bars show the standard error of the mean. (b) Asymmetry in the cluster-bound PomZ density at the left and right edge of the cluster, A_{clu} (see SI text A.7), for different values of the residence length of cluster-bound PomZ dimers λ. The intermediate λ value corresponds to the parameter values in Table S5.1. (c)-(d) The PomZ flux difference into the cluster, j_{diff}, along the long cell axis for a cluster at a fixed position, which is varied from 10% to 50% of nucleoid length, is shown. In c), the cluster's length is varied and in d) the cluster's width. For a ring-shaped cluster, $w_{\mathrm{clu}} = 100\% \cdot w_{\mathrm{nuc}}$, the simulation results agree with those from the one-dimensional model (black crosses). To understand how the cluster's length and width affects the flux difference, the values are scaled with the number of PomZ dimers in the cytosol, N_{cyt} (for each cluster position separately), and, in d) also with the fraction of the cluster's width to the nucleoid's width (figures on the right hand side). The second smallest value, 32% of nucleoid length, corresponds to the width of the cluster given in Table S5.1 (0.7 μm), and 100% corresponds to the full cluster's width of 2.2 μm. In d) an analytical estimate for the flux difference is plotted (dashed line), which agrees with the simulation results for a ring-shaped cluster (see SI text A.2 for details). If not given explicitly, we used the parameter values as in Table S5.1.

PomZ dimers into the cluster, which is non-zero for clusters positioned off-centre (Fig. 5.7c), the forces exerted on the cluster via PomZ dimers and the friction of the cluster tethered to the nucleoid via the PomZ dimers [120]. The latter is only important if the number of cluster-bound PomZ dimers varies significantly. The PomZ flux difference can be regarded as the frequency a net force is exerted on the cluster. Thus, together with the magnitude of the net force exerted by a single PomZ dimer, it determines the bias in the movement of the cluster. However, there are differences due to the three-dimensional model geometry: For a rectangular-shaped cluster, PomZ dimers can attach to the cluster not only from the long, but also from the short cell axis direction. Furthermore, as long as the cluster does not cover the whole nucleoid's circumference, there is a chance for PomZ dimers to diffuse past the cluster without interacting with it. This happens with a higher probability, the smaller the cluster is in one of its linear dimensions and leads to a mass exchange of PomZ dimers on the nucleoid between the regions left and right of the cluster. This partially equalizes the asymmetry in the PomZ density along the nucleoid and therefore also reduces the flux difference into the cluster along the long cell axis. Finally, increasing the length or width of the cluster while keeping the other variable constant, results in an increased number of cluster-bound PomZ dimers, as the cluster becomes more accessible for nucleoid-bound PomZ dimers. The increase in PomZ dimers bound to the cluster leads to a larger turnover of PomZ dimers cycling between the nucleoid-bound and cytosolic state, which increases the diffusive flux of PomZ dimers on the nucleoid and hence results in a larger net force exerted on the cluster.

In addition to the PomZ fluxes into the cluster, the forces exerted by PomZ dimers also depend on the shape of the cluster. PomZ dimers mainly exert a force at the edges of the cluster as discussed in section 5.2.2 and shown in Fig. 5.9. We approximate the diffusion constant of a cluster-bound PomZ dimer by $D_{\mathrm{nuc}}/2$ with D_{nuc} the diffusion constant of PomZ dimers bound to the nucleoid only. The reduction in the diffusion constant is due to the reduced mobility of PomZ dimers bound to both the cluster and the nucleoid. To understand the magnitude and direction of forces generated by PomZ dimers at the cluster the *residence length* $\lambda = \sqrt{D_{\mathrm{nuc}}/(2k_h)}$, measuring the typical length a cluster-bound PomZ dimer diffuses before detaching, needs to be compared to the length and width of the cluster. For a small residence length, a PomZ dimer that binds to the cluster in close proximity to one of the cluster's edges, stays close to this edge until it detaches and hence, on average, exerts a force that is perpendicular to this edge and points outwards of the cluster region (see Fig. 5.9). In contrast, when the residence length is large, the asymmetry in the cluster-bound PomZ distribution, which results from different fluxes of PomZ dimers into the cluster, flattens. This effect can be quantified by comparing the asymmetry in the diffusive fluxes into the cluster from either side along the long or short cell axis, A_{flux}, with the asymmetry in the cluster-bound PomZ density at the corresponding edges of the cluster, A_{clu}. We find that the longer the size of the cluster and the smaller the residence length, the closer the asymmetry in the fluxes is reflected in the asymmetry of the PomZ gradient (Fig. 5.8b, for a detailed derivation see SI text A.7).
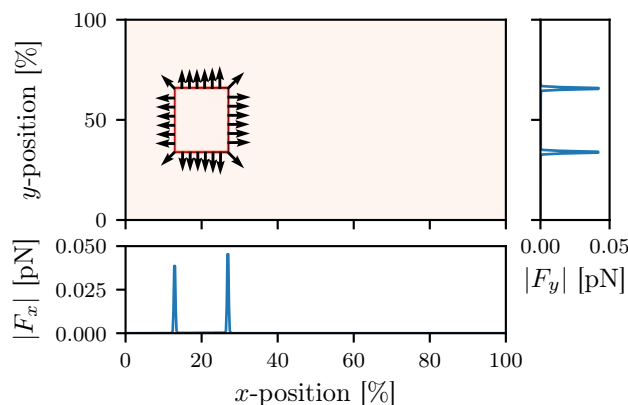
Figure 5.9 PomZ dimers exert a force on the cluster when they encounter the cluster's edge. For a fixed cluster position (here at 20% nucleoid length), the average forces the PomZ dimers exert on the cluster are recorded per nucleoid site. The color code shows the magnitude of the average force vector, which is highest at the cluster's edges (darker red indicates higher values). At the cluster's edges, the average force vectors are plotted, $\vec{F} = (F_x, F_y)$. The average x-component of the force, F_x, (summed over all y-positions) is shown in the lower panel. We find that the forces that point towards midcell are larger than the forces pointing in the opposite direction, resulting in a net force towards midcell. For the average y-component of the force, F_y (summed over all x-positions) the situation is different: The average forces acting on the cluster along the short cell axis balance each other and hence do not result in a net force (panel on the right). The parameters in Table S5.1 were used.

With these observations, we rationalize the dependence of the arrival time on the length of the cluster as follows. An increase in cluster length while keeping the width constant increases the amount of PomZ dimers interacting with the cluster and with it the cycling frequency of PomZ between the nucleoid and the cytosol. This enhances the flux difference in PomZ dimers arriving at the cluster along the long cell axis direction. Indeed, our simulation results for a cluster that is kept at a fixed position show that the longer the cluster, the larger the difference in the total PomZ dimer fluxes from either side along the direction of the long cell axis (Fig. 5.8c). To test if the increased flux of PomZ dimers in the system is the main determinant for the observed increase in the flux difference, we scaled the fluxes by the number of PomZ dimers in the cytosol, N_{cyt}, which is proportional to the on-flux of PomZ dimer to the nucleoid. Hence, if the flux difference depends only on N_{cyt} and it is proportional to N_{cyt}, the curves would fall on one master curve after rescaling. Indeed we find that for longer clusters the flux difference curves collapse to one master curve (Fig. 5.8c, right), confirming our hypothesis. However, for small cluster lengths the rescaled flux differences are smaller than for longer clusters. This is probably because for short clusters more PomZ dimers can diffuse past the cluster, which reduces the flux difference into the cluster along the long cell axis.

The PomZ flux difference results in a force exerted on the cluster that also depends on the cluster size: For a longer cluster, the asymmetry in the PomZ dimer fluxes lead to a steeper cluster-bound PomZ gradient and hence a larger net force pointing towards midnucleoid (see Fig. 5.8b). In total, a longer cluster increases both the diffusive flux of PomZ dimers into the cluster and the force exerted by a single PomZ dimer at the cluster. Hence, the frequency and the magnitude of the forces exerted on the cluster increase, implying a larger net force, which explains the shorter arrival times of the Pom cluster at midnucleoid (Fig. 5.8a).

Next, we discuss the dependence of the arrival time on the cluster width. Similar to an increase in length, the overall turnover of PomZ dimers increased with cluster width. In addition to this, the width of the cluster determines how many PomZ dimers attach to the cluster from the long cell axis direction and also how many pass the cluster without interacting with it. The broader the cluster is, the smaller the flux of PomZ dimers that pass the cluster. Our simulation results (for clusters at fixed positions) show an increased PomZ flux difference when the cluster width is increased from 16% to 100% of the nucleoid's circumference (Fig. 5.8d). When the cluster covers the entire circumference of the nucleoid, we call it a ring. To test if the increase in the flux difference is due to the increased cycling frequency of PomZ and the larger width of the cluster, we scale the fluxes by N_{cyt} and the fraction the cluster covers the nucleoid circumference, $w_{\text{clu}}/w_{\text{nuc}}$. However, we find that upon rescaling the curves do not collapse to one master curve (Fig. 5.8d, right). Instead, the scaled flux profiles are larger for smaller widths. The reason is that, as long as the cluster is not a ring, there is a net flux of PomZ dimers along the short cell axis towards the cluster or its extension along the long cell axis, which also contributes to the flux difference of PomZ dimers into the cluster along the long cell axis direction.

Regarding the forces exerted by PomZ dimers, a change in the width of the cluster does affect the forces exerted on the cluster in the short, but not significantly in the long cell axis direction, which is the observable of interest to understand the observed arrival times for the PomXY clusters. To summarize, the decrease in arrival time for wider clusters can be explained by an increased PomZ flux difference into the cluster along the long cell axis.

5.2.6 Fast cytosolic diffusion is important for flux asymmetry

So far, we assumed that the cytosolic PomZ distribution is spatially uniform. This assumption is justified by the time delay between detachment of PomZ from the nucleoid and reattachment to the nucleoid as well as fast diffusion of PomZ in the cytosol [52, 56]. Now we investigate how the PomXY cluster dynamics change when spatial heterogeneity in the cytosolic PomZ distribution is accounted for in our model. To this end, we explicitly incorporate the cytosol by approximating the cytosolic volume as a one-dimensional layer of the same length as the nucleoid (see Fig. 5.6a) and formulate reaction-diffusion equations for the density of cytosolic PomZ-ADP (c_D) and PomZ-ATP (c_T) along the long cell axis. For simplicity (and to allow for a closed analytical solution), we consider only an active (ATP-bound) and inactive

(ADP-bound) conformation of PomZ, and disregard an explicit monomeric and dimeric state of PomZ in the cytosol. Furthermore, we reduce the ATPase cycle to three processes: attachment of PomZ-ATP to the nucleoid, detachment of PomZ-ADP at the cluster, and nucleotide exchange.

The dynamics of PomZ-ATP and PomZ-ADP in the cytosol are modeled as follows: At the position of the cluster, $x_c(t)$, PomZ-ADP is released into the cytosol. Due to the time scale separation of the PomZ and cluster dynamics (adiabatic approximation), we can assume that the cluster is stationary, $x_c(t) = x_c$, when investigating the PomZ dynamics. The local increase in cytosolic PomZ-ADP at the cluster position due to detachment facilitated by ATP hydrolysis is approximated as a point source: $s_0\delta(x-x_c)$. The constant s_0 depends on the hydrolysis rate k_h and the amount of PomZ dimers bound to the cluster. However, the normalized steady-state PomZ-ATP distribution will not depend on this constant (for details see SI text A.3). In the cytosol, PomZ-ADP exchanges ADP for ATP nucleotides with an effective rate k_{ne}. We assume that cytosolic PomZ diffuses in both nucleotide states with the same diffusion constant, D_{cyt}. However, only the ATP-bound form of PomZ can attach to the nucleoid with an effective rate k_{on}. In total, we obtain the following reaction-diffusion equations for the cytosolic PomZ-ADP and PomZ-ATP concentrations:

$$\partial_t c_D = D_{cyt}\partial_x^2 c_D - k_{ne}c_D + s_0\delta(x - x_c)\Theta(t) \ , \tag{5.12a}$$

$$\partial_t c_T = D_{cyt}\partial_x^2 c_T - k_{on}c_T + k_{ne}c_D \ . \tag{5.12b}$$

Solving these equations in the stationary state results in a PomZ-ATP density that is maximal at the cluster position for finite D_{cyt} values (Fig. 5.10a, for the analytical solutions see SI text A.3).

We find that the smaller the cytosolic diffusion constant, the larger the deviations from a uniform distribution (Fig. 5.10a). In the limit of infinitely large cytosolic PomZ diffusion constants, the cytosolic PomZ distribution becomes spatially uniform, as expected.

To investigate the effect of the cytosolic PomZ distribution on the cluster's trajectory qualitatively, we replaced the spatially uniform cytosolic PomZ-ATP distribution by the stationary solution of Eq. 5.12b, $c_T(x)$, in our three-dimensional model. The distribution $c_T(x)$ changes with the cluster position, x_c. As described before, we assume a uniform distribution of cytosolic PomZ-ATP along the circumference of the nucleoid. The attachment rate of PomZ dimers to the nucleoid at site (x, y) is then proportional to $c_T(x)$ times the number of PomZ dimers in the cytosol. With this spatially heterogeneous attachment rate to the nucleoid, our simulations show that for a larger deviation of the cytosolic PomZ distribution from a spatially uniform one (decreasing D_{cyt}), the movement of the clusters is less biased towards midnucleoid (Fig. 5.10b). Hence, we conclude that the cytosolic PomZ distribution has an impact on the cluster trajectories and the velocity of the cluster towards midnucleoid is maximal for a uniform cytosolic PomZ-ATP distribution compared to the distributions resulting from the reduced model for the PomZ ATPase cycle discussed here.
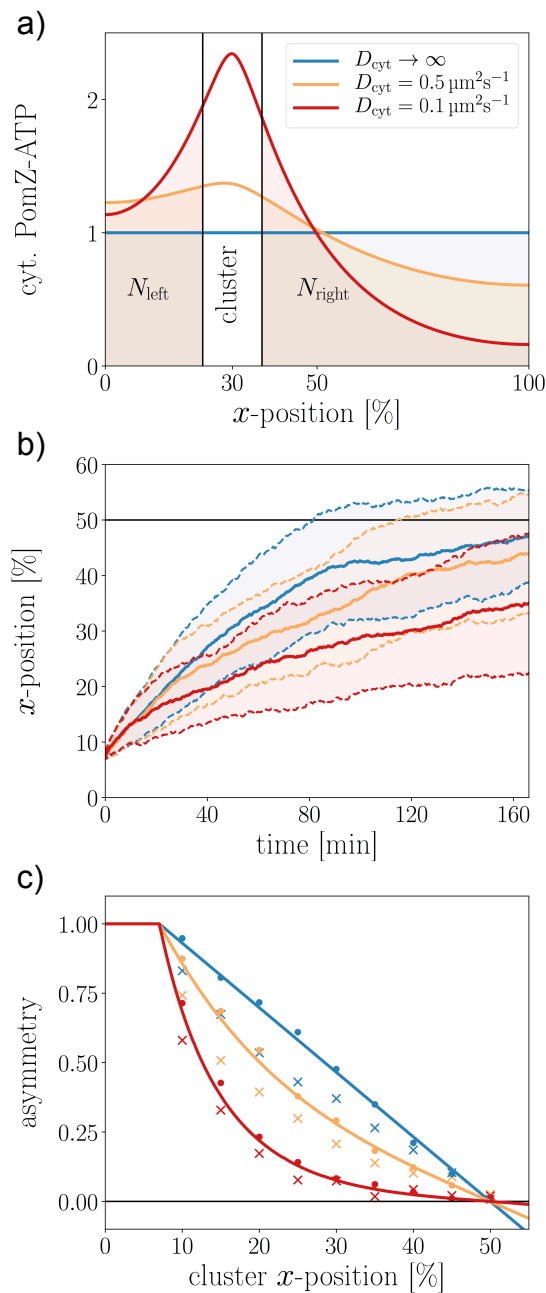
a)

b)

c)

Figure 5.10 Fast cytosolic diffusion accelerates midcell localization. (a) Cytosolic PomZ-ATP distribution along the long axis (x-axis) for different cytosolic PomZ diffusion constants D_{cyt}. Integrating the distributions along the long cell axis left and right of the cluster yields the total number of PomZ-ATP proteins left and right of the cluster, N_{left} and N_{right}. (b) Average cluster trajectories along the x-direction for the different cytosolic PomZ diffusion constants in a). The shading denotes the regions of one standard deviation around the average trajectories. Midnucleoid is indicated by the solid black line. In the simulations, the clusters are positioned initially such that the left edge of the cluster coincides with the left edge of the nucleoid. (c) Asymmetry measure of the number of cytosolic PomZ-ATP left and right of the cluster, $A_{\mathrm{cyt}} = (N_{\mathrm{right}} - N_{\mathrm{left}})/(N_{\mathrm{right}} + N_{\mathrm{left}})$, (solid lines) compared to the PomZ flux asymmetry into the cluster, A_{flux} (Eq. 5.16), for different cytosolic PomZ diffusion constants. The dots indicate the flux asymmetry into a cluster that forms a ring. Crosses indicate the asymmetry for a cluster with a width of 32% of the nucleoid's circumference (same value as in Table S5.1). We averaged over 100 runs of the simulation. The parameter values given in Table S5.1 are used.

How does the cytosolic PomZ distribution affect the cluster's movement? As argued before (section 5.2.2), the flux of PomZ dimers onto the nucleoid regions to the left and right of the cluster and the diffusive flux of PomZ dimers into the cluster from the left and right side are equal, respectively, in the one-dimensional model geometry and for a stationary cluster (adiabatic approximation) (see SI text A.2). Since the total on-flux of PomZ dimers to the nucleoid left and right of the cluster depends on the cytosolic PomZ-ATP distribution, we expect the diffusive PomZ fluxes into the cluster to depend on this distribution as well. To investigate this further, we define the

following asymmetry measure

$$A_{\text{cyt}} = \frac{N_{\text{right}} - N_{\text{left}}}{N_{\text{right}} + N_{\text{left}}}, \tag{5.13}$$

which compares the total number of cytosolic PomZ-ATP left and right of the cluster (see Fig. 5.10a):

$$N_{\text{left}} = \int_0^{x_c - l_{\text{clu}}/2} c_T(x)\mathrm{d}x \ , \tag{5.14}$$

$$N_{\text{right}} = \int_{x_c + l_{\text{clu}}/2}^{l_{\text{nuc}}} c_T(x)\mathrm{d}x \ , \tag{5.15}$$

using the stationary PomZ-ATP distribution $c_T(x)$ for a given cluster location x_c. Furthermore, the corresponding asymmetry in the PomZ fluxes into the cluster from the left, j_{left}, and right side, j_{right}, is given by

$$A_{\text{flux}} = \frac{j_{\text{right}} - j_{\text{left}}}{j_{\text{right}} + j_{\text{left}}} \ . \tag{5.16}$$

We measured this flux asymmetry in our simulations for two scenarios: First, for a PomXY cluster that forms a ring around the nucleoid and second, for a cluster that does not cover the whole nucleoid's circumference. We find that the asymmetry in the flux, A_{flux}, obtained from simulations for a cluster that forms a ring, and the corresponding asymmetry in the cytosolic PomZ-ATP density, A_{cyt}, agree nicely (Fig. 5.10c). Hence, an asymmetry in the cytosolic distribution of PomZ-ATP is directly reflected in the diffusive PomZ fluxes of PomZ into the cluster, which affects the net force exerted on the cluster. For an infinitely large cytosolic PomZ diffusion constant, both asymmetry measures decay linearly when the cluster position is varied from far off-centre towards midnucleoid. Decreasing the cytosolic PomZ diffusion constant results in asymmetry curves that decay faster than linearly towards zero (Fig. 5.10c). For a PomXY cluster that does not cover the whole nucleoid's circumference the asymmetry in the PomZ fluxes into the cluster is smaller than the asymmetry in the cytosolic PomZ-ATP concentration (Fig. 5.10c). This can be attributed to a reduction in the diffusive fluxes of PomZ dimers into the cluster along the long cell axis direction, since PomZ dimers can diffuse past the cluster or attach to the cluster from the short cell axis direction. Hence the flux onto the nucleoid left and right of the cluster is no longer equivalent to the flux into the cluster from the left and right, respectively, as for a one-dimensional model or a cluster that forms a ring. The reduced asymmetry in the diffusive PomZ fluxes explains the less biased movement of the PomXY cluster towards midnucleoid and the slightly increased variance in the cluster trajectories observed for smaller cytosolic PomZ diffusion constants (Fig. 5.10b).

5.2.7 Two clusters localize at one- and three-quarter positions

Intracellular positioning systems often involve not only one, but several cargoes, such as plasmids, which are equidistantly positioned along the nucleoid [3, 10, 13–15]. Motivated by this observation, we studied the dynamics of two PomXY clusters in our three-dimensional model geometry. The positions of the two clusters are denoted by (x_1, y_1) and (x_2, y_2) with the x-direction along the long and the y-direction along the short axis of the nucleoid. We performed numerical simulations of the trajectories of two clusters using the same model parameters as before (Table S5.1). Our simulations show localization of the clusters at the one- and three-quarter positions, i.e. equidistant cluster positioning (Fig. 5.11a).

In ParABS systems both oscillatory plasmid movements around [10] and localization at their equally distant positions [3] along the long cell axis are observed. Interestingly, we also find both localization patterns in our simulations of two clusters moving on a three-dimensional nucleoid depending on the parameter choice. For the parameters as in Table S5.1, the two clusters localize at the one- and three-quarter positions along the nucleoid length (Fig. 5.11a,b). The clusters fluctuate around these positions without a dominant frequency as indicated by the absence of a peak in the Fourier spectrum (Fig. 5.11b). However, when we reduce the diffusion constant of PomZ dimers on the nucleoid, D_{nuc}, and, in addition, increase the total number of PomZ dimers in the system, N, the two clusters show oscillatory movements around the equidistant positions (Fig. 5.11c).

Flux-based positioning of two clusters can be heuristically explained as follows (see [3, 16, 100]): At the protein clusters nucleoid-bound PomZ dimers detach into the cytosol. Hence, if two protein clusters approach each other, the PomZ density and fluxes on the nucleoid between the clusters are reduced. Since the clusters move into the direction of the highest PomZ flux, two clusters effectively repel each other. Due to this repelling interaction, the clusters are separated from each other. The average positions of the two clusters and the average PomZ density on the nucleoid has to be symmetric with respect to the midnucleoid plane. Hence there is no net flux of nucleoid-bound PomZ at midnucleoid, on average. Therefore, in the stationary state, we can map the system to one that consists of two subsystems with half the size of the original system and each subsystem contains one PomXY cluster. The positioning mechanism previously discussed for one cluster explains midcell localization in each of the subsystems, which corresponds to the one- and three-quarter positions on the nucleoid.

5.2.8 Discussion

In this work, we investigated a mathematical model for midcell localization in *M. xanthus* using a biologically realistic three-dimensional geometry for the nucleoid, which allows nucleoid-bound PomZ dimers to diffuse past the PomXY cluster. Our numerical simulations show that the PomXY cluster localizes at midnucleoid by a mechanism that is based on the nucleoid-bound PomZ fluxes [3] and the elasticity of the nucleoid

Figure 5.11 Two clusters are localized at the one- and three-quarter positions. (a) Average cluster movement along the x-direction (using 100 runs). The shaded region indicates the standard deviation of the ensemble. Initially, the two clusters are positioned side by side along the long cell axis such that the left edge of one and the right edge of the other cluster are positioned at midnucleoid. (b)-(c) Averaged Fourier spectrum of the cluster trajectories with one example trajectory shown in the inset. For the parameters as in Table S5.1, the Fourier spectrum does not show a peak in b), indicating that the clusters do not oscillate around their equal flux positions with a prevalent frequency. In contrast, if the diffusion constant of PomZ dimers on the nucleoid and cluster is reduced ($D_{\mathrm{nuc}} = D_{\mathrm{clu}} = 0.0002\,\mu\mathrm{m}^2\mathrm{s}^{-1}$) and the total number of PomZ dimers increased ($N = 500$), the Fourier spectrum has a peak at a frequency of about $0.004\,\mathrm{min}^{-1}$, c). When calculating the Fourier spectrum we ignore trajectories with two clusters that cross each other. If not explicitly stated otherwise, we used the parameter set given in Table S5.1.
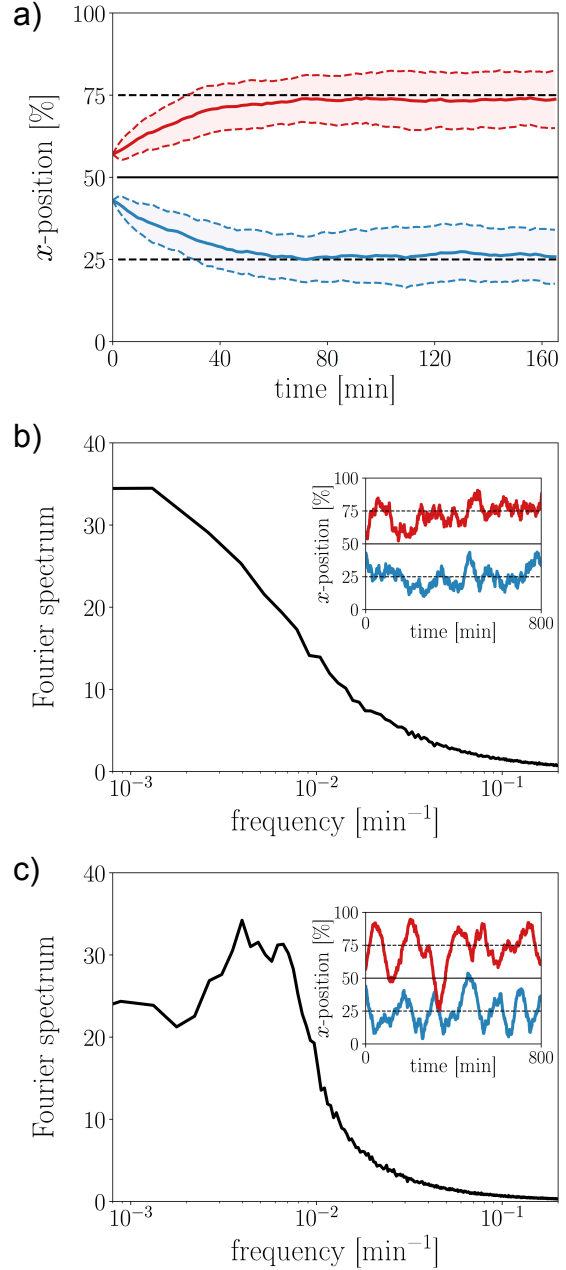
[5, 6], such that cluster-bound PomZ dimers can exert forces on the cluster. This result is consistent with our previous findings for a one-dimensional model geometry [2, 120].

However, the work presented here offers additional insights into flux-based positioning: most importantly, we find that a flux-based mechanism also leads to midnucleoid positioning if PomZ dimers can diffuse past the cluster. The cargo — here the PomXY cluster — acts as a sink. If the cargo is located off-centre the steady state PomZ density on the nucleoid reflects this asymmetry implying that more PomZ dimers arrive at the cluster from the side with the larger distance between the cluster and the nucleoid end.

A flux of PomZ dimers past the cluster diminishes the asymmetry in the PomZ density on the nucleoid, but does not entirely equilibrate the PomZ density left and right of the cluster along the long cell axis. Hence, we conclude that a flux-based mechanism can explain midnucleoid positioning even in the full three-dimensional geometry of a cell.

To investigate the effect of the flux of PomZ dimers past the cluster, we studied the dynamics of the cluster in dependence of its width and length. We find that increasing the width of the cluster, which reduces the PomZ flux past the cluster, accelerates the movement of the cluster to midnucleoid, but a ring-shaped cluster is not a necessary requirement for midnucleoid positioning. Qualitatively we observe the same behavior for an increased length of the cluster: the required time for the cluster to reach midcell is reduced. This can be attributed to both an increase in the flux difference of PomZ dimers into the cluster from each side along the long cell axis and a larger net force exerted by a single PomZ dimer.

Ietswaart et al. [3] previously suggested a flux-based mechanism for the segregation of the low copy number plasmid pB171 in *E. coli*. They provided experimental evidence that ParA forms structures within the nucleoid region and stated that ParA-ATP should form a "1d-like structure" [3] along the nucleoid to achieve equal plasmid partitioning. Their reasoning is as follows: if ParA does not form such structures, ParA can diffuse past a plasmid without interacting with it and hence the ParA concentrations on both sides would equalize even if the plasmids are not at equally spaced positions. In this work we showed that if the ParA-like PomZ dimers can diffuse past the PomXY cluster, they still form an asymmetric density profile along the nucleoid, if the cluster is located off-centre, which leads to a bias in the cluster movement towards midnucleoid. We conclude that a flux-based mechanism can explain equal positioning of one or several cargoes even if the ATPase can diffuse past the cargo.

Additionally, our simulation data demonstrates that fast cytosolic diffusion of PomZ proteins optimizes the time until positioning is achieved. The asymmetry in the cytosolic PomZ density left and right of the cluster along the long cell axis is reflected in the diffusive flux difference of PomZ dimers into the cluster and thus crucially influences the cluster dynamics. This is plausible, as the PomZ dimers released into the cytosol locally at the cluster need to "measure" the position of the cluster to guide it towards midnucleoid. For fast diffusion of cytosolic PomZ or slow rates for PomZ dimers to gain the non-specific DNA binding competence, the cytosolic PomZ distribution becomes spatially uniform. In this case, the flux of PomZ dimers onto the nucleoid scales with the length of the nucleoid regions left and right of the cluster, which leads to the largest PomZ flux differences for off-centre clusters compared to realistic, but spatially non-uniform cytosolic PomZ distributions. This prediction might be tested experimentally by significantly decreasing the diffusion constant of PomZ in the cytosol or reducing the time between detachment of PomZ at the cluster and reattachment to the nucleoid. Interestingly, spatial redistribution of proteins in the cytosol is also found to be important for Min protein pattern formation [52, 54] and for ParA-mediated cargo movement [97].

Finally, we also investigated the dynamics of two clusters in the realistic three-dimensional cell geometry and find equidistant positioning along the nucleoid. Since

the nucleoid-bound PomZ dimers are shared between the two clusters, the PomZ fluxes in the region between the clusters are reduced when the two clusters approach each other. This leads to an effective repulsive interaction between the two clusters and in total to the observed positioning at equally distant locations. We conclude that a flux-based mechanism can not only explain midnucleoid localization of one cargo, but also equidistant positioning of two cargoes along the nucleoid in the full three-dimensional geometry.

Interestingly, in our simulations the two clusters either localize at or oscillate around the one- and three-quarter positions. Both localization patterns are observed experimentally in ParAB*S* plasmid partitioning systems, although there is evidence that the oscillatory case occurs less frequently [3]. In our simulations, localization of two clusters at the one- and three-quarter positions changes to oscillatory movements around these positions when we decrease the diffusion constant of PomZ on the nucleoid and increase the PomZ dimer numbers in the cell. This observation is in accordance with previous findings for one cluster in a one-dimensional model geometry [120]. Although our simulations predict that two Pom clusters are spaced at equally distant positions along the nucleoid reminiscent of equal plasmid spacing, we expect a high density of PomZ at the cluster in contrast to a low ParA density typically observed at the plasmids [10, 76] as observed *in vivo* for one cluster [2]. It would be highly interesting to test the model prediction of equidistant positioning for multiple PomXY clusters experimentally in *M. xanthus* cells. Here, the cell would need to be modified in such a way that two PomXY clusters exist in one cell on the same nucleoid. This is very challenging because the PomX proteins tend to cluster together in the cell resulting in one spot only. Finding a method to induce the formation of several Pom clusters *in vivo* will help us to test our model predictions for multiple cargoes.

Le Gall et al. [12] showed that partition complexes as well as plasmids move within the nucleoid volume. In contrast, based on the large size of the PomXY cluster, we assumed that the movement of a PomXY cluster tethered to the nucleoid via PomZ dimers is restricted to the surface of the nucleoid. To verify our assumption, the position of the PomXY cluster relative to the nucleoid needs to be measured *in vivo* using e.g. super-resolution experiments. In addition, since PomZ dimers are a lot smaller than the Pom cluster, they might be able to diffuse into the nucleoid volume although the cluster does not. It would be interesting to investigate this aspect further.

Moreover, in *M. xanthus* there is no evidence for PomZ filament formation *in vivo* [1]. However, due to inhomogeneities in the chromosome density, the PomZ dimers might also form structures on or within the nucleoid as observed for ParA [3, 12]. Experimental insights into the localization of the Pom cluster and the PomZ dimers relative to the nucleoid will increase our understanding of the molecular mechanism and its regulation. Possible extensions of our model could be to include the PomZ dynamics within the nucleoid volume and to account for the dynamics of the chromosome in more detail.

So far our model for the PomXY cluster dynamics in *M. xanthus* cells allows a qualitative, but not a quantitative comparison with experiments. To arrive at a

quantitative model, the rates for all relevant biological processes need to be measured experimentally, which is an important task for future research.

In summary, we showed that a flux-based mechanism can explain midcell localization of one, and equidistant positioning of two Pom clusters in a model geometry that allows the ATPase PomZ to diffuse past the clusters on the nucleoid. This observation is also important for other positioning systems, such as the Par system to equidistantly space low copy number plasmids along the nucleoid, as nucleoid-bound ParA proteins likely also diffuse past the plasmids. Understanding the differences and similarities between these positioning systems will help us to understand the generic mechanisms underlying the localization patterns of cargoes inside the cell.

A Supporting information

A.1 Details on the mathematical model

Hopping of PomZ dimers on the nucleoid and the PomXY cluster

Nucleoid-bound PomZ dimers can diffuse on the nucleoid and on the PomXY cluster, when attached to the cluster, with the diffusion constants, D_{nuc} and D_{clu}, respectively. In the lattice gas model, these two diffusive processes are implemented as stochastic hopping events that occur with rate $k^0_{\mathrm{hop,\,nuc}} = D_{\mathrm{nuc}}/a^2$ and $k^0_{\mathrm{hop,\,clu}} = D_{\mathrm{clu}}/a^2$, respectively. By a we denote the lattice spacing, which we chose to have the same value in x- and y-direction. More concretely, a nucleoid-bound PomZ dimer at site (i, j), with i denoting the lattice site in x-direction and j in y-direction, can move to site $(i \pm 1, j)$ or $(i, j \pm 1)$ with hopping rate $k^0_{\mathrm{hop,\,nuc}}$. As we are using periodic boundary conditions in y-direction, a particle may also hop from site $(i, N_{\mathrm{nuc},y})$ to the site $(i, 1)$ and vice versa; here $N_{\mathrm{nuc},y} = w_{\mathrm{nuc}}/a$ denotes the number of sites along the y-axis. In x-direction we assume reflecting boundary conditions for the PomZ dimer movements.

If a PomZ dimer is bound to both the cluster and the nucleoid, a hopping event may lead to a gain or loss in elastic energy; note that PomZ dimers are modeled as springs to account for the elasticity of the nucleoid. In this case we introduce additional Boltzmann factors such that detailed balance holds, similar to Lansky et al. [105]:

$$k_{\mathrm{hop,clu}} = k^0_{\mathrm{hop,clu}} \cdot \exp\left[-\frac{1}{4}\,\beta k \left[(\vec{x}_{\mathrm{clu,\,new}} - \vec{x}_{\mathrm{nuc}})^2 - (\vec{x}_{\mathrm{clu,\,old}} - \vec{x}_{\mathrm{nuc}})^2 \right] \right], \qquad \text{(S5.1)}$$

$$k_{\mathrm{hop,nuc}} = k^0_{\mathrm{hop,nuc}} \cdot \exp\left[-\frac{1}{4}\,\beta k \left[(\vec{x}_{\mathrm{clu}} - \vec{x}_{\mathrm{nuc,\,new}})^2 - (\vec{x}_{\mathrm{clu}} - \vec{x}_{\mathrm{nuc,\,old}})^2 \right] \right]. \qquad \text{(S5.2)}$$

Here, k denotes the effective spring stiffness of the PomZ dimers and β is the inverse of the thermal energy, $\beta = 1/k_B T$, at temperature T. The positions of the cluster and nucleoid binding site of the PomZ dimer are denoted as $\vec{x}_{\mathrm{clu}}$ and $\vec{x}_{\mathrm{nuc}}$, respectively. The

labels "old" and "new" refer to the positions of the binding site before and after the hopping event.

We expect that the position of a cluster, which is tethered to the nucleoid, does not change remarkably in the direction perpendicular to the nucleoid's surface because the cluster is unlikely to penetrate into the nucleoid's volume due to its large size and, on the other hand, cannot move far away from the nucleoid due to the tethering. Hence we neglect the forces that a PomZ dimer exerts on the cluster in the direction perpendicular to the nucleoid's surface by approximating the positions of the cluster and nucleoid binding site by their projections on the rectangular sheet representing the nucleoid: $\vec{x}_{\mathrm{clu}} = (x_{\mathrm{clu}}, y_{\mathrm{clu}})$ and $\vec{x}_{\mathrm{nuc}} = (x_{\mathrm{nuc}}, y_{\mathrm{nuc}})$.

Attachment of PomZ to and detachment from the PomXY cluster

A nucleoid-bound PomZ dimer can bind, with a second binding site, to a lattice site on the PomXY cluster. For the rate with which a PomZ dimer bound to the nucleoid at site $\vec{x}_{\mathrm{nuc}}$ attaches to the cluster at site $\vec{x}_{\mathrm{clu}}$ we choose:

$$k_a(\vec{x}_{\mathrm{clu}}) = k_a^0 \cdot \exp\left[-\frac{1}{2}\beta k(\vec{x}_{\mathrm{clu}} - \vec{x}_{\mathrm{nuc}})^2\right] . \tag{S5.3}$$

The constant rate k_a^0 is multiplied with a Boltzmann factor corresponding to the distribution of the elongation of a spring in a thermal heat bath with temperature T.

The rate for a PomZ dimer located at $\vec{x}_{\mathrm{nuc}}$ to attach, with its second binding site, to any site of the nucleoid ("total attachment rate") is then given by the integration of $k_a(\vec{x}_{\mathrm{clu}})$ over all possible cluster binding sites:

$$k_a^{\mathrm{tot}} = \int_{\mathcal{A}_{\mathrm{clu}}} k_a^0 \cdot \exp\left[-\frac{1}{2}\beta k(\vec{x}_{\mathrm{clu}} - \vec{x}_{\mathrm{nuc}})^2\right] d\vec{x}_{\mathrm{clu}} \approx \begin{cases} k_a^0 \cdot \frac{2\pi}{\beta k}, & \text{if } \vec{x}_{\mathrm{nuc}} \in \mathcal{A}_{\mathrm{clu}} , \\ 0, & \text{otherwise} . \end{cases} \tag{S5.4}$$

Here, $\mathcal{A}_{\mathrm{clu}}$ denotes the area on the nucleoid that is covered by the cluster. Since the Boltzmann factor decays quickly ($1/\sqrt{\beta k} = 0.01\,\mu\mathrm{m}$, for the spring stiffness used, see Table S5.1), we can neglect the boundaries of the region $\mathcal{A}_{\mathrm{clu}}$ for $\vec{x}_{\mathrm{nuc}} \in \mathcal{A}_{\mathrm{clu}}$ and approximate the attachment rate of a PomZ dimer bound to the nucleoid outside of the cluster region by zero.

The fact that the Boltzmann factor decays quickly towards zero when increasing the distance between the cluster and the nucleoid binding site, is also used in the model implementation to save computation time. We introduce a cut-off distance above which we set the attachment rate to zero. The cut-off is defined as the smallest distance $\Delta x = |\vec{x}_{\mathrm{clu}} - \vec{x}_{\mathrm{nuc}}|$ in multiples of the lattice spacing a for which the attachment rate per lattice site, $k_a \cdot a^2$, is smaller than 10^{-5}. This value is chosen such that, on the time scale for the cluster to move towards midcell $\approx 4800\,\mathrm{s}$, this event occurs on average not even once.

We assume that nucleoid-bound PomZ dimers that are also bound to the PomXY cluster can only be released into the cytosol by ATP hydrolysis resulting in a conformational change of the protein. Detachment from the cluster alone such that the PomZ

dimer still remains attached to the nucleoid, is not included in our model. The reason for this assumption is that experiments with a mutant of PomZ that cannot hydrolyze ATP show a high concentration of PomZ dimers at the PomXY cluster and a nearly zero concentration away from the cluster suggesting that the PomZ dimers are captured at the cluster in this case [2]. If cluster-bound PomZ dimers would likely detach from the cluster without ATP hydrolysis, there would be a fraction of cluster-bound and unbound PomZ dimers. The latter ones would diffuse on the nucleoid increasing the PomZ concentration on the nucleoid away from the cluster.

The ATPase activity of PomZ is stimulated by DNA, PomX and PomY, which leads to a conformational change of the ATP-bound PomZ dimer, and subsequently the release of two ADP-bound PomZ monomers into the cytosol [2]. In our model, we combine the different processes involved (ATP hydrolysis, conformational change and PomZ-ADP detachment into the cytosol) into one effective detachment process and denote the corresponding rate as the ATP hydrolysis rate k_h. We assume that k_h is independent of the degree of stretching of the dimer.

PomZ dimers are released into the cytosol at the cluster via ATP hydrolysis, but when they are in the cytosolic state (as ADP-bound monomers) they cannot directly rebind to the nucleoid and the cluster, but instead need to become ATP-bound dimers and then first bind to the nucleoid before binding to the cluster. Hence, detailed balance is broken and the system is out of equilibrium.

Attachment rate of PomZ to the nucleoid

In our simulations we either assume that the PomZ density in the cytosol is homogeneous such that the flux of PomZ dimers onto the nucleoid is constant along the nucleoid or we account for the cytosolic PomZ distribution qualitatively. In the former case, a cytosolic PomZ dimer attaches to each lattice site of the nucleoid with the same rate (also where the cluster is located). This rate is given by the attachment rate to the entire surface of the nucleoid, k_{on}, divided by the number of lattice sites $l_{\mathrm{nuc}} \cdot w_{\mathrm{nuc}}/a^2$. In the latter case, when we account for the cytosolic PomZ distribution, we replace the homogeneous with the steady-state cytosolic PomZ-ATP distribution derived in SI text A.3 in our model. Here, we use a one-dimensional solution for the cytosolic PomZ-ATP density, which describes the variation of the protein density along the long cell axis. In our model, which has a three-dimensional geometry, we then assume that the cytosolic PomZ-ATP density is homogeneous along the short cell axis and changes along the long cell axis according to the one-dimensional distribution.

Movement of the PomXY cluster

Cluster-bound PomZ dimers can exert forces, which lead to a net movement of the cluster. Let us denote the position of the nucleoid binding site of the i-th PomZ dimer as $\vec{x}_{i,\mathrm{nuc}}$ and the position of the cluster binding site as $\vec{x}_{i,\mathrm{clu}} = \vec{x}_c + \Delta\vec{x}_{i,\mathrm{clu}}$ with $\vec{x}_c$ the position of the cluster ($\vec{x}_c \in \mathbb{R}^2$). Here, we decomposed the position of a cluster binding site into the cluster position, $\vec{x}_c$, and the additional vector $\Delta\vec{x}_{i,\mathrm{clu}}$. This is done

because we are interested in the equation of motion for the cluster position, $\vec{x}_c$, and when the cluster moves the cluster binding sites of the PomZ dimers move accordingly. As long as the PomZ dimer does not diffuse on the nucleoid or the cluster, the two vectors $\vec{x}_{i,\mathrm{nuc}}$ and $\Delta\vec{x}_{i,\mathrm{clu}}$ are constant.

A single PomZ dimer exerts a force $\vec{F}_i(t)$ on the cluster:

$$\vec{F}_i(t) = -k\left(\vec{x}_{i,\mathrm{clu}}(t) - \vec{x}_{i,\mathrm{nuc}}\right) = -k\left(\vec{x}_c(t) + \Delta\vec{x}_{i,\mathrm{clu}} - \vec{x}_{i,\mathrm{nuc}}\right) . \tag{S5.5}$$

In a friction dominated regime, the sum over all forces exerted by N_b cluster-bound PomZ dimers has to balance with the friction force acting on the cluster (friction coefficient γ):

$$\gamma\dot{\vec{x}}_c(t) = \sum_{i=1}^{N_b}\vec{F}_i(t) = -k\sum_{i=1}^{N_b}\left(\vec{x}_c(t) + \Delta\vec{x}_{i,\mathrm{clu}} - \vec{x}_{i,\mathrm{nuc}}\right) . \tag{S5.6}$$

This equation is solved by separation of variables, yielding

$$\vec{x}_c(t) = \left(\vec{x}_c(t_0) - \vec{x}_f\right)\exp\left(-\frac{N_b k}{\gamma}(t - t_0)\right) + \vec{x}_f , \tag{S5.7}$$

with

$$\vec{x}_f = \frac{1}{N_b}\left(\sum_{i=1}^{N_b}\vec{x}_{i,\mathrm{nuc}} - \Delta\vec{x}_{i,\mathrm{clu}}\right) . \tag{S5.8}$$

We find that the cluster approaches the position $\vec{x}_f$, at which no net force is acting on the cluster, exponentially fast with the characteristic time $\tau = \gamma/(N_b k)$.

A.2 Flux difference into the cluster for different cluster shapes

PomZ dimers detach from the nucleoid into the cytosol upon ATP hydrolysis, which breaks detailed balance and leads to a net flux of PomZ through the system. In the following we consider the fluxes of PomZ for the one- and three-dimensional model geometry (see Fig. S5.1). If the cluster position is fixed, which can be assumed in the adiabatic limit, the fluxes in and out of each region (cytosol, cluster and nucleoid region left and right of the cluster) have to balance in the steady state. Hence, the flux of PomZ dimers to the nucleoid left and right of the cluster, j_1 and j_3, balance the fluxes into the cluster region, j_2 and j_4, respectively. If we assume that the cytosolic PomZ distribution is homogeneous, the on-fluxes to the nucleoid scale with the length of the respective nucleoid region:

$$j_1 = k_{\mathrm{on}}\frac{l_{\mathrm{nuc}} - x_c - l_{\mathrm{clu}}/2}{l_{\mathrm{nuc}}}N_{\mathrm{cyt}} , \tag{S5.9}$$

$$j_3 = k_{\mathrm{on}}\frac{x_c - l_{\mathrm{clu}}/2}{l_{\mathrm{nuc}}}N_{\mathrm{cyt}} , \tag{S5.10}$$

with x_c the position of the cluster. This results in the following formula for the flux difference of PomZ into the cluster

$$j_{\text{diff}} = j_2 - j_4 = j_1 - j_3 = k_{\text{on}} N_{\text{cyt}} \left(1 - \frac{2x_c}{l_{\text{nuc}}} \right). \qquad (\text{S5.11})$$

The flux difference is proportional to the attachment rate of PomZ to the nucleoid, k_{on}, and the number of PomZ dimers in the cytosol, N_{cyt}. It is important to note, that N_{cyt} also depends, among other parameters on the clusters length, l_{nuc} and its position.
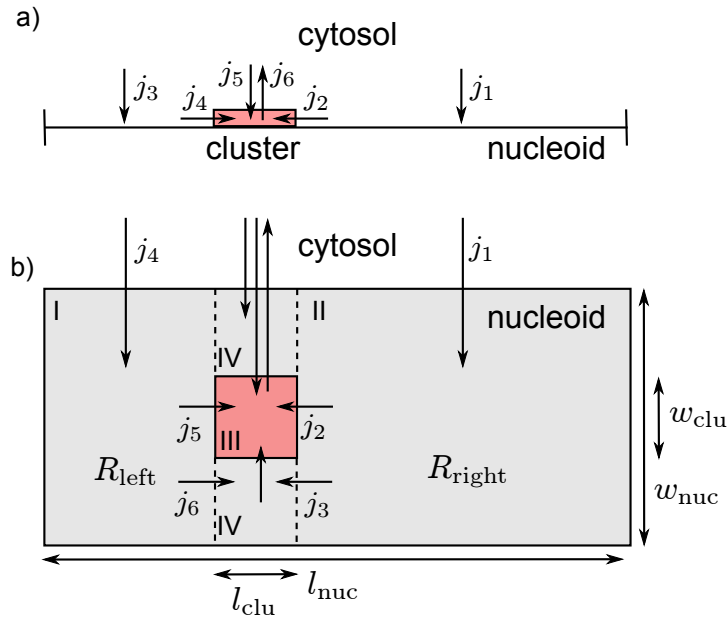
Figure S5.1 Sketch of the one- and three-dimensional model geometry with the PomZ fluxes. (a) In the one-dimensional model, nucleoid and cluster are incorporated as one-dimensional lattices. The cluster region is shown as a red rectangle. PomZ dimers attach to and diffuse on the nucleoid with reflecting boundary conditions at the nucleoid ends. The arrows show the different PomZ fluxes from one region (cytosol, cluster and nucleoid left and right of the cluster) to another. (b) Similar to a), but for the three-dimensional model geometry. The grey region shows the nucleoid of size $l_{\text{nuc}} \times w_{\text{nuc}}$ and the red region the cluster of size $l_{\text{clu}} \times w_{\text{clu}}$. The area of the nucleoid regions left and right of the cluster are denoted by R_{left} and R_{right}, respectively.

In the three-dimensional model geometry there are additional fluxes if the cluster does not cover the entire nucleoid width, i.e. if $w_{\text{clu}} < w_{\text{nuc}}$ holds (see Fig. S5.1b). Nucleoid-bound PomZ dimers can leave the nucleoid regions either by entering the cluster region and then attaching to the cluster, or by diffusing into the region in the extension of the cluster along the short cell axis direction (region IV in Fig. S5.1b). PomZ dimers in region IV either diffuse back into the region they came from, or enter the cluster or diffuse past the cluster. In the steady state, the fluxes in and out of each

region (I to IV) have to balance, such that we find:

$$j_1 = j_2 + j_3 \ , \tag{S5.12}$$

$$j_4 = j_5 + j_6 \ . \tag{S5.13}$$

If we assume that the flux into the cluster region (region III) and into region IV scale with their respective lengths, i.e. $j_2/j_3 = w_{\mathrm{clu}}/(w_{\mathrm{nuc}} - w_{\mathrm{clu}})$ and similarly for j_5 and j_6, the flux difference into the cluster reads:

$$j_{\mathrm{diff}} = j_2 - j_5 = k_{\mathrm{on}} N_{\mathrm{cyt}} \frac{w_{\mathrm{clu}}}{w_{\mathrm{nuc}}} \left(1 - \frac{2x_c}{l_{\mathrm{nuc}}} \right) \ , \tag{S5.14}$$

which agrees with the formula for the one-dimensional system if the cluster is ring-shaped, i.e. $w_{\mathrm{clu}} = w_{\mathrm{nuc}}$. This curve agrees well with our simulation results for a ring-shaped cluster (see Fig. 5.8d). However, if the cluster does not cover the full nucleoid's width, it deviates. The smaller the nucleoid width is, the larger the rescaled flux difference, $j_{\mathrm{diff}}/N_{\mathrm{cyt}} \cdot w_{\mathrm{clu}}/w_{\mathrm{nuc}}$. This deviation can be attributed to the fact that PomZ dimers that diffuse into region IV are not absorbed here, but can diffuse back into region I or II. Hence, the fluxes into the cluster are larger than the values obtained from the simple estimate we used before. For the fluxes into the cluster from the right hand side, we have

$$\frac{j_2}{j_3} > \frac{w_{\mathrm{clu}}}{w_{\mathrm{nuc}} - w_{\mathrm{clu}}} \ . \tag{S5.15}$$

Furthermore, PomZ dimers can pass the cluster by diffusion from region I to region II or vice versa. However, this flux only matters if the cluster is small both in length and width.

A.3 Derivation of the cytosolic PomZ distribution

In the main text we introduced the following coupled partial differential equations for the cytosolic PomZ-ATP (c_T) and PomZ-ADP (c_D) density:

$$\partial_t c_D(x,t) = D_{\mathrm{cyt}} \partial_x^2 c_D(x,t) - k_{\mathrm{ne}} c_D(x,t) + s_0 \delta(x - x_c)\Theta(t) \ , \tag{S5.16}$$

$$\partial_t c_T(x,t) = D_{\mathrm{cyt}} \partial_x^2 c_T(x,t) - k_{\mathrm{on}} c_T(x,t) + k_{\mathrm{ne}} c_D(x,t) \ . \tag{S5.17}$$

Here, the cluster position x_c is a constant. To obtain the stationary PomZ-ATP distribution, we solved this system of two coupled differential equations with the time derivative set to zero. In a coordinate system where the cluster position is at the origin

the solution reads:

$$c_T(x) = \tilde{c}_1 \left[-\lambda_T \cosh\left(\frac{L_1}{\lambda_T}\right) \cosh\left(\frac{L_2 + x}{\lambda_T}\right) \sinh\left(\frac{L}{\lambda_D}\right) + \right.$$
$$\left. + \lambda_D \cosh\left(\frac{L_1}{\lambda_D}\right) \cosh\left(\frac{L_2 + x}{\lambda_D}\right) \sinh\left(\frac{L}{\lambda_T}\right) \right] , \quad \text{for} \quad -L_1 \leq x \leq 0 ,$$

$$\text{(S5.18)}$$

$$c_T(x) = \tilde{c}_1 \left[-\lambda_T \cosh\left(\frac{L_2}{\lambda_T}\right) \cosh\left(\frac{L_1 - x}{\lambda_T}\right) \sinh\left(\frac{L}{\lambda_D}\right) + \right.$$
$$\left. + \lambda_D \cosh\left(\frac{L_2}{\lambda_D}\right) \cosh\left(\frac{L_1 - x}{\lambda_D}\right) \sinh\left(\frac{L}{\lambda_T}\right) \right] , \quad \text{for} \quad 0 \leq x \leq L_2 , \quad \text{(S5.19)}$$

with

$$\tilde{c}_1 = \frac{4 s_0 \lambda_T^2 e^{L(1/\lambda_D + 1/\lambda_T)}}{D_{\text{cyt}} \left(\lambda_D^2 - \lambda_T^2\right) \left(e^{2L/\lambda_D} - 1\right) \left(e^{2L/\lambda_T} - 1\right)} . \quad \text{(S5.20)}$$

Here, L_1 and L_2 denote the lengths of the nucleoid left and right of the cluster position, x_c, respectively. The total length of the nucleoid, L, is then given by the sum of these two lengths: $L = L_1 + L_2$. Furthermore, we defined the diffusive length scales for PomZ-ATP until it attaches to the nucleoid and PomZ-ADP until it exchanges its ATP for ADP as λ_D and λ_T, respectively:

$$\lambda_D = \sqrt{\frac{D_{\text{cyt}}}{k_{\text{ne}}}} \quad \text{and} \quad \lambda_T = \sqrt{\frac{D_{\text{cyt}}}{k_{\text{on}}}} . \quad \text{(S5.21)}$$

The above solution for the cytosolic PomZ-ATP density holds true for $\lambda_T \neq \lambda_D$. If the two length scales are equal, $\tilde{c}_1$ becomes singular and hence this case needs to be considered separately. For $\lambda_D = \lambda_T \equiv \lambda$ the solution is given by:

$$c_T(x) = \tilde{c}_2 \left[(2L_1 - x) \cosh\left(\frac{2L_2 + x}{\lambda}\right) - x \cosh\left(\frac{2L + x}{\lambda}\right) + \right.$$
$$+ (2L + x) \cosh\left(\frac{x}{\lambda}\right) + (2L_2 + x) \cosh\left(\frac{2L_1 - x}{\lambda}\right) +$$
$$\left. + 4\lambda \cosh\left(\frac{L_1}{\lambda}\right) \cosh\left(\frac{L_2 + x}{\lambda}\right) \sinh\left(\frac{L}{\lambda}\right) \right] , \quad \text{for} \quad -L_1 \leq x \leq 0 , \quad \text{(S5.22)}$$

$$c_T(x) = \tilde{c}_2 \left[(2L_2 + x) \cosh\left(\frac{2L_1 - x}{\lambda}\right) + x \cosh\left(\frac{2L - x}{\lambda}\right) + \right.$$
$$+ (2L - x) \cosh\left(\frac{x}{\lambda}\right) + (2L_1 - x) \cosh\left(\frac{2L_2 + x}{\lambda}\right) +$$
$$\left. + 4\lambda \cosh\left(\frac{L_2}{\lambda}\right) \cosh\left(\frac{L_1 - x}{\lambda}\right) \sinh\left(\frac{L}{\lambda}\right) \right] , \quad \text{for} \quad 0 \leq x \leq L_2 , \quad \text{(S5.23)}$$

with

$$\tilde{c}_2 = \frac{s_0}{8 D_{\text{cyt}} \sinh^2\left(L/\lambda\right)} . \quad \text{(S5.24)}$$
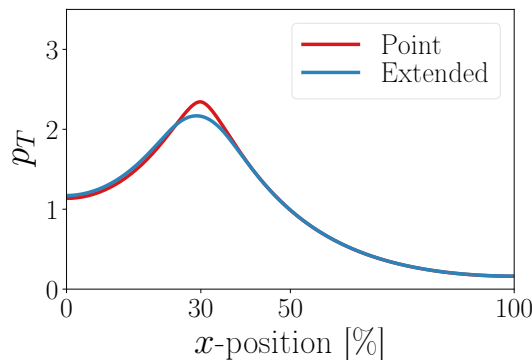
Figure S5.2 Cytosolic PomZ distribution. a) Comparison of the steady-state solutions for the cytosolic PomZ-ATP density if detachment of PomZ-ADP at the PomXY cluster is modeled as a point source (red curve) or a source with the same extension as the cluster (blue curve).

With the analytical solution for the PomZ-ATP density in the cytosol, we can now define the attachment rate of a PomZ dimer to the nucleoid, accounting for the cytosolic PomZ distribution. Previously, we used a constant attachment rate of PomZ dimers to the nucleoid, k_{on}. Now, we normalize the steady-state solution for $c_T(x)$ to one to obtain a probability density:

$$p_T(x) = \frac{k_{\mathrm{on}}}{s_0} c_T(x) \ . \tag{S5.25}$$

The rate with which a PomZ dimer attaches to site x along the long cell axis is then defined by:

$$k_{\mathrm{on}}(x) \equiv k_{\mathrm{on}} \, p_T(x) \ . \tag{S5.26}$$

In the derivation of the cytosolic PomZ-ATP density above, we reduced the cytosol to a one-dimensional line and the PomXY cluster to a point source. To investigate how the PomZ-ATP density changes when the cluster's extension is accounted for, we also solved Eqs. S5.16 and S5.17 with the Dirac delta distribution replaced by a Heaviside step function $\Theta(x - x_c + l_{\mathrm{clu}}/2)\Theta(x_c + l_{\mathrm{clu}}/2 - x)/l_{\mathrm{clu}}$. For the parameters considered (Table S5.1) we find that the solution for the steady-state PomZ-ATP density, when the cluster is included as a point source (Eqs. S5.18 and S5.19), is a good approximation to the solution considering a one-dimensional cytosolic lane and an extended cluster (Fig. S5.2a, "Point" and "Extended"). The PomZ density profiles only deviate significantly in close proximity to the cluster ($x_c = 30\%$ of nucleoid length), which can be attributed to the different shapes of the cluster used.

A.4 Discussion of parameters used in the simulations

The total PomZ dimer number, the length and width of the cluster and the length of the nucleoid are chosen in accordance with experimental observations in *M. xanthus* [2].

For the ATP hydrolysis rate we use a value obtained from an *in vitro* assay to measure the ATP turnover rate of PomZ in contact with PomX, PomY and DNA [2]. The attachment rate of cytosolic PomZ to the nucleoid is approximated by literature values for the related Par system ($50\,\mathrm{s}^{-1}$ [3] and $0.03\,\mathrm{s}^{-1}$ [6]). To get a double attachment rate that is comparable to the one-dimensional case, we chose k_a^0 such that the total attachment rate k_a^{tot} is equal in both models. This implies that the rate used in the one-dimensional model has to be multiplied by a factor of $\sqrt{\beta k/2\pi}$ to account for the additional dimension.

Parameter	Variable	Value
M. xanthus cell length	l_{cell}	$7.7\,\mathrm{\mu m}$
Nucleoid length	l_{nuc}	$5.0\,\mathrm{\mu m}$
Nucleoid width (circumference)	w_{nuc}	$2.2\,\mathrm{\mu m}$
PomXY cluster length	l_{clu}	$0.7\,\mathrm{\mu m}$
PomXY cluster width	w_{clu}	$0.7\,\mathrm{\mu m}$
Effective spring stiffness of a PomZ dimer	k	$10^4\,\mathrm{k_B T \mu m^{-2}}$
Attachment rate of cytosolic PomZ to nucleoid	k_{on}	$0.1\,\mathrm{s}^{-1}$
Attachment rate of nucleoid-bound PomZ to cluster	k_a^0	$2.0\times10^4\,\mathrm{s^{-1}\mu m^{-2}}$
Diffusion constant of PomZ on nucleoid	D_{nuc}	$0.01\,\mathrm{\mu m^2 s^{-1}}$
Diffusion constant of PomZ on cluster	D_{clu}	$0.01\,\mathrm{\mu m^2 s^{-1}}$
ATP hydrolysis rate of PomZ at the cluster	k_h	$0.01\,\mathrm{s}^{-1}$
Total number of PomZ dimers in the cell	N	100
Diffusion constant of the PomXY cluster in the cytosol	D_{cluster}	$2\times10^{-4}\,\mathrm{\mu m^2/s}$
Diffusion constant of PomZ in the cytosol	D_{cyt}	$0.1\,\mathrm{\mu m^2 s^{-1}}$
Nucleotide exchange rate of PomZ	k_{ne}	$6\,\mathrm{s}^{-1}$
Lattice spacing	a	$0.01\,\mathrm{\mu m}$

Table S5.1 Parameters used in the simulations.

The diffusion constant of PomZ on the nucleoid and on the PomXY cluster is approximated by the effective diffusion constant of ParA dimers on the nucleoid used in models for the Par system. However, these values vary a lot: $0.001\,\mathrm{\mu m^2/s} - 1\,\mathrm{\mu m^2/s}$ [3, 115]. The friction coefficient of the cluster, γ, is related to its diffusion constant, D_{cluster}, via Stokes-Einstein: $\gamma = k_B T/D_{\mathrm{cluster}}$. We approximate the diffusion constant D_{cluster} by the corresponding literature values for plasmids. However, since the PomXY cluster seems to be larger than plasmids, these values are only an upper bound for the diffusion constant of the Pom cluster: $D_{\mathrm{cluster}} \leq 3\times10^{-4}\,\mathrm{\mu m^2 s^{-1}}$[3, 6].

The cytosolic diffusion constant of PomZ can be estimated from bleaching experiments (data shown in [2]). Here, cytosolic PomZ dimers that cannot bind to the nucleoid are bleached close to one of the cell poles. After a bleaching time of $t_{\mathrm{bleach}} = 3\,\mathrm{s}$ the

fluorescence intensity in the cell is drastically decreased. This indicates that cytosolic PomZ dimers can diffuse a distance of the cell length, l_{cell}, in 3 s, which results in the following estimate for the diffusion constant:

$$D_{\text{cyt}} \geq \frac{l_{\text{cell}}^2}{2t_{\text{bleach}}} \approx \frac{(7.7\,\mu\text{m})^2}{6\,\text{s}} \approx 10\,\mu\text{m}^2/\text{s} \; . \tag{S5.27}$$

When we tested the effect of a non-homogeneous PomZ-ATP distribution in the cytosol on the cluster dynamics, we reduced the diffusion constant by about a factor of 100. The nucleotide exchange rate of PomZ-ADP to PomZ-ATP is approximated by the corresponding rate for MinD proteins [104].

A.5 Details on the stochastic simulation

Initial PomZ distribution

Initially all PomZ proteins are in the cytosol. Then we let the simulations run for a time t_{min} of at least 10 minutes with a fixed cluster position such that the PomZ proteins can approach their steady-state distribution. After this initial time t_{min} recording starts. The cluster can now start to move or is kept at a fixed position ("stationary simulation") during the entire simulation.

Gillespie algorithm

We implement our model using the Gillespie algorithm [112, 120], a stochastic simulation algorithm. Since the cluster position, $\vec{x}_c \in \mathbb{R}^2$, changes over time according to the forces cluster-bound PomZ dimers exert on the cluster (Eq. S5.7), all rates that depend on the position of the cluster binding site of a PomZ dimer depend on time. These include the attachment rate of a nucleoid-bound PomZ dimer to the cluster and the hopping rates of a PomZ dimer bound to the nucleoid and the cluster. If the cluster only moves slightly in one time step of the Gillespie algorithm, we can approximate the time-dependent rates as constant.

To quantify the effect of the time dependence of the rates, let us consider a PomXY cluster with N_b PomZ dimers bound to it such that a non-zero net force acts on the cluster. According to Eq. S5.7 the time scale for the cluster to relax to the force-free position, $\vec{x}_f$, is given by $t_{\text{clu}} = \gamma/(N_b k)$. The number of cluster-bound PomZ dimers, N_b, changes with the position of the cluster along the nucleoid. For a cluster positioned at 10% of nucleoid length and one at midnucleoid the number of cluster bound PomZ dimers as obtained from simulations leads to $t_{\text{clu}} \approx 0.04\,\text{s}$ and $t_{\text{clu}} \approx 0.02\,\text{s}$, respectively (for the parameters as in Table S5.1).

Next, we consider the time step, Δt, until the next event happens in the Gillespie algorithm. It can be approximated by the time until a PomZ dimer hops on the nucleoid because hopping on the nucleoid occurs most frequently compared to the other events for the parameters we consider (Table S5.1). The rate for the event that any of the nucleoid-bound PomZ dimers, N_{nuc}, hops in any of the four possible directions

on the nucleoid (ignoring the boundaries) is given by $4\,k_{\text{hop,nuc}}^0 N_{\text{nuc}}$. The typical time until the next event happens can then be approximated by the inverse of this rate. Again, the number of nucleoid-bound PomZ dimers, N_{nuc}, varies with the position of the cluster. For a cluster at 10% of nucleoid length and one at midnucleoid, we get $\Delta t \approx 4 \times 10^{-5}\,\text{s}$ and $\Delta t \approx 3 \times 10^{-5}\,\text{s}$, respectively. Since the typical time until the next event happens, Δt, is much smaller than the time scale for the movement of the cluster, t_{clu}, we can approximate all rates in the Gillespie algorithm as time-independent, which significantly improves the computational speed of the algorithm.

A.6 Analysis of PomZ density and flux on the nucleoid

To determine the PomZ density and flux along the nucleoid for a specific cluster position from our simulations we recorded the PomZ density / flux at any time the cluster is in a small region ($\pm 0.5\%$ of nucleoid length) around the x-position of interest. In the case of the density, we averaged it over the complete y-axis (short cell axis) to obtain the density along the long cell axis. In contrast, the PomZ flux was averaged only over the part of the nucleoid that corresponds to the extension of the cluster region along the long cell axis (see Fig. S5.3a) because we are interested in the flux of PomZ dimers into the cluster. In both cases the data was additionally averaged over an ensemble of 100 simulations. This leads to a flux profile as shown in Fig. S5.3b. To obtain the difference in the PomZ dimer fluxes into the cluster from each side along the long cell axis, the maximal / minimal values of the average flux profile left / right of the PomXY cluster were determined (red lines in Fig. S5.3b) and then the two values of different signs were added together to obtain the flux difference.
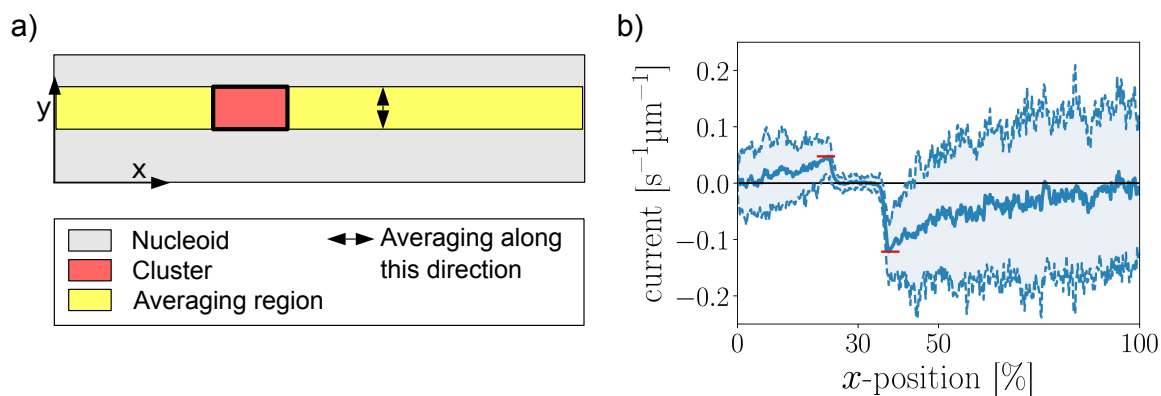
Figure S5.3 *In silico* **measurement of the nucleoid-bound PomZ flux.** (a) Sketch of the region used for averaging the flux. Only hopping events in the yellow region are taken into account when determining the PomZ flux profile along the long cell axis. The fluxes are averaged over the y-axis. (b) Simulated flux profile of nucleoid-bound PomZ along the long cell axis with the averaging performed as illustrated in a). The flux into the cluster is given by the maximal value left of the cluster and the minimal value right of the cluster (red horizontal lines). We used the same parameters as in Table S5.1.

A.7 Cluster-bound PomZ density gradient

Let us consider a simplified, one-dimensional model for the cluster-bound PomZ distribution. Here, we consider the cluster as a linear object of size s, which either refers to the width, w_{clu}, or length, l_{clu}, of the cluster. Let $c_b(x, t)$ denote the concentration of cluster-bound PomZ dimers. We assume that nucleoid-bound PomZ dimers quickly attach to the cluster when they are in close proximity to the cluster. Hence, we can approximate the dynamics of the cluster-bound PomZ dimers by an influx of PomZ dimers at each cluster end. The influx corresponds to the diffusive flux of PomZ dimers into the cluster from either side. The diffusion constant of cluster-bound PomZ dimers is reduced, compared to that of PomZ dimers bound to the nucleoid only, because the movement of the two binding sites on the nucleoid and cluster is limited due to the spring connecting them. We approximate the diffusion constant of the cluster-bound PomZ dimers as $D_b = D_{\text{nuc}}/2$, with the diffusion constant of PomZ on the nucleoid, D_{nuc}. Besides diffusion, PomZ may detach from the cluster with rate k_h (ATP hydrolysis), which, in total, results in the following reaction-diffusion equations

$$\partial_t c_b(x, t) = D_b \partial_x^2 c_b(x, t) - k_h c_b(x, t) \ , \tag{S5.28}$$

with constant flux boundary conditions

$$-D_b \partial_x c_b(x, t)|_{x=0} = j_{\text{left}} \ , \tag{S5.29a}$$
$$D_b \partial_x c_b(x, t)|_{x=s} = j_{\text{right}} \ . \tag{S5.29b}$$

The steady-state solution is given by

$$c_b(x) = \frac{\lambda}{D_b} \left(e^{-x/\lambda} \frac{j_{\text{right}} + j_{\text{left}} e^{s/\lambda}}{e^{s/\lambda} - e^{-s/\lambda}} + e^{x/\lambda} \frac{j_{\text{right}} + j_{\text{left}} e^{-s/\lambda}}{e^{s/\lambda} - e^{-s/\lambda}} \right) \ , \tag{S5.30}$$

with *the residence length* $\lambda = \sqrt{D_b/k_h}$ measuring the typical length a PomZ dimer diffuses while bound to the cluster before detaching. This yields an asymmetry in the protein concentrations between the left and right edge of the cluster (Fig. 5.8b),

$$A_{\text{clu}} = \frac{c_b(s) - c_b(0)}{c_b(s) + c_b(0)} = \frac{j_{\text{right}} - j_{\text{left}}}{j_{\text{right}} + j_{\text{left}}} \tanh\left(\frac{s}{2\lambda}\right)^2 = A_{\text{flux}} \tanh\left(\frac{s}{2\lambda}\right)^2 \ . \tag{S5.31}$$

The relative magnitude of the length s (length or width of the cluster) and the residence length determines how significant the PomZ protein gradients on the cluster are. They are most pronounced for small diffusion constants of cluster-bound PomZ (D_b) and large ATP hydrolysis rates (k_h).

Chapter 6

Conclusion and outlook

Summary of the results

We investigated how midcell is localized in the bacterium *M. xanthus*, which is necessary for the cell to determine the site of division. First, we searched for a computational model that can explain the experimentally observed Pom cluster movement from a position close to the nucleoid pole to midcell. Together with our experimental collaboration partners, Dominik Schumacher and Lotte Søgaard-Andersen from the MPI for Terrestrial Microbiology in Marburg, Germany, we developed a one-dimensional mathematical model that leads to midcell localization of the cluster on the experimentally observed time scale with physiologically relevant parameters. The positioning mechanism is based on the diffusive fluxes of the ATPase PomZ into the cluster. If the cluster is positioned off-center, more PomZ dimers arrive at the cluster from the site with the longer cluster-to-nucleoid-end distance. The mechanism is self-correcting: if the cluster overshoots midcell, the PomZ flux difference reverses its sign and the cluster is guided back to midcell.

It remained to be analyzed how the model parameters affect the cluster dynamics and for which parameter regions midcell localization breaks down. For this purpose we performed extensive *in silico* parameter sweeps. Reassuringly, we found midcell localization of the cluster for a broad parameter range. By varying the ATP hydrolysis rate of PomZ we found that the time the cluster needs to reach midcell is minimized for intermediate hydrolysis rates. A qualitative change was observed when the diffusion constant of PomZ on the nucleoid was reduced: the cluster started to oscillate around midcell. This can be explained by the time scales of the cluster dynamics and the PomZ dynamics. If the PomZ dimers diffuse quickly on the nucleoid and the cluster moves slowly, the PomZ distribution almost immediately readjusts to the new steady state distributions while the cluster is moving (adiabatic limit). However, if the PomZ dynamics is slow, the build-up of the PomZ gradient lacks behind the movement of the cluster. Due to this time delay, the cluster overshoots midcell. At some point, it slows down and the PomZ gradient can catch up, such that the cluster reverses it direction, leading to oscillatory movements.

To get further mechanistic insights into the positioning process, we developed, for the non-oscillatory case, a theoretical approach that predicts the average cluster trajectory. We found that the net velocity of the cluster is determined by three factors. One factor is the flux difference in nucleoid-bound PomZ into the cluster from each side, which measures how far away the cluster is from midnucleoid. The other two

factors are the force a single PomZ dimer exerts on the cluster and the effective friction coefficient of the cluster when tethered to the nucleoid via PomZ dimers. With this approach we get mechanistic insights into the cluster movement. For example, we found that the time the clusters need to reach midcell is minimized for an intermediate ATP hydrolysis rate of PomZ, k_h. When k_h increases, the flux difference in PomZ also increases, but the force a single PomZ dimer exerts on the cluster decreases. The average velocity of the cluster is proportional to the product of these two factors, which results in a maximum for intermediate k_h values.

Since we modeled the nucleoid and the cluster as one-dimensional objects, the question was raised whether a flux-based mechanism can lead to midcell positioning of the cluster also in a biologically more realistic, three-dimensional cell geometry. To answer this question we generalized our previous model to one that incorporates the nucleoid as a cylinder and the cluster as a rectangular object moving on the surface of the cylinder. Our simulation results showed that clusters can still be positioned at midcell although nucleoid-bound PomZ dimers can diffuse past the cluster without interaction. Increasing the length or width of the cluster, leads to faster midcell localization. The main reasons are faster cycling of PomZ between the nucleoid and cytosol and larger forces exerted by a single PomZ dimer. Furthermore, we investigated the effect of the cytosolic distribution of PomZ, which was previously assumed to be homogeneous. Our results showed that spatial redistribution of PomZ due to a time delay between detachment from and reattachment to the nucleoid and fast cytosolic diffusion, speeds up the time for midcell positioning. We also simulated the dynamics of two clusters, which we found to localize at the one- and three-quarter positions along nucleoid length.

Discussion

Comparison with Par models for plasmid and chromosome segregation

The Pom system in *M. xanthus* has several similarities with Par systems for plasmid and chromosome segregation. Both systems involve an ATPase (PomZ or ParA) that binds in its ATP-bound dimeric state to the nucleoid. Its ATPase activity is triggered by an ATPase activating protein (PomX/PomY or ParB), which either forms the cargo itself (PomXY cluster) or binds to the cargo (plasmids, partition complex). The cargo is then positioned in an ATPase-dependent manner at equidistant positions along the nucleoid, i.e. midcell for one cargo.

Despite these commonalities between the two positioning systems, some experimental findings for the Pom system are in contrast to those for Par systems. The key differences in our experimental observations [2] are: First, PomZ has a high density at the cluster, which is different to a low ParA density at the cargo observed for some Par systems [10, 76]. However, in other positioning systems the ATPase also accumulates at the cargo, similar to the Pom system [60, 99]. Second, we did not observe a clear depletion zone in PomZ in the wake of the cluster, which was observed in Par systems [10, 72]. Third, the Pom cluster is relatively large (about 0.7 µm in length [2]) compared

to plasmids (about 0.1 µm [6]). This observation could explain the low mobility of the cluster in the absence of PomZ. Finally, the typical dynamics of the Pom cluster in *M. xanthus* is movement to and localization at midcell until the cell divides. For Par systems several different cargo dynamics have been observed, including oscillatory cargo movement [10, 13, 72], movement from one cell pole to the other [6] and equidistant positioning of the cargoes [3, 10, 13–15]. In contrast to the observed Pom cluster dynamics, a single plasmid typically localizes at midcell until it duplicates and then the two plasmids are positioned at the one- and three-quarter positions.

Due to these differences in the experimental observations we developed a model for midcell positioning in *M. xanthus* that is distinct from previously proposed models for positioning by Par systems. Nevertheless, it is based on and has similarities with models explaining translocation and localization of cargoes by ParA proteins.

A flux-balance mechanism was originally suggested by Ietswaart et al. [3] for equal plasmid spacing and also applied to the localization of dynamic protein clusters on the nucleoid [16]. In our continuum description of the stochastic model (section 4.4) we calculated an analytical expression for the PomZ flux difference into the cluster, which is a generalization of the result from Ietswaart et al. [3]. We extended their results by incorporating the cluster as an object of finite size, instead of a point, and also explicitly included a cluster- and nucleoid-bound species that is captured at the cluster until it detaches into the cytosol. This was motivated by the experimental finding that the Pom cluster is large and a significant fraction of PomZ dimers accumulate at the cluster. Moreover, we considered the PomZ flux differences also for a non-zero detachment rate of PomZ from the nucleoid away from the cluster. We found that a flux-based mechanism only leads to midcell positioning if the length a PomZ dimer diffuses on the nucleoid before it detaches into the cytosol is sufficiently large compared to the nucleoid length, in agreement with previous findings [16, 77]. Other necessary conditions for flux-based positioning are that the ATPase diffuses faster on the nucleoid than the cargo and cycles between a nucleoid-bound and cytosolic state [2, 3, 16].

How forces are generated by the ATPase to move the cargo is still not completely understood. A chemophoresis force [74–77] and the elasticity of the nucleoid [5, 6] have been suggested. In our model we incorporated the elasticity of the nucleoid, which can lead to translocation forces acting on the cluster via the nucleoid-bound PomZ dimers, similar to the DNA-relay model for plasmid and chromosome segregation [6, 100]. In the DNA-relay model nucleoid-bound ParA dimers are spatially restricted in their movement, similar to a Brownian particle in a trap. This model assumption is in contrast to the experimentally observed fast dynamics of PomZ across the entire nucleoid. It can explain the different cargo dynamics observed for the DNA-relay model (oscillatory cargo movement) and our model (midcell localization). Interestingly, we also observed oscillations around midcell, when the PomZ diffusion constant is reduced. Our finding that the cluster movement changes from midcell localization to oscillatory when the time scale of the PomZ dynamics is slow compared to the cluster dynamics is in agreement with previous findings for the Par system [75, 79], although their models differ from ours.

Fast cargo dynamics compared to slow diffusion of the ParA proteins is also assumed in diffusion-ratchet models [78, 79]. It ensures that a depletion zone in the wake of the cargo forms, such that the cargo continues to move in one direction and only turns if it encounters the nucleoid pole. Our experimental findings show the opposite, a fast PomZ dynamics and a slowly diffusing cargo. In this case, a region on the nucleoid with a reduced PomZ density is quickly refilled and hence no depletion zone in the wake of the cluster can form.

Motivated by experimental findings, we assume that cluster-bound PomZ dimers can diffuse on both the nucleoid and the cluster in our model. We found that forces are not only generated when the PomZ dimers attach to the cluster in a stretched configuration. They also produce a net force on the cluster when the cluster-bound PomZ dimers encounter the cluster's edge. Our simulations showed that for the parameters we consider, the latter contribution to the overall force of a single PomZ dimer is much more important than binding in a stretched configuration. This is in stark contrast to the situation in the DNA-relay model, where only the initial deflection of the ParA dimer from its equilibrium position accounts for the generated force. Thus, we showed that force generation based on elasticity can be sufficient for cargo translocation even if the motility of the transporting proteins is higher than the motility of the cargo. This is still true even in a three-dimensional geometry where proteins can diffuse past the cargo without interaction.

Comparison with the Min system in *E. coli*

Although the Min system in *E. coli* has the same biological function as the Pom system, i.e. localization of the Z-ring at midcell, both systems differ in several aspects. The two key differences are: i) MinD binds to the cell membrane and PomZ to the nucleoid, and ii) in contrast to MinD, the proteins PomX and PomY form a single cluster in the cell that can be approximated as a fixed structure.

Common features of the Min and the Pom system are that the ATPase proteins (MinD and PomZ) cycle between two states, one of which has a high affinity to bind to the cell membrane or nucleoid, respectively. Both, PomZ and MinD, are spatially redistributed in the cytosol before they reattach to their respective scaffold. These principles have been identified also in other positioning systems (e.g. PAR system in *C. elegans* or cell polarization in yeast) [53, 54, 97].

Another key feature to explain the observed Min oscillations is cooperative binding of MinD to the membrane, which leads to a non-linear term in the corresponding reaction-diffusion equations. For PomZ it is not known whether it binds cooperatively to the nucleoid. However, our results indicate that the positioning mechanism does not rely on such a property of PomZ.

Model predictions

By studying the Pom system both analytically and in simulations we could make several model predictions that would be highly interesting to test experimentally. First, we found that midcell localization of the cluster changes to oscillatory cluster movements

around midcell, when the PomZ dynamics is slow compared to the cluster dynamics. It would be interesting to test this theoretical prediction experimentally, which might be possible by performing experiments with a reduced diffusion constant of PomZ on the nucleoid. Second, we predicted that midcell localization is fastest for an intermediate ATP hydrolysis rate of PomZ. Experiments with a smaller hydrolysis rate indeed indicated that the cluster movement towards midcell is reduced [2]. However, whether this is also the case for large hydrolysis rates remains to be tested. A third prediction is that two Pom clusters localize at the one- and three-quarter positions along the nucleoid length. This is challenging to test experimentally, as the Pom proteins accumulate into one cluster inside the cell.

Outlook

Possible extensions of our model for midcell positioning in *M. xanthus*
We modeled the biological processes in the Pom system in *M. xanthus* to a high level of detail in order to capture the main mechanistic features. However, there are still interesting aspects that could be incorporated in even more detail in the future. This includes, for example, accounting for further biochemical processes, e.g. dimerization and nucleotide exchange of PomZ, as well as the assembly and maintenance of the Pom cluster. This could shed more light on the cytosolic distribution of PomZ and the interplay between PomZ with both PomX and PomY. During the cell cycle, the PomZ protein number is doubled to maintain a constant particle number upon cell division. Furthermore, the chromosome is duplicated and segregated to the two cell halves, leading to significant changes of its geometry and size. Hence, it would be further interesting to study changes of the nucleoid length and shape, as well as protein production and degradation.

We have studied the effects of the three-dimensional cell geometry on the cluster dynamics in two ways: First, by considering the PomZ dynamics in the full three-dimensional cell geometry for a fixed cluster position by using reaction-diffusion equations evaluated with a finite element solver. Second, we used the stochastic particle-based model to simulate cluster trajectories with a three-dimensional representation of both nucleoid and cluster. In the latter, we incorporated the cytosolic PomZ distribution explicitly, though in a reduced, effective manner. A next step could be to combine the two approaches and incorporate the full cytosolic volume, confined by the cell membrane, into the stochastic model. In this way one could investigate the influence of the geometry of the cytosolic volume to even more detail. Moreover, we assumed that PomZ dimers bind to and diffuse on the nucleoid surface only. Since these proteins are small, it cannot be excluded that they are able to move into the nucleoid volume. A future model could account for this possibility and study the effects. However, we expect that the results change only quantitatively (by decreasing the fluxes), but not qualitatively. The reason is that moving into the volume provides a way for PomZ to diffuse past the cluster without interaction, which is already incorporated in the three-dimensional particle-based model we have presented in this thesis.

Furthermore, the chromosome is a highly complicated, dynamic structure that reshapes remarkably over time. The density of the chromosome was found to be non-homogeneously distributed along the nucleoid [12]. This observation is in agreement with a patchy fluorescence signal for the nucleoid in *M. xanthus* cells [2]. If the density of the nucleoid differs spatially and temporally, the elasticity of the chromosome might also depend on space and time. Including the chromosome organization and structure in models for the positioning of cargoes is an interesting opportunity for future research.

A quantitative model for midcell localization in *M. xanthus*

Our computational model can explain the experimentally observed cluster dynamics qualitatively. Since not all rates have been measured yet, we approximated these values by the corresponding ones from the Par system or varied the parameters over a broad range. Determining all rates of the biochemical processes involved is an important task for future research and one step towards a quantitative description of the system. In this regard, it would be also helpful to further improve the quantification of the experimental cluster trajectories by including more and longer time lapses that show the whole trajectory of the cluster from the nucleoid pole to midcell. Moreover, with super-resolution experiments it might be possible to determine the unknown rates for the biochemical processes. We predicted a relatively high density of PomZ over the cluster, but still an asymmetry in the density distribution. We would welcome the possibility to test that PomZ assumes the distribution suggested by our model.

Translocation forces

In our model we assume that the elasticity of the nucleoid and, to a minor extent, the PomZ dimers generate the forces to move the cargo. It remains to be tested experimentally if the elasticity of the nucleoid is sufficient to generate the forces required to move the cargo and if the force mainly has an elastic or chemophoretic origin. This question might be answered by *in vitro* experiments with a PomXY-coated cargo tethered to PomZ proteins bound to a DNA-carpet, similar to an *in vitro* Par system considered previously [76]. When the stiffness of the DNA-carpet is varied, we would expect that the cluster dynamics is affected, if the elasticity of the nucleoid is important for the cluster's movement (for very stiff nucleoids, the cluster should move less). In contrast, if the forces are mainly due to chemophoresis, only the gradient of PomZ proteins on the DNA-carpet should matter, such that the two possible mechanisms, how forces can be generated, could be distinguished.

In this thesis, I presented our theoretical approaches to assess the Pom positioning system in *M. xanthus* cells. We found that a flux-based mechanism can explain the experimentally observed cluster dynamics, both in a one- and three-dimensional model cell geometry. Our work contributes to identifying generic principles of positioning inside bacteria, which is investigated also in the context of Par and Min protein systems. The presented results add more details to the big picture derived in this very important and active field of research.

Bibliography

[1] A. Treuner-Lange *et al.* PomZ, a ParA-like protein, regulates Z-ring formation and cell division in Myxococcus xanthus. *Mol Microbiol* **87**(2), 235–253, 2013. DOI: 10.1111/mmi.12094.

[2] D. Schumacher *et al.* The PomXYZ Proteins Self-Organize on the Bacterial Nucleoid to Stimulate Cell Division. *Dev Cell* **41**(3), 299–314.e13, 2017. DOI: 10.1016/j.devcel.2017.04.011.

[3] R. Ietswaart, F. Szardenings, K. Gerdes and M. Howard. Competing ParA Structures Space Bacterial Plasmids Equally over the Nucleoid. *PLoS Comput Biol* **10**(12), e1004009, 2014. DOI: 10.1371/journal.pcbi.1004009.

[4] M. Schliwa and G. Woehlke. Molecular motors. *Nature* **422**(6933), 759–765, 2003. DOI: 10.1038/nature01601.

[5] P. A. Wiggins *et al.* Strong intranucleoid interactions organize the Escherichia coli chromosome into a nucleoid filament. *Proc Natl Acad Sci U S A* **107**(11), 4991–4995, 2010. DOI: 10.1073/pnas.0912062107.

[6] H. C. Lim *et al.* Evidence for a DNA-relay mechanism in ParABS-mediated chromosome segregation. *Elife* **3**, e02758, 2014. DOI: 10.7554/eLife.02758.

[7] L. Rothfield, A. Taghbalout and Y.-L. Shih. Spatial control of bacterial division-site placement. *Nat Rev Microbiol* **3**(12), 959–968, 2005. DOI: 10.1038/nrmicro1290.

[8] M. Thanbichler and L. Shapiro. MipZ, a Spatial Regulator Coordinating Chromosome Segregation with Cell Division in Caulobacter. *Cell* **126**(1), 147–162, 2006. DOI: 10.1016/j.cell.2006.05.038.

[9] J. Lutkenhaus. The ParA/MinD family puts things in their place. *Trends Microbiol* **20**(9), 411–418, 2012. DOI: 10.1016/j.tim.2012.05.002.

[10] S. Ringgaard, J. van Zon, M. Howard and K. Gerdes. Movement and equipositioning of plasmids by ParA filament disassembly. *Proc Natl Acad Sci U S A* **106**(46), 19369–19374, 2009. DOI: 10.1073/pnas.0908347106.

[11] *COMSOL Multiphysics® v. 5.2. www.comsol.com, COMSOL AB.* Stockholm, Sweden.

[12] A. Le Gall *et al.* Bacterial partition complexes segregate within the volume of the nucleoid. *Nat Commun* **7**, 12107, 2016. DOI: 10.1038/ncomms12107.

[13] G. Ebersbach *et al.* Regular cellular distribution of plasmids by oscillating and filament-forming ParA ATPase of plasmid pB171. *Mol Microbiol* **61**(6), 1428–42, 2006. DOI: 10.1111/j.1365-2958.2006.05322.x.

[14] T. Hatano and H. Niki. Partitioning of P1 plasmids by gradual distribution of the ATPase ParA. *Mol Microbiol* **78**(5), 1182–1198, 2010. DOI: 10.1111/j.1365-2958.2010.07398.x.

[15] M. Sengupta, H. J. Nielsen, B. Youngren and S. Austin. P1 Plasmid Segregation: Accurate Redistribution by Dynamic Plasmid Pairing and Separation. *J Bacteriol* **192**(5), 1175–1183, 2010. DOI: 10.1128/JB.01245-09.

[16] S. M. Murray and V. Sourjik. Self-organization and positioning of bacterial protein clusters. *Nat Phys* **13**(10), 1006–1013, 2017. DOI: 10.1038/nphys4155.

[17] D. F. Savage, B. Afonso, A. H. Chen and P. A. Silver. Spatially Ordered Dynamics of the Bacterial Carbon Fixation Machinery. *Science* **327**(5970), 1258–1261, 2010. DOI: 10.1126/science.1186090.

[18] G. Laloux and C. Jacobs-Wagner. How do bacteria localize proteins to the cell pole? *J Cell Sci* **127**(1), 11–19, 2014. DOI: 10.1242/jcs.138628.

[19] L. Shapiro, H. H. McAdams and R. Losick. Why and How Bacteria Localize Proteins. *Science* **326**(5957), 1225–1228, 2009. DOI: 10.1126/science.1175685.

[20] A. Treuner-Lange and L. Søgaard-Andersen. Regulation of cell polarity in bacteria. *J Cell Biol* **206**(1), 7–17, 2014. DOI: 10.1083/jcb.201403136.

[21] S. R. Thompson, G. H. Wadhams and J. P. Armitage. The positioning of cytoplasmic protein clusters in bacteria. *Proc Natl Acad Sci U S A* **103**(21), 8209–8214, 2006. DOI: 10.1073/pnas.0600919103.

[22] M. R. Alley, J. R. Maddock and L. Shapiro. Polar localization of a bacterial chemoreceptor. *Genes Dev* **6**(5), 825–836, 1992. DOI: 10.1101/gad.6.5.825.

[23] G. Ebersbach, A. Briegel, G. J. Jensen and C. Jacobs-Wagner. A Self-Associating Protein Critical for Chromosome Attachment, Division, and Polar Organization in Caulobacter. *Cell* **134**(6), 956–968, 2008. DOI: 10.1016/j.cell.2008.07.016.

[24] Z. Hu and J. Lutkenhaus. Topological regulation of cell division in Escherichia coli involves rapid pole to pole oscillation of the division inhibitor MinC under the control of MinD and MinE. *Mol Microbiol* **34**(1), 82–90, 1999. DOI: 10.1046/j.1365-2958.1999.01575.x.

[25] D. M. Raskin and P. A. J. de Boer. Rapid pole-to-pole oscillation of a protein required for directing division to the middle of Escherichia coli. *Proc Natl Acad Sci U S A* **96**(9), 4971–4976, 1999. DOI: 10.1073/pnas.96.9.4971.

[26] J. S. Schuhmacher, K. M. Thormann and G. Bange. How bacteria maintain location and number of flagella? *FEMS Microbiol Rev* **39**(6), 812–822, 2015. DOI: 10.1093/femsre/fuv034.

[27] E. Bi and J. Lutkenhaus. FtsZ ring structure associated with division in Escherichia coli. *Nature* **354**(6349), 161–164, 1991. DOI: 10.1038/354161a0.

[28] K. Gerdes, M. Howard and F. Szardenings. Pushing and Pulling in Prokaryotic DNA Segregation. *Cell* **141**(6), 927–942, 2010. DOI: 10.1016/j.cell.2010.05.033.

[29] K. A. Michie and J. Löwe. Dynamic Filaments of the Bacterial Cytoskeleton. *Annu Rev Biochem* **75**(1), 467–492, 2006. DOI: 10.1146/annurev.biochem.75.103004.142452.

[30] J. Moller-Jensen. Prokaryotic DNA segregation by an actin-like filament. *EMBO J* **21**(12), 3119–3127, 2002. DOI: 10.1093/emboj/cdf320.

[31] R. A. Larsen *et al.* Treadmilling of a prokaryotic tubulin-like protein, TubZ, required for plasmid stability in Bacillus thuringiensis. *Genes Dev* **21**(11), 1340–1352, 2007. DOI: 10.1101/gad.1546107.

[32] D. A. Fletcher and R. D. Mullins. Cell mechanics and the cytoskeleton. *Nature* **463**(7280), 485–492, 2010. DOI: 10.1038/nature08908.

[33] G. Bange and I. Sinning. SIMIBI twins in protein targeting and localization. *Nat Struct Mol Biol* **20**(7), 776–80, 2013. DOI: 10.1038/nsmb.2605.

[34] T. A. Leonard, P. J. Butler and J. Löwe. Bacterial chromosome segregation: structure and DNA binding of the Soj dimer – a conserved biological switch. *EMBO J* **24**(2), 270–82, 2005. DOI: 10.1038/sj.emboj.7600530.

[35] L. L. Lackner, D. M. Raskin and P. A. J. de Boer. ATP-Dependent Interactions between Escherichia coli Min Proteins and the Phospholipid Membrane In Vitro. *J Bacteriol* **185**(3), 735–749, 2003. DOI: 10.1128/JB.185.3.735-749.2003.

[36] J. Lutkenhaus. Assembly Dynamics of the Bacterial MinCDE System and Spatial Regulation of the Z Ring. *Annu Rev Biochem* **76**(1), 539–562, 2007. DOI: 10.1146/annurev.biochem.75.103004.142652.

[37] Z. Hu, A. Mukherjee, S. Pichoff and J. Lutkenhaus. The MinC component of the division site selection system in Escherichia coli interacts with FtsZ to prevent polymerization. *Proc Natl Acad Sci U S A* **96**(26), 14819–14824, 1999. DOI: 10.1073/pnas.96.26.14819.

[38] Z. Hu, E. P. Gogol and J. Lutkenhaus. Dynamic assembly of MinD on phospholipid vesicles regulated by ATP and MinE. *Proc Natl Acad Sci U S A* **99**(10), 6761–6766, 2002. DOI: 10.1073/pnas.102059099.

[39] Z. Hu and J. Lutkenhaus. Topological Regulation of Cell Division in E. coli. *Mol Cell* **7**(6), 1337–1343, 2001. DOI: 10.1016/S1097-2765(01)00273-8.

[40] H. Meinhardt and P. A. J. de Boer. Pattern formation in Escherichia coli: A model for the pole-to-pole oscillations of Min proteins and the localization of the division site. *Proc Natl Acad Sci U S A* **98**(25), 14202–14207, 2001. DOI: 10.1073/pnas.251216598.

[41] M. Howard, A. D. Rutenberg and S. de Vet. Dynamic Compartmentalization of Bacteria: Accurate Division in E. Coli. *Phys Rev Lett* **87**(27), 278102, 2001. DOI: 10.1103/PhysRevLett.87.278102.

[42] K. Kruse. A Dynamic Model for Determining the Middle of Escherichia coli. *Biophys J* **82**(2), 618–627, 2002. DOI: 10.1016/S0006-3495(02)75426-X.

[43] K. C. Huang, Y. Meir and N. S. Wingreen. Dynamic structures in Escherichia coli: Spontaneous formation of MinE rings and MinD polar zones. *Proc Natl Acad Sci U S A* **100**(22), 12724–12728, 2003. DOI: 10.1073/pnas.2135445100.

[44] K. C. Huang and N. S. Wingreen. Min-protein oscillations in round bacteria. *Phys Biol* **1**(4), 229–235, 2004. DOI: 10.1088/1478-3967/1/4/005.

[45] M. Loose *et al.* Spatial Regulators for Bacterial Cell Division Self-Organize into Surface Waves in Vitro. *Science* **320**(5877), 789–792, 2008. DOI: 10.1126/science.1154413.

[46] D. Fange and J. Elf. Noise-Induced Min Phenotypes in E. coli. *PLoS Comput Biol* **2**(6), e80, 2006. DOI: 10.1371/journal.pcbi.0020080.

[47] A. Touhami, M. Jericho and A. D. Rutenberg. Temperature Dependence of MinD Oscillation in Escherichia coli: Running Hot and Fast. *J Bacteriol* **188**(21), 7661–7667, 2006. DOI: 10.1128/JB.00911-06.

[48] J. Halatek and E. Frey. Highly Canalized MinD Transfer and MinE Sequestration Explain the Origin of Robust MinCDE-Protein Dynamics. *Cell Rep* **1**(6), 741–752, 2012. DOI: 10.1016/j.celrep.2012.04.005.

[49] J. Halatek and E. Frey. Effective 2D model does not account for geometry sensing by self-organized proteins patterns. *Proc Natl Acad Sci U S A* **111**(18), E1817–E1817, 2014. DOI: 10.1073/pnas.1220971111.

[50] F. Wu, B. G. C. van Schie, J. E. Keymer and C. Dekker. Symmetry and scale orient Min protein patterns in shaped bacterial sculptures. *Nat Nanotechnol* **10**(8), 719–726, 2015. DOI: 10.1038/nnano.2015.126.

[51] F. Wu *et al.* Multistability and dynamic transitions of intracellular Min protein patterns. *Mol Syst Biol* **12**(6), 873, 2016. DOI: 10.15252/msb.20156724.

[52] J. Halatek and E. Frey. Rethinking pattern formation in reaction–diffusion systems. *Nat Phys* **14**(5), 507–514, 2018. DOI: 10.1038/s41567-017-0040-5.

[53] E. Frey, J. Halatek, S. Kretschmer and P. Schwille. Protein Pattern Formation. 1–17, 2018. arXiv: 1801.01365.

[54] J. Halatek, F. Brauns and E. Frey. Self-organization principles of intracellular pattern formation. *Philos Trans R Soc Lond B Biol Sci* **373**(1747), 20170107, 2018. DOI: 10.1098/rstb.2017.0107.

[55] J. Denk *et al.* MinE conformational switching confers robustness on self-organized Min protein patterns. *Proc Natl Acad Sci U S A*, 201719801, 2018. DOI: 10.1073/pnas.1719801115.

[56] D. Thalmeier, J. Halatek and E. Frey. Geometry-induced protein pattern formation. *Proc Natl Acad Sci U S A* **113**(3), 548–553, 2016. DOI: 10.1073/pnas.1515191113.

[57] G. del Solar *et al.* Replication and control of circular bacterial plasmids. *Microbiol Mol Biol Rev* **62**(2), 434–64, 1998.

[58] R. Reyes-Lamothe *et al.* High-copy bacterial plasmids diffuse in the nucleoid-free space, replicate stochastically and are randomly partitioned at cell division. *Nucleic Acids Res* **42**(2), 1042–1051, 2014. DOI: 10.1093/nar/gkt918.

[59] J. C. Baxter and B. E. Funnell. Plasmid Partition Mechanisms. *Microbiol Spectr* **2**(6), 135–155, 2014. DOI: 10.1128/microbiolspec.PLAS-0023-2014.

[60] M. A. J. Roberts *et al.* ParA-like protein uses nonspecific chromosomal DNA binding to partition protein complexes. *Proc Natl Acad Sci U S A* **109**(17), 6698–6703, 2012. DOI: 10.1073/pnas.1114000109.

[61] B. Galán *et al.* Nucleoid-associated PhaF phasin drives intracellular location and segregation of polyhydroxyalkanoate granules in Pseudomonas putida KT2442. *Mol Microbiol* **79**(2), 402–418, 2011. DOI: 10.1111/j.1365-2958.2010.07450.x.

[62] J. T. Henry and S. Crosson. Chromosome replication and segregation govern the biogenesis and inheritance of inorganic polyphosphate granules. *Mol Biol Cell* **24**(20), 3177–3186, 2013. DOI: 10.1091/mbc.e13-04-0182.

[63] L. R. Racki *et al.* Polyphosphate granule biogenesis is temporally and functionally tied to cell cycle exit during starvation in Pseudomonas aeruginosa. *Proc Natl Acad Sci U S A* **114**(12), E2440–E2449, 2017. DOI: 10.1073/pnas.1615575114.

[64] J. Livny, Y. Yamaichi and M. K. Waldor. Distribution of Centromere-Like parS Sites in Bacteria: Insights from Comparative Genomics. *J Bacteriol* **189**(23), 8693–8703, 2007. DOI: 10.1128/JB.01239-07.

[65] C. M. Hester and J. Lutkenhaus. Soj (ParA) DNA binding is mediated by conserved arginines and is essential for plasmid segregation. *Proc Natl Acad Sci U S A* **104**(51), 20326–20331, 2007. DOI: 10.1073/pnas.0705196105.

[66] G. Scholefield, R. Whiting, J. Errington and H. Murray. Spo0J regulates the oligomeric state of Soj to trigger its switch from an activator to an inhibitor of DNA replication initiation. *Mol Microbiol* **79**(4), 1089–1100, 2011. DOI: 10.1111/j.1365-2958.2010.07507.x.

[67] J. L. Ptacin *et al.* A spindle-like apparatus guides bacterial chromosome segregation. *Nat Cell Biol* **12**(8), 791–798, 2010. DOI: 10.1038/ncb2083.

[68] W. B. Schofield, H. C. Lim and C. Jacobs-Wagner. Cell cycle coordination and regulation of bacterial chromosome segregation dynamics by polarly localized proteins. *EMBO J* **29**(18), 3068–3081, 2010. DOI: 10.1038/emboj.2010.207.

[69] A. G. Vecchiarelli, L. C. Hwang and K. Mizuuchi. Cell-free study of F plasmid partition provides evidence for cargo transport by a diffusion-ratchet mechanism. *Proc Natl Acad Sci U S A* **110**(15), E1390–E1397, 2013. DOI: 10.1073/pnas.1302745110.

[70] G. E. Lim, A. I. Derman and J. Pogliano. Bacterial DNA segregation by dynamic SopA polymers. *Proc Natl Acad Sci U S A* **102**(49), 17658–17663, 2005. DOI: 10.1073/pnas.0507222102.

[71] G. Ebersbach, D. J. Sherratt and K. Gerdes. Partition-associated incompatibility caused by random assortment of pure plasmid clusters. *Mol Microbiol* **56**(6), 1430–1440, 2005. DOI: 10.1111/j.1365-2958.2005.04643.x.

[72] T. Hatano, Y. Yamaichi and H. Niki. Oscillating focus of SopA associated with filamentous structure guides partitioning of F plasmid. *Mol Microbiol* **64**(5), 1198–1213, 2007. DOI: 10.1111/j.1365-2958.2007.05728.x.

[73] M. Howard and K. Gerdes. MicroCommentary: What is the mechanism of ParA-mediated DNA movement? *Mol Microbiol* **78**(1), 9–12, 2010. DOI: 10.1111/j.1365-2958.2010.07316.x.

[74] T. Sugawara and K. Kaneko. Chemophoresis as a driving force for intracellular organization: Theory and application to plasmid partitioning. *Biophysics* **7**, 77–88, 2011. DOI: 10.2142/biophysics.7.77.

[75] J.-C. Walter *et al.* Surfing on Protein Waves: Proteophoresis as a Mechanism for Bacterial Genome Partitioning. *Phys Rev Lett* **119**(2), 028101, 2017. DOI: 10.1103/PhysRevLett.119.028101.

[76] A. G. Vecchiarelli, K. C. Neuman and K. Mizuuchi. A propagating ATPase gradient drives transport of surface-confined cellular cargo. *Proc Natl Acad Sci U S A* **111**(13), 4880–4885, 2014. DOI: 10.1073/pnas.1401025111.

[77] E. J. Banigan and J. F. Marko. Self-propulsion and interactions of catalytic particles in a chemically active medium. *Phys Rev E* **93**(1), 012611, 2016. DOI: 10.1103/PhysRevE.93.012611.

[78] L. Hu *et al.* Directed and persistent movement arises from mechanochemistry of the ParA/ParB system. *Proc Natl Acad Sci U S A* **112**(51), 201505147, 2015. DOI: 10.1073/pnas.1505147112.

[79] L. Hu *et al.* Brownian ratchet mechanisms of ParA-mediated partitioning. *Plasmid* **92**, 12–16, 2017. DOI: 10.1016/j.plasmid.2017.05.002.

[80] E. J. Banigan *et al.* Filament Depolymerization Can Explain Chromosome Pulling during Bacterial Mitosis. *PLoS Comput Biol* **7**(9), e1002145, 2011. DOI: 10.1371/journal.pcbi.1002145.

[81] B. Shtylla and J. P. Keener. A mathematical model of ParA filament-mediated chromosome movement in Caulobacter crescentus. *J Theor Biol* **307**, 82–95, 2012. DOI: 10.1016/j.jtbi.2012.05.004.

[82] J. Palacci *et al.* Colloidal Motility and Pattern Formation under Rectified Diffusiophoresis. *Phys Rev Lett* **104**(13), 138302, 2010. DOI: 10.1103/PhysRevLett.104.138302.

[83] F. Jülicher and J. Prost. Generic theory of colloidal transport. *Eur Phys J E Soft Matter* **29**(1), 27–36, 2009. DOI: 10.1140/epje/i2008-10446-8.

[84] J. Anderson. Colloid Transport By Interfacial Forces. *Annu Rev Fluid Mech* **21**(1), 61–99, 1989. DOI: 10.1146/annurev.fluid.21.1.61.

[85] L. Jindal and E. Emberly. Operational Principles for the Dynamics of the In Vitro ParA-ParB System. *PLoS Comput Biol* **11**(12), e1004651, 2015. DOI: 10.1371/journal.pcbi.1004651.

[86] A. G. Vecchiarelli, Y. Seol, K. C. Neuman and K. Mizuuchi. A moving ParA gradient on the nucleoid directs subcellular cargo transport via a chemophoresis force. *Bioarchitecture* **4**(4-5), 154–159, 2014. DOI: 10.4161/19490992.2014.987581.

[87] E. Toro and L. Shapiro. Bacterial Chromosome Organization and Segregation. *Cold Spring Harb Perspect Biol* **2**(2), a000349, 2010. DOI: 10.1101/cshperspect. a000349.

[88] X. Wang, P. M. Llopis and D. Z. Rudner. Organization and segregation of bacterial chromosomes. *Nat Rev Genet* **14**(3), 191–203, 2013. DOI: 10.1038/ nrg3375.

[89] M. Thanbichler, S. C. Wang and L. Shapiro. The bacterial nucleoid: A highly organized and dynamic structure. *J Cell Biochem* **96**(3), 506–521, 2005. DOI: 10.1002/jcb.20519.

[90] N. J. Kuwada, K. C. Cheveralls, B. Traxler and P. A. Wiggins. Mapping the driving forces of chromosome structure and segregation in Escherichia coli. *Nucleic Acids Res* **41**(15), 7370–7377, 2013. DOI: 10.1093/nar/gkt468.

[91] C. Peskin, G. Odell and G. Oster. Cellular motions and thermal fluctuations: the Brownian ratchet. *Biophys J* **65**(1), 316–324, 1993. DOI: 10.1016/S0006-3495(93)81035-X.

[92] S. Saffarian *et al.* Powering a burnt bridges Brownian ratchet: A model for an extracellular motor driven by proteolysis of collagen. *Phys Rev E* **73**(4), 041909, 2006. DOI: 10.1103/PhysRevE.73.041909.

[93] A. Y. Morozov and A. B. Kolomeisky. Transport of molecular motor dimers in burnt-bridge models. *J Stat Mech* **2007**(12), P12008, 2007. DOI: 10.1088/1742-5468/2007/12/P12008.

[94] B. Shtylla and J. P. Keener. Mathematical modeling of bacterial track-altering motors: Track cleaving through burnt-bridge ratchets. *Phys Rev E* **91**(4), 042711, 2015. DOI: 10.1103/PhysRevE.91.042711.

[95] M. A. Fogel and M. K. Waldor. A dynamic, mitotic-like mechanism for bacterial chromosome segregation. *Genes Dev* **20**(23), 3269–3282, 2006. DOI: 10.1101/ gad.1496506.

[96] F. Szardenings, D. Guymer and K. Gerdes. ParA ATPases can move and position DNA and subcellular structures. *Curr Opin Microbiol* **14**(6), 712–718, 2011. DOI: 10.1016/j.mib.2011.09.008.

[97] A. G. Vecchiarelli *et al.* ATP control of dynamic P1 ParA-DNA interactions: a key role for the nucleoid in plasmid partition. *Mol Microbiol* **78**(1), 78–91, 2010. DOI: 10.1111/j.1365-2958.2010.07314.x.

[98] L. C. Hwang *et al.* ParA-mediated plasmid partition driven by protein pattern self-organization. *EMBO J* **32**(9), 1238–1249, 2013. DOI: 10.1038/emboj.2013.34.

[99] I. V. Surovtsev, H. C. Lim and C. Jacobs-Wagner. The Slow Mobility of the ParA Partitioning Protein Underlies Its Steady-State Patterning in Caulobacter. *Biophys J* **110**(12), 2790–2799, 2016. DOI: 10.1016/j.bpj.2016.05.014.

[100] I. V. Surovtsev, M. Campos and C. Jacobs-Wagner. DNA-relay mechanism is sufficient to explain ParA-dependent intracellular transport and patterning of single and multiple cargos. *Proc Natl Acad Sci U S A* **113**(46), E7268–E7276, 2016. DOI: 10.1073/pnas.1616118113.

[101] D. Schumacher and L. Søgaard-Andersen. Regulation of Cell Polarity in Motility and Cell Division in Myxococcus xanthus. *Annu Rev Microbiol* **71**(1), 61–78, 2017. DOI: 10.1146/annurev-micro-102215-095415.

[102] A. Harms, A. Treuner-Lange, D. Schumacher and L. Søgaard-Andersen. Tracking of Chromosome and Replisome Dynamics in Myxococcus xanthus Reveals a Novel Chromosome Arrangement. *PLoS Genet* **9**(9), e1003802, 2013. DOI: 10.1371/journal.pgen.1003802.

[103] A. A. Iniesta. ParABS System in Chromosome Partitioning in the Bacterium Myxococcus xanthus. *PLoS One* **9**(1), e86897, 2014. DOI: 10.1371/journal.pone.0086897.

[104] G. Meacci *et al.* Mobility of Min-proteins in Escherichia coli measured by fluorescence correlation spectroscopy. *Phys Biol* **3**(4), 255–263, 2006. DOI: 10.1088/1478-3975/3/4/003.

[105] Z. Lansky *et al.* Diffusible Crosslinkers Generate Directed Forces in Microtubule Networks. *Cell* **160**(6), 1159–1168, 2015. DOI: 10.1016/j.cell.2015.01.051.

[106] M. Hamdi, G. Sharma, A. Ferreira and C. Mavroidis. Characterization of protein based spring-like elastic joints for biorobotic applications. *Proc IEEE Int Conf Robot Autom*, 1794–1799, 2006. DOI: 10.1109/ROBOT.2006.1641966.

[107] H. Dietz and M. Rief. Elastic Bond Network Model for Protein Unfolding Mechanics. *Phys Rev Lett* **100**(9), 098101, 2008. DOI: 10.1103/PhysRevLett.100.098101.

[108] P. Montero Llopis, O. Sliusarenko, J. Heinritz and C. Jacobs-Wagner. In Vivo Biochemistry in Bacterial Cells Using FRAP: Insight into the Translation Cycle. *Biophys J* **103**(9), 1848–1859, 2012. DOI: 10.1016/j.bpj.2012.09.035.

[109] I. V. Surovtsev and C. Jacobs-Wagner. Subcellular Organization: A Critical Feature of Bacterial Cell Replication. *Cell* **172**(6), 1271–1293, 2018. DOI: 10.1016/j.cell.2018.01.014.

[110] D. T. Gillespie. A general method for numerically simulating the stochastic time evolution of coupled chemical reactions. *J Comput Phys* **22**(4), 403–434, 1976. DOI: 10.1016/0021-9991(76)90041-3.

[111] D. T. Gillespie. Exact stochastic simulation of coupled chemical reactions. *J Chem Phys* **81**(25), 2340–2361, 1977. DOI: 10.1021/j100540a008.

[112] D. T. Gillespie. Stochastic Simulation of Chemical Kinetics. *Annu Rev Phys Chem* **58**(1), 35–55, 2007. DOI: 10.1146/annurev.physchem.58.032806.104637.

[113] C. Gardiner. *Stochastic Methods: A Handbook for the Natural and Social Sciences.* 4th edition. Springer-Verlag, Berlin, Germany, 2009.

[114] K. Ahnert *et al.* Odeint – Solving Ordinary Differential Equations in C++. *AIP Conf Proc 1389.* 2011, pp. 1586–1589. DOI: 10.1063/1.3637934.

[115] L. Hu *et al.* Brownian Ratchet Mechanism for Faithful Segregation of Low-Copy-Number Plasmids. *Biophys J* **112**(7), 1489–1502, 2017. DOI: 10.1016/j.bpj.2017.02.039.

[116] P. G. De Gennes. Dynamics of Entangled Polymer Solutions. I. The Rouse Model. *Macromolecules* **9**(4), 587–593, 1976. DOI: 10.1021/ma60052a011.

[117] *Mathematica, Version 11.1, Wolfram Research, Inc.* Champaign, IL, 2017.

[118] S. H. Strogatz. *Nonlinear Dynamics and Chaos: With Applications to Physics, Biology, Chemistry, and Engineering.* 2nd edition. Westview Press, Boulder, Colorado, USA, 2015.

[119] W. H. Press, S. A. Teukolsky, W. T. Vetterling and B. P. Flannery. *Numerical Recipes: The Art of Scientific Computing.* 3rd edition. Cambridge University Press, Cambridge, UK, 2007.

[120] S. Bergeler and E. Frey. Regulation of Pom cluster dynamics in Myxococcus xanthus. *submitted for publication*, 2018. arXiv: 1801.06133.

Acknowledgements

having a very good time! For proof-reading my thesis I want to thank Christoph Brand, Isabella Graf, Marianne Bauer, Jacob Halatek and Jonas Denk.

Finally, I would like to express a cordial thanks to my parents, Iris and Jürgen Bergeler, my sister Maike Bergeler and Stephan Bachmann for encouraging and supporting me. A very special thanks goes to Christoph Brand for your love, continuous support and encouragement, and many helpful discussions.